Characterization of FERM domain proteins, Merlin and Moesin, in Drosophila

by

Namal Wijeratne Abeysundara

A thesis submitted in partial fulfillment of the requirements for the degree of

Doctor of Philosophy

Medical Sciences - Medical Genetics
University of Alberta

ABSTRACT

Merlin and the ezrin-radixin-moesin (ERM) proteins are key organizers of the cell cortex through linking membrane-associated proteins to the underlying actin cytoskeleton. Merlin and the ERM proteins have been implicated in the maintenance of cell integrity, adhesion, and motility during tissue development and organization. Functional redundancies between the ERM proteins remain a challenge to further elucidating ERM protein function in mammals. Furthermore, the precise mechanisms underlying the tissue-specific defects associated with the loss of merlin still remain unclear. Thus, we use *Drosophila melanogaster* as a model organism to further investigate the functional significance of Merlin and Moesin, the single Drosophila orthologues of merlin and the ERM proteins.

Biochemical studies have demonstrated that mammalian merlin interacts with ezrin-binding phosphoprotein 50 (EBP50), which is an essential scaffold protein in ERM-mediated membrane organization. However, the functional significance of the merlin and EBP50 interaction still remains unclear. We used Drosophila as a model organism to further characterize the interaction between Merlin and Sip1, the Drosophila orthologue of EBP50. We found that Merlin and Sip1 genetically interact. *In vitro* binding assays showed that the α-helical domain of Merlin was important for Sip1 binding. Specifically, mutation of two conserved arginine residues within the α-helical domain of Merlin reduced binding to Sip1 and altered Merlin subcellular localization and trafficking in Drosophila wing epithelia and cell culture. When Merlin with reduced binding to Sip1 was expressed in the adult wings, the area of the wing region increased. Furthermore, reduced Merlin and Sip1 binding led to defects in epithelial organization in the follicle cell epithelium surrounding the developing oocyte. These findings suggest that Merlin and Sip1 binding is important for growth inhibition and epithelial organization in Drosophila.

As the loss of merlin is associated with the development of central nervous system tumours in humans, the functional significance of Drosophila Merlin was further investigated in a neuronal context. Within the Drosophila optic lobe, neuroepithelial cells differentiate into neural progenitors or neuroblasts, which give rise to the neurons essential for the adult visual system. Multiple signaling pathways have been linked to neuroepithelial cell proliferation and differentiation. We found that both Merlin and Sip1 localized to the neuroepithelial cells and neuroblasts within the developing optic lobe. Loss of Merlin and Sip1 led to defects in optic lobe development. Although the mechanisms still remain largely unknown, these findings suggest that Merlin and Sip1 may regulate neuroepithelial cell proliferation or differentiation.

Drosophila neuroblast asymmetric cell division requires an intact actomyosin network for anchoring polarity proteins to the cell cortex and maintaining cell size asymmetry. However, the mechanisms that regulate actomyosin dynamics during neuroblast asymmetric cell division have not been extensively studied. We found that Moesin is essential for neuroblast proliferation and mitotic progression in the developing brain. During metaphase, phosphorylated Moesin (p-Moesin) was enriched at the apical cortex and loss of Moesin led to defects in apical polarity maintenance and cortical stability. This asymmetric distribution of p-Moesin was regulated by components of the apical polarity complex. During early anaphase, p-Moesin remained enriched at the apical cortex, which appeared to contribute to asymmetric cortical extension and myosin basal furrow positioning. Therefore, our findings reveal Moesin as a novel apical polarity protein that drives cortical remodelling of dividing neuroblasts, essential for polarity maintenance and initial establishment of cell size asymmetry.

Together, this work provides further insight into the role of Merlin and Moesin in cell or tissue organization during Drosophila development.

PREFACE

The majority of Chapter 2 (Characterization of Merlin and Sip1 interaction) has been published as Abeysundara, N., Leung, A. C., Primrose, D. A. and Hughes, S. C. (2014), Regulation of cell proliferation and adhesion by means of a novel region of Drosophila Merlin interacting with Sip1. Developmental Dynamics, 243: 1554–1570. doi:10.1002/dvdy.24187 (License no. 4152010495684). Technical assistance with scanning electron microscopy was provided by Arlene Oatway. For Section 2.3.2 (Identification of Merlin and Sip1 interaction region), the experiments were conducted and data was analyzed by Albert C. Leung.

In Chapter 4 (Determining the role of Sip1 and Moesin in central brain neuroblasts), technical assistance with live imaging was provided by Andrew J. Simmonds and technical assistance with sample preparation for mass spectrometry was provided by David A. Primrose.

The remaining parts of this thesis are original work by Namal Wijeratne Abeysundara.

ACKNOWLEDGEMENTS

I would like to express my sincere gratitude to my supervisor, Dr. Sarah Hughes, for taking me on as an undergraduate student, where I had my first glimpse into the world of research, and for having the trust and confidence in me to continue on with my graduate studies. I truly appreciated the freedom and encouragement she gave me to pursue various projects, which allowed me to grow as a scientist. I will be forever grateful for her endless support and understanding during times of stress, in both my academic and personal life.

I would like to thank my supervisory committee, Dr. John Locke and Dr. Fred Berry, for their support and guidance, and my examining committee, including Dr. Martin Srayko and Dr. Gregory Emery, for their helpful suggestions and feedback regarding my work and moving forward in my academic career.

Sincere thanks to David Primrose for training me as an undergraduate student and for his continuous support and help in keeping things running over the years. The mid-afternoon breaks to Tim Hortons were always a nice stress relief, especially during "roll up the rim to win" season when we needed a few extra wins in life!

I would also like to thank Dr. Rika Maruyama for always listening and providing invaluable advice during the course of my graduate degree. It was always nice having someone to literally turn to in the lab.

Special thanks go to my friend and former labmate, Kirsten Arnold, for sharing in the excitement and frustrations that come with research and life in general. Whether it was cooking fly food or tipping stocks, I always enjoyed our time together in the lab.

I would also like to thank Dr. Andrew Simmonds for being a constant support for the lab and for always lending a helping hand. I also appreciated the life advice and the friendly reminder to have fun once in a while!

Thanks to all the past and current members of the Hughes and Simmonds labs for their helpful feedback along the way and for always creating a supportive and enjoyable research environment.

I am also very grateful for the labs of Drs. M. Bhat, C. Berg, R. Fehon, D. Hipfner, J. Knoblich, F. Matsuzaki, J. Skeath, and A. Wodarz for generously sharing their fly stocks and antibody reagents and the Fly Group at the University of Alberta for sharing ideas and offering helpful comments on my work.

Lastly, I would like to express my sincere appreciation for my family and friends and their unconditional love and support over the years. It is always comforting knowing that I have such caring people to share my successes and failures with at the end of the day.

TABLE OF CONTENTS

LIST OF FIGURES

LIST OF TABLES

LIST OF ABBREVIATIONS

AEL	After egg laying
ALH	After larval hatching
A/P	Anterior/posterior
aPKC	Atypical kinase C
ATPα	Na^+/K^+-ATPase α-subunit
Baz	Bazooka
Cand1	Cullin-associated NEDD8-dissociated protein 1
DAPI	4′,6-Diamidine-2′-phenylindole dihydrochloride
DCAD	DE-Cadherin
Dpn	Deadpan
DSHB	Developmental Studies Hybridoma Bank
dsRNA	Double stranded RNA
EBP50	ezrin-binding phosphoprotein 50
EGFR	epidermal growth factor receptor
ERM	ezrin-radixin-moesin
F-actin	filamentous actin
FERM	four-point-one ezrin, radixin, moesin
Flw	Flapwing
GFP	Green fluorescent protein
Hts	Hu li tai shao
Insc	Inscuteable
IPC	Inner proliferation center
L(1)sc	Lethal of Scute
Lgl	Lethal (2) giant larvae
MARCM	Mosaic analysis with a repressible cell marker
MDCK	Madin-Darby canine kidney

Mer	Merlin
Moe	Moesin
Mira	Miranda
Mud	Mushroom body defect
NF2	Neurofibromatosis 2
NHERF1	Na^+/H^+ exchanger regulatory cofactor 1
OPC	Outer proliferation center
PDGF	platelet derived growth factor
PDZ	Post-synaptic density protein 95, Discs large 1, Zonula occludens-1
PH3	Phospho-histone H3
Pins	Partner of Inscuteable
PIP_2	Phosphatidylinositol 4,5-bisphosphate
PPF	Post-puparium formation
Pros	Prospero
Ptc	Patched
RFP	Red fluorescent protein
ROK	Rho kinase
S2	Schneider 2
shRNA	Short hairpin RNA
Sip1	Sry-interacting protein 1
siRNA	Small interfering RNA
Slik	Sterile20-like kinase
UAS	Upstream activation sequence
YAP	Yes-associated protein

Chapter 1: General Introduction

1.1 THE ERM PROTEINS AND MERLIN

The ezrin-radixin-moesin (ERM) proteins and merlin are membrane-associated proteins that have the ability to regulate changes in cell morphology, adhesion, and motility at the cell cortex (Bretscher et al., 2002). The ERM proteins and merlin interact with the actin cytoskeleton and localize to actin-rich structures and regions of cell-cell contact (Amieva and Furthmayr, 1995; Berryman et al., 1993; Gonzalez-Agosti et al., 1996; Sainio et al., 1997). Changes in these structures can lead to tumour development and progression due to the loss of cell polarity, contact-dependent inhibition of proliferation, and increased cell motility and invasiveness (McClatchey, 2003). The ERM proteins are essential for the formation and alteration of specialized membrane domains through linking membrane-associated proteins to the underlying actin cytoskeleton (Lamb et al., 1997; Mackay et al., 1997; Takeuchi et al., 1994). Although the ERM proteins and merlin are structurally similar and display some overlapping function, merlin acts as a tumour suppressor protein (Rouleau et al., 1993; Trofatter et al., 1993); whereas the ERM proteins have been proposed to promote cancer progression (Elliott et al., 2005; Estecha et al., 2009; Valderrama et al., 2012). The loss of merlin is not compensated by the ERM proteins, further supporting that merlin functions as a distinct protein (McClatchey et al., 1997). Merlin regulates contact dependent inhibition of the proliferation through the stabilization and formation of cell-cell contacts and negative regulation of mitogenic signaling (Lallemand et al., 2003; Morrison et al., 2001; Shaw et al., 2001). However, it still remains unclear how merlin precisely coordinates these processes in specific tissues. Thus, studying how the ERM proteins and merlin regulates changes in cell morphology, adhesion, and proliferation during development can provide further insight into their role during cancer progression.

1.1.1 Identification

The gene family consisting of ezrin, radixin, and moesin belong to the band 4.1 superfamily, defined by the presence of a Four-point-one ERM (FERM) domain involved in regulating interactions between the plasma membrane and actin cytoskeleton (Funayama et al., 1991; Gould et al., 1989; Lankes and Furthmayr, 1991; Sato et al., 1992). Ezrin was initially identified as a protein substrate of receptor tyrosine kinases (Cooper and Hunter, 1981) and was purified as a component of the microvillus cytoskeleton isolated from intestinal epithelial cell brush borders (Bretscher, 1983). Sequence analysis revealed that the amino (N)-terminal of ezrin was similar to that of the band 4.1 protein, an essential structural protein at erythrocyte membranes (Conboy et al., 1986; Gould et al., 1989; Turunen et al., 1989). Ezrin was also found to be enriched in surface structures of cultured

cells, including microvilli, cortical blebs, and retraction fibers (Bretscher, 1983; Gould et al., 1989; Pakkanen et al., 1987; Pakkanen and Vaheri, 1989; Pakkanen et al., 1988; Turunen et al., 1989). Radixin was first isolated from the adherens junctions of liver cells (Tsukita et al., 1989) and localized to the microvilli of hepatocytes and other actin-rich structures, including the cleavage furrow (Amieva et al., 1994; Sato et al., 1991). Moesin was identified as a heparin-binding protein (Lankes et al., 1988; Tsukita et al., 1989) and was later found to be closely related to ezrin (Lankes and Furthmayr, 1991). Moesin localized to endothelial cells and surface structures of cultured cells (Amieva and Furthmayr, 1995; Franck et al., 1993). Thus, ezrin, radixin, and moesin, collectively known as the ERM proteins, were identified as potential cytoskeletal linkers given their homology to the band 4.1 protein and localization to actin-rich structures.

Linkage studies revealed that the gene associated with Neurofibromatosis Type 2 (NF2) mapped to chromosome 22 (Rouleau et al., 1987), which led to the identification of the *NF2* gene encoding for a protein related to the ERM protein family, merlin (for moesin-ezrin-radixin-like protein) (Rouleau et al., 1993; Trofatter et al., 1993). Similar to the ERM proteins, merlin localized to motile structures such as membrane ruffles and the leading edge of human fibroblasts, but was not associated with stress fibers (Gonzalez-Agosti et al., 1996). Furthermore, merlin was found to co-localize with ezrin near the cell surface and accumulated in surface extensions and blebs of cultured COS-1 cells (Sainio et al., 1997). However, in human meningioma cells, merlin did not localize to the same motile structures as either ezrin or moesin, suggesting merlin functions as a distinct protein in these cells (Gonzalez-Agosti et al., 1996).

1.1.2 Structure and regulation

The ERM proteins share approximately 75% overall sequence identity with each other and all three members are 45-47% identical to merlin (Figure 1-1) (Trofatter et al., 1993). Merlin and the ERM proteins exhibit similar structural domains, consisting of an N-terminal FERM domain, a central α-helical domain, and a carboxyl (C)-terminal domain, which includes an actin-binding site in the ERM proteins but not in merlin (Kang et al., 2002; Pearson et al., 2000; Shimizu et al., 2002). The FERM domain adopts a cloverleaf structure consisting of three independent lobes that allow for the association of multiple proteins at the plasma membrane (Algrain et al., 1993; Pearson et al., 2000), including Rho GTPase regulators (Kissil et al., 2003; Maeda et al., 1999; Takahashi et al., 1998; Takahashi et al., 1997), transmembrane receptors CD44 and CD43 (Morrison et al., 2001; Tsukita et al., 1994; Yonemura et al., 1998), and the ezrin-binding phosphoprotein 50

(EBP50) (Murthy et al., 1998; Reczek et al., 1997). The C-terminal tail of the ERM proteins can bind filamentous actin (F-actin) (Pestonjamasp et al., 1995; Turunen et al., 1994). An actin-binding site within the N-terminal domain of ezrin has also been identified *in vitro*, which is conserved in moesin, radixin, and merlin (Martin et al., 1997). Even though merlin lacks the C-terminal actin-binding site, merlin has been shown to associate with the actin cytoskeleton via its N-terminal domain (Brault et al., 2001; James et al., 2001; Xu and Gutmann, 1998).

The isolation of heterotypic and homotypic interactions between ezrin and moesin, revealed that an intramolecular interaction occurs between the N-terminal FERM domain and the C-terminal domain of the ERM proteins (Gary and Bretscher, 1993; Gary and Bretscher, 1995; Nguyen et al., 2001). Previously, it has been shown that full-length ezrin does not bind F-actin (Bretscher, 1983; Shuster and Herman, 1995). Thus, the intramolecular interaction between the N- and C-terminal domains of the ERM proteins prevent F-actin binding (Turunen et al., 1994) and the association of the N-terminus with membrane-associated proteins (Gary and Bretscher, 1995; Reczek and Bretscher, 1998; Takahashi et al., 1997). The α-helical domain was also shown to associate with the FERM domain and mask known binding sites for protein interactions (Li et al., 2007b). Phosphorylation of a conserved threonine residue in the actin-binding region of the ERM proteins relieves the intramolecular interaction and thus is essential for protein activation (Hayashi et al., 1999; Huang et al., 1999; Matsui et al., 1998; Nakamura et al., 1995; Nakamura et al., 1999; Oshiro et al., 1998; Pietromonaco et al., 1998; Simons et al., 1998; Tran Quang et al., 2000). Multiple kinases phosphorylate this conserved threonine residue, including the lymphocyte-oriented kinase, Rho-kinase (ROK), protein kinase C, Nck-interacting kinase, and MST4 (Baumgartner et al., 2006; Belkina et al., 2009; Matsui et al., 1998; Ng et al., 2001; Pietromonaco et al., 1998; Simons et al., 1998; ten Klooster et al., 2009). Phosphorylation of tyrosine and threonine residues in the N-terminal domain of the ERM proteins have also been demonstrated (Berryman et al., 1993; Bretscher, 1989; Krieg and Hunter, 1992; Yang and Hinds, 2003). Furthermore, phosphatidylinositol 4,5-bisphosphate (PIP_2) binding of the ERM proteins at the plasma membrane acts as a prerequisite to ERM phosphorylation and activation (Fievet et al., 2004; Hirao et al., 1996; Matsui et al., 1999; Niggli et al., 1995; Yonemura et al., 2002).

Similar to the ERM proteins, association between the N-terminal FERM domain and C-terminal tail of merlin has also been demonstrated (Gonzalez-Agosti et al., 1999; Gronholm et al., 1999; Huang et al., 1998; Nguyen et al., 2001; Sherman et al., 1997). However, mammalian studies suggest that the intramolecular interaction of merlin is

important for tumour suppressor activity, as NF2 patient mutations displayed a reduced ability to self-associate and the over-expression of the self-associated form of merlin was able to inhibit growth of a rat schwannoma cell line (Gutmann et al., 1999a; Morrison et al., 2001; Shaw et al., 1998a; Sherman et al., 1997). Phosphorylation of merlin at serine 518 by p21-activated kinase and protein kinase A was shown to inactivate its growth suppressive function (Alfthan et al., 2004; Kissil et al., 2002; Shaw et al., 2001; Surace et al., 2004; Xiao et al., 2002). Furthermore, dephosphorylation of merlin at serine 518 by the myosin phosphatase targeting subunit 1 and phosphatase PP1δ complex leads to the activation of the growth suppressive function of merlin (Jin et al., 2006). Based mostly on studies of ERM protein conformation, it was hypothesized that merlin phosphorylation at serine 518 would disrupt the intramolecular interaction and adopt an open conformation; whereas dephosphorylation of serine 518 would lead to a closed conformation (Shaw et al., 2001). However, alternative models have been proposed for merlin conformation (Ali Khajeh et al., 2014; Hennigan et al., 2010; Sher et al., 2012). Studies have shown that merlin phosphorylation at serine 518 either has minimal effects on conformation (Hennigan et al., 2010) or leads to a more closed form compared to non-phosphorylated merlin (Sher et al., 2012). Thus, the conformation of active and inactive forms of merlin still remains controversial. Merlin can also be phosphorylated at serine 10, threonine 230, and serine 315 by Akt, which regulates merlin ubiquitination and degradation (Laulajainen et al., 2011; Tang et al., 2007).

1.1.3 Functional Significance

As the ERM proteins are enriched in areas of contact between the plasma membrane and actin filaments, it was hypothesized that the ERM proteins function as linkers between membrane proteins and the underlying actin cytoskeleton. The ERM proteins function in Rho- and Rac-dependent reorganization of the actin cytoskeleton (Mackay et al., 1997) and have been shown to influence the Rho family of GTPases through association with GTPase-activating proteins, guanine nucleotide exchange factors, and guanine nucleotide dissociation inhibitors (D'Angelo et al., 2007; Hamada et al., 2001; Hatzoglou et al., 2007; Takahashi et al., 1998; Takahashi et al., 1997). The ERM proteins have been implicated in the organization of specialized actin-rich structures such as, retraction fibers, lamellipodia, filopodia, and microvilli (Amieva and Furthmayr, 1995; Lamb et al., 1997; Oshiro et al., 1998; Takeuchi et al., 1994). Moesin was found to be associated with the filopodia and microvilli of cultured fibroblasts, macrophages, and epithelial cells (Amieva and Furthmayr, 1995). In transformed rat fibroblast cells, ezrin co-localized with F-actin to membrane

ruffles at the tips of pseudopodia (Lamb et al., 1997). Chromochore-assisted laser inactivation of ezrin in these transformed fibroblast cells resulted in the loss of membrane ruffling and pseudopodial retraction, suggesting that ezrin mediates pseudopodial extension during oncogenic transformation (Lamb et al., 1997). In nerve growth cones, radixin ablation also led to lamellipodial retraction (Castelo and Jay, 1999). Furthermore, the expression of a phosphomimetic form of ezrin resulted in the formation of lamellipodia, membrane ruffles, and microvilli in epithelial cells derived from kidney proximal tubules, compared to the expression of wild-type or the non-phosphorylated form of ezrin (Gautreau et al., 2000). Similarly, expression of a phosphomimetic form of moesin in COS7 cells led to the formation of microvilli-like structures (Oshiro et al., 1998). These findings suggest that phosphorylation of the ERM proteins induce the formation of actin-rich structures. Interfering with ERM protein synthesis using antisense oligonucleotides demonstrated that the ERM proteins are essential for microvilli formation in mouse epithelial and thymoma cells (Takeuchi et al., 1994). In addition, ezrin was shown to be involved in microvilli organization in the retinal pigment epithelium, small intestine, and the blastocyst of mice (Bonilha et al., 1999; Dard et al., 2001; Saotome et al., 2004). Thus, the ERM proteins are essential for the formation of specialized actin-rich structures in cultured cells and mammalian tissues.

Through the ability to form specialized actin-rich membrane domains, the ERM proteins can regulate many structural and dynamic processes at the cell cortex, including cell adhesion (Pujuguet et al., 2003; Takeuchi et al., 1994) and migration (Baeyens et al., 2013; Crepaldi et al., 1997; Legg et al., 2002). Interfering with ERM protein synthesis disrupted cell-substrate and cell-cell adhesion of cultured mouse epithelial cells, demonstrating a role for the ERM proteins in mediating cell adhesion (Takeuchi et al., 1994). Expression of the phosphomimetic form of ezrin resulted in E-cadherin accumulation in intracellular compartments of Madin-Darby canine kidney (MDCK) cells (Pujuguet et al., 2003) and the inability of mouse epithelial cells to form cysts or tubules in cell culture (Gautreau et al., 2000). These findings suggest that ezrin is involved in establishing functional cell-cell contacts in cell culture. Furthermore, studies in the mouse blastocyst revealed an essential role for ezrin in adherens junction assembly, as expression of mutations affecting ezrin phosphorylation impaired E-cadherin function and early morphogenetic events (Dard et al., 2004; Dard et al., 2001; Louvet et al., 1996). Protein kinase C-dependent phosphorylation of CD44 was shown to promote its association with ezrin and influence cell motility (Legg et al., 2002). The ERM proteins localize to polarized structures of vascular smooth muscle cells, in response to platelet-derived growth factor

(PDGF) stimulation (Baeyens et al., 2013). The depletion of the ERM proteins inhibited PDGF-induced formation of lamellipodia and cell migration (Baeyens et al., 2013). In addition, hepatocyte growth factor stimulation promoted the recruitment of ezrin to lateral membranes, enhancing cell motility of cultured epithelial cells (Crepaldi et al., 1997). Although the ERM proteins are important for the formation of polarized membrane domains in response to extracellular cues during migration, the spatiotemporal regulation and function of the ERM proteins in the establishment and maintenance of polarity still remains unclear.

Similar to the ERM proteins, merlin can also associate with cortical actin and influence cytoskeletal organization and assembly (Gonzalez-Agosti et al., 1996; James et al., 2001; Lallemand et al., 2003; Laulajainen et al., 2008; Sainio et al., 1997). Even though merlin lacks the C-terminal actin-binding site present in the ERM proteins, the N-terminal domain of merlin can bind to actin (Brault et al., 2001; James et al., 2001). Alternatively, merlin can indirectly associate with the actin cytoskeleton through interaction with cytoskeletal proteins such as, βII-spectrin, paxillin, or the ERM proteins (Fernandez-Valle et al., 2002; Gronholm et al., 1999; Scoles et al., 1998). The expression of merlin in CHO cells induced an elongated cell morphology, where merlin localized near the plasma membrane and at surface blebs (Sainio et al., 1997). Cultured human schwannoma cells displayed aberrant membrane ruffling and disorganized stress fibers, suggesting that a disorganized actin cytoskeleton is associated with the loss of merlin (Pelton et al., 1998). When merlin was over-expressed in rat schwannoma cell lines, cell motility and substrate attachment was reduced (Gutmann et al., 1999b). Merlin was shown to mediate cytoskeletal assembly and function through the negative regulation of Rac GTPase signaling (Kissil et al., 2003; Shaw et al., 2001). Furthermore, merlin association with cortical actin was important for growth inhibition in liver-derived epithelial cells (Cole et al., 2008). However, the expression of merlin chimeras that were unable to associate with actin, were still able to inhibit proliferation in *Nf2*-deficient primary Schwann cells; whereas other chimeras that did not inhibit proliferation, localized to cortical actin (Lallemand et al., 2009b). Thus, actin association is not required for merlin-mediated growth inhibition in Schwann cells, suggesting alternative mechanisms exist for merlin function.

Although the ERM proteins and merlin have high sequence similarity and some overlapping functions, merlin also has distinct functions. The loss of merlin is lethal in mice, demonstrating a functional requirement for merlin during development and the inability of the ERM proteins to compensate for the loss of merlin (McClatchey et al., 1997). Merlin was shown to be essential for early embryogenesis as mouse embryos homozygous for *Nf2*

mutations were lethal between embryonic days 6.5-7.0, displaying defects in extraembryonic tissues and gastrulation (McClatchey et al., 1997). Heterozygous *Nf2* mutant mice developed a wide variety of tumour types, suggesting that merlin is essential for growth inhibition in multiple tissues (McClatchey et al., 1998).

Merlin has been implicated in mediating contact-dependent inhibition of proliferation (Curto et al., 2007; Johnson et al., 2002; Lallemand et al., 2003; Morrison et al., 2001; Okada et al., 2005; Shaw et al., 1998b). When cultured cells were plated at increasing cell density, merlin levels increased with the non-phosphorylated form being the most prominent when cells established cell-cell contact (Shaw et al., 1998b). Furthermore, loss of cell adhesion led to merlin dephosphorylation, which was reversed when cells were re-plated, suggesting that cell-cell contact and cell spreading can influence merlin phosphorylation (Shaw et al., 1998b). Similarly, merlin levels and the hypo-phosphorylated form of merlin were shown to increase in rat Schwann cells cultured at high cell density, compared to low density cultures (Morrison et al., 2001). However, in a rat schwannoma cell line, merlin levels did not increase in confluent cultures but when merlin was over-expressed, merlin was hypo-phosphorylated and growth inhibition was observed only at high cell density (Morrison et al., 2001). These findings demonstrate that the hypo-phosphorylated form of merlin is essential for contact-mediated inhibition of proliferation.

In mouse embryonic fibroblasts, merlin associates with β-catenin at regions of cell-cell contact and the loss of merlin appeared to destabilize the adherens junctions, leading to the loss of contact-dependent inhibition of proliferation (Lallemand et al., 2003). Merlin association with tight junctions was also shown to be essential for its growth suppressive function (Yi et al., 2011). Defects in tight junction formation and cell polarity were observed in the embryonic epidermis with the loss of merlin (Gladden et al., 2010). In addition, merlin regulates the assembly of cell junctions and the loss of merlin led to neuroepithelial cell detachment and tissue fusion defects during early mouse development (McLaughlin et al., 2007). Together, these findings support a role for merlin in stabilizing regions of cell adhesion and polarity, which are essential for contact-mediated inhibition of proliferation and tissue organization.

Merlin can also influence contact-dependent inhibition of proliferation through the interaction with transmembrane proteins and the regulation of signalling pathway activity (Curto et al., 2007; Morrison et al., 2001; Shaw et al., 2001). Similar to the ERM proteins, merlin was shown to interact with the transmembrane receptor, CD44 (Sainio et al., 1997; Tsukita et al., 1994). CD44 specifically interacted with the hypo-phosphorylated form of merlin under confluent culture conditions, which was important for the growth suppressive

function of merlin (Morrison et al., 2001). Merlin can also inhibit Rac recruitment to the plasma membrane and signalling during contact-dependent inhibition of proliferation (Okada et al., 2005; Shaw et al., 2001). Furthermore, merlin loss in the liver resulted in hepatocyte and biliary epithelial over-proliferation, which was suppressed by the heterozygous deletion of *Yap* (Zhang et al., 2010), the transcriptional coactivator downstream of the Hippo pathway (Zhao et al., 2007). However, abnormal epidermal growth factor receptor (EGFR) signaling was also shown to contribute to over-proliferation of liver progenitors cells lacking merlin (Benhamouche et al., 2010). Merlin can associate with and negatively regulate EGFR signaling by sequestering EGFR into a membrane compartment (Cole et al., 2008; Curto et al., 2007). Furthermore, the loss of merlin in Schwann cells resulted in elevated levels of multiple growth factor receptors, ErbB2/3, insulin-like growth factor 1 receptor, and PDGF receptor (Lallemand et al., 2009a). Thus, merlin has the ability to influence cytoskeletal organization, cell adhesion, and the localization and function of multiple growth factor receptors during growth inhibition.

It is unclear how merlin coordinately regulates growth inhibition at so many levels but it likely involves its tissue-specific protein interactions. Merlin has been shown to interact with the ezrin-binding phosphoprotein 50 (EBP50), also referred to as the Na^+/H^+ exchanger regulatory cofactor 1 (NHERF1) (Gonzalez-Agosti et al., 1999; Murthy et al., 1998; Nguyen et al., 2001). EBP50 and merlin co-localize to actin-rich structures of cultured cells (Murthy et al., 1998). Although, merlin negatively regulates EGFR in an EBP50-dependent manner (Curto et al., 2007), the functional significance of the merlin and EBP50 interaction remains largely unknown.

1.2 NHERF1/EBP50

1.2.1 Identification

NHERF1 was originally identified as an essential cofactor involved in Na^+/H^+ exchanger 3 (NHE3) inhibition in renal brush border epithelium (Weinman et al., 1993). NHERF1 was also identified in human placenta microvilli as an ezrin-binding protein and thus is also referred to as ezrin-binding phosphoprotein 50 or EBP50 (Reczek et al., 1997). The NHERF1/EBP50 protein belongs to the NHERF family of PDZ (Post-synaptic density protein 95, Discs large 1, Zonula occludens-1)-domain containing proteins, which mediate protein-protein interactions (Custer et al., 1997; Kocher et al., 1999; Scott et al., 2002; Weinman et al., 1995; Yun et al., 1997). The presence of ERM-binding domains in NHERF1/EBP50 and the NHERF family member, NHERF2/E3KARP, suggests a role for linking membrane-associated proteins to the underlying actin cytoskeleton (Reczek et al., 1997).

1.2.2 Structure and regulation

NHERF proteins have been shown to homo- and hetero-dimerize through their PDZ domains, enhancing the ability to form multiprotein complexes (Fouassier et al., 2000; Lau and Hall, 2001; Shenolikar et al., 2001). An intramolecular interaction between the PDZ2 and the C-terminal domains of EBP50 reduces binding to PDZ domain ligands (Cheng et al., 2009; Li et al., 2007a; Morales et al., 2007). This intramolecular interaction is relieved by ezrin binding at the C-terminal domain of EBP50 and mutations disrupting this C-terminal region resulted in a cytoplasmic distribution in opossum proximal tubule cells (Morales et al., 2007). Several kinases have been shown to phosphorylate EBP50, including PKC, AKT, G protein-coupled kinase, Cdc2, and RSK1 (Fouassier et al., 2005; Hall et al., 1999; He et al., 2001; Li et al., 2007a; Lim and Jou, 2016; Raghuram et al., 2003; Song et al., 2015; Voltz et al., 2007). EBP50 phosphorylation within the ERM-binding domain or the PDZ2 domain can influence the EBP50 intramolecular interaction and binding to specific protein partners (Li et al., 2007a; Raghuram et al., 2003; Song et al., 2015). Phosphorylation within the PDZ1 domain was also shown to reduce EBP50 binding to target proteins (Voltz et al., 2007). Furthermore, phosphorylation of EBP50 can affect oligomerization (Fouassier et al., 2005; He et al., 2001; Lau and Hall, 2001; Shenolikar et al., 2001). In cultured cells, the expression of phosphomimetic and non-phosphorylated forms of EBP50 affected its localization at the plasma membrane (Chen et al., 2012; Voltz et al., 2007). In addition, phosphorylation of EBP50 can also regulate the cytoplasmic-to-nuclear trafficking of EBP50 (Lim and Jou, 2016). Thus, EBP50 binding activity, oligomeric state, and subcellular localization are regulated by phosphorylation.

1.2.3 Functional significance

EBP50 localizes to the apical membrane of epithelial cells in both human and rodent tissues (Fouassier et al., 2001; Georgescu et al., 2014; Ingraffea et al., 2002; Shenolikar et al., 2002; Stemmer-Rachamimov et al., 2001; Weinman et al., 1993). Analysis of mutant mice lacking EBP50 demonstrated that EBP50 was essential for stabilizing active phosphorylated ERM proteins at the apical plasma membrane of kidney and intestinal epithelial cells (Morales et al., 2004). Furthermore, structural defects in the intestinal microvilli were observed with the loss of EBP50, such that they resembled the intestinal microvilli of *ezrin* mutant mice (Morales et al., 2004; Saotome et al., 2004). In human JEG-3 cells, siRNA-mediated knockdown of EBP50 or the over-expression of an EBP50 construct lacking the ezrin binding region led to defects in microvilli formation (Garbett et al., 2010; Hanono et al., 2006). Thus, EBP50 acts as an essential scaffold protein for ERM-mediated

membrane organization. In mouse embryonic fibroblasts and intestinal epithelial cells, EBP50 was also shown to stabilize β-catenin at cell junctions and the apical brush border membrane, respectively (Kreimann et al., 2007). Furthermore, the loss of EBP50 from the apical plasma membrane disrupted epithelial morphology and cell junctions of Caco-2 cells (Hayashi et al., 2010), which normally form polarized monolayers with apical microvilli in culture (Simon-Assmann et al., 2007). Together, these studies support a role for EBP50 in maintaining epithelial integrity and organization. EBP50 has also been shown to bind to and regulate many other transmembrane proteins containing a PDZ-binding motif, including ion transporters (Short et al., 1998; Weinman et al., 1993), the PDGF receptor (Maudsley et al., 2000), G protein-coupled receptors (Hall et al., 1998; Li et al., 2002; Wheeler et al., 2007), and receptor tyrosine kinases (Lazar et al., 2004; Takahashi et al., 2006). Thus, EBP50 has essential functions in organizing multiprotein signaling complexes.

1.3 DISEASE RELEVANCE OF ERM PROTEINS, MERLIN, AND EBP50

Generally, the over-expression of the ERM proteins have been linked to cancer progression (Akisawa et al., 1999; Bartholow et al., 2011; Kobayashi et al., 2004). Increased ezrin expression levels were shown in a variety of invasive and metastatic cancers, including pancreatic carcinomas, osteosarcomas, and gliomas (Akisawa et al., 1999; Geiger et al., 2000; Khanna et al., 2001; Nestl et al., 2001; Tokunou et al., 2000; Wick et al., 2001). In a study that examined ezrin expression in over 5000 human cancers, it was found that enhanced ezrin expression was associated more with cancers of mesenchymal origin (Bruce et al., 2007). Analysis of human breast cancer cell lines revealed that total ezrin levels were not altered but ezrin localization to motile structures and the cytoplasm was associated with invasive breast cancer cell lines (Sarrio et al., 2006). Expression of ezrin and activated non-receptor tyrosine kinase c-Src disrupted cell adhesion and enhanced cell scattering, motility, and invasion in mouse mammary carcinoma cell lines (Elliott et al., 2005; Elliott et al., 2004). The over-expression of a truncated N-terminal domain of ezrin, which blocks hepatocyte growth factor-induced migration and morphogenesis of epithelial cells (Crepaldi et al., 1997), inhibited metastasis of mammary carcinoma cell lines (Elliott et al., 2005; Elliott et al., 2004). It was also shown that the shRNA-mediated knockdown of ezrin reduced the invasive potential of MDA-MB-231 breast cancer cells (Li et al., 2008). Furthermore, ezrin over-expression induced cell protrusions, anchorage-independent growth, cell motility, and invasiveness in a pancreatic cancer cell line, which were reversed by siRNA-mediated knockdown of ezrin (Meng et al., 2010). Thus, the over-expression and silencing of ezrin in cancer models demonstrate that ezrin is

necessary and sufficient for tumour metastasis. Radixin was also found to be over-expressed in high-grade prostate intraepithelial neoplasia, the proposed precursor lesion to prostate cancer (Bartholow et al., 2011; Bostwick et al., 1993; Pang et al., 2004). Similar to ezrin, radixin promoted cell motility in the PC3 prostate cancer cell line (Valderrama et al., 2012). In addition, increased expression levels and the subcellular localization of moesin have been linked to oral squamous cell carcinoma invasiveness and metastatic potential (Kobayashi et al., 2004). Moesin was shown to be essential for early colonization of melanoma cells in the lung and invasion of melanoma cells in 3D matrices (Estecha et al., 2009) and promoted the epithelial-to-mesenchymal transition in breast and pancreatic cancers (Abiatari et al., 2010; Haynes et al., 2011; Wang et al., 2012). Thus, increased ERM protein expression and activity have been implicated in tumourigenesis and metastasis in a wide variety of cancers.

Deletions or loss-of-function mutations in the *NF2* gene can lead to the development of the NF2 cancer syndrome, characterized by the presence of bilaterial vestibular schwannomas and other tumours associated with the central nervous system, including ependymomas and mengiomas (Evans et al., 1992; Rouleau et al., 1993; Trofatter et al., 1993). However, transcriptional inactivation by aberrant *NF2* promoter methylation was also observed in schwannomas or meningiomas (Gonzalez-Gomez et al., 2003; Kino et al., 2001; Lomas et al., 2005). Furthermore, in schwannomas and meningiomas lacking detectable *NF2* mutations, increased degradation of merlin by the calpain protease has also been demonstrated (Kimura et al., 1998). NF2 patients may also present with neuropathy due to compression from surrounding tumours or inactivation of merlin within the neurons (Schulz et al., 2013; Schulz et al., 2014; Sperfeld et al., 2002). Heterozygous *Nf2* mutant mice do not spontaneously develop schwannomas or meningiomas but lead to the development of multiple tumour types, including osteosarcomas and hepatocellular carcinomas (McClatchey et al., 1998). However, the Schwann cell- or arachnoidal cell-specific knockout of *Nf2* led to the formation of schwannomas and meningiomas, similar to the human tumours (Giovannini et al., 2000; Kalamarides et al., 2002). More recently, a genetically engineered NF2 mouse model was generated, which more closely recapitulated the human disease with the consistent development of vestibular schwannomas correlating with hearing loss and imbalance (Gehlhausen et al., 2015). *NF2* mutations have also been identified in 40% of malignant mesotheliomas (Baser et al., 2002; Cheng et al., 1999; Sekido et al., 1995; Thurneysen et al., 2009). Although, *NF2* mutations were found in other non-neuronal cancers including, breast, colorectal, and prostate cancers, mutational

analysis revealed a low incidence of *NF2* mutations in these common cancers (Yoo et al., 2012).

The over-expression of EBP50 has been found in various cancers (Cardone et al., 2007; Shibata et al., 2003; Song et al., 2007; Stemmer-Rachamimov et al., 2001), suggesting an oncogenic role in tumour progression. EBP50 over-expression in human breast tumour samples was associated with metastasis (Cardone et al., 2007). In hepatocellular carcinoma and colorectal cancer cell lines, increased EBP50 expression specifically enhanced β-catenin-mediated transcriptional activity (Shibata et al., 2003). Some studies have also suggested a tumour suppressive role for EBP50. Allelic loss of the gene encoding for EBP50 was frequently observed in breast and ovarian cancers (Dai et al., 2004; Kalikin et al., 1996; Orsetti et al., 1999; Plummer et al., 1997; Presneau et al., 2005; Radford et al., 1995). EBP50 interactions with β-catenin and PTEN have been shown to contribute to its tumour suppressor function (Kreimann et al., 2007; Takahashi et al., 2006). Furthermore, the loss of EBP50 in immortalized mouse embryonic fibroblasts promoted anchorage-independent growth and cell motility (Kreimann et al., 2007), supporting a tumour suppressive role in cancer progression. As the over-expression of EBP50 was shown to be cytoplasmic in cancer cells (Cardone et al., 2007; Shibata et al., 2003; Song et al., 2007; Stemmer-Rachamimov et al., 2001), it is proposed that cytoplasmic EBP50 acts as an oncogenic protein (Takahashi et al., 2006); whereas cortical EBP50 acts as a tumour suppressor (Kreimann et al., 2007). Thus, further understanding the functional significance of EBP50 subcellular localization and regulation during development may provide further insight into its role during cancer progression.

1.4 DROSOPHILA AS A MODEL ORGANISM

Drosophila melanogaster is a very powerful and versatile genetic model that can be used to study fundamental biological processes and pathways. The technical advantages to using Drosophila as a model organism, including short life cycle, the ability to generate large numbers of progeny, and the availability of a wide variety of genetic tools and reagents, make this an ideal time and cost-effective system to study development and disease (Hales et al., 2015). Comparisons of the human and Drosophila genomes revealed that approximately 75% of known human disease genes have highly similar counterparts in Drosophila (Reiter et al., 2001), further supporting the use of Drosophila as a relevant model for human disease.

Although distinct functions have been described among the ERM proteins (Bonilha et al., 1999; Lamb et al., 1997; Paglini et al., 1998), functional redundancies between these

proteins, revealed by the tissue-specific or subtle defects of individual mutant mice (Doi et al., 1999; Kikuchi et al., 2002; Saotome et al., 2004), remain a challenge to further elucidating ERM protein function in mammals. Thus, studies investigating the single Drosophila ERM orthologue can provide great insight into ERM protein function in development and disease. The single Drosophila ERM orthologue was found to be 58% identical to both human moesin and human ezrin, and was referred to as DMoesin (hereafter referred to as Moesin) due to the absence of a polyproline tract, which is present in both human ezrin and radixin (Figure 1-1) (McCartney and Fehon, 1996). Drosophila Moesin partially co-localized with actin in the microvilli of embryos during cellularization and was also found at the apical surface of polarized tissues (McCartney and Fehon, 1996), consistent with ERM protein localization in mammalian cells and tissues. The loss of Moesin in Drosophila results in larval lethality, suggesting that Moesin is required for Drosophila development (Speck et al., 2003). Similar to the ERM proteins, several studies reveal a structural role for Drosophila Moesin in maintaining cell integrity and epithelial organization (Carreno et al., 2008; Jankovics et al., 2002; Karagiosis and Ready, 2004; Kunda et al., 2008; Polesello et al., 2002; Speck et al., 2003). The critical phosphorylation residue at the C-terminus of the ERM proteins is also conserved in Drosophila and corresponds to the threonine residue at amino acid position 559 (McCartney and Fehon, 1996). *Moesin* mutants were rescued to viability by the ubiquitous expression of the phosphomimetic form of Moesin (Moesin^{T559D}), whereas the non-phosphorylated form of Moesin (Moesin^{T559A}) did not rescue the mutant (Speck et al., 2003). These findings confirm that phosphorylation of the conserved threonine residue is also essential for Moesin function in Drosophila. Several studies have shown that the Sterile20-like kinase, Slik, regulates Moesin phosphorylation (Carreno et al., 2008; Hipfner et al., 2004; Hughes and Fehon, 2006; Kunda et al., 2008). Furthermore, the Drosophila orthologue of EBP50 was identified as Sip1, which also functions as a scaffold protein in Moesin-mediated epithelial integrity (Hughes et al., 2010).

The Drosophila Merlin orthologue shares 55% identity with human merlin (McCartney and Fehon, 1996). Human *NF2* was able to functionally replace a *Merlin* null mutant allele in Drosophila, strongly suggesting that there is functional conservation between mammals and Drosophila (Gavilan et al., 2014). Although, Drosophila Moesin and Merlin were both found in embryonic and larval tissues, the subcellular localization within these tissues were distinct (McCartney and Fehon, 1996). Merlin was found in punctate structures associated with the plasma membrane and cytoplasm, whereas Moesin associated more with the plasma membrane within Drosophila cell culture and tissues (McCartney and Fehon, 1996). Both mammalian and Drosophila Merlin associate with the plasma membrane and punctate

cytoplasmic structures of cells (Kissil et al., 2002; McCartney and Fehon, 1996; Scherer and Gutmann, 1996; Schmucker et al., 1997). Mammalian studies have shown that multiple phosphorylation states exist for merlin (Shaw et al., 1998b; Shaw et al., 2001). Similarly, Drosophila Merlin was shown to migrate as multiple forms and λ phosphatase treatment resulted in a single, faster migrating band via western blot analysis, suggesting that Drosophila Merlin is also phosphorylated (Hughes and Fehon, 2006) The critical threonine residue of Drosophila Moesin is conserved in Drosophila Merlin at amino acid position 616 (McCartney and Fehon, 1996). When the phosphomimetic form of Merlin ($Merlin^{T616D}$) was expressed in Drosophila cell culture, the slower migrating band was enhanced, relative to the expression of the non-phosphorylated form of Merlin ($Merlin^{T616A}$), thus the threonine 616 residue of Merlin is phosphorylated in Drosophila (Hughes and Fehon, 2006). Similar to mammalian studies, Drosophila Merlin has been implicated in growth inhibition through the regulation of multiple signaling pathways, including the Hippo, Notch, and EGFR pathways (Hamaratoglu et al., 2006; LaJeunesse et al., 1998; LaJeunesse et al., 2001; McCartney et al., 2000).

1.5 THESIS OVERVIEW

This thesis addresses how the FERM domain proteins, Merlin and Moesin, and their interacting partners function in Drosophila. A variety of Drosophila cells and tissues were used in this work, including the wing and follicle cell epithelium, neuroepithelial cells in the optic lobe, and central brain neuroblasts, which all share the ability to establish polarity or adhesion. Investigating Merlin and Moesin function in this context provides insight into their roles in regulating cell or tissue organization during development.

Chapter 2 describes the **characterization of a Merlin and Sip1 interaction region in Drosophila cell culture and epithelial tissues**. The relatively uncharacterized α-helical domain of Merlin was shown to be important for Sip1 binding. The Merlin and Sip1 interaction regulates the growth suppressive function of Merlin in Drosophila adult wings and the maintenance of epithelial organization in the follicle cells surrounding the developing oocyte. We propose that Sip1 influences Merlin activity by facilitating the dephosphorylation and activation of Merlin. Thus, this work reveals Sip1 as an important interacting partner and regulator of Merlin function in Drosophila.

Chapter 3 describes the **investigation of Merlin and Sip1 function in the developing optic lobes of the larval brain**. This work was done to further investigate the functional significance of Merlin and Sip1 in a neuronal context. Merlin and Sip1 localizes to the neuroepithelial cells and neuroblasts within the larval optic lobe. The loss of Merlin and Sip1 function impairs optic lobe development, suggesting potential roles in regulating neuroepithelial cell proliferation or differentiation. However, further work is required to determine the mechanisms underlying the role of Merlin and Sip1 during optic lobe development.

Chapter 4 describes the **investigation of Sip1 and Moesin in the central brain neuroblasts of the larval brain**. Sip1 localizes to the cytoplasm of central brain neuroblasts and the loss of Sip1 function appears to alter neuroblast self-renewal and differentiation. The precise mechanisms underlying the role of Sip1 in the neuroblasts still remain unknown. Moesin localizes to the cortex of neuroblasts, where is it apically enriched during asymmetric cell division. This asymmetric and dynamic distribution of Moesin is important for polarity maintenance and cortical remodelling of dividing neuroblasts.

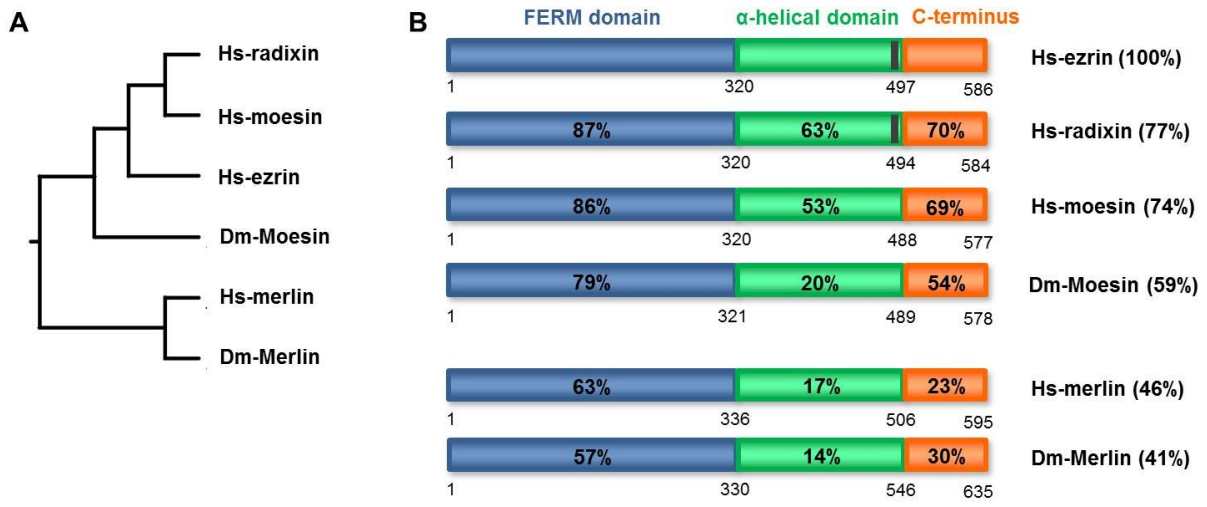

Figure 1-1: Sequence comparisons and schematic representation of the ERM and merlin proteins in *Homo sapiens* and *Drosophila melanogaster*. (A) Phylogenetic analysis of human ezrin (Hs-ezrin), human radixin (Hs-radixin), human moesin (Hs-moesin), Drosophila Moesin (Dm-Moesin), human merlin (Hs-merlin), and Drosophila Merlin (Dm-Merlin). The phylogenetic tree was constructed using the UPGMA method and web-based version of CLUSTALW. (B) The sequence comparisons to human ezrin (Hs-ezrin) are shown for human radixin (Hs-radixin), human moesin (Hs-moesin), Drosophila Moesin (Dm-Moesin), human merlin (Hs-merlin), and Drosophila Merlin (Dm-Merlin). The ERM proteins and merlin consist of a FERM domain (blue), an α-helical domain (green), and C-terminal domain (orange), with amino acid positions indicated below the schematic protein structures. The polyproline tract in human ezrin and radixin are shown in the α-helical domain. The overall sequence identity is indicated following the protein name and the sequence similarity of the specific domains are shown. This figure was generated using the following accession numbers: Hs-ezrin: P15311; Hs-radixin: P35241; Hs-moesin: P26038; Dm-Moesin: P46150; Hs-merlin: P35240; Dm-Merlin: Q24564. Figure adapted from (Bretscher et al., 2000).

Chapter 2: Characterization of Merlin and Sip1 interaction

2.1 INTRODUCTION

Human merlin has been shown to interact with the scaffold protein EBP50 (Murthy et al., 1998; Nguyen et al., 2001). Mammalian cell culture studies demonstrated that merlin associates with and negatively regulates EGFR signaling by sequestering EGFR into a membrane compartment, preventing it from signaling and being internalized (Curto et al., 2007). This interaction is EBP50-dependent as reduced EBP50 expression abolished the association of merlin and EGFR (Curto et al., 2007). Even though there is biochemical evidence suggesting merlin and EBP50 interactions, the functional significance of this interaction remains unclear. Thus, we used Drosophila as model to further examine the interaction between Merlin and Sip1, the Drosophila orthologue of EBP50.

Previously, it was shown that, upon induction, wild-type Merlin was initially associated with the plasma membrane but over time, Merlin localized to punctate cytoplasmic structures in Drosophila Schneider 2 (S2) cells (McCartney and Fehon, 1996). Using this pulse-trafficking assay, multiple studies have examined how the expression of various domains within Merlin and interacting proteins alter Merlin subcellular localization and trafficking (Bensenor et al., 2010; Hughes and Fehon, 2006; LaJeunesse et al., 1998; McCartney and Fehon, 1996). It was found that the phosphomimetic form of Merlin remained at the plasma membrane for an extended period of time; whereas the non-phosphorylated form of Merlin traffics away from the plasma membrane faster than wild-type Merlin (Hughes and Fehon, 2006). Furthermore, the Sterile20-like kinase, Slik, has been proposed to regulate Merlin phosphorylation and expression of Slik in pulse-trafficking assays resulted in slower Merlin trafficking in S2 cells, similar to the expression of the phosphomimetic form of Merlin (Hughes and Fehon, 2006). These findings suggest that Merlin localization and trafficking are linked to the phosphorylation status of Merlin.

Multiple studies have also used Drosophila adult wings and imaginal disc epithelium to examine Merlin function in growth suppression and epithelial organization (Hughes and Fehon, 2006; LaJeunesse et al., 1998; LaJeunesse et al., 2001; Maitra et al., 2006). The expression of a dominant negative form of Merlin resulted in an increase in adult wing area (LaJeunesse et al., 1998), which is observed when mutations led to increased cell proliferation in the wing (Boedigheimer and Laughon, 1993; Bryant et al., 1993; Mahoney et al., 1991). Genetic studies suggested that *Merlin* genetically interacts with components of signaling pathways to regulate cell proliferation during wing epithelial development (LaJeunesse et al., 2001). Indeed, Merlin and the Protein 4.1 superfamily member, Expanded, were shown to function together in receptor localization at the cell surface and endocytic trafficking in wing epithelial tissue (Maitra et al., 2006). Merlin and Expanded

were also shown to regulate localization of apical polarity complexes in wing imaginal discs (Hamaratoglu et al., 2009). Furthermore, the expression of a phosphomimetic and non-phosphorylated form of Merlin resulted in defects in epithelial integrity in the wing imaginal discs (Yang et al., 2012). Thus, Merlin phosphorylation and activity are important for inhibiting tissue growth and maintaining epithelial organization in the Drosophila adult wings and imaginal disc epithelium.

The follicle cells surrounding the developing oocyte is another system used in Drosophila to study aspects of proliferation, polarity, and adhesion during epithelial patterning and morphogenesis (Figure 2-1). The follicle cells proliferate during early stages of oogenesis (Margolis and Spradling, 1995) and then stop dividing and undergo endoreplication from stages 7-9 (Deng et al., 2001; Lopez-Schier and St Johnston, 2001). The follicle cells are also patterned along the anterior-posterior and dorsal-ventral axes of the developing egg chamber (Gonzalez-Reyes et al., 1995; Roth et al., 1995). In addition, junctional complexes, such as adherens, gap, and septate junctions, connect the follicle cell epithelium (Mahowald, 1972). The ability to generate mosaic clones within the follicle cells allow for relatively easy genetic manipulation and analysis of factors essential for epithelial tissues (Duffy et al., 1998). Previously, Merlin was found to be apically localized in follicle cells (McCartney and Fehon, 1996) and was required in the most posterior follicle cells for axis specification during oogenesis (MacDougall et al., 2001). Furthermore, Sip1 was shown to regulate Moesin phosphorylation and epithelial integrity in the follicle cells (Hughes et al., 2010), however it is not known whether Merlin and Sip1 function together in maintaining epithelial organization. Thus, we utilized Drosophila cell culture and epithelial tissues, including the adult wings and follicle cell epithelium, to examine the functional significance of the Merlin and Sip1 interaction.

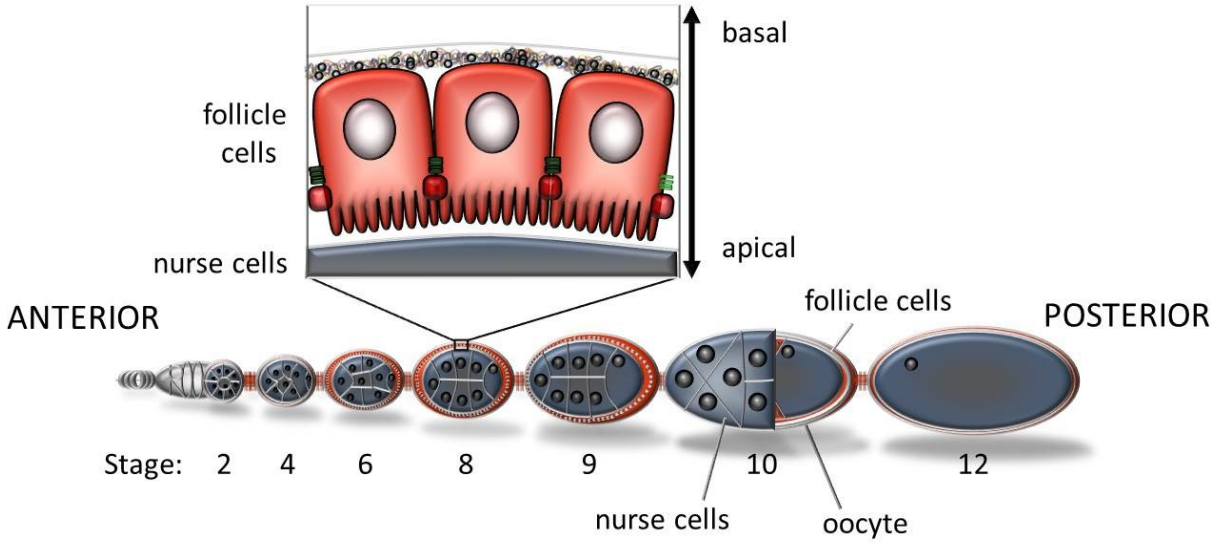

Figure 2-1: Drosophila oogenesis and the follicle cell epithelium. The schematic shown here is a single ovariole consisting of a chain of developing egg chambers at the indicated stages (2-12). The youngest egg chambers are found at the anterior end of the ovariole and progressively older egg chambers are found more posteriorly. Follicle cells (red) surround the developing oocyte/nurse cells (blue), with a magnified view of the follicle cells shown. The follicle cells are oriented such that the apical surfaces make contact with the oocyte/nurse cells and the basal surfaces contact the basement membrane. Junctional complexes also form in between the follicle cells. Figure provided by Andrew J. Simmonds, with permission.

2.2 MATERIALS AND METHODS

2.2.1 Fly strains and genetics

All stocks were raised on standard Bloomington media at 25°C. All stocks including *patched* (*ptc*)-GAL4 and *actin-GAL4* were obtained from the Bloomington stock center. 42D FRT *Sip1*^{06373}/CyO was obtained from R. Fehon (Hughes et al., 2010). The 19A FRT MARCM line was obtained from Celeste Berg. For generation of Merlin arginine mutant transgenic lines, the confirmed inserts in pENTR/D were cloned into MYC-tagged UAS vectors (Drosophila Gateway vectors) and multiple independent lines were generated (BestGene, CA).

2.2.2 Wing measurements

The following crosses were set up for wing size analysis: *w*^{1118}, *UAS-MYC-Merlin*^{WT}, *UAS-MYC-Merlin*^{T616D}, *UAS-MYC-Merlin*^{T616A}, *UAS-MYC-Merlin*^{R325A}, *UAS-MYC-Merlin*^{R335L}, and *UAS-MYC-Merlin*$^{R325A\ R335L}$ were crossed to *ptc-GAL4*. For the rescue experiments, *UAS-MYC-Merlin*^{T616A} was combined *UAS-MYC-Merlin*^{WT}, *UAS-MYC-Merlin*^{R325A}, *UAS-MYC-Merlin*^{R335L}, and *UAS-MYC-Merlin*$^{R325A\ R335L}$ and crossed to *ptc-GAL4.* Adult wings from the male progeny were prepared and measured as described previously (Yang et al., 2012). The area of the *patched* region (between wing veins L3 and L4) of at least 84 wings over three biological replicates were measured.

2.2.3 Scanning electron microscopy

Adult fly heads were collected and prepared for SEM using the hexamethyldisilazane (HMDS) method (Li et al., 2013) and imaged using a Philips/FEI (XL30) Scanning Electron Microscope (Philips, Hillsboro, OR) at the Advanced Microscopy Facility of the Department of Biological Sciences, University of Alberta.

2.2.4 Immunofluorescence

Larval/pupal wing tissues were dissected in 1X PBS and fixed in 4% paraformaldehyde for 20 min. Dissected tissues were rinsed at least 5 times in 1X PBS and blocked in 0.1% Triton X-100, and 1% normal donkey serum in 1X PBS (PTN) for at least 1 hr at room temperature (RT). Primary antibodies in PTN were incubated overnight at 4°C. Tissues were rinsed/washed for at least 1 hr in PTN at RT. Secondary antibodies in PTN were incubated for 2-4 hours at RT and rinsed/washed for at least 2 hours in PTN at RT. Tissues were incubated in DAPI (1:10 000) for 10 min and rinsed at least 3 times in PTN and at least 3 times in 1X PBS prior to mounting in ProLong® Gold Antifade Reagent (Invitrogen). Primary antibodies used were: guinea pig anti-Merlin (1:1000), rabbit anti-c-MYC (1:500; Sigma),

rat anti-DE-Cadherin (1:200; Developmental Studies Hybridoma Bank, DSHB), rabbit anti-Phospho-histone H3 (1:2000; Millipore #06-570), Phalloidin Alexa Fluor 546 (1:1000; Invitrogen), Phalloidin Alexa Fluor 488 (1:1000; Invitrogen). Secondary antibodies used were: Donkey anti-Rabbit, -Mouse, -Guinea pig, and -Rat Alexa Fluor® 488/555/647 (Abcam). Imaging was performed using a Zeiss LSM 700 confocal microscope using a 40× NA 1.3 oil immersion objective (EC Plan-Neofluar; Zeiss), and 63× NA 1.4 oil immersion objective (Plan-Apochromat; Zeiss). Acquisition software used was Zen 2009. Adobe Photoshop and Illustrator were used to generate figures.

2.2.5 Drosophila S2R+ cell transfections

Transfections were carried out as previously described (Yang et al., 2012) using the DDAB (dimethyldiocta-decyl ammonium bromide; Sigma Aldrich) transfection reagent and Hyclone Serum free SFX insect cell culture medium (ThermoScientific). For pulse-trafficking assays, the transfection mix was then added dropwise into 3 ml of $S2R^+$ cells (10^6 cells per ml) in a six well plate and were then incubated for 48 hours at 25°C. S2 cell lines stably expressing HS-MYC-$Merlin^{WT}$, HS-MYC-$Merlin^{T616A}$ and HS-MYC-$Merlin^{T616D}$ were established using DDAB transfection reagent and the Invitrogen *Drosophila* expression protocol with hygromycin B as a selection agent. S2 cell lines were co-transfected with Actin5c-Flag-Sip1 and one of the expression plasmids HS-HA-Merlin, HS-HA-$Merlin^{325A}$, HS-HA-$Merlin^{335L}$ or HS-HA-$Merlin^{325A335L}$ for co-immunoprecipitation.

2.2.6 Pulse-trafficking experiments

Pulse-trafficking experiments were performed as previously described (Hughes and Fehon, 2006). Transfected cells were induced by heat shock at 37°C for 30 minutes and cells were collected and fixed in 2% PF for 10 min at 1 hour, 3 hour and 6 hour post-heat shock. HA-tagged constructs were detected using mouse anti-HA at 1:500 (Sigma-Aldrich) and mouse secondary antibody (raised in donkey) conjugated to Alexa 488 (Invitrogen). A minimum of 100 transfected cells were counted for each time point and three experimental replicates were averaged. Statistical analysis was performed using Student's t-test.

2.2.7 Somatic mosaic analysis

Animals of the genotype *Mer^4* neoFRT19A/FM7YFP; *UAS-MYC-$Merlin^{WT}$* or *UAS-MYC-$Merlin^{R325A\ R335L}$*/CyOYFP were crossed to the 19A FRT MARCM line (*hsFLP, TubPGAL80, 19A FRT*;;*TubPGAL4, UAS-MCD8-GFP/MKRS*) and were heat shocked for 1 hr at 37°C, 1 hr at 25°C, 1 hr at 37°C at 40-48 hrs after egg laying and were dissected 4 days after eclosion or adults of 2 days of age were heat shocked in the same way and dissected 4 days later.

Ovaries were dissected and fixed as described in (Hughes et al., 2010). Primary antibodies were used as follows: DE-Cadherin (1:200; DSHB), DAPI, and secondary Donkey anti-Rat Alexa 647 antibodies at 1:2000. Images were taken on a Zeiss 700 confocal microscope, 40X NA 1.4 lens and figures prepared using Adobe Photoshop Adobe Illustrator. No alteration to the images was carried out.

2.3 RESULTS

2.3.1 Genetic interaction between Merlin and Sip1

To test the genetic interaction between *Merlin* and *Sip1*, I examined whether the loss of Sip1 modified the phenotypes observed with a *Merlin* hypomorphic allele, Mer^3 (Fehon et al., 1997; LaJeunesse et al., 1998). Mer^3 flies carry a missense mutation of Methionine 177 to Isoleucine resulting in a semi-viable phenotype, with hemizygous males exhibiting smaller rough eyes and abnormal head cuticle at the ventral region of the eye (LaJeunesse et al., 2001; McCartney et al., 2000). Thus, I examined whether the loss of one copy of the *Sip1* mutant allele, $Sip1^{06373}$ (Hughes et al., 2010; Spradling et al., 1999), modified the Mer^3 mutant eye phenotype using scanning electron microscopy. In 28.33% of Mer^3 adult males, the eyes appeared similar to w^{1118} controls (*n*=60 males; Figure 2-2, A-A'). However, the majority of Mer^3 adult male eyes appeared smaller, with a narrowed ventral region and disorganized bristle formation between the individual ommatidia (60%, *n*=60 males; Figure 2-2, B-B'). In a small proportion of the Mer^3 adult males, the eye phenotype was more severe as multiple bristles formed between the individual ommatidia and the ventral region of the eye was dramatically disrupted with abnormal growth (3.33%, *n*=60 males; Figure 2-2, C-C'). The remaining Mer^3 adults males displayed an intermediate eye phenotype (8.33%, *n*=60 males). These eye defects were partially rescued with the loss of one copy of *Sip1* in a Mer^3 mutant background (Mer^3/Y; $Sip1^{06373}$/+). I found that 48% of the Mer^3/Y; $Sip1^{06373}$/+ adult males eyes were similar to controls, with 46% displaying minimal ventral narrowing and more regular bristle formation (*n*=35 males; Figure 2-2, D-D'). I did not observe any Mer^3/Y; $Sip1^{06373}$/+ adult males exhibiting the severe eye phenotypes present in the Mer^3 alone (Figure 2-2, C-C'). The remaining adult males (6%, *n*=35 males) exhibited the intermediate phenotype, with abnormal growth in the most ventral region of the eye and some irregular bristle formation (Figure 2-2, E-E'). Thus, the loss of one copy of *Sip1* suppresses the *Merlin* mutant phenotype, consistent with a genetic interaction between *Merlin* and *Sip1.*

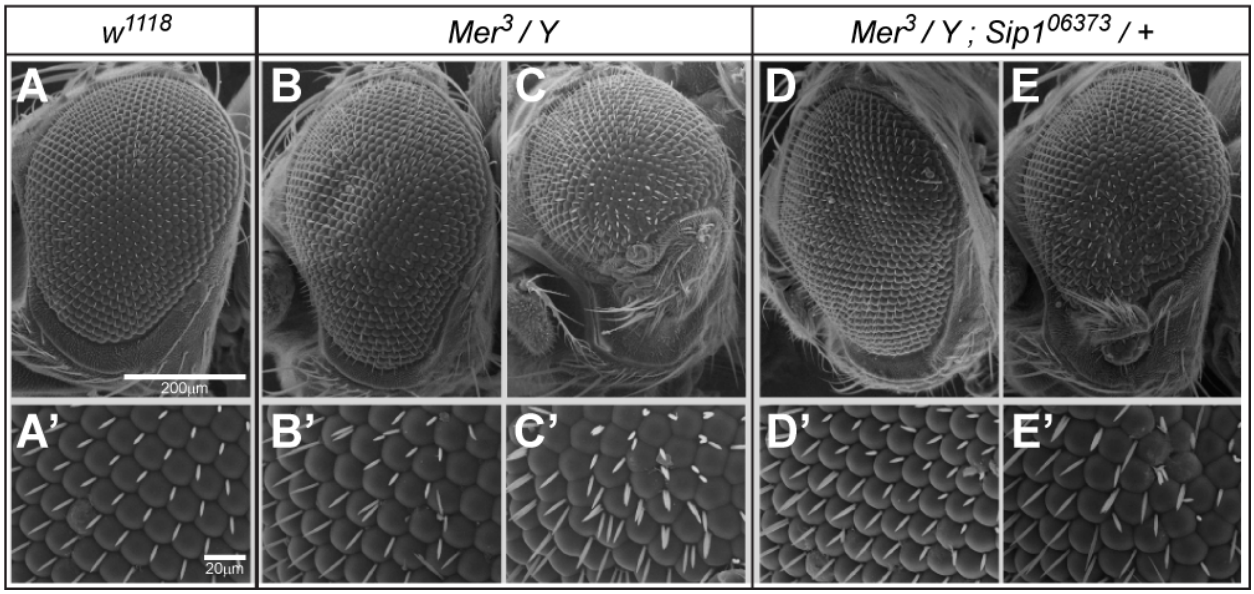

Figure 2-2: *Merlin* and *Sip1* genetically interact. Scanning electron microscopy images of representative (A) w^{1118}, (B-C) Mer^3, and (D-E) Mer^3/Y; $Sip1^{06373}$/+ male adult eyes, with corresponding zoomed images displaying the ommatidia and sensory bristles (A'-E'). (B-B') The majority (60%, *n*=60) of Mer^3 male progeny displayed ventral narrowing and irregular bristle formation. (C-C') A small proportion (3.33%, *n*=60) of Mer^3 males showed abnormal growth in the ventral region of the eye, with (C') multiple bristles forming between the ommatidia, when compared to controls (A-A'). (D-D') The loss of one copy of *Sip1* in a Mer^3 mutant background, resulted in the majority (48%, *n*=35) of the male progeny displaying normal eye development with minor ventral narrowing. (E-E') A small proportion (6%, *n*=35) of Mer^3/Y; $Sip1^{06373}$/+ adult males displayed abnormal growth in the ventral region of the eye. Scale bars in (A-E) 200 µm and (A'-E') 20 µm. Figure obtained from (Abeysundara et al., 2014), with permission.

2.3.2 Identification of Merlin and Sip1 interaction region

To identify the potential regions essential for Merlin and Sip1 interaction, full-length and fragments of ^{35}S radiolabelled Merlin protein, as outlined in (Figure 2-3, A), were incubated with GST-tagged full-length Sip1 protein coupled to glutathione sepharose beads in GST pull-down assays, performed by Albert C. Leung (Abeysundara et al., 2014). It was found that ^{35}S radiolabelled full-length Merlin interacted with full-length Sip1 (GST-Sip1) (Figure 2-3, B). In addition, the FERM domain of Merlin (Merlin^{FERM}) and the C-terminal tail of Merlin (Merlin $^{CC\ Tail}$) bound to GST-Sip1 (Figure 2-3, B). There appeared to be a small amount of non-specific binding of the Merlin protein fragments to GST alone, yet the amount of binding of full-length Merlin, Merlin^{FERM}, or Merlin$^{CC\ Tail}$ to GST-Sip1 increased above background levels, suggesting a specific interaction. When the FERM domain of Merlin was further subdivided, the Merlin^{F1} and Merlin^{F2} subdomains bound to GST-Sip1, whereas the F3 subdomain of Merlin (Merlin^{F3}) did not bind to GST-Sip1 (Figure 2-3, B). A protein consisting of 100 amino acids immediately downstream of the FERM domain of Merlin (Merlin$^{306-405}$) interacted with GST-Sip1 (Figure 2-3, B). However, proteins corresponding to amino acids past residue 405 (Merlin$^{406-480}$, Merlin$^{481-635}$) did not bind GST-Sip1 protein (Figure 2-3, B). Furthermore, when region 306-405 was subdivided into 50 amino acid regions (Merlin$^{306-355}$, Merlin$^{330-380}$ Merlin$^{356-405}$), these Merlin fragments did not bind GST-Sip1, suggesting that the complete 100 amino acid region is essential for Sip1 binding (Figure 2-3, B). Interestingly, amino acids 313-359 of human merlin, which correspond to a part of this 100 amino acid region of Drosophila Merlin, were not included in an *in vitro* analysis of the interactions between merlin and EBP50 (Nguyen et al., 2001). Thus, the significance of this region of merlin interacting with EBP50 is not known.

To identify which amino acids within 306-405 of Drosophila Merlin were involved in Sip1 binding, Merlin constructs carrying smaller deletions within amino acids 306-405 were generated (Figure 2-4, A). Deletion of the entire 100 amino acid region (Merlin$^{\Delta 306-405}$) reduced binding of GST-Sip1 to background levels (Figure 2-4, B), confirming that this region of Merlin is important for Sip1 binding. Furthermore, smaller deletions of 50 amino acids of Merlin (Merlin$^{\Delta 306-355}$ and Merlin$^{\Delta 330-380}$) displayed reduced binding to GST-Sip1 (Figure 2-4, B). However, deletion of amino acids 356-405 had no effect on GST-Sip1 binding as binding was similar to that observed for full length Merlin (Figure 2-4, B). These findings suggest that amino acids 306-355 of Merlin are important for Sip1 binding.

Protein alignment of amino acids 305-355 of Drosophila Merlin against different species revealed two conserved arginine residues (Figure 2-5, A). These arginine residues present in Merlin were not conserved in either human or Drosophila Moesin (Figure 2-5, A).

To investigate whether these two arginine residues were important for Merlin binding to Sip1, the arginine residues were substituted to the corresponding residues found in Drosophila Moesin, using site-directed mutagenesis. Three Merlin arginine mutant constructs were created: a construct carrying an arginine to alanine substitution at amino acid position 325 (R325A), another with an arginine to leucine substitution at amino acid position 335 (R335L), and the third construct containing both substitutions (R325A R335L). Using GST pull-down assays, Merlin^{R325A}, Merlin^{R335L}, and Merlin$^{R325A\ R335L}$ proteins displayed reduced binding to GST-Sip1, when compared to GST-alone and full-length Merlin (Figure 2-5, B), suggesting that these Merlin arginine residues are important for Sip1 binding.

For the Materials and Methods of this section, please refer to (Abeysundara et al., 2014).

A

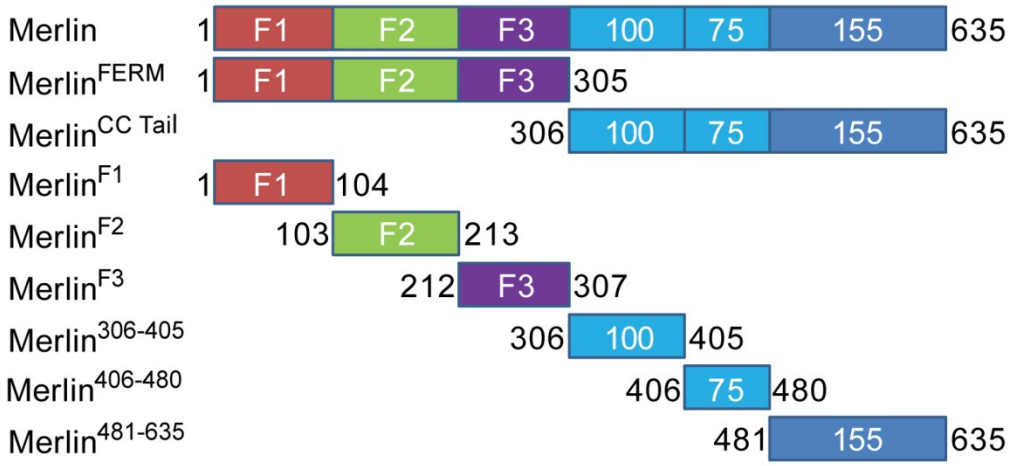
Merlin
1
F1
F2
F3
100
75
155
635
Merlin^FERM
1
F1
F2
F3
305
Merlin^CC Tail
306
100
75
155
635
Merlin^F1
1
F1
104
Merlin^F2
103
F2
213
Merlin^F3
212
F3
307
Merlin^306-405
306
100
405
Merlin^406-480
406
75
480
Merlin^481-635
481
155
635

B

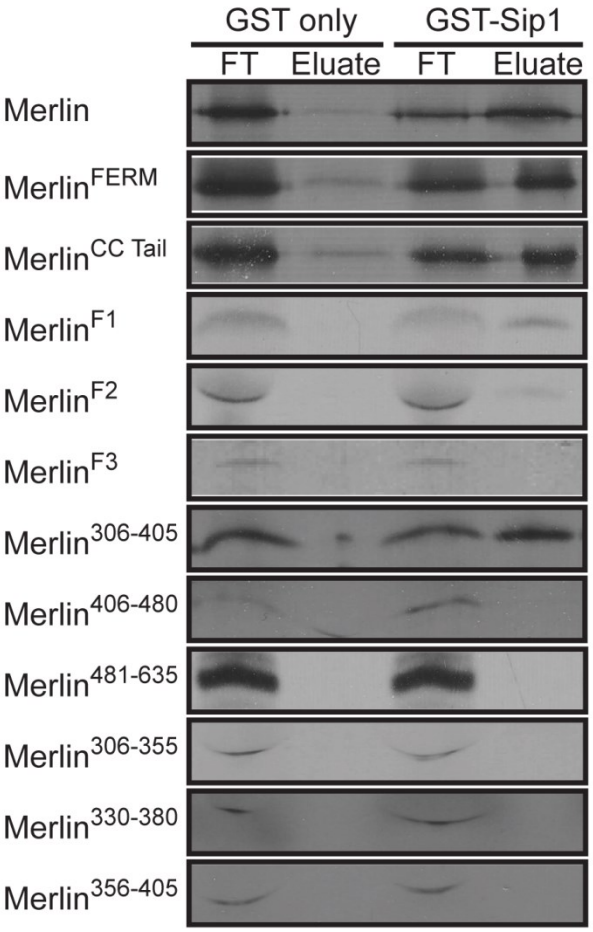
GST only
GST-Sip1
FT
Eluate
FT
Eluate
Merlin
Merlin^FERM
Merlin^CC Tail
Merlin^F1
Merlin^F2
Merlin^F3
Merlin^306-405
Merlin^406-480
Merlin^481-635
Merlin^306-355
Merlin^330-380
Merlin^356-405

Figure 2-3: Identification of regions of Merlin binding to Sip1 using *in vitro* GST pull-down assays. (A) Schematic representation of the Merlin protein constructs used in the mapping of specific interaction domains. The indicated amino acid positions are included in each construct in relation to the full-length protein. (B) GST pull-downs of each Merlin construct with GST-Sip1 construct and GST beads alone, which were used as the control for background levels of binding. Full-length Merlin, the FERM domain, and C-terminal domain bound to GST-Sip1. When the FERM domain was divided into subdomains, Merlin F1 and F2 showed binding to GST-Sip1, but Merlin F3 did not. Within the C-terminal domain of Merlin, only Merlin$^{306\text{-}405}$ showed binding to GST-Sip1. FT = Flow through. Experiments conducted and data analyzed by Albert C. Leung. Figure adapted from (Abeysundara et al., 2014), with permission.

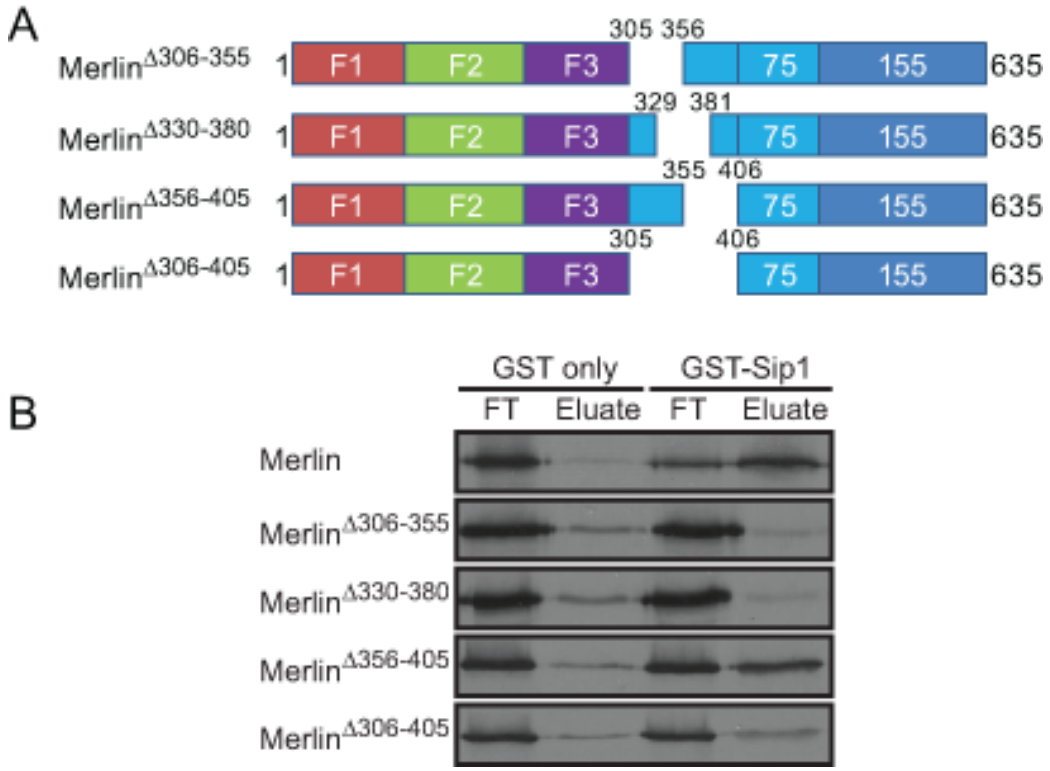

Figure 2-4: Determining the minimal Merlin domain essential for binding to Sip1 using *in vitro* GST pull-down assays. (A) Schematic representation of overlapping deletion constructs within the 100 amino acid region (305-406) of Merlin. (B) GST pull-downs of full-length Merlin and each of the deletions. Deletion of the entire 100 amino acid region or deletion of 306-355 or 330-380 had reduced binding to Sip1. Deletion of 356-405 was able to bind Sip1. Experiments conducted and data analyzed by Albert C. Leung. Figure obtained from (Abeysundara et al., 2014), with permission.

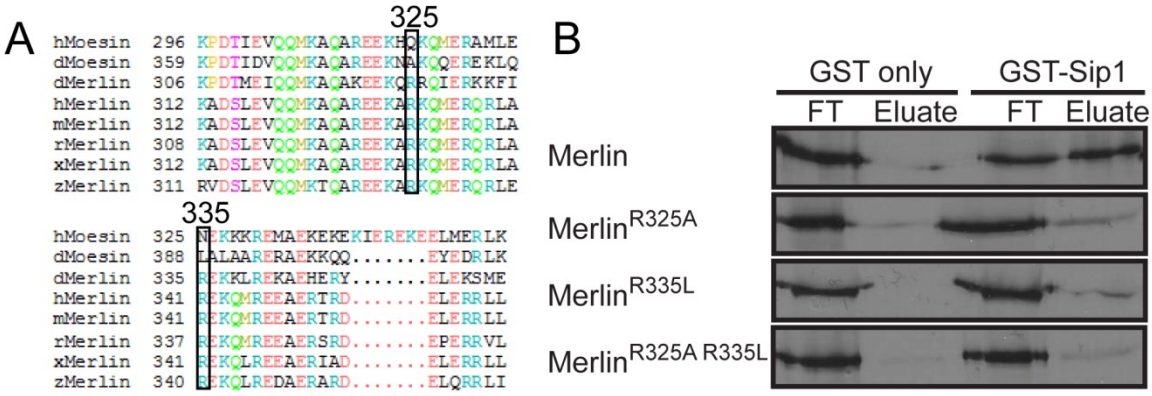

Figure 2-5: Conserved arginine residues in Merlin are important for binding to Sip1. (A) An alignment of the amino acids around the conserved arginine residues including human (h), and Drosophila (d) Moesin, and human (h), Drosophila (d), mouse (m), rat (r), Xenopus (x) and zebrafish (z) Merlin. The arginine residues at Drosophila residue 325 and 335 were conserved in all species, but were not conserved in either human or Drosophila Moesin. (B) GST pull-down assays of Merlin proteins with the conserved arginine residues mutated to the corresponding residues found in Drosophila Moesin. Full-length Merlin was present in the eluate of GST-Sip1 but not the GST-only control. The amount of binding observed for Merlin^{R325A}, Merlin^{R335L} was reduced as compared to full-length Merlin. Merlin$^{R325A\ R335L}$ showed the greatest reduction in binding to Sip1. Experiments conducted and data analyzed by Albert C. Leung. Figure adapted from (Abeysundara et al., 2014), with permission.

2.3.3 Functional significance of Merlin and Sip1 interaction region

Previously, it was shown that Merlin localization and trafficking were linked to the phosphorylation status of Merlin (Hughes and Fehon, 2006). To determine whether Sip1 binding was important for Merlin trafficking, I performed pulse-trafficking assays on heat shock-inducible HA-tagged Merlin (hs-Merlin^{WT}) and Merlin arginine mutants (hs-Mer^{R325A}, hs-Mer^{R335L}, and hs-Mer$^{R325A\ R335L}$) expressed in S2R^{+} cells. Similar to previous results (Hughes and Fehon, 2006; McCartney and Fehon, 1996), wild-type Merlin initially localized to the plasma membrane, with some cytoplasmic structures (phenotypes A-B) at 1 hour post-induction (Figure 2-6, E). Over time, wild-type Merlin trafficked off the plasma membrane and localized primarily to large cytoplasmic structures (phenotype D) in the majority of S2R^{+} cells at 6 hours post-induction (Figure 2-6, E). However, trafficking of Merlin^{R335L} and Merlin$^{R325A\ R335L}$ arginine mutants appeared to be delayed at 6 hours post-induction, when compared to wild-type Merlin (Figure 2-6, G-H). At 6 hours post-induction, there were a smaller proportion of cells displaying phenotype D in the Merlin^{R335L} and Merlin$^{R325A\ R335L}$ expressing cells, with an increase in the proportion of cells displaying phenotype B (Figure 2-6, G-H). Thus, Merlin binding to Sip1 appears to be important for Merlin subcellular trafficking in Drosophila S2R^{+} cells. Interestingly, this delay in trafficking is similar but not as severe as the inactive, phosphomimetic form of Merlin (Hughes and Fehon, 2006), suggesting that binding between Merlin and Sip1 may be important for Merlin localization and activity.

To determine whether Merlin and Sip1 binding influences Merlin localization *in vivo*, the localization of the MYC-tagged Merlin arginine mutant (*MYC-Mer$^{R325A\ R335L}$*) was analyzed and compared to MYC-tagged wild-type Merlin (*MYC-Mer^{WT}*), the active/non-phosphorylated form of Merlin (*MYC-Mer^{T616A}*), and the inactive/phosphomimetic form of Merlin (*MYC-Mer^{T616D}*) expressed in the anterior/posterior (A/P) boundary of the wing imaginal disc using *patched* (*ptc)-GAL4* (Capdevila and Guerrero, 1994). I found that wild-type Merlin localized near the plasma membrane of the epithelial cells within the *patched* region of the wing imaginal disc (Figure 2-7, A-D). The active form of Merlin, Mer^{T616A}, primarily localized to punctate structures near the plasma membrane (Figure 2-7, E-H); whereas the inactive form Merlin^{T616D} localized to the cytoplasm and some punctate structures (Figure 2-7, I-L). However, Mer$^{R325A\ R335L}$ appeared largely cytoplasmic and was not as concentrated near the plasma membrane (Figure 2-7, M-P). Thus, the Merlin arginine mutant may not completely function as an inactive form of Merlin as they display different localization patterns.

Previously, *Merlin* hypomorphic mutant adult wings and the expression of a dominant negative form of Merlin in the posterior half of the wing resulted in an increase in the wing

area, compared to the expression of wild-type Merlin (LaJeunesse et al., 1998). Thus, the growth suppressive function of Merlin can be readily examined in the adult wings and reducing or disrupting Merlin function leads to tissue overgrowth. To investigate whether Sip1 binding was important for the growth suppressive function of Merlin *in vivo*, I expressed the Merlin arginine mutants in the A/P boundary of the wing using *ptc-GAL4* and measured changes in wing area of the *patched* region (Figure 2-8, A). The average area of the *patched* region increased when the Merlin arginine mutants were expressed, compared to the w^{1118} and wild-type Merlin controls (Figure 2-8, B). This increase in wing area was similar to that observed with the expression of $Merlin^{T616D}$, the phosphomimetic and inactive form of the growth suppressive function of Merlin (Figure 2-8, B). This suggests that when Merlin and Sip binding was reduced, Merlin appeared to behave as an inactive form leading to an increase in wing area. Furthermore, when the non-phosphorylated and active form of Merlin ($Merlin^{T616A}$) was co-expressed with the Merlin arginine mutants, the area of the *patched* region decreased (Figure 2-8, B). Thus, expression of active Merlin partially rescued the Merlin arginine mutant phenotype observed in the adult wings, suggesting that Merlin and Sip1 binding is important for Merlin activity and growth suppressive function.

As the expression of the Merlin arginine mutants increased the area of the *patched* region in adult wings, we then asked whether proliferation or adhesion was affected during early wing development. When $Mer^{R325A\ R335L}$ was expressed in the *patched* region, obvious defects in proliferation or epithelial organization were not observed (Figure 2-9; Table 1). As merlin and EBP50 were previously shown to affect EGFR signaling (Curto et al., 2007), I also analyzed EGFR in third instar wing imaginal discs expressing the $Mer^{R325A\ R335L}$ and found no obvious defects (Table 1). As the expression of the Merlin arginine mutants may alter proliferation or adhesion during pupal stages, I also analyzed pupal wing epithelium. At 28 hours post-puparium formation (PPF), I did not observe any defects in proliferation or epithelial organization when $Mer^{R325A\ R335L}$ was expressed in the *patched* region, compared to controls (Figure 2-10). I also analyzed EGFR, cell death, and other adhesion markers in pupal wing epithelium expressing the various Merlin arginine mutants but found no obvious defects at various stages of post-puparium formation, as summarized in Table 2.

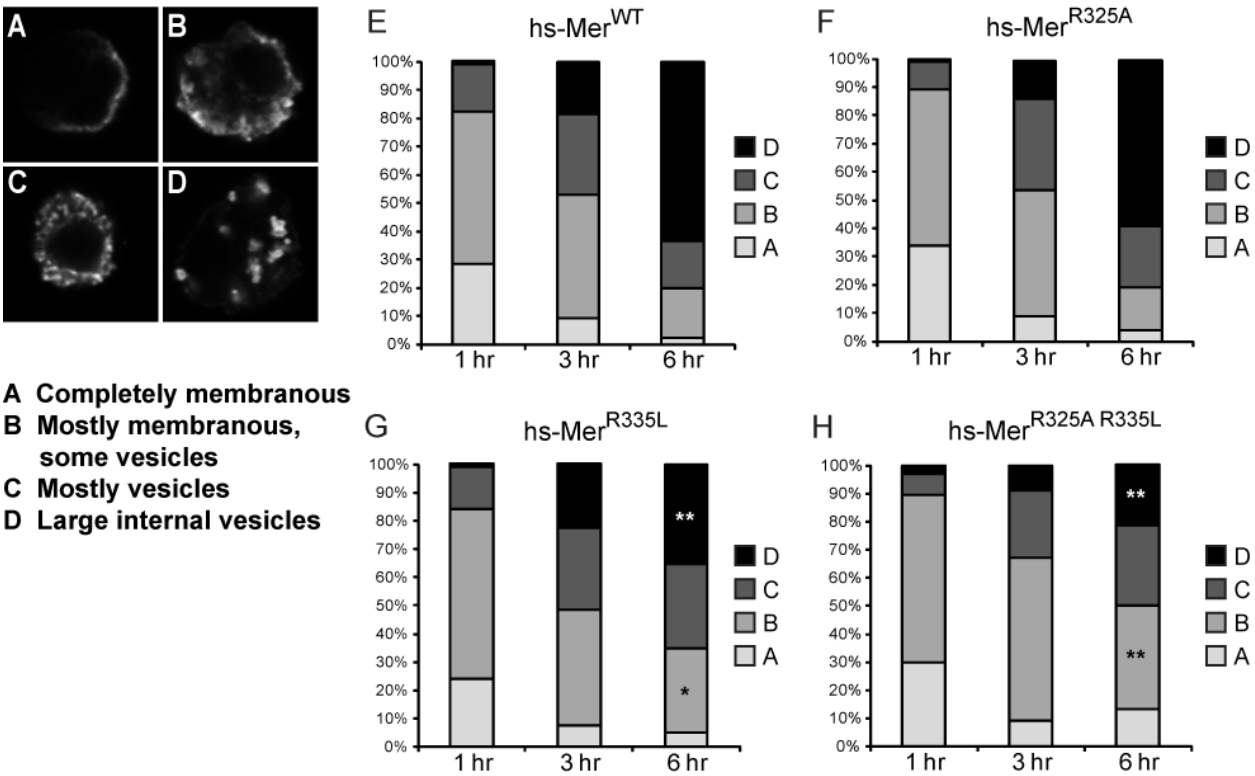

Figure 2-6: Subcellular localization and trafficking of Merlin and the Merlin arginine mutants in S2R$^+$ cells. Heat shock (hs)-inducible HA-tagged Merlin (hs-Merlin^{WT}) and Merlin arginine mutants (hs-Mer^{R325A}, hs-Mer^{R335L}, and hs-Mer$^{R325A\ R335L}$) were expressed in S2R$^+$ cells. Following heat shock, the subcellular localization of HA-tagged constructs were described as (A) completely membranous, (B) mostly membranous with some vesicles, (C) mostly vesicles, and (D) large internal vesicles. The proportions of cells displaying phenotypes A-D were scored 1 hour (hr), 3 hr and 6 hr post-induction. The subcellular localization of the HA-tagged Merlin arginine mutants, (F) hs-Mer^{R325A}, (G) hs-Mer^{R335L}, and (H) hs-Mer$^{R325A\ R335L}$ were compared to (E) hs-Mer^{WT}. At 6 hours post-induction, the proportion of cells displaying phenotype B increased and phenotype D decreased when (G) Merlin^{R335L} and (H) Merlin$^{R325A\ R335L}$ were expressed, compared to (E) Merlin^{WT}. ** represents *p*-value ≤0.01 and * represents p-value ≤0.05. Figure obtained from (Abeysundara et al., 2014), with permission.

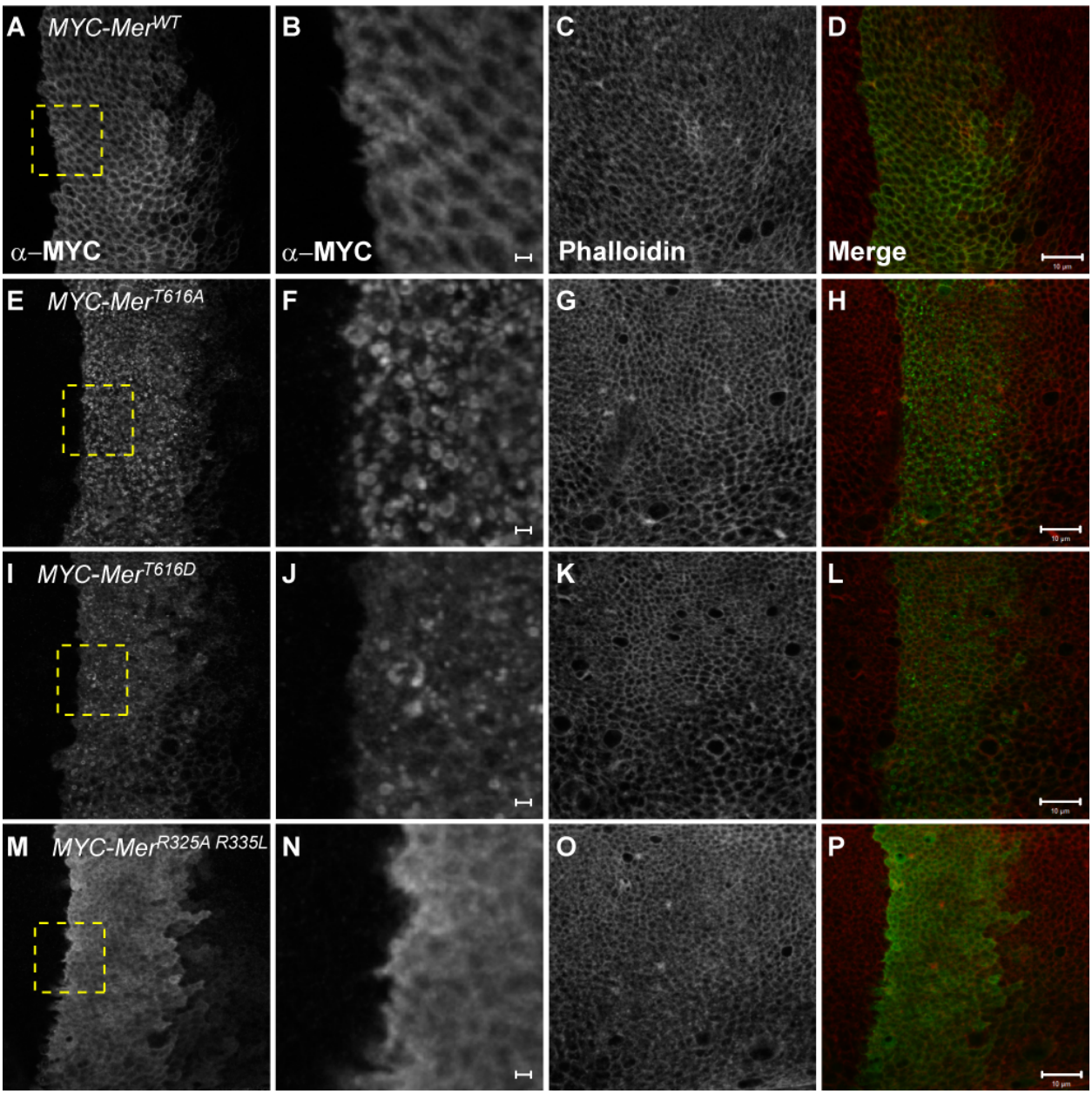
A MYC-Mer^WT
α–MYC
B
α–MYC
C
Phalloidin
D
Merge
E MYC-Mer^T616A
F
G
H
I MYC-Mer^T616D
J
K
L
M MYC-Mer^R325A R335L
N
O
P

Figure 2-7: Subcellular localization of the MYC-tagged forms of Merlin expressed using *ptc-GAL4*. (A-D) *UAS-MYC-Merlin* (*MYC-Mer*^{WT}), (E-H) *UAS-MYC-Merlin*^{T616A} (*MYC-Mer*^{T616A}), (I-L) *UAS-MYC-Merlin*^{T616D} (*MYC-Mer*^{T616D}), and (M-P) *UAS-MYC-Merlin* $^{R325A\ R335L}$ (*MYC-Mer*$^{R325A\ R335L}$) were expressed using *ptc-GAL4* in third instar wing imaginal discs. Localization of MYC-tagged Merlin (anti-MYC; green) and the actin cytoskeleton (Phalloidin; red) are shown in the merge panels (D, H, L, P). The area outlined with the yellow boxes (A, E, I, M) correspond to the zoomed images shown in B, F, J and N, respectively. (A-B) *MYC-Mer*^{WT} localized near the plasma membrane. (E-F) *MYC-Mer*^{T616A} localized to punctate structures near the plasma membrane and (I-J) *MYC-Mer*^{T616D} was cytoplasmic with some punctae. (M-N) *MYC-Mer*$^{R325A\ R335L}$ appeared largely cytoplasmic and was not as concentrated near the plasma membrane. Scale bars represent (B, F, J, and M) 1 μm and (D, H, L, and P) 10 μm. Figure obtained from (Abeysundara et al., 2014), with permission.

A

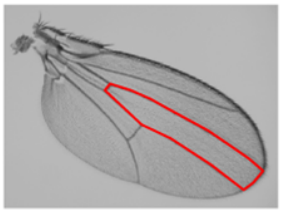

B

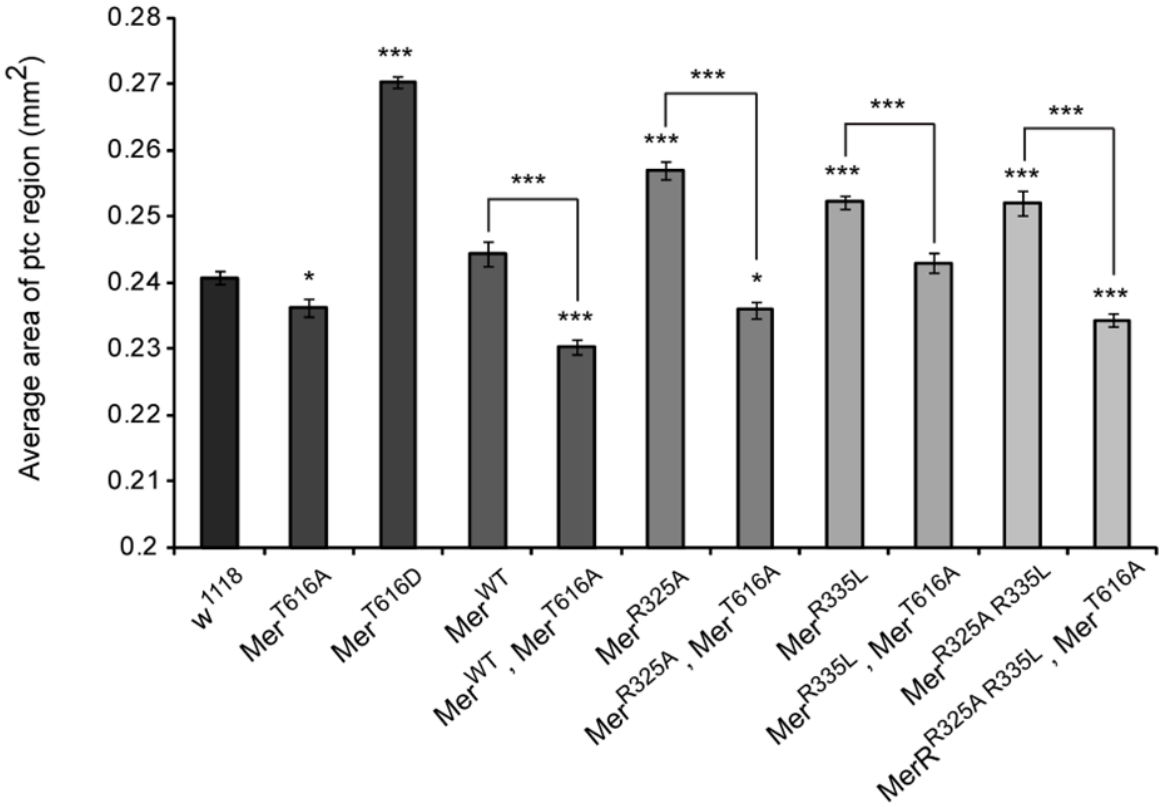
Average area of ptc region (mm2)
0.28
0.27
0.26
0.25
0.24
0.23
0.22
0.21
0.2
***
*
***
***
***
*
***
***
***
***
***
w1118
MerT616A
MerT616D
MerWT
MerWT , MerT616A
MerR325A
MerR325A , MerT616A
MerR335L
MerR335L , MerT616A
MerR325A R335L
MerR325A R335L , MerT616A

Figure 2-8: Expression of an active form of Merlin partially rescues the Merlin arginine mutant phenotype. (A) A wild-type adult wing with the *patched* (*ptc*) region between wing veins L3 and L4 outlined. (B) w^{1118}, *UAS-MYC-Merlin*^{T616A} (Mer^{T616A}), *UAS-MYC-Merlin*^{T616D} (Mer^{T616D}), *UAS-MYC-Merlin* (Mer^{WT}), *UAS-MYC-Merlin*^{R325A} (Mer^{R325A}), *UAS-MYC-Merlin*^{R335L} (Mer^{R335L}), and *UAS-MYC-Merlin*$^{R325A\ R335L}$ (Mer$^{R325A\ R335L}$) transgenic flies were crossed to *ptc-GAL4* and the average area of the *ptc* region was quantified. Expression of the Merlin arginine mutants increased the area of the *ptc* region, similar to the expression of Mer^{T616D}. When Mer^{T616A} was co-expressed with the Merlin arginine mutants, the area decreased, suggesting that an active form of Merlin partially rescues the Merlin arginine mutant phenotype. Except where indicated by brackets, wing areas were compared to the w^{1118} control for statistical analysis. Error bars represent standard error. *** represents p-value ≤0.0001 and * p-value ≤0.02. Figure obtained from (Abeysundara et al., 2014), with permission.

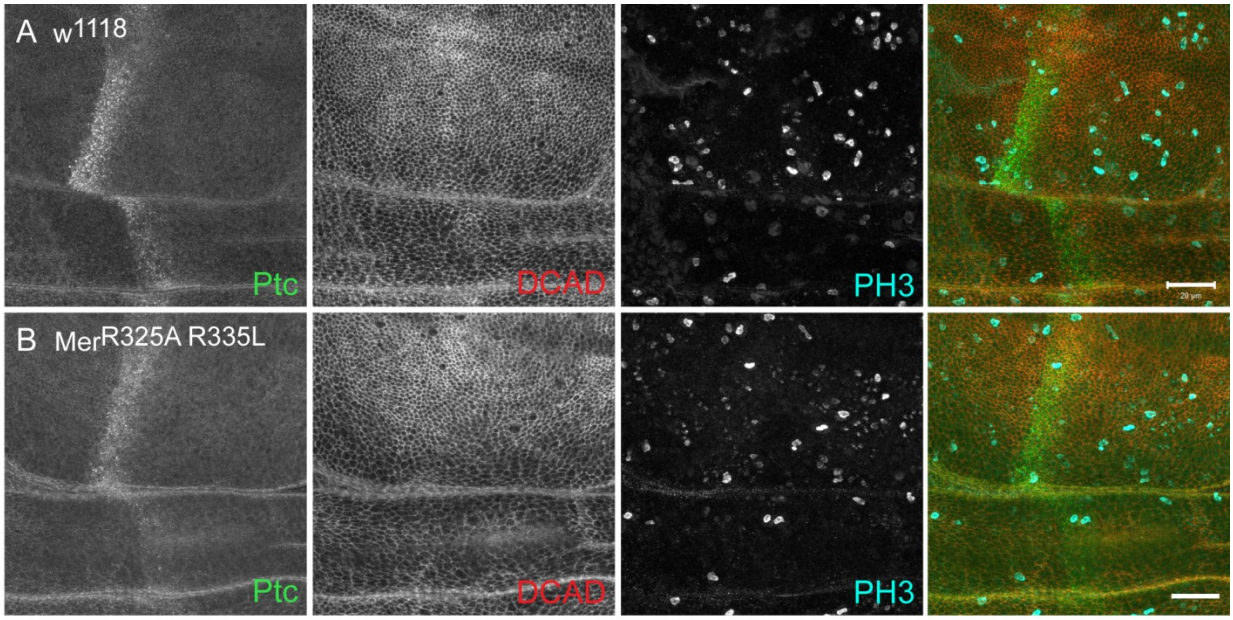

Figure 2-9: Expression of Merlin with reduced binding to Sip1 does not alter proliferation or epithelial organization in wing imaginal epithelium. (A) *w*^{1118} and (B) *UAS-MYC-Mer*$^{R325A\ R335L}$ were crossed to *ptc-GAL4* and third instar wing imaginal discs were labelled for anti-Ptc (green), anti-DE-Cadherin (DCAD; red), and anti-phospho-histone H3 (PH3; cyan) as shown in merge panels. Mer$^{R325A\ R335L}$ expression did not lead to obvious defects in proliferation or epithelial organization in the *ptc* region, when compared to controls. Scale bar represents 20 μm.

Table 1: Antibodies tested for changes in third instar wing imaginal discs when Merlin transgenes were expressed using *ptc-GAL4* [a]

Antibodies used	Mer^{T616A}	Mer^{R335L}	$Mer^{R325A\ R335L}$
Rat anti-DCAD	N/A	•	•
Rabbit anti-EGFR	•	N/A	•
Rabbit anti-PH3	N/A	•	•
Phalloidin	•	N/A	•
Mouse anti-Ptc	•	•	•

[a] *UAS-MYC-Mer*^{T616A}, *UAS-Mer*^{R335L}, and *UAS-MYC-Mer*$^{R325A\ R335L}$ were crossed to *ptc-GAL4* and third instar wing imaginal discs of progeny were analyzed.

• denotes no change in localization observed for the progeny tested, compared to controls (progeny of w^{1118} crossed to *ptc-GAL4*).

N/A indicates that the particular progeny was not analyzed for a change in localization of the specific marker.

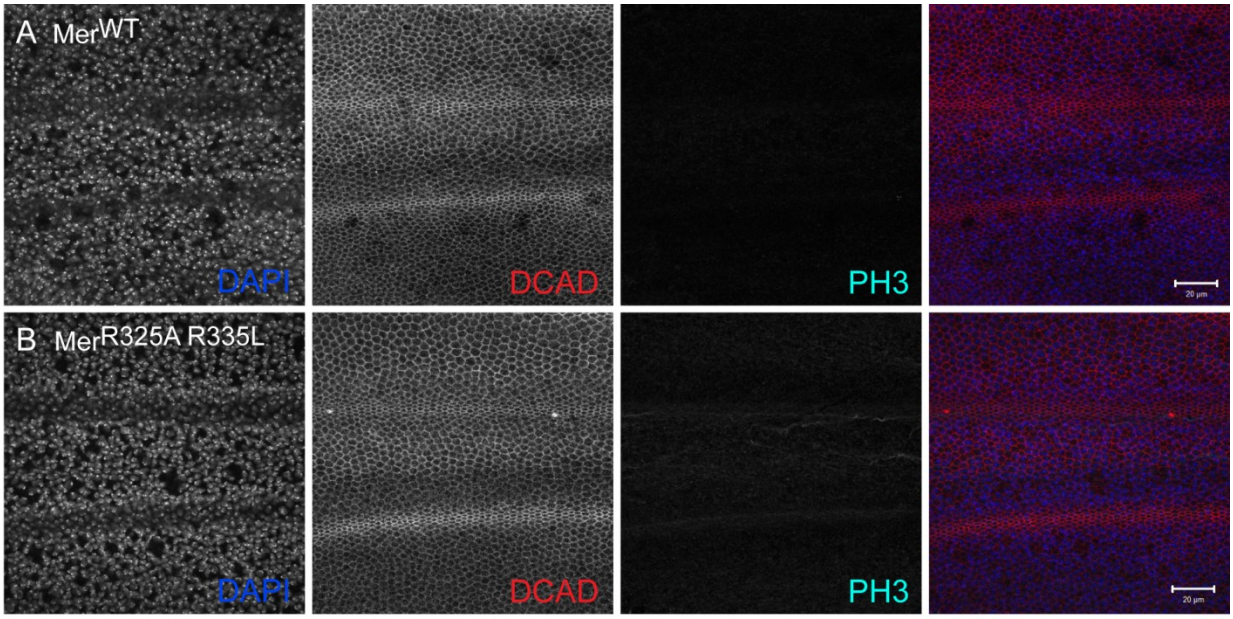

Figure 2-10: Expression of Merlin with reduced binding to Sip1 does not alter proliferation or epithelial organization in pupal wing epithelium. (A) *UAS-MYC-Mer*^{WT} and (B) *UAS-MYC-Mer*$^{R325A\ R335L}$ were crossed to *ptc-GAL4* and pupal wing epithelium were labelled for DAPI (blue), anti-DE-Cadherin (DCAD; red), and anti-phospho-histone H3 (PH3; cyan) at 28 hours post-puparium formation. Mer$^{R325A\ R335L}$ expression did not lead to ectopic proliferation or defects in epithelial organization in the *ptc* region, when compared to controls. Scale bar represents 20 μm.

Table 2: Antibodies tested for changes in pupal wing epithelium when Merlin arginine mutants were expressed using *ptc-GAL4* [a]

Hours PPF[b]	Antibodies used	Mer^{R325A}	Mer^{R335L}	$Mer^{R325A\ R335L}$
18	Rat anti-DCAD	●	N/A	N/A
	Rabbit anti-PH3	●	N/A	N/A
	Mouse anti-Ptc	●	N/A	N/A
26-28	Rabbit anti-Active caspase 3	N/A	●	N/A
	Mouse anti-Coracle	N/A	N/A	●
	Rat anti-DCAD	●	●	●
	Rabbit anti-dpERK	N/A	●	N/A
	Mouse anti-Dpp	N/A	●	●
	Rabbit anti-EGFR	●	●	●
	Mouse anti-Fas III	●	N/A	●
	Rabbit anti-PH3	●	●	●
	Phalloidin	N/A	●	●
	Mouse anti-Ptc	●	●	●
38	Rabbit-anti Active caspase 3	●	●	N/A
	Mouse anti-Crumbs	●	●	N/A
	Rat anti-DCAD	N/A	●	●
	Mouse anti-Fas III	N/A	●	●
	Rabbit anti-PH3	N/A	●	●
	Phalloidin	●	●	N/A

[a] *UAS-MYC-Mer*^{R325A}, *UAS-Mer*^{R335L}, and *UAS-MYC-Mer*$^{R325A\ R335L}$ were crossed to *ptc-GAL4* and pupal wings of progeny were analyzed at indicated stages.

[b] PPF indicates post-puparium formation

● denotes no change in localization observed for the progeny tested, compared to controls (progeny of w^{1118} or *UAS-MYC-Mer*^{WT} crossed to *ptc-GAL4*).

N/A indicates that the particular progeny was not analyzed for a change in localization of the specific marker.

2.3.4 Merlin and Sip1 function in the follicle cells of the developing oocyte

As the expression of the Merlin arginine mutants did not appear to alter proliferation and adhesion in larval and pupal wing epithelial tissues, we hypothesized that endogenous Merlin function may interfere with the expression of the Merlin arginine mutants. Thus, to further investigate the functional significance of reduced binding between Merlin and Sip1 in the absence of endogenous Merlin, the expression of the Merlin arginine mutants were analyzed in *Merlin* null mutant clones using the mosaic analysis with a repressible cell marker (MARCM) technique. MARCM uses FLP/FRT recombination to create groups of mutant cells that ubiquitously express a transgene of interest, marked by GFP expression (Lee and Luo, 1999). As Sip1 was shown to be essential for Moesin phosphorylation and epithelial organization in the follicle cells surrounding the developing oocyte (Hughes et al., 2010), we wanted to determine whether Sip1 also regulated Merlin function in these epithelial cells.

Using MARCM, the expression of the Merlin arginine mutant ($Mer^{R325A\ R335L}$) in *Merlin* null mutant (*Mer*^{4}) clones altered follicle cell organization (Figure 2-11). *Mer*^{4} mutant clones expressing $Mer^{R325A\ R335L}$ displayed disorganized cell morphology (Figure 2-11, I-L and O), compared to the expression of wild-type Merlin (Figure 2-11, E-H and N) or the *Mer*^{4} mutant clones alone (Figure 2-11, A-D and M). In addition, follicle cells expressing $Mer^{R325A\ R335L}$ in a *Mer*^{4} mutant background formed multiple layers of cells compared to the surrounding wild-type cells (Figure 2-11, P-S). Therefore, reduced Merlin binding to Sip1 disrupts follicle cell organization.

When *Sip1* mutant clones were analyzed for changes in Merlin localization, I found that the loss of Sip1 did not affect Merlin localization in the follicle cells during early stages of oocyte development, specifically stages 2-8 (Figure 2-12). However, during later stages of oocyte development, Merlin appeared mis-localized and cytoplasmic in *Sip1* mutant follicle cells, compared to surrounding wild-type cells (Figure 2-13, C and Figure 2-14, C). These findings provide further evidence that Sip1 is important for the subcellular localization of Merlin. The loss of Sip1 also appeared to increase proliferation in the follicle cells, as indicated by the presence of PH3-positive cells within the *Sip1* mutant clones compared to the surrounding wild-type cells (Figure 2-13, D). In addition, EGFR localization appeared mis-localized and cytoplasmic in the follicle cells with the loss of Sip1 (Figure 2-14, D), suggesting that Sip1 may affect the EGFR pathway, which has been previously shown in mammalian studies (Curto et al., 2007).

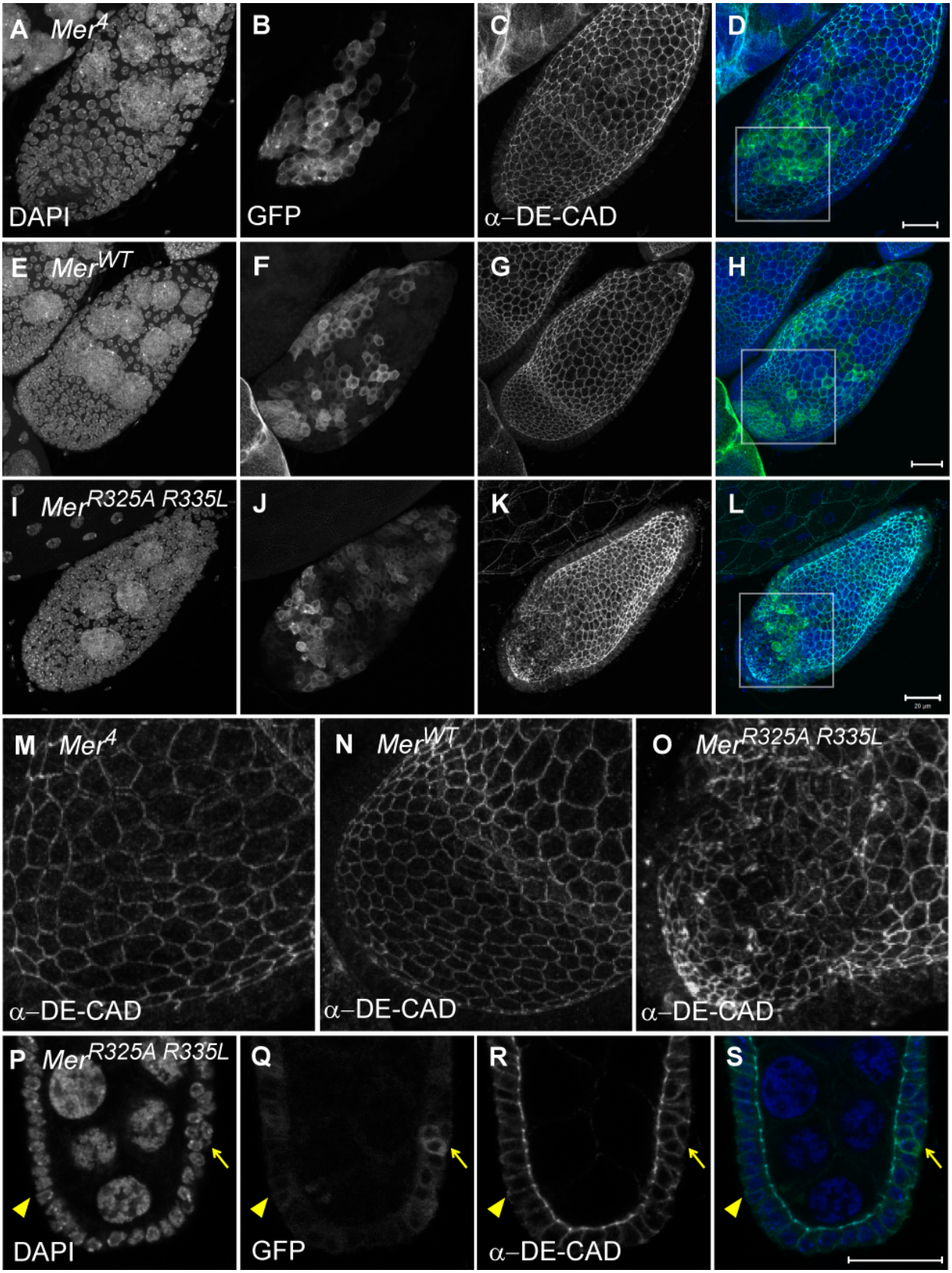
A Mer4
DAPI
B
GFP
C
α–DE-CAD
D
E MerWT
F
G
H
I MerR325A R335L
J
K
L
20 µm
M Mer4
α–DE-CAD
N MerWT
α–DE-CAD
O MerR325A R335L
α–DE-CAD
P MerR325A R335L
DAPI
Q
GFP
R
α–DE-CAD
S

Figure 2-11: Loss of Merlin and Sip1 binding disrupts DE-cadherin in follicle cell epithelium. Follicle cells expressing *UAS-MYC-Merlin* (*Mer*^{WT}) and *UAS-MYC-Merlin*$^{R325A\ R335L}$ (*Mer*$^{R325A\ R335L}$) in a *Merlin* null mutant (*Mer*^{4}) background were generated using MARCM and mutant clones were positively labelled with mCD8::GFP (GFP; green). Egg chambers were fluorescently labelled with DAPI (blue) and anti-DE-Cadherin (α-DE-Cad; cyan) as shown in merge panels, along with GFP. (A-D) *Mer*^{4} mutant clones showed no defects in follicle cell organization in stage 9 egg chambers. (E-H) *Mer*^{4} mutant clones in which *Mer*^{WT} was expressed also showed no defects in follicle cell organization in stage 8 egg chambers. (I-L) When *Mer*$^{R325A\ R335L}$ was expressed in *Mer*^{4} mutant clones, epithelial integrity appeared disorganized at the posterior pole of stage 8 egg chambers. (D, H, L) Boxed areas shown in merge panels correspond to the zoomed images in M-O. (P-S) Multi-layering of nuclei (yellow arrows) was observed within the clones expressing *Mer*$^{R325A\ R335L}$ in the *Mer*^{4} mutant background, compared to wild-type clones (yellow arrowhead). Maximum projection images are shown in A-O and single focal plane images are shown in P-S. Scale bars represent 20 μm. Figure obtained from (Abeysundara et al., 2014), with permission.

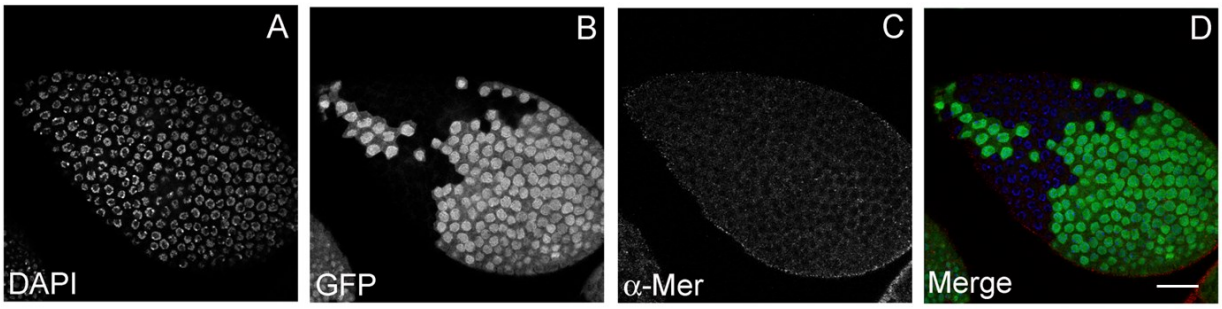

Figure 2-12: Loss of Sip1 in the follicle cells does not affect Merlin at early stages of oocyte development. *Sip1*^{06373} mutant clones (GFP-negative) were generated using somatic mosaic recombination and developing oocytes were fluorescently labelled with DAPI (blue) and anti-Merlin (α-Mer; red) as shown in merge panel (D), along with GFP (green). (B) *Sip1* mutant clones are indicated by the absence of GFP. (C) Merlin localization was unaltered within the *Sip1* mutant clone, compared to surrounding GFP-positive, wild-type follicle cells. Scale bar represents 20 μm.

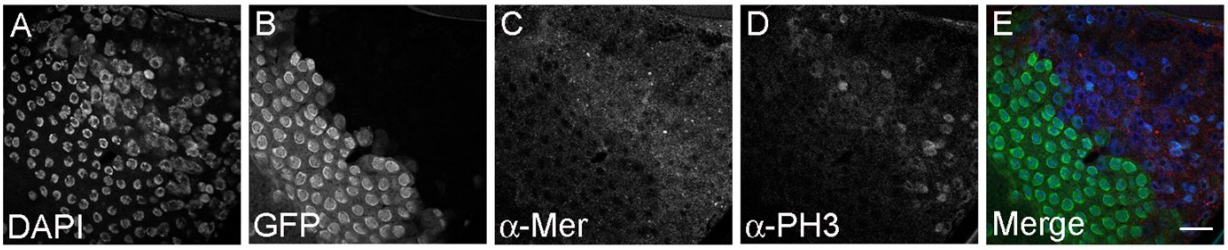

Figure 2-13: Loss of Sip1 in the follicle cells affects Merlin and proliferation at later stages of oocyte development. *Sip1*^{06373} mutant clones (GFP-negative) were generated using somatic mosaic recombination and stage 10 egg chambers were fluorescently labelled with DAPI (blue), anti-Merlin (α-Mer; red), and anti-phospho-histone H3 (α-PH3; cyan) as shown in merge panel (E), along with GFP (green). (B) *Sip1* mutant clones are indicated by the absence of GFP. (C) Merlin was mis-localized and appeared cytoplasmic and (D) an increase in PH3-positive cells were observed within the *Sip1* mutant clones, compared to surrounding GFP-positive, wild-type follicle cells. Scale bar represents 20 μm.

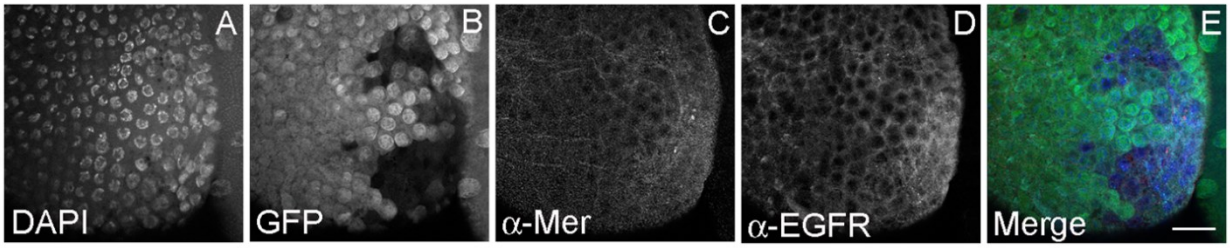

Figure 2-14: Loss of Sip1 in the follicle cells affects Merlin and EGFR localization at later stages of oocyte development. *Sip1*^{06373} mutant clones (GFP-negative) were generated using somatic mosaic recombination and stage 10 egg chambers were fluorescently labelled with DAPI (blue), anti-Merlin (α-Mer; red), and anti-EGFR (α-EGFR; cyan) as shown in merge panel (E), along with GFP (green). (B) *Sip1* mutant clones are indicated by the absence of GFP. (C-D) Merlin and EGFR were mis-localized and appeared cytoplasmic within the *Sip1* mutant clones, compared to surrounding GFP-positive, wild-type follicle cells. Scale bar represents 20 μm.

2.4 DISCUSSION AND FUTURE DIRECTIONS

Using Drosophila, we found that the NHERF1/EBP50 orthologue, Sip1, modified the *Merlin* hypomorphic mutant phenotype in the adult eye, suggesting a genetic interaction between *Merlin* and *Sip1*. Furthermore, we found that the FERM domain and C-terminal tail of Drosophila Merlin bound directly with Sip1, consistent with mammalian *in vitro* studies (Murthy et al., 1998; Nguyen et al., 2001). Interestingly, a previously uncharacterized α-helical domain immediately downstream of the FERM domain of Drosophila Merlin was also important for binding to Sip1. Comparison of the sequences within this region from several vertebrates and Drosophila species identified two conserved arginine residues in the α-helical domain of Merlin, which were not conserved in human or Drosophila Moesin. When the conserved arginine residues were substituted to the corresponding residues present in Drosophila Moesin, we confirmed that these residues were important for Sip1 binding *in vitro*. To demonstrate that these arginine residues were important for Merlin binding to Sip1 *in vivo*, transgenic Drosophila lines were generated where MYC-tagged constructs of $Merlin^{R325A}$, $Merlin^{R335L}$, and $Merlin^{R325A\ R335L}$ were under control of the upstream activation sequence (UAS). When MYC-tagged wild-type Merlin ($Merlin^{WT}$), $Merlin^{R325A}$, $Merlin^{R335L}$, and $Merlin^{R325A\ R335L}$ were expressed using *actin-GAL4* and immunoprecipitated from pupal lysates, David Primrose showed that the Merlin arginine mutants displayed reduced binding to endogenous Sip1, compared to wild-type Merlin (Abeysundara et al., 2014). Furthermore, when FLAG-tagged Sip1 was co-expressed with HA-tagged wild-type Merlin and the Merlin arginine mutants in $S2R^+$ cells, the relative amount of $Merlin^{R335L}$ and $Merlin^{R325A\ R335L}$ that co-immunoprecipitated with Sip1 was reduced, compared to wild-type Merlin (Abeysundara et al., 2014). Together, these findings suggest that the Merlin arginine residues within the α-helical domain are important for binding to Sip1 *in vitro* and *in vivo*.

To analyze the functional significance of Merlin and Sip1 binding, we utilized multiple approaches to investigate how reduced binding to Sip1 may affect Merlin localization and activity. We showed that expression of Merlin with reduced binding to Sip1 displayed altered Merlin localization and trafficking in cultured cells, which has previously been linked to Merlin phosphorylation and activity (Bensenor et al., 2010; Hughes and Fehon, 2006; LaJeunesse et al., 1998). Following induction, a phosphomimetic, inactive form of Merlin remained closely associated with the plasma membrane; whereas a non-phosphorylated, active form of Merlin trafficked off the plasma membrane faster and primarily localized to large cytoplasmic structures, when compared to wild-type Merlin over time (Hughes and Fehon, 2006). We found that $Merlin^{R335L}$ and $Merlin^{R325A\ R335L}$ trafficking off the plasma membrane appeared delayed in $S2R^+$ cells, consistent with but not as severe as the

phosphomimetic form of Merlin (Bensenor et al., 2010; Hughes and Fehon, 2006). When the Merlin$^{R325A\ R335L}$ transgene was expressed in the *patched* region of the wing imaginal disc, the Merlin arginine mutant appeared more cytoplasmic, compared to wild-type Merlin. These differences observed in S2R^{+} cells and wing imaginal discs may be due to differences in cell type and expression of factors regulating Merlin localization. However, the loss of Sip1 from the follicle cells using somatic mosaic recombination lead to the mis-localization of Merlin to the cytoplasm. Together, these findings demonstrate the Sip1 is important for proper Merlin subcellular localization and thus may affect Merlin phosphorylation and activity.

We found that Sip1 binds to the phosphomimetic Merlin^{T616D} form more efficiently than the non-phosphorylated form, Merlin^{T616A} (Abeysundara et al., 2014). Given that reducing Sip1 binding affected Merlin localization in cell culture and epithelial tissues, and Sip1 appeared to interact with the phosphomimetic form of Merlin, this led us to hypothesize that the Merlin and Sip1 interaction may facilitate the dephosphorylation and activation of Merlin. Indeed, we found that, when Merlin$^{R325A\ R335L}$ was expressed using *actin-GAL4* and immunoprecipitated from pupal lysates, the arginine mutant appeared to be hyper-phosphorylated, compared to the expression of wild-type Merlin (Abeysundara et al., 2014). Furthermore, dsRNA-mediated knockdown of Sip1 using *actin-GAL4* led to an increase in phosphorylated Merlin in pupal lysates via western blot analysis (Abeysundara et al., 2014). Thus, reducing binding between Merlin and Sip1 or the knockdown of Sip1 resulted in an increase in Merlin phosphorylation. We also found that the over-expression of Sip1 in S2 cells reduced Merlin phosphorylation, further supporting our model that Sip1 facilitates the dephosphorylation of Merlin.

To further test this model *in vivo*, we over-expressed the Merlin arginine mutants in the *patched* region of the adult wing and measured the wing area. We found that reducing Merlin and Sip1 binding resulted in a larger wing area compared to the expression of wild-type Merlin and controls. This increase in wing area was also observed when the phosphomimetic and inactive Merlin^{T616D} form was expressed. When the non-phosphorylated and active Merlin^{T616A} form was co-expressed with the Merlin arginine mutants, the increase in wing area was partially rescued. Thus, Merlin binding to Sip1 is important for the growth suppressive function of Merlin. However, when we examined whether the change in wing size was due to defects in proliferation or adhesion, we did not observe any obvious defects in larval imaginal discs and pupal wings. It is possible that the interaction between Merlin and Sip1 is very transient or stage-specific, explaining why we could not observe any defects at the specific stages we examined. Quantification of mitotic cells during early wing development may be necessary to capture subtle defects in proliferation. Alternatively,

generating Merlin arginine mutant clones in a *Merlin* null mutant background in the wing imaginal disc may provide further insight into the precise mechanism underlying the increase in adult wing area when binding between Merlin and Sip1 is reduced. Previously, Merlin and Moesin were shown to localize to the apical surface of wing epithelial tissues and were coordinately regulated by the Slik kinase and Flapwing phosphatase (Hughes and Fehon, 2006; Yang et al., 2012). *Moesin* and *Sip1* were also found to genetically interact in adult wings (Hughes et al., 2010). If Sip1 potentially acts as the scaffold protein essential for both Merlin and Moesin regulation, it is possible that the expression of Merlin with reduced binding to Sip1 may affect Moesin localization and activity in the wing epithelium. Thus, future studies would need to confirm that the expression of the Merlin arginine mutants increase adult wing size, independent of Moesin.

To exclude the possibility of endogenous Merlin interfering with the expression of the Merlin arginine mutants, we then analyzed the effect of expressing the Merlin arginine mutants in the absence of Merlin using the MARCM technique in the follicle cells. Previously, the loss of Merlin in the posterior follicle cells led to multi-layering of the epithelium and defects in oocyte nuclear migration (MacDougall et al., 2001). We found that the loss of Merlin did not affect DE-Cadherin organization in the follicle cells of stage 9 oocytes, likely because these mutant clones were not generated in the most posterior follicle cells. Furthermore, we did not confirm whether oocyte nuclear migration was affected with the loss of Merlin. When the Merlin arginine mutants were expressed in a *Merlin* null mutant background, we observed defects in DE-Cadherin organization in the follicle cells surrounding the developing oocyte. In addition, the follicle cells were not maintained in a single epithelial layer. Previously, the loss of Sip1 displayed dramatic defects in F-actin organization and DE-Cadherin localization in the follicle cells of stage 13 oocytes, through the Slik-mediated loss of phosphorylated Moesin (Hughes et al., 2010). We found that the expression of the Merlin arginine mutants with the loss of Merlin affected DE-Cadherin organization in the follicle cells of stage 8 oocytes, suggesting that Merlin binding to Sip1 is important for epithelial organization during earlier stages of oogenesis. As Sip1 promotes the Slik-dependent phosphorylation of Moesin in follicle cells (Hughes et al., 2010), it is possible that expressing Merlin with reduced binding to Sip1 may enhance Moesin phosphorylation in these follicle cells due to more freely available endogenous Sip1. Thus, the phosphorylation levels of Moesin would need to be examined in the Merlin arginine mutant follicle cells to confirm that increased Moesin activity is not leading to the defects in epithelial integrity observed with reduced binding between Merlin and Sip1. Furthermore, multiple studies have demonstrated that the loss of proteins within the polarity complexes

result in rounded cells and multi-layering of the follicle cell epithelium (Abdelilah-Seyfried et al., 2003; Bilder et al., 2000; De Lorenzo et al., 1999; Genova et al., 2000; Goode and Perrimon, 1997; Manfruelli et al., 1996; Tanentzapf et al., 2000). Thus, it would be interesting to further examine how reduced Merlin binding to Sip1 affects the polar domains in the follicle cells.

In summary, we found that the Merlin and Sip1 interaction appeared to facilitate the dephosphorylation of Merlin, which is important for its growth suppressive function and epithelial organization (Abeysundara et al., 2014). Previously, the Flapwing phosphatase was shown to bind to Merlin and Sip1 *in vitro* and altering Flapwing levels affected Merlin phosphorylation (Yang et al., 2012). Thus, studies examining whether the interaction between Merlin and Sip1 is essential for Flapwing-mediated dephosphorylation of Merlin would provide further insight into the role of Merlin regulation during growth and the maintenance of epithelial integrity (Figure 2-15).

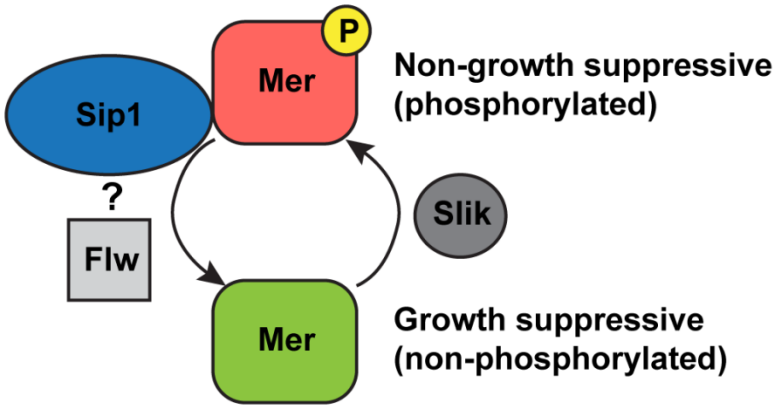

Figure 2-15: Sip1 interaction is essential for Merlin activation via dephoshorylation. Sip1 binds to the phosphorylated or inactive form of Merlin (Mer) and facilitates the dephosphorylation or activation of Merlin. It remains to be determined how the phosphatase Flapwing (Flw) functions along with Sip1 and Merlin. Figure obtained from (Abeysundara et al., 2014), with permission.

Chapter 3: Investigation of Merlin and Sip1 function in the developing optic lobes

3.1 INTRODUCTION

The Drosophila visual system is composed of the compound eye and the optic lobe located in the brain. The optic lobe develops from an optic placode during embryogenesis (Green et al., 1993). During early larval development, the cells within the optic placode proliferate and separate into the inner and outer proliferation centers (IPC and OPC, respectively) and adopt a crescent-like shape (Hofbauer and Camposortega, 1990; Nassif et al., 2003; White and Kankel, 1978). The IPC produces the inner medulla, the lobula, and the lobula plate neurons; whereas the OPC produces the outer medulla and lamina neurons (Meinertzhagen and Hanson, 1993). The early cells within the IPC and OPC express epithelial junctional markers such as, PatJ and DE-Cadherin, and the proneural protein, Scute, and thus, are referred to as neuroepithelial cells (Egger et al., 2007). During early larval stages, the neuroepithelial cells of the OPC proliferate by symmetric divisions and expand the progenitor pool (Egger et al., 2007). During late larval stages, the neuroepithelial cells undergo at least two distinct modes of neurogenesis in the lateral and medial margins of the OPC to generate the lamina neurons and medulla neuroblasts, respectively (refer to Figure 3-1 for a schematic representation of the optic lobe) (Egger et al., 2007; Yasugi et al., 2008). The neuroepithelial cells located at the lateral margin give rise to lamina precursor cells, which undergo cell cycle arrest and differentiate into the lamina neurons in response to signals from the innervating retinal axons (Huang and Kunes, 1996; Huang and Kunes, 1998; Selleck et al., 1992; Selleck and Steller, 1991). However, the neuroepithelial cells along the medial margin of the OPC, differentiate into medulla neuroblasts in response to the coordinated activity of multiple signaling pathways (Egger et al., 2007; Egger et al., 2010; Ngo et al., 2010; Orihara-Ono et al., 2011; Reddy et al., 2010; Wang et al., 2011a; Wang et al., 2011b; Weng et al., 2012; Yasugi et al., 2010; Yasugi et al., 2008). The medulla neuroblasts express neuroblast markers, Deadpan and Miranda (Bier et al., 1992; Ikeshima-Kataoka et al., 1997), and lack the localization of junctional proteins (Egger et al., 2007; Hofbauer and Camposortega, 1990). The transition from neuroepithelial cells to medulla neuroblasts occurs as a wave of differentiation that sweeps across the neuroepithelial cells, where the most medial neuroepithelial cells transiently express the proneural protein, Lethal of Scute (L(1)sc), prior to differentiation (Yasugi et al., 2008). This wave of differentiation, referred to as the proneural wave, occurs in a medial to lateral direction and is regulated by the JAK/STAT, Hippo, Notch, and EGFR signaling pathways (Egger et al., 2010; Ngo et al., 2010; Orihara-Ono et al., 2011; Reddy et al., 2010; Wang et al., 2011a; Wang et al., 2011b; Weng et al., 2012; Yasugi et al.,

2010; Yasugi et al., 2008). In addition to signaling pathways regulating neuroepithelial cell proliferation and differentiation, glial cells that surround the developing optic lobe have also been shown to regulate the neuroepithelial to neuroblast transition (Morante et al., 2013; Perez-Gomez et al., 2013). During mammalian forebrain development, neuroepithelial cells undergo symmetric cell divisions to expand the neural stem cell pool, followed by asymmetric cell divisions that generate the neuronal population (Chenn and McConnell, 1995). Furthermore, a meningeal-derived cue regulates the switch from symmetric to asymmetric divisions in the neuroepithelium (Siegenthaler et al., 2009). Thus, the transition of optic lobe neuroepithelial cells to medulla neuroblasts closely models the transition of neuroepithelial cells to radial glia during mammalian neurogenesis, making it a suitable system to study factors regulating self-renewal and differentiation.

Drosophila Merlin and Sip1 appear to play roles in regulating both proliferation and maintaining epithelial integrity (Hughes et al., 2010; LaJeunesse et al., 1998; Yang et al., 2012). Previous studies have shown that the Hippo pathway controls the growth and differentiation of Drosophila optic lobe neuroepithelial cells, by regulating the co-activator protein, Yorkie (Reddy et al., 2010). In addition, the EGFR and Notch signaling pathways are also required for neuroepithelial cell maintenance and differentiation (Wang et al., 2011b; Yasugi et al., 2010). Merlin is one of many upstream regulators of the Hippo pathway (Hamaratoglu et al., 2006), but its role during optic lobe development still remains unclear. Furthermore, Merlin and Expanded function together in Notch receptor clearance from the plasma membrane of Drosophila epithelial tissues (Maitra et al., 2006). Mammalian merlin has been shown to negatively regulate EGFR signaling in liver-derived epithelial cells, in an EBP50-dependent manner (Curto et al., 2007). Mammalian cell culture studies have also shown that EBP50 interacts with YAP, the human orthologue of Yorkie (Mohler et al., 1999). Given that merlin and EBP50 regulate multiple signaling pathways in different cellular contexts, it is possible that Drosophila Merlin and Sip1 may coordinately influence these signaling pathways during optic lobe development. As the spatiotemporal progression of the proneural wave across the neuroepithelial cells of the OPC has been well characterized, I focused on the potential role of Merlin and Sip1 in regulating the neuroepithelial to neuroblast transition at the medial edge of the OPC.

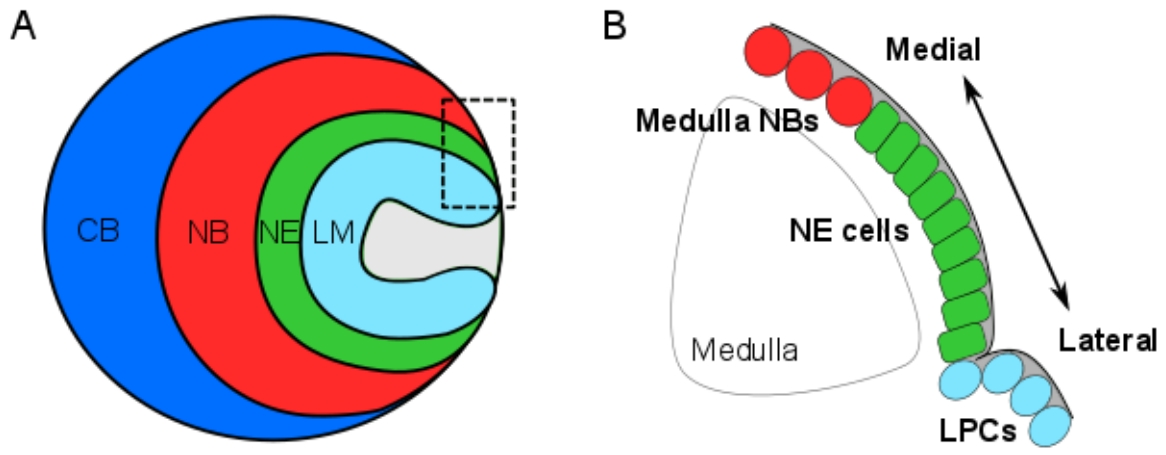

Figure 3-1: Schematic representation of the larval brain lobe. (A) The lateral view of the larval brain lobe displaying the outer proliferation center (OPC) of the developing optic lobe, consisting of the lamina (LM; cyan), neuroepithelial cells (NE; green) and medulla neuroblasts (NB; red). The central brain (CB; blue) is also shown. The region outlined in A represents the zoomed cross-sectional area shown in B. (B) The NE cells differentiate into lamina precursor cells (LPCs) at the lateral edge and differentiate into medulla NBs at the medial edge of the OPC. Medulla NBs are the progenitors that give rise to neurons located in the medulla. The gray area in B represents the glial cells surrounding the developing larval brain/optic lobe. Figure adapted from (Yasugi et al., 2008).

3.2 MATERIALS AND METHODS

3.2.1 Fly strains and genetics

The following lines were obtained from Bloomington Stock Centre: *Mer*^{3} 19A FRT/FM7c, *Mer*^{4} 19A FRT/FM7,*actin-GFP*, *UAS-Mer*^{dsRNA} (#34958), *actin-GAL4*, *Insc-GAL4*, *c855a-GAL4*, *Repo-GAL4*, *Pros-GAL4*, *Ey-GAL4*, and *GMR-GAL4*. *UAS-Sip1*^{dsRNA} (RNA interference inverted repeat transgene) was obtained from Richard Fehon. The 19A FRT MARCM line (*hsFLP, TubPGAL80, 19A FRT*;;*TubPGAL4, UAS-MCD8-GFP/*MKRS) was obtained from Celeste Berg. When necessary, stocks were maintained over *actin-GFP* balancer chromosomes and larvae of interest were chosen by lack of GFP. *w*^{1118} flies were used as wild-type control. Flies were maintained on standard Bloomington media.

3.2.2 Immunofluorescence

Larvae were dissected in 1X PBS and fixed in 4% paraformaldehyde for 20 min. Dissected tissues were rinsed at least 5 times in 1X PBS and blocked in 0.1% Triton X-100, and 1% normal donkey serum in 1X PBS (PTN) for at least 1 hr at room temperature (RT). Tissues were incubated in primary antibodies in PTN overnight at 4°C. Tissues were rinsed/washed for at least 1 hr in PTN at RT and incubated in secondary antibodies in PTN for 2-4 hours at RT. Tissues were rinsed/washed for at least 2 hours in PTN at RT. Tissues were incubated in DAPI (1:10 000) for 10 min and sinsed at least 3 times in PTN and at least 3 times in 1X PBS prior to mounting in ProLong® Gold Antifade Reagent (Invitrogen). Primary antibodies used were: Guinea pig anti-Sip1 (1:1000), guinea pig anti-Merlin (1:1000), rat anti-DE-Cadherin (1:200; DSHB), mouse anti-Repo (1:500; DSHB), rabbit anti-PatJ (1:1000; M. Bhat), mouse anti-Miranda (1:200; F. Matsuzaki), guinea pig anti-Deadpan (1:500; J. Skeath), mouse anti-Prospero (1:500; DSHB MR1A), rabbit anti-Phospho-histone H3 (1:2000; Millipore #06-570), mouse anti-GFP 3E6 (1:500; Invitrogen), Phalloidin Alexa Fluor 546 (1:1000; Invitrogen), Phalloidin Alexa Fluor 488 (1:1000; Invitrogen). Secondary antibodies used were: Donkey anti-Rabbit, -Mouse, -Guinea pig, and -Rat Alexa Fluor® 488/555/647 (Abcam). Imaging was performed using a Zeiss LSM 700 confocal microscope using a 40× NA 1.3 oil immersion objective (EC Plan-Neofluar; Zeiss), and 63× NA 1.4 oil immersion objective (Plan-Apochromat; Zeiss). The acquisition software used was Zen 2009 and Adobe Photoshop/Illustrator were used to generate figures.

3.2.3 Somatic mosaic analysis

Animals of the genotype *Mer*^{4} 19A FRT/FM7*, actin-GFP* line were crossed to the 19A FRT MARCM line (*hsFLP, TubPGAL80, 19A FRT*;;*TubPGAL4, UAS-MCD8-GFP/*MKRS) and allowed

to lay eggs for approximately 12 hours. Larvae were heat shocked approximately 48 hours after egg laying for 1 hr at 37°C, 1hr at 25°C, and 1hr at 37°C. Three days following heat shock, larval brains were dissected, fixed, and immunofluorescence was performed as described in Section 3.2.2.

3.3 RESULTS

3.3.1 Merlin and Sip1 localization in the larval brain lobes

To investigate whether Merlin and Sip1 are involved in optic lobe development, I first examined whether Merlin and Sip1 localized within the developing optic lobe during larval stages. Indirect immunofluorescence revealed that Merlin was expressed throughout the late larval brain lobes and it partially co-localized with DE-Cadherin at the cortex of the neuroepithelial cells and neuroblasts within the optic lobe (Figure 3-2). As neuroepithelial cells proliferate during early larval stages and differentiate into neuroblasts during late larval stages (Egger et al., 2007), Merlin localization might change during optic lobe development. Thus, I examined Merlin localization at 45 to 56 hours and 57 to 69 hours after egg laying (AEL; Figure 3-3). At 45 to 56 hours AEL, Merlin was detected in the larval brain lobes (Figure 3-3, B). However, at 57 to 69 hours AEL, Merlin immunofluorescence appeared to increase at the cortex of the neuroepithelial cells, partially co-localizing with F-actin (Phalloidin; Figure 3-3, F-J). Thus, Merlin localization in the neuroepithelial cells during early larval stages suggests that Merlin may be involved in larval optic lobe development.

I also found that Sip1 partially co-localized with DE-Cadherin at the cortex but was largely cytoplasmic in the neuroepithelial cells and neuroblasts within the late larval optic lobe (Figure 3-4). Sip1 also localized to the cytoplasm of the neuroblasts within the larval central brain (Figure 3-4), which will be analyzed and discussed further in Chapter 4. In addition, Sip1 localized to the neuroepithelial cells of the optic lobe and central brain neuroblasts during early larval stages (Figure 3-5). Given that Merlin and Sip1 localize within the developing optic lobes, we hypothesize that these proteins may be involved in neuroepithelial cell proliferation or differentiation.

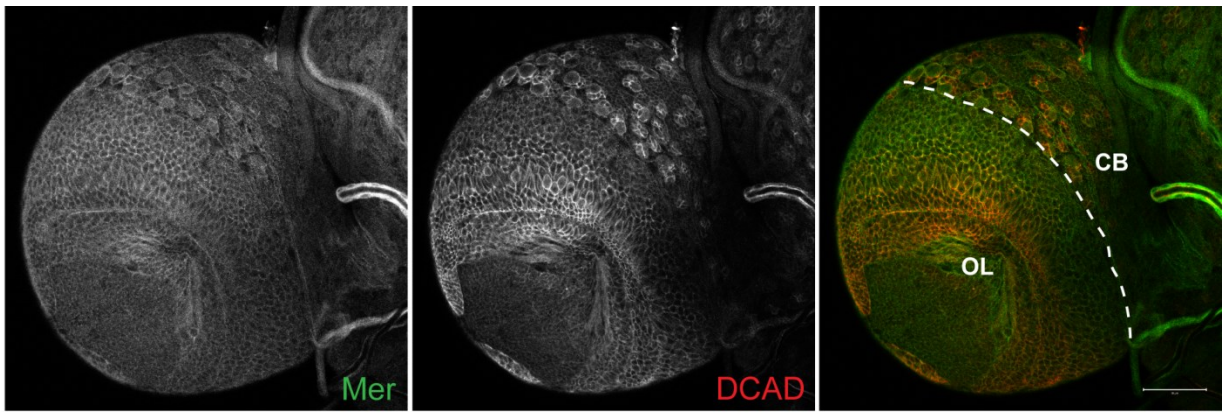

Figure 3-2: Merlin localizes ubiquitously in late larval brains. Third instar larval brain lobe fluorescently labelled with anti-Merlin (Mer; green) and anti-DE-Cadherin (DCAD; red). Merlin was ubiquitously localized in larval brain lobes and partially co-localized with DCAD at the cortex of neuroepithelial cells and neuroblasts within the optic lobe (OL), as shown in the merge. White dashed line in merge marks the boundary between the OL and central brain (CB). Scale bar represents 50 μm.

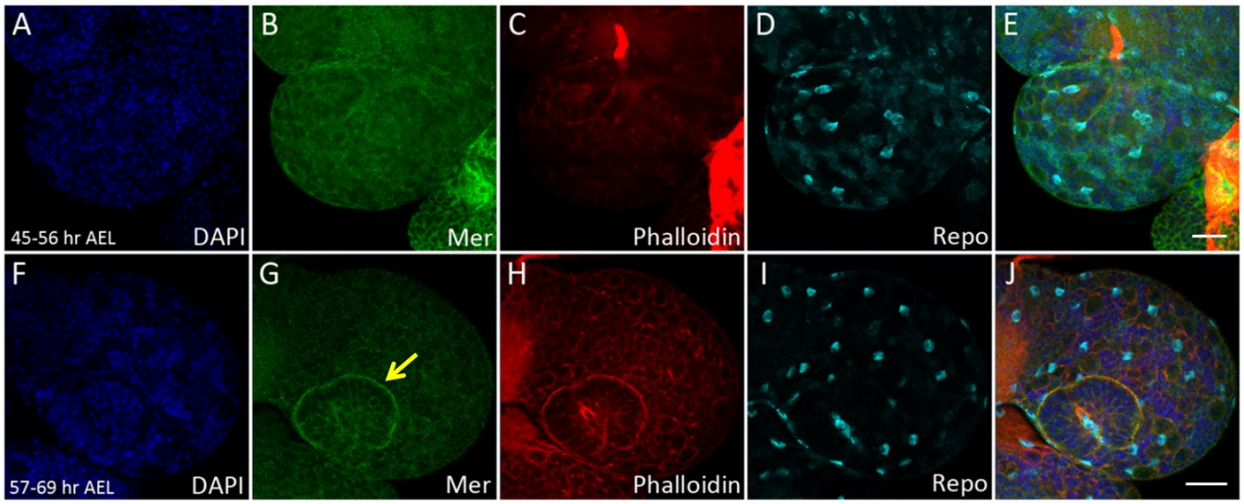

Figure 3-3: Merlin localization in the developing optic lobes during early larval stages. Brains dissected from *w*^{1118} larvae at (A-E) 45-56 hours (hr) after egg laying (AEL) and (F-J) 57-69 hr AEL. Larval brains were fluorescently labelled with DAPI (blue), anti-Merlin (green), Phalloidin (red), and anti-Repo (cyan). Merlin localized (B) ubiquitously in larval brain lobes at 45-56 hr AEL. (G) The Merlin immunofluorescent signal increased in the neuroepithelial cells of the optic lobe at 57-69 hr AEL, as indicated by the yellow arrow. Merge is shown in E and J. Scale bars represent 20 μm.

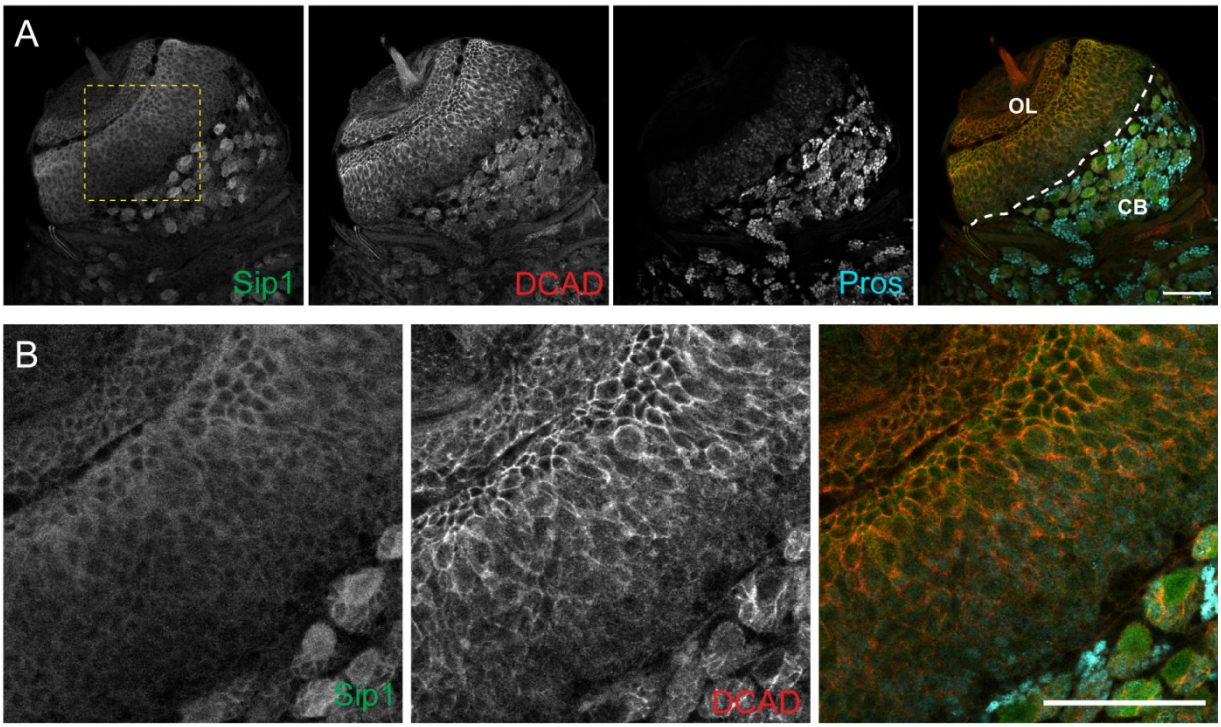

Figure 3-4: Sip1 localizes to the cortex and cytoplasm of the neuroepithelial cells and neuroblasts within the late larval optic lobes. (A-B) Third instar larval brain lobe fluorescently labelled with anti-Sip1 (green), anti-DE-Cadherin (DCAD; red), and anti-Prospero (cyan). The area outlined with the yellow dashed box in A corresponds to the zoomed images shown in B. Sip1 co-localized with DCAD at the cortex and localized to the cytoplasm of neuroepithelial cells and neuroblasts within the optic lobe (OL). Cytoplasmic Sip1 was observed in the neuroblasts of the central brain (CB). White dashed line in merge marks the boundary between the OL and CB. Scale bar represents 50 μm.

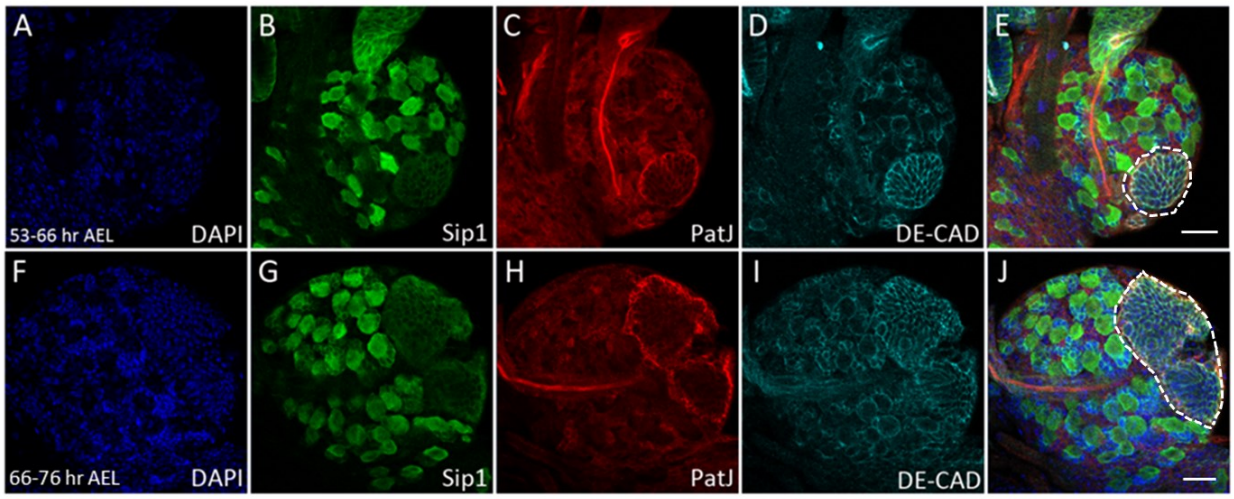

Figure 3-5: Sip1 localizes to the neuroepithelial cells and central brain neuroblasts during early larval stages. Brains dissected from w^{1118} larvae at (A-E) 53-66 hours (hr) after egg laying (AEL) and (F-J) 66-76 hr AEL. Larval brains were fluorescently labelled with DAPI (blue), anti-Sip1 (green), anti-PatJ (red), and anti-DE-Cadherin (DE-CAD; cyan). Sip1 localized to the neuroepithelial cells within the developing optic lobes and to the cytoplasm of central brain neuroblasts at (B) 53-66 hr and (G) 66-76 hr AEL. The developing optic lobe is outlined with the white dashed line in the merge shown in E and J. Scale bars represent 20 μm.

3.3.2 Investigation of Merlin function in the developing optic lobes

To determine whether Merlin was involved in optic lobe development, larval brains of *Merlin* hypomorphic mutants (*Mer*^{3}) (Fehon et al., 1997; LaJeunesse et al., 1998) were examined. The IPC and OPC appeared expanded in the *Merlin* hypomorphic mutant brains, as shown by the neuroepithelial cell-specific marker, PatJ (Figure 3-6) (Egger et al., 2007)). I did not observe defects in Sip1 localization in the *Merlin* hypomorphic mutant brains, although epithelial integrity appeared disorganized within the OPC, as indicated by DE-Cadherin localization (Figure 3-6). Thus, Merlin does not appear to alter Sip1 localization in the larval brain lobe but may affect neuroepithelial cell integrity, proliferation, or differentiation.

In addition, homozygous *Merlin* null mutants (*Mer*^{4}) (Fehon et al., 1997; LaJeunesse et al., 1998) were analyzed for defects in optic lobe development. The *Merlin* null mutant larval brain lobes displayed a similar phenotype to the *Merlin* hypomorphic mutants (Figure 3-7). *Merlin* null mutants displayed an expanded OPC, as shown by neuroepithelial cells marked by PatJ, and compared to *w*^{1118} controls (Figure 3-7, A-B). Conversely, the medulla neuroblast population (Dpn) appeared to be reduced in size in the *Merlin* mutant optic lobes, when compared to *w*^{1118} controls (Figure 3-7, A-B). In severe cases, the overall larval brain size appeared reduced, as optic lobe development was severely impaired in the *Merlin* mutants (Figure 3-7, C). Together, these findings suggest that Merlin is essential for proper optic lobe development.

To investigate whether the loss of Merlin affects the neuroepithelial to neuroblast transition, *Merlin* null mutant clones were generated at the proneural wavefront using the MARCM technique (Lee and Luo, 1999). When *Merlin* null mutant clones were generated in the developing optic lobe, GFP-positive clones were only observed in the dorsal and ventral tips of the OPC crescent (Figure 3-8, A). Defects in the neuroepithelial to neuroblast transition were not observed in the GFP-positive *Merlin* mutant clones, relative to the surrounding non-GFP cells (Figure 3-8, B). However, neuroepithelial cell size appeared reduced in the *Merlin* mutant clones, when compared to the surrounding wild-type neuroepithelial cells (Figure 3-8, B). Thus, the loss of Merlin within the dorsal and ventral tips of the OPC does not alter neuroepithelial cell differentiation but may reduce neuroepithelial cell size.

As generating *Merlin* null mutant clones in the neuroepithelial cells did not alter the proneural wavefront, it is possible that Merlin may function in a different cell type during optic lobe development. Therefore, Merlin was reduced in a tissue-specific manner using the UAS/GAL4 system (Brand and Perrimon, 1993) and the larval optic lobe was examined. To

confirm the *Merlin* hypomorphic and null mutant phenotypes, I initially analyzed the ubiquitous knockdown of Merlin using *actin-GAL4*. To further enhance Merlin knockdown levels, Merlin dsRNA was over-expressed along with Dicer. Similar to *Merlin* mutant larval brains, the ubiquitous Merlin knockdown resulted in an expanded neuroepithelial cell population, compared to controls (Figure 3-9, PatJ panels). Furthermore, there appeared to be a reduction in medulla neuroblasts and epithelial integrity was severely disrupted (Figure 3-9, C-D; Dpn and DCAD panels). The neuroepithelial cells also appeared reduced in size with the ubiquitous knockdown of Merlin (Figure 3-9, C-D; PatJ panels). Thus, the phenotypes observed in the optic lobe when Merlin was ubiquitously reduced, were very similar to the *Merlin* hypomorphic and null mutants. Together, these findings confirm that Merlin is essential for optic lobe development.

To further examine the specific cell type that Merlin may function in during optic lobe development, dsRNA-mediated knockdown of Merlin was performed in the neuroblasts using *Insc-GAL4* and in the neuroepithelial cells using *c855a-GAL4* (Egger et al., 2007; Hrdlicka et al., 2002; Manseau et al., 1997). Merlin knockdown in the neuroblasts and neuroepithelial cells did not lead to obvious defects in the neuroepithelial cells (PatJ) or medulla neuroblasts (Miranda), when compared to the w^{1118} and Dicer controls (Figure 3-10). In addition, epithelial integrity within the optic lobe appeared normal in these tissue-specific Merlin knockdowns (Figure 3-10, DCAD panels). I also examined phospho-histone H3 and showed that there was no obvious difference in the mitotic cells when Merlin was knocked down using *Insc-GAL4* and *c855a-GAL4* (Figure 3-11). Merlin was also knocked down in differentiated cells, including the glial cells (*Repo-GAL4*) and ganglion mother cells (*Prospero-GAL4*). Merlin knockdown in differentiated cells did not alter the neuroepithelial cells (PatJ) or medulla neuroblasts (Miranda) within the optic lobe, when compared to w^{1118} and Dicer controls (Figure 3-12). Furthermore, epithelial integrity within the optic lobe was also largely normal (Figure 3-12, DCAD panels).

In Drosophila, eye and optic lobe development are closely linked as the development of the lamina depends on innervating retinal axons from the eye (Selleck and Steller, 1991). Thus, I examined whether Merlin knockdown using eye-specific GAL4 drivers altered optic lobe development. When Merlin was knocked down using *Eyeless-GAL4* and *GMR-GAL4*, overall defects in mitotic cells (phospho-histone H3), neuroblasts (Miranda), and larval brain morphology were not observed, when compared to controls (Figure 3-13). Thus, reducing Merlin in the eyes did not alter optic lobe development. As I was not able to identify a specific cell type that required Merlin function, it is possible that Merlin is essential in multiple tissues during optic lobe development.

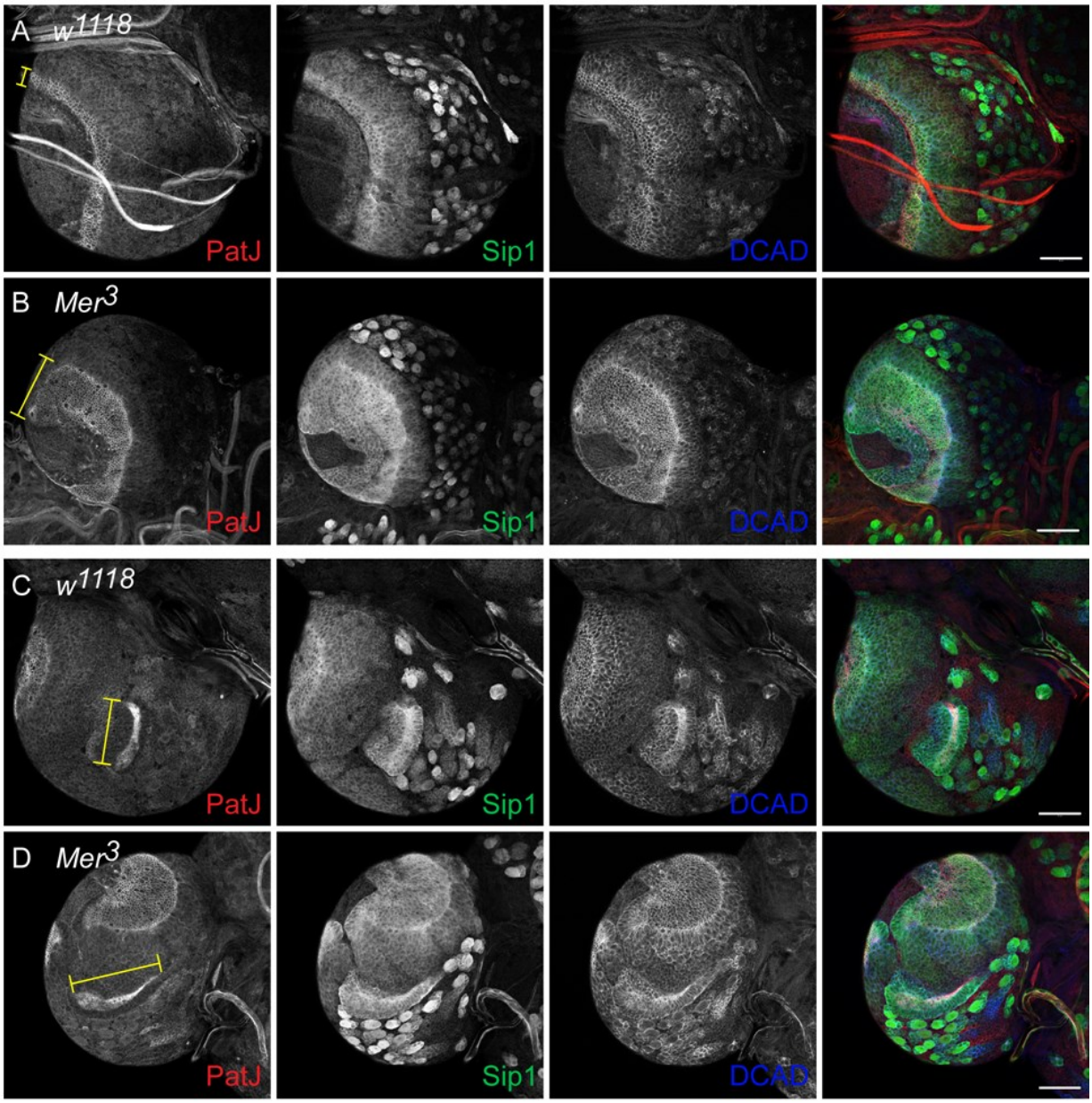

Figure 3-6: Merlin hypomorphic mutants display expanded proliferation centers within the developing optic lobe. Third instar larval brain lobes of (A and C) w^{1118} and (B and D) $y^{-}w^{-}Mer^{3}$/Y (Mer^{3}) males. Larval brains were fluorescently labelled with anti-PatJ (red), anti-Sip1 (green), and anti-DE-Cadherin (DE-CAD; blue) as shown in merge. (A-B) The width of the outer proliferation centers (OPCs) and (C-D) the length of the inner proliferation centers (IPCs) of the optic lobe are indicated by the yellow brackets. (B and D) Merlin hypomorphic mutant brains displayed an expanded OPC and IPC, when compared to respective (A and C) w^{1118} controls. Scale bars represent 50 µm.

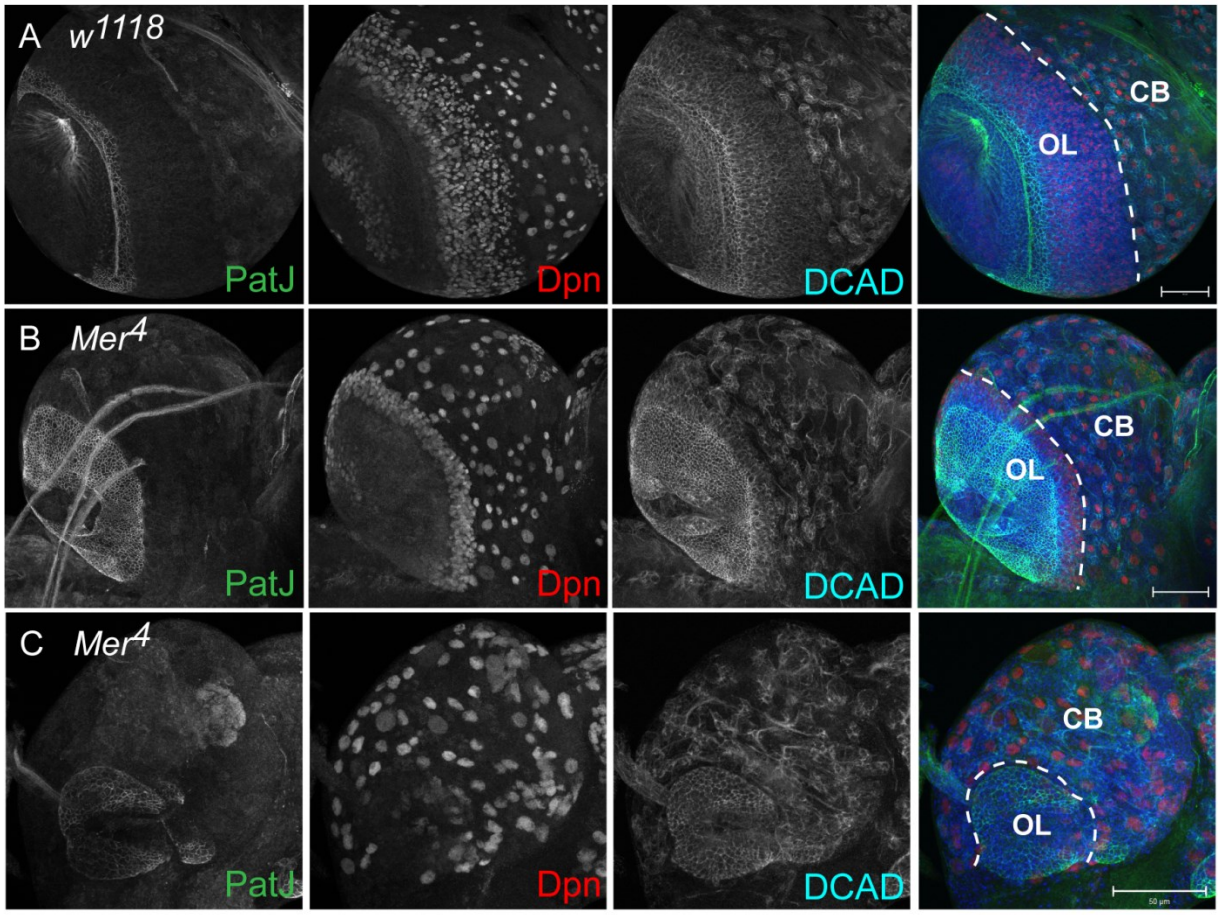

Figure 3-7: *Merlin* null mutants display an expanded neuroepithelial cell population and a reduction in neuroblasts. Third instar larval brains of (A) w^{1118} and (B-C) *Merlin* null mutant (Mer^{4}) males were fluorescently labelled for DAPI, anti-PatJ (green), anti-Deadpan (Dpn; red), and anti-DE-Cadherin (DCAD; cyan) as shown in merge. (B) *Merlin* mutants displayed an expanded neuroepithelial cell population (PatJ region) and a reduction in neuroblasts (Dpn region) within the optic lobe (OL), compared to w^{1118} larval OLs. (C) In severe cases, the neuroepithelial cells have not proliferated nor differentiated into neuroblasts in the *Merlin* mutant brains, as indicated by reduced OL size and the lack of neuroblasts within the OL. Images are maximum intensity projections and white dashed line in merge marks the boundary between the OL and central brain (CB). Scale bars represent 50 μm.

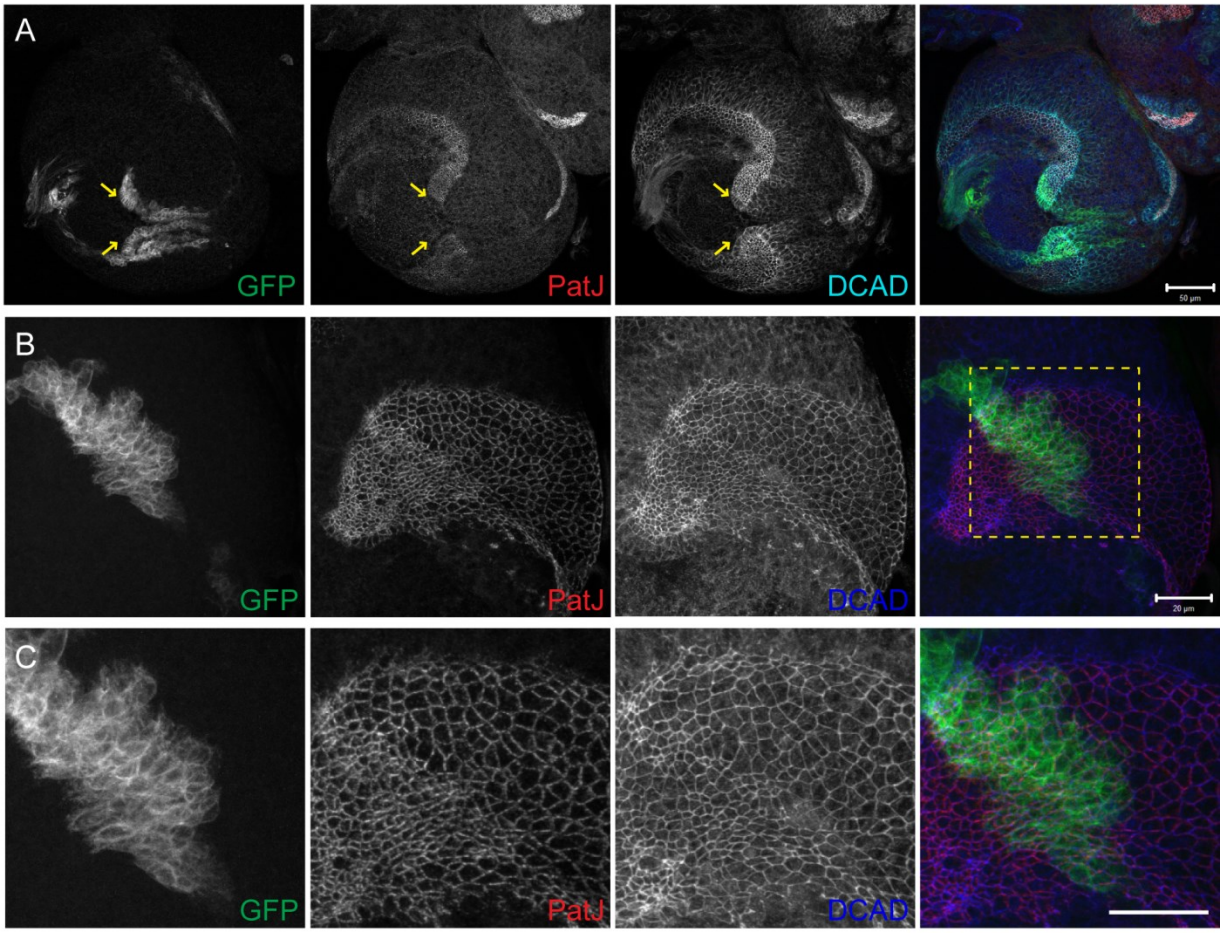

Figure 3-8: The loss of Merlin at the proneural wavefront does not alter the neuroepithelial to neuroblast transition. *Merlin* null mutant clones were generated using MARCM and positively labelled with mCD8::GFP (GFP). Larval brains were fluorescently labelled with DAPI (blue) in A, anti-GFP (green), anti-PatJ (red), and anti-DE-Cadherin (DCAD; cyan in A and blue in B and C), as shown in merge. (A) *Merlin* mutant clones (GFP-positive) were observed in the dorsal and ventral tips of the OPC crescent, as indicated by yellow arrows. (B-C) *Merlin* mutant clones did not alter the neuroepithelial to neuroblast transition but the apical domain appeared reduced in size, when compared to surrounding non-GFP wild-type cells. The area outlined with the yellow dashed box in B represents the zoomed images shown in C. (A) Single focal plane and (B-C) maximum intensity projection images are shown. Scale bars represent (A) 50 μm and (B-C) 20 μm.

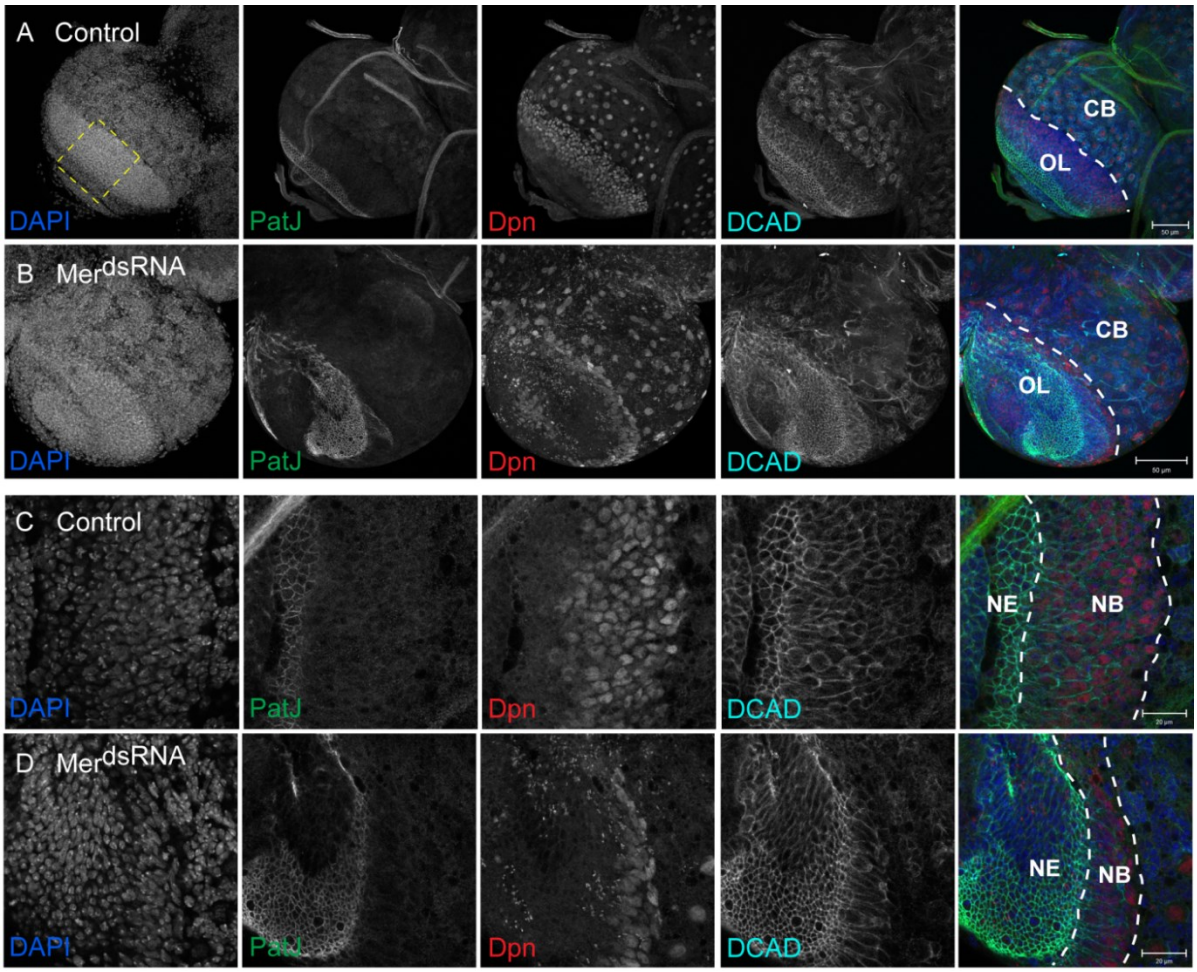

Figure 3-9: Ubiquitous Merlin knockdown displays an expanded neuroepithelial cell population and a reduction in neuroblasts. The ubiquitous GAL4 driver, *actin-GAL4*, was crossed to (A and C) w^{1118} (Control) and (B and D) *UAS-Dicer*;;*UAS-Merlin*^{dsRNA} (Mer^{dsRNA}) and third instar larval brains were fluorescently labelled with DAPI, anti-PatJ (green), anti-Deadpan (Dpn; red), and anti-DE-Cadherin (DCAD; cyan) as shown in merge. (C-D) Magnified images of the optic lobe (OL) areas, indicated by the yellow dashed box in A. (B and D) Merlin knockdown displayed an expanded neuroepithelial cell layer (NE; PatJ region) and a reduction in neuroblasts (NB; Dpn region) within the OL, compared to (A and C) control OLs. (D) Epithelial integrity of the NBs within the OL, as shown in DCAD panels, was disorganized in Merlin knockdown, compared to (C) controls. Images are maximum intensity projections and white dashed line in merge marks the boundary between either (A-B) the OL and central brain (CB) within the larval brain lobe and (C-D) the NE and NB within the larval optic lobe. Scale bars represent (A-B) 50 µm and (C-D) 20 µm.

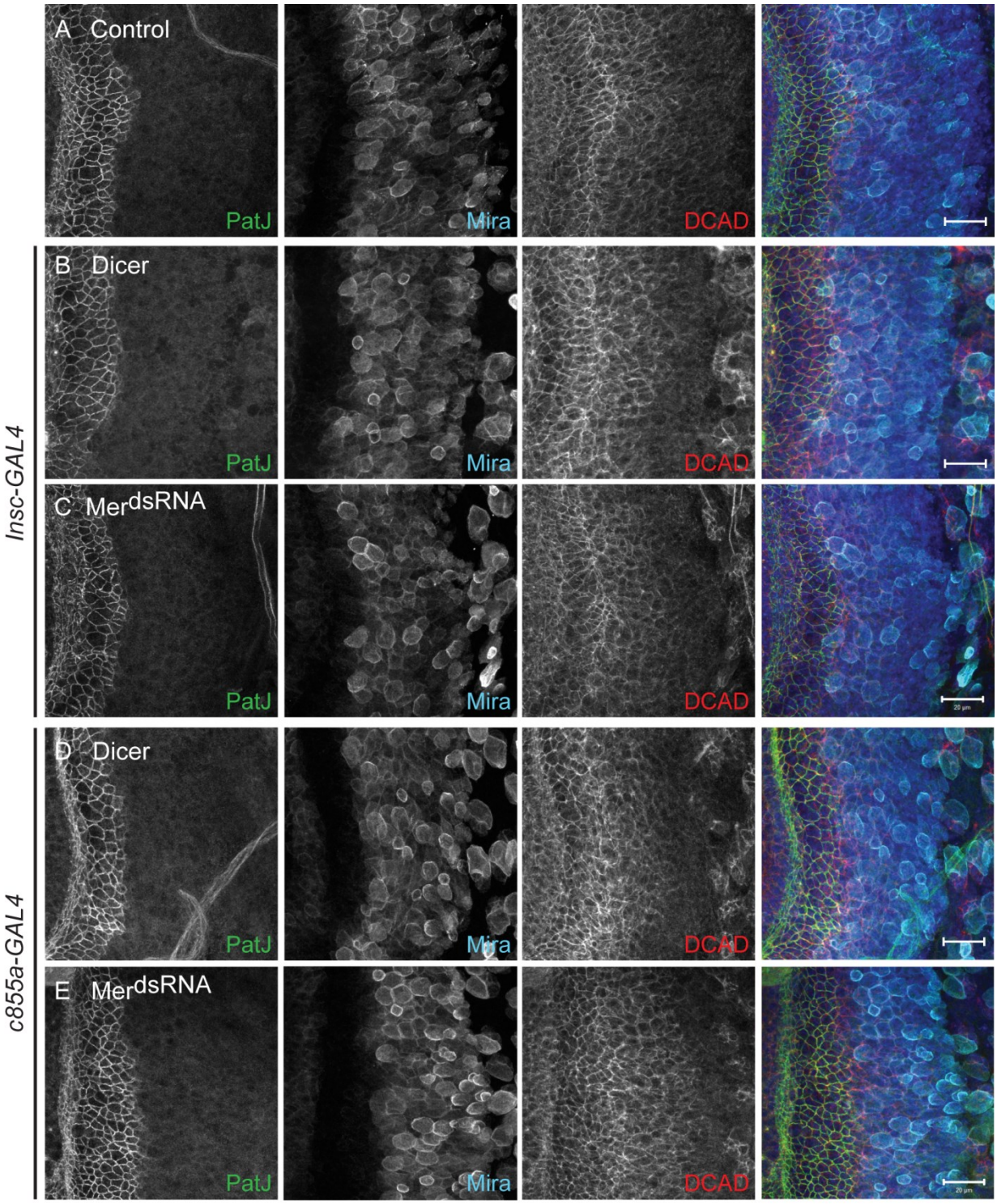
A Control
PatJ
Mira
DCAD
B Dicer
PatJ
Mira
DCAD
C MerdsRNA
PatJ
Mira
DCAD
Insc-GAL4
D Dicer
PatJ
Mira
DCAD
E MerdsRNA
PatJ
Mira
DCAD
c855a-GAL4

Figure 3-10: Merlin knockdown using neuroblast and neuroepithelial cell-specific GAL4 drivers do not alter the neuroepithelial cells or the neuroblasts within the optic lobe. Third instar larval brains were dissected from progeny of *UAS-Dicer*;;*UAS-Merlin*^{dsRNA} (Mer^{dsRNA}) crossed to (A) *w*^{1118} (Control), (C) *Insc-GAL4*, and (E) *c855a-GAL4*. *UAS-Dicer* (Dicer) was crossed to (B) *Insc-GAL4* and (D) *c855a-GAL4* for Dicer controls. Larval brains were fluorescently labelled with DAPI, anti-PatJ (green), anti-Miranda (Mira; cyan), and anti-DE-Cadherin (DCAD; red) as shown in merge. Merlin knockdown using (C) the neuroblast GAL4 driver, *Insc-GAL4*, and (E) the optic lobe GAL4 driver, *c855a-GAL4*, did not alter the neuroepithelial cells (PatJ), the neuroblasts (Mira), nor epithelial integrity (DCAD) within the optic lobe, when compared to (A) *w*^{1118} and (B and D) respective Dicer controls. Images are maximum intensity projections. Scale bars represent 20 μm.

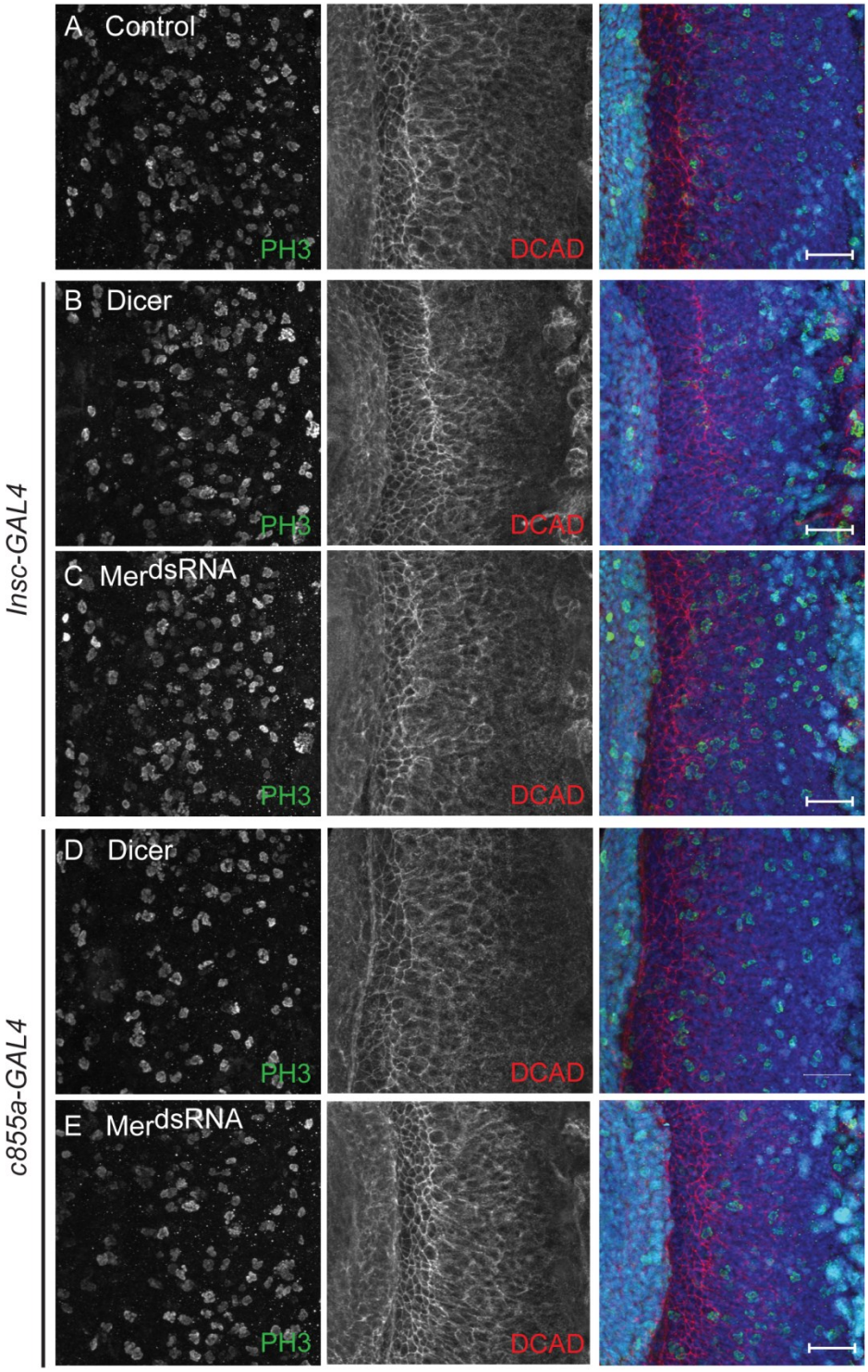
A Control
PH3
DCAD
B Dicer
PH3
DCAD
C Mer^dsRNA
PH3
DCAD
Insc-GAL4
D Dicer
PH3
DCAD
E Mer^dsRNA
PH3
DCAD
c855a-GAL4

Figure 3-11: Merlin knockdown using neuroblast and neuroepithelial cell-specific GAL4 drivers do not alter proliferation within the optic lobe. Third instar larval brains were dissected from progeny of *UAS-Dicer*;;*UAS-Merlin*^{dsRNA} (Mer^{dsRNA}) crossed to (A) *w*^{1118} (Control), (C) *Insc-GAL4*, and (E) *c855a-GAL4*. *UAS-Dicer* (Dicer) was crossed to (B) *Insc-GAL4* and (D) *c855a-GAL4* for Dicer controls. Larval brains were fluorescently labelled with DAPI, anti-phospho-histone H3 (PH3; green), anti-Dachshund (cyan), and anti-DE-Cadherin (DCAD; red) as shown in merge. Merlin knockdown using (C) the neuroblast GAL4 driver, *Insc-GAL4*, and (E) the optic lobe GAL4 driver, *c855a-GAL4*, did not alter proliferation (PH3) nor epithelial integrity (DCAD) within the optic lobe, when compared to (A) *w*^{1118} and (B and D) respective Dicer controls. Images are maximum intensity projections. Scale bars represent 20 μm.

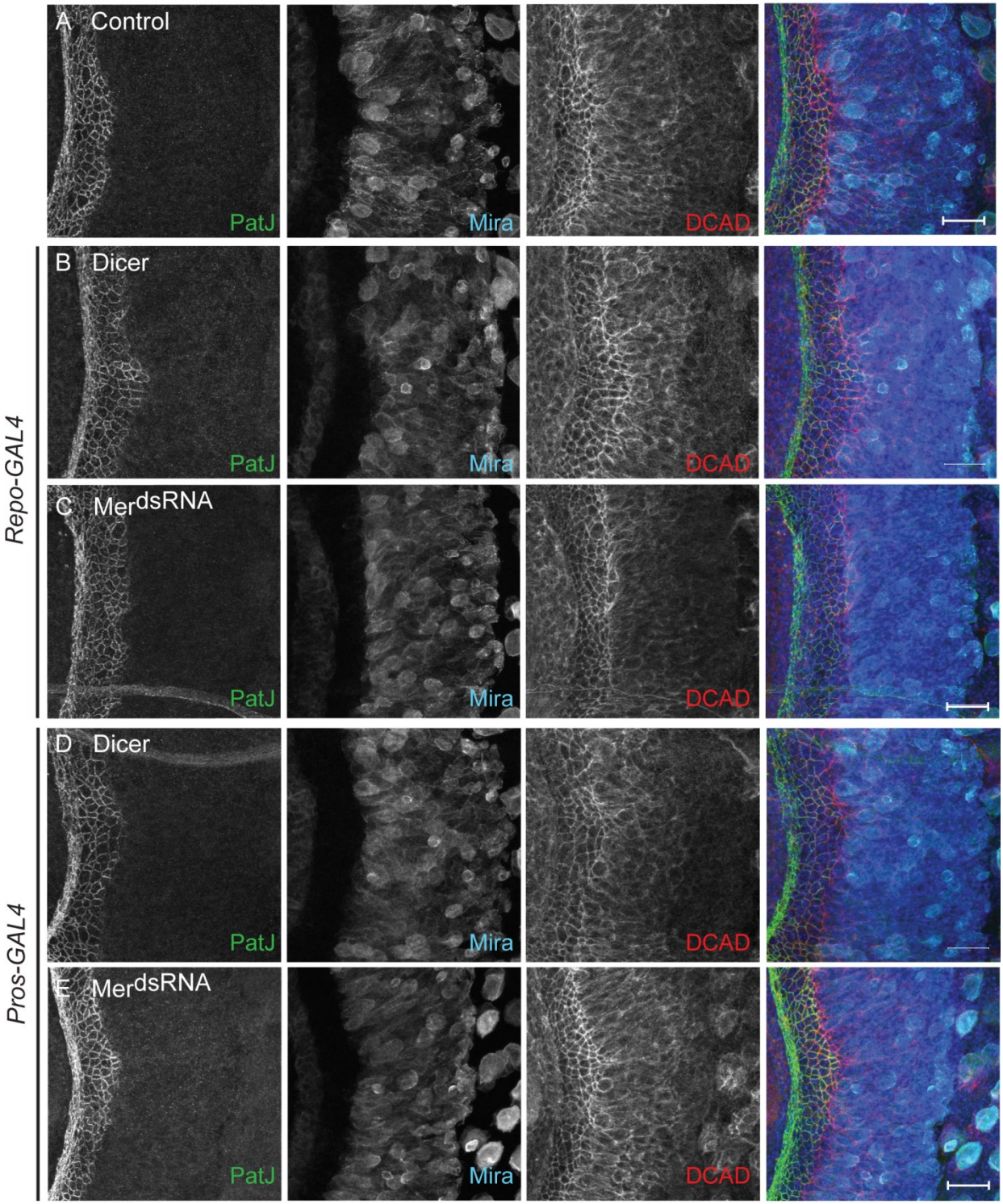
A Control
PatJ
Mira
DCAD
B Dicer
PatJ
Mira
DCAD
C MerdsRNA
PatJ
Mira
DCAD
Repo-GAL4
D Dicer
PatJ
Mira
DCAD
E MerdsRNA
PatJ
Mira
DCAD
Pros-GAL4

Figure 3-12: Merlin knockdown using differentiated cell-specific GAL4 drivers do not alter the neuroepithelial cells or neuroblasts within the optic lobe. Third instar larval brains were dissected from progeny of *UAS-Dicer*;;*UAS-Merlin*^{dsRNA} (Mer^{dsRNA}) crossed to (A) *w*^{1118} (Control), (C) *Repo-GAL4*, and (E) *Prospero (Pros)-GAL4*. *UAS-Dicer* (Dicer) was crossed to (B) *Repo-GAL4* and (D) *Pros-GAL4* for Dicer controls. Larval brains were fluorescently labelled with DAPI, anti-PatJ (green), anti-Miranda (Mira; cyan), and anti-DE-Cadherin (DCAD; red) as shown in merge. Merlin knockdown using (C) the glial-cell specific GAL4 driver, *Repo-GAL4*, and (E) the ganglion mother cell-specific GAL4 driver, *Pros-GAL4*, did not alter the neuroepithelial cells (PatJ), the neuroblasts (Mira), nor epithelial integrity (DCAD) within the optic lobe, when compared to (A) *w*^{1118} and (B and D) respective Dicer controls. Images are maximum intensity projections. Scale bars represent 20 μm.

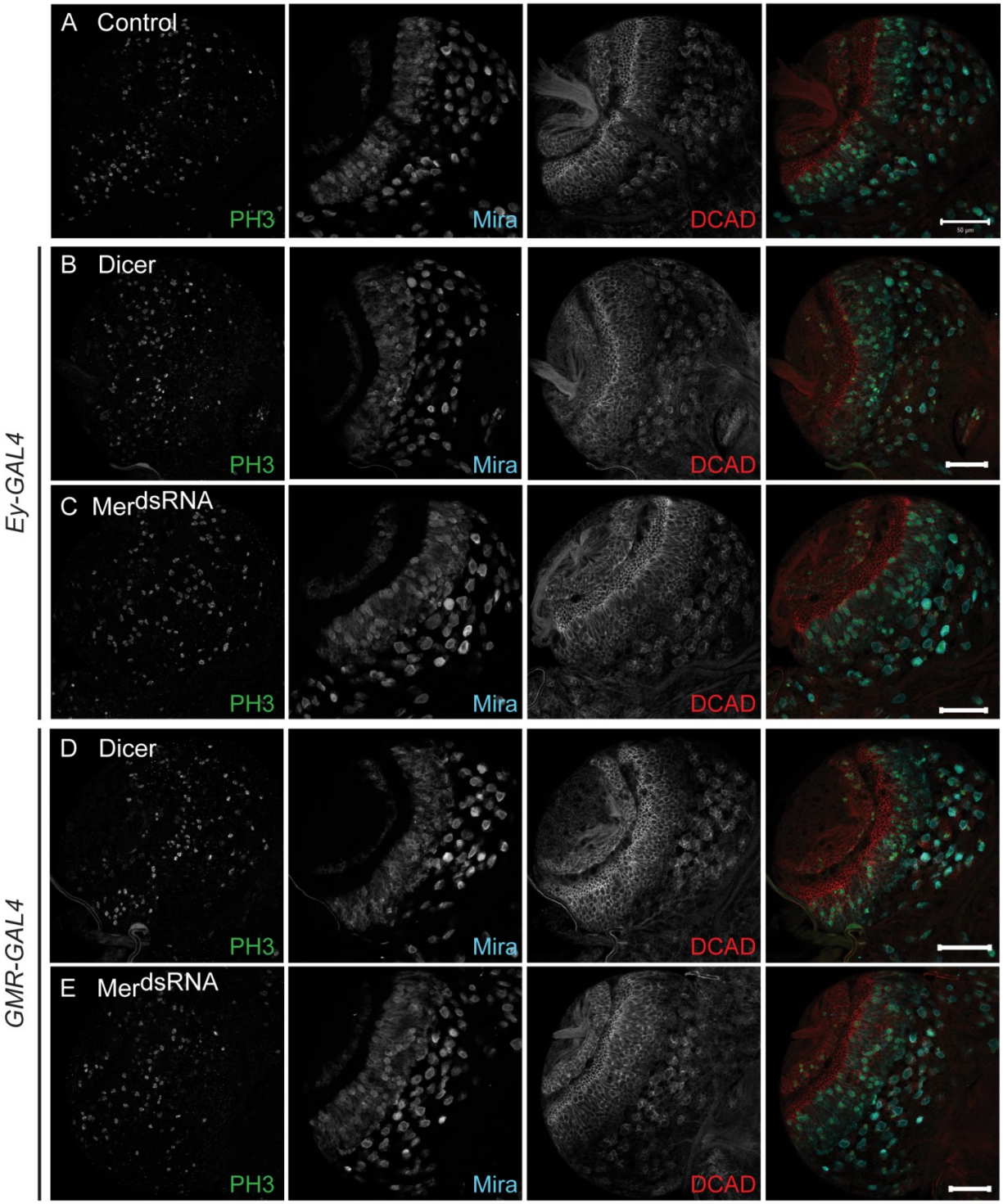
A Control
PH3
Mira
DCAD
B Dicer
PH3
Mira
DCAD
C MerdsRNA
PH3
Mira
DCAD
D Dicer
PH3
Mira
DCAD
E MerdsRNA
PH3
Mira
DCAD
Ey-GAL4
GMR-GAL4

Figure 3-13: Merlin knockdown using eye-specific GAL4 drivers do not alter optic lobe development. Third instar larval brains were dissected from progeny of *UAS-Dicer*;;*UAS-Merlin*^{dsRNA} (Mer^{dsRNA}) crossed to (A) *w*^{1118} (Control), (C) *Eyeless (Ey)-GAL4*, and (E) *GMR-GAL4*. *UAS-Dicer* (Dicer) was crossed to (B) Ey-*GAL4* and (D) *GMR-GAL4* for Dicer controls. Larval brains were fluorescently labelled with anti-phospho-histone H3 (PH3; green), anti-Miranda (Mira; cyan), and anti-DE-Cadherin (DCAD; red) as shown in merge. Merlin knockdown using eye-specific GAL4 drivers, (C) *Ey-GAL4* and (E) *GMR-GAL4*, did not alter proliferation (PH3), the neuroblasts (Mira), nor overall brain morphology, when compared to (A) *w*^{1118} and (B and D) respective Dicer controls. Images are maximum intensity projections. Scale bars represent 50 μm.

3.3.3 Investigation of Sip1 function in the developing optic lobes

Sip1 localization within the neuroepithelial cells and medulla neuroblasts of the optic lobe (Figure 3-4), suggests that Sip1 may be involved in larval optic lobe development. To determine the functional significance of Sip1 in the larval optic lobe, dsRNA-mediated knockdown of Sip1 was performed in a ubiquitous manner using *actin-GAL4*. The ubiquitous knockdown of Sip1 resulted in abnormal optic lobe development (Figure 3-14). The neuroepithelial cell size (PatJ) appeared reduced in the ubiquitous Sip1 knockdown, compared to the controls (Figure 3-14, C-D). Furthermore, there was a reduction in the medulla neuroblast population (Dpn) and epithelial integrity (DCAD) was severely disorganized (Figure 3-14, C-D). Thus, Sip1 appears to be important for optic lobe development and organization.

To identify the specific cell type that Sip1 may function in during optic lobe development, Sip1 was reduced using *Insc-GAL4*, *c855a-GAL4*, and *Repo-GAL4*. I found that when Sip1 was knocked down in the neuroblasts (*Insc-GAL4*) and optic lobe (*c855a-GAL4*), the neuroepithelial cells (PatJ), the medulla neuroblasts (Miranda), and epithelial integrity (DCAD) were largely unaffected, when compared to controls (Figure 3-15, A-C). However, Sip1 knockdown in the glial cells using *Repo-GAL4* resulted in the appearance of fewer medulla neuroblasts, compared to controls (Figure 3-15, A and D; outlined with yellow dashed lines). Furthermore, the neuroepithelial cell size appeared slightly reduced in the glial-specific Sip1 knockdown (Figure 3-15). Thus, reduced Sip1 in the glial cells appeared to affect optic lobe development.

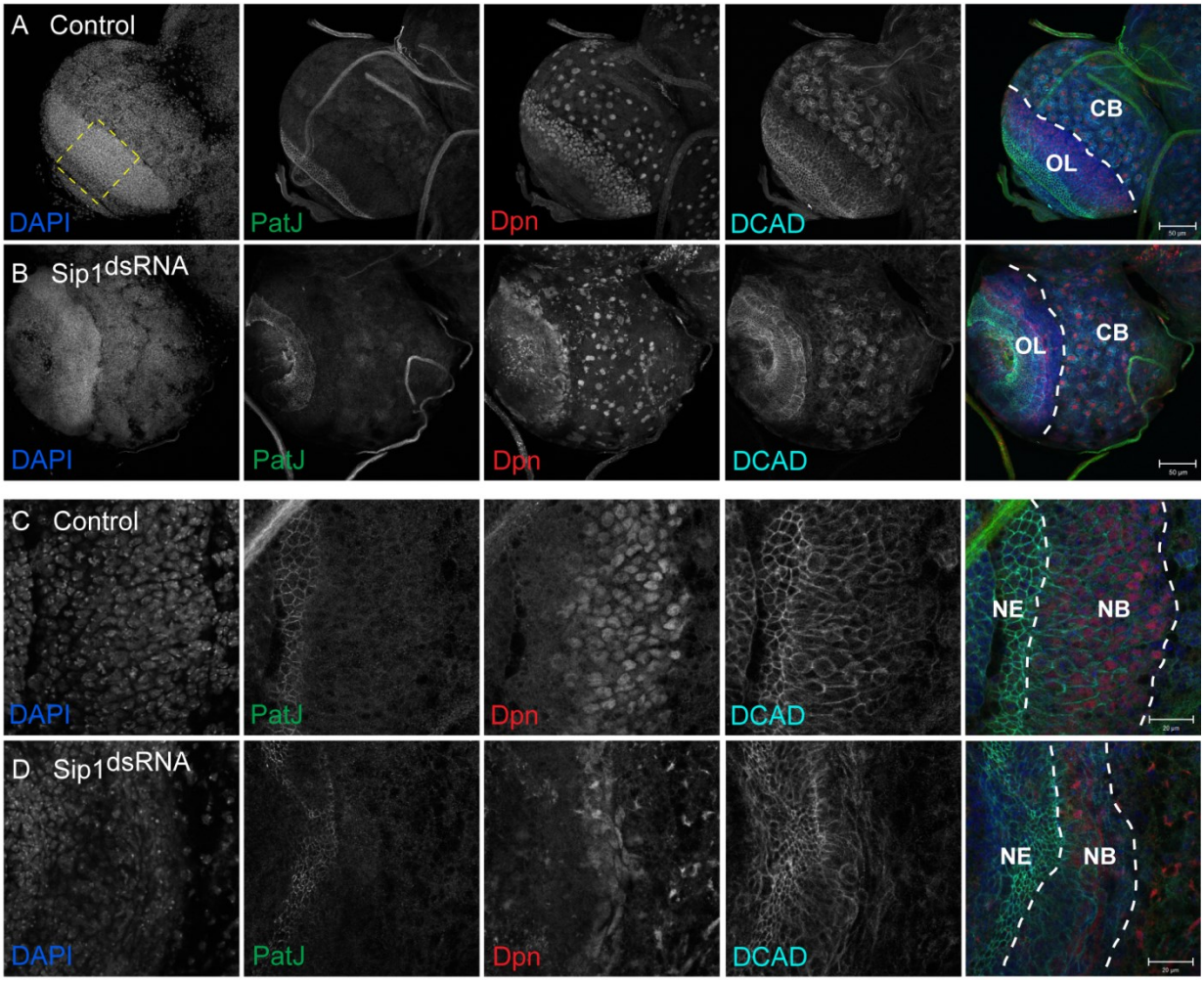

Figure 3-14: Ubiquitous Sip1 knockdown alters optic lobe development. The ubiquitous GAL4 driver, *actin-GAL4*, was crossed to (A and C) w^{1118} (Control) and (B and D) *UAS-Dicer*;;*UAS-Sip1*^{dsRNA} (Sip1^{dsRNA}) and third instar larval brains were fluorescently labelled with DAPI, anti-PatJ (green), anti-Deadpan (Dpn; red), and anti-DE-Cadherin (DCAD; cyan) as shown in merge. (C-D) Magnified images of the optic lobe (OL) region, indicated by the yellow dashed box in A. (B and D) The apical domain of the neuroepithelial cells (NE; PatJ) appeared reduced and fewer neuroblasts (NB; Dpn) were observed in the OL of the Sip1 knockdown, compared to (A and C) control OLs. (D) Epithelial integrity of the NE cells and NBs within the OL, as shown in DCAD panels, was disorganized in Sip1 knockdown, compared to (C) controls. Images are maximum intensity projections and white dashed line in merge marks the boundary between either (A-B) the OL and central brain (CB) within the larval brain lobe and (C-D) the NE and NB within the larval optic lobe. Scale bars represent (A-B) 50 µm and (C-D) 20 µm.

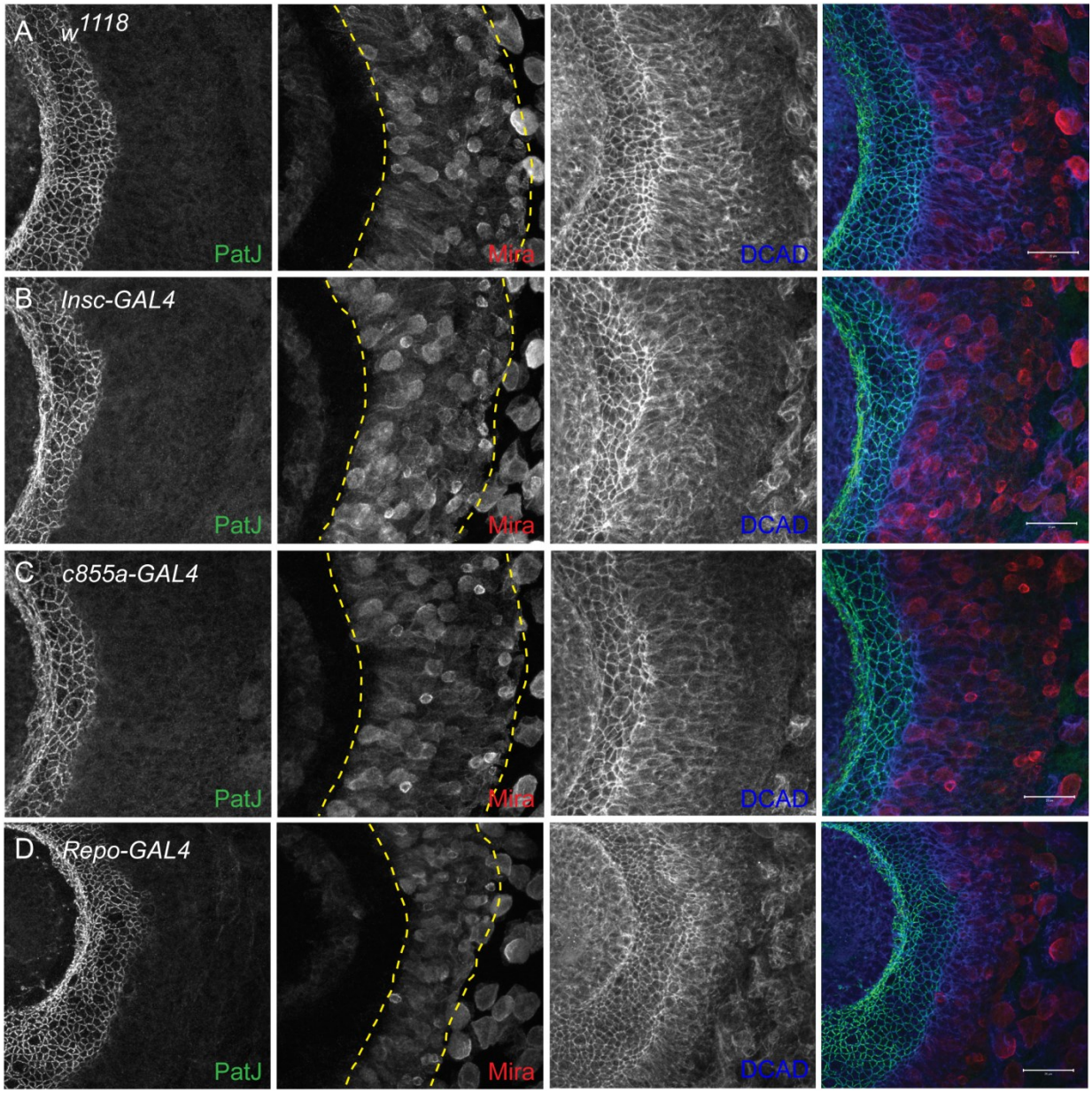
A
w1118
PatJ
Mira
DCAD
B
Insc-GAL4
PatJ
Mira
DCAD
C
c855a-GAL4
PatJ
Mira
DCAD
D
Repo-GAL4
PatJ
Mira
DCAD

Figure 3-15: Sip1 knockdown using tissue-specific GAL4 drivers and optic lobe development. Third instar larval brains were dissected from progeny of *UAS-Dicer*;;*UAS-Sip1*^{dsRNA} crossed to (A) *w*^{1118} (Control), (B) *Insc-GAL4*, (C) *c855a-GAL4*, and (D) *Repo-GAL4*. Larval brains were fluorescently labelled with anti-PatJ (green), anti-Miranda (Mira; red), and anti-DE-Cadherin (DCAD; blue) as shown in merge. Sip1 knockdown using (B) the neuroblast GAL4 driver, *Insc-GAL4*, and (C) the optic lobe GAL4 driver, *c855a-GAL4*, did not alter the neuroepithelial cells (PatJ), the neuroblasts (Mira), nor epithelial integrity (DCAD) within the optic lobe, when compared to (A) *w*^{1118} controls. (D) Sip1 knockdown using the glial-specific GAL4 driver, *Repo-GAL4*, resulted in the appearance of fewer neuroblasts (Mira) within the OL, when compared (A) *w*^{1118} controls. Images are maximum intensity projections. Scale bars represent 20 μm.

3.4 DISCUSSION AND FUTURE DIRECTIONS

I found that the loss of Merlin led to defects in larval optic lobe development, suggesting a functional role for Merlin during neuroepithelial cell proliferation or differentiation, which occur during larval development (Egger et al., 2007). In both *Merlin* hypomorphic and null mutant larval brains, the neuroepithelial cell population within the OPC appeared expanded, with an appearance of a reduced medulla neuroblast population compared to controls. These findings suggest that Merlin may inhibit the symmetric cell divisions that increase the neuroepithelial cell population or Merlin may promote the neuroepithelial to neuroblast transition.

To confirm these findings, *Merlin* null mutant clones were generated at the proneural wavefront located at the medial edge of the OPC. If Merlin promoted the neuroepithelial to neuroblast transition, I would have expected a delay in proneural wave progression in the *Merlin* mutant clones compared to the surrounding wild-type cells. However, when *Merlin* null mutant clones were generated at the proneural wavefront, neuroepithelial cell differentiation into neuroblasts was not affected. Instead, the apical domain of the neuroepithelial cells appeared reduced in size. Furthermore, the PatJ immunofluorescent signal appeared elevated with the loss of Merlin. In Drosophila imaginal discs, the simultaneous loss of Merlin and Expanded also resulted in elevated levels of apical determinants aPKC, Crumbs, and PatJ, with the appearance of a reduced apical domain area of these epithelial cells (Hamaratoglu et al., 2009). Thus, Merlin may also be involved in maintaining the apical domain in neuroepithelial cells. In addition, I found that *Merlin* null mutant clones were commonly generated in the ventral or dorsal tips of the OPC. The OPC can be subdivided into at least six known compartments defined by the expression of certain factors (Erclik et al., 2008; Erclik et al., 2017; Gold and Brand, 2014; Kaphingst and Kunes, 1994). Wingless and the TGF-β family member, Decapentaplegic, have been shown to be expressed in adjacent domains at the ventral and dorsal tips of the OPC (Kaphingst and Kunes, 1994), where *Merlin* null mutant clones were generated. Furthermore, the neuroepithelial cells of the Wingless domain appear to behave in a distinct manner compared to the rest of the OPC (Bertet et al., 2014; Chen et al., 2016). It is possible that the *Merlin* null mutant clones generated in the non-Wingless or non–Decapentaplegic expressing cells of the OPC may result in cell death and extrusion of the neuroepithelial cells, thus explaining the lack of *Merlin* null mutant clones generated in these domains of the OPC. To address this possibility, further studies may require the co-expression of an inhibitor of apoptosis, p35 (Zhou et al., 1997), along with the *Merlin* null mutant to investigate the potential functional significance of Merlin in these regions of the OPC.

Alternatively, it was shown that *pointed* mutant clones were not generated in the neuroepithelial cell region unless the *Minute* technique was performed (Morata and Ripoll, 1975; Yasugi et al., 2010). Thus, future studies could address the functional significance of Merlin in neuroepithelial cells by utilizing the *Minute* technique with mosaic analysis.

To determine the specific cell type that requires Merlin function for optic lobe development, dsRNA-mediated knockdown of Merlin in a tissue-specific manner was performed using the UAS/GAL4 system. The ubiquitous knockdown of Merlin resulted in similar defects in the optic lobe as the *Merlin* hypomorphic and null mutants, confirming that Merlin is essential for optic lobe development. However, when Merlin was knocked down specifically in the individual cells of the optic lobe (neuroblasts, neuroepithelial cells, glial cells, ganglion mother cells, or eye imaginal discs), I did not find any observable defects in the optic lobe. It is possible that Merlin may be required in multiple tissues during optic lobe development. Previously, it was shown that early neuroepithelial cell expansion is dependent on nutrients via Insulin/PI3K signaling (Lanet et al., 2013). As optic lobe development was severely disrupted in *Merlin* null mutant brains, it is possible that Merlin may not function within the optic lobe itself but is important for activating a systemic signal required for optic lobe development in the fat body. Therefore, loss of Merlin in a fat body-specific manner may reveal the functional significance of Merlin during optic lobe development. It is important to note that during my analysis, I focused on neuroepithelial cell differentiation into medulla neuroblasts at the medial edge of the OPC. However, the neuroepithelial cells also differentiate into lamina precursor cells at the lateral edge of the OPC by means of an entirely different mechanism (Huang and Kunes, 1996; Huang and Kunes, 1998; Selleck et al., 1992; Selleck and Steller, 1991). Therefore, analysis of neuroepithelial cell differentiation at the lateral edge of the OPC may be essential to address the functional role of Merlin during optic lobe development.

Sip1 also localized to the neuroepithelial cells and medulla neuroblasts. The ubiquitous knockdown of Sip1 led to defects in optic lobe development. Sip1 was shown to be important for epithelial integrity of the optic lobe, as the neuroepithelial cells and medulla neuroblasts appeared disorganized. Furthermore, the medulla neuroblast population appeared to be reduced with the loss of Sip1, suggesting that Sip1 is essential for medulla neuroblast formation or maintenance. When Sip1 was knocked down in a tissue-specific manner in the neuroblasts and the neuroepithelial cells, optic lobe development at the medial edge of the OPC was not affected. However, when Sip1 was knocked down in the glial cells, the medulla neuroblast population appeared reduced. Thus, Sip1 function in the glial cells may be essential for the neuroepithelial to neuroblast transition at the medial

edge of the OPC or medulla neuroblast differentiation. Early studies have shown that glial cells can affect optic lobe organization and development (Ebens et al., 1993). Recently, the perineurial and subperineurial glial subtypes that ensheath the Drosophila central nervous system (Awasaki et al., 2008; Bainton et al., 2005; Pereanu et al., 2005; Schwabe et al., 2005; Stork et al., 2008), were shown to express the Notch ligand, Serrate (Perez-Gomez et al., 2013). The generation of *serrate* mutant clones in the glial cells resulted in ectopic L(1)sc localization in the underlying neuroepithelial cells, thus affecting the neuroepithelial to neuroblast transition (Perez-Gomez et al., 2013). Furthermore, a distinct population of cortex glia associated with the optic lobe have also been shown to regulate neuroepithelial growth and differentiation (Morante et al., 2013). Thus, the interaction between the surrounding glia and neuroepithelial cells are important for optic lobe development. The optic lobe-associated cortex glia express the Drosophila microRNA, *miR-8*, which regulates glial cell morphology and neuroblast formation in the developing optic lobe (Morante et al., 2013). Interestingly, *EBP50* mRNA was identified as a target of the *miR-8* family in zebrafish embryos (Chen et al., 2005; Flynt et al., 2009). Thus, it is possible that Drosophila *miR-8* regulates Sip1 levels in the cortex glia surrounding the optic lobe. Future studies investigating Sip1 localization and the mechanisms underlying Sip1 function in the glial cells are necessary to address its potential role during optic lobe development.

Chapter 4: Determining the role of Sip1 and Moesin in central brain neuroblasts

4.1 INTRODUCTION

Coordinated self-renewal and differentiation via asymmetric cell division is essential for generating cellular diversity during development. Drosophila neuroblasts have become an attractive model for studying the mechanisms involved in progenitor cell self-renewal and differentiation (Jiang and Reichert, 2014; Li et al., 2014). During Drosophila neurogenesis, neuroblasts undergo asymmetric division, renewing the neuroblast and producing a ganglion mother cell (GMC), which differentiates into the neurons and the glia of the adult nervous system (Figure 4-1). Neuroblast asymmetric cell division requires the appropriate segregation of basal cell fate determinants such as, Prospero (Pros) and Numb, through adaptor proteins Miranda and Partner of Numb, respectively, into the GMC (Doe et al., 1991; Ikeshima-Kataoka et al., 1997; Li et al., 1997; Lu et al., 1998; Shen et al., 1997). Segregation of basal cell fate determinants depend on the localization of two apical protein complexes linked by the adaptor protein, Inscuteable (Insc) (Kraut and Campos-Ortega, 1996; Parmentier et al., 2000; Schaefer et al., 2000; Schober et al., 1999; Tio et al., 1999; Yu et al., 2000)). The Par polarity complex, consisting of Bazooka (Baz), Par-6, and atypical PKC (aPKC), is the first complex to localize to the neuroblast cortex and is primarily involved in excluding basal determinants from the apical cortex (Betschinger et al., 2003; Petronczki and Knoblich, 2001; Wodarz et al., 2000; Wodarz et al., 1999). The second apical protein complex, consisting of Partner of Inscuteable (Pins), the heterotrimeric G protein subunit Gαi, and Mushroom body defect (Mud), is generally involved in regulating mitotic spindle formation and alignment relative to the apical/basal axis (Bowman et al., 2006; Izumi et al., 2004; Nipper et al., 2007; Schaefer et al., 2001; Schaefer et al., 2000; Yu et al., 2003; Yu et al., 2000). Basal protein targeting during asymmetric cell division is also dependent on the cortical tumour suppressors, Discs large (Dlg), Lethal (2) giant larvae (Lgl), and Scribble (Albertson and Doe, 2003; Betschinger et al., 2003; Ohshiro et al., 2000; Peng et al., 2000). Thus, proper localization of apical polarity proteins, orientation of the mitotic spindle, and segregation of cell fate determinants all ensure the appropriate balance between neuroblast self-renewal and differentiation. A schematic representation summarizing the key players involved in asymmetric cell division are shown in Figure 4-2. Furthermore, an intact actin cytoskeleton has also been shown to be essential for cortical anchoring of apical/basal proteins to their respective neuroblast poles (Broadus and Doe, 1997; Knoblich et al., 1997; Kraut et al., 1996; Lu et al., 1999; Shen et al., 1998). In addition, Drosophila myosins are involved in maintaining cell size asymmetry and function downstream of the apical complex in basal targeting of cell fate determinants (Barros et al., 2003; Cabernard et al., 2010; Connell et al., 2011; Ohshiro et

al., 2000; Peng et al., 2000; Petritsch et al., 2003). However, the precise mechanisms underlying actomyosin regulation and dynamics during Drosophila asymmetric cell division have not been studied extensively.

The ezrin, radixin, and moesin (ERM) proteins are key organizers of the cell cortex through the ability to bind directly to F-actin and link membrane-associated proteins to the underlying actin cytoskeleton (Algrain et al., 1993; Hirao et al., 1996; Turunen et al., 1994). Investigating the single Drosophila ERM orthologue, Moesin, provides unique insight into ERM function during development (McCartney and Fehon, 1996). Drosophila Moesin has been implicated in regulating epithelial tissue integrity (Hipfner et al., 2004; Karagiosis and Ready, 2004; Molnar and de Celis, 2006; Pilot et al., 2006; Speck et al., 2003). In embryonic epithelium, the synaptotagmin-like protein, Bitesize, and Moesin were shown to regulate adherens junction stability, through maintaining local actin organization (Pilot et al., 2006). Furthermore, the loss of Moesin led to defects in actin organization and altered distribution of the adherens junction marker, E-cadherin, in wing imaginal discs and follicle cell epithelium (Hughes et al., 2010; Speck et al., 2003). The scaffold protein Sip1 was shown to promote the Slik-dependent phosphorylation of Moesin in the follicle cells, which was essential for maintaining epithelial integrity (Hughes et al., 2010). Moesin has also been implicated in maintaining oocyte polarity, through the stabilization of F-actin (Jankovics et al., 2002; Polesello et al., 2002). Although, Moesin interacts with the apical determinant Crumbs and other apical membrane proteins in Drosophila embryos (Medina et al., 2002), Moesin does not appear to be directly involved in establishing apical/basal polarity. Numerous studies in Drosophila cell culture have shown that the uniform distribution of Moesin at the cell cortex is involved in mitotic cell rounding and cortically remodelling in symmetrically dividing cells (Carreno et al., 2008; Kunda et al., 2008; Kunda et al., 2012; Roubinet et al., 2011). Thus, Moesin is essential for the regulation of actin organization in Drosophila epithelial tissues and cell culture. However, a role for Moesin in remodelling the cortex during asymmetric cell division remains largely unknown.

We found that both Drosophila Sip1 and Moesin localized to mitotic neuroblasts. Although the functional significance of Sip1 in the neuroblasts still remains unclear, Moesin was shown to be essential for proliferation and stable cortical remodelling in asymmetrically dividing neuroblasts. Moesin appears to be a novel apical polarity protein involved in polarity maintenance and cortical integrity. Known components of the apical polarity complex regulate the polar distribution of phosphorylated Moesin in metaphase neuroblasts. Furthermore, Slik kinase was also found to be important for neuroblast proliferation and aPKC polarity maintenance, likely through regulating Moesin activity in the neuroblasts.

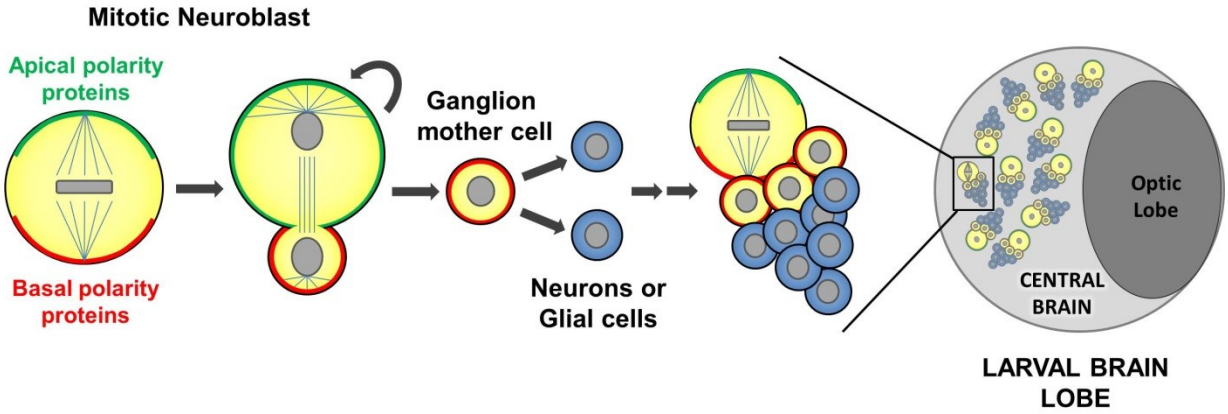

Figure 4-1: Neuroblast asymmetric cell division in the larval central brain. The balance between self-renewal and differentiation is maintained through asymmetric cell division. During metaphase apical polarity proteins and basal polarity proteins localize to their respective poles and the mitotic spindle is oriented such that during telophase the apical determinants are retained in the self-renewing neuroblast and the basal determinants segregate into the differentiating GMC. The GMC further differentiates into neurons or glial cells. Repeated rounds of asymmetric cell division result in a single large neuroblast with a cluster of differentiated cells surrounding it. Multiple lineages are found within the central brain region. A single larval brain lobe consists of the central brain and optic lobe.

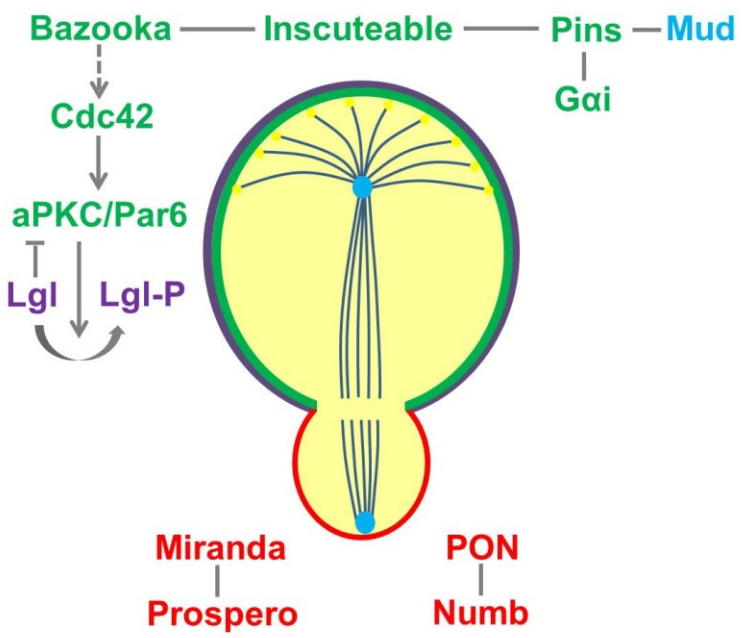

Figure 4-2: Known key players during neuroblast asymmetric cell division. Apically localized protein complexes (green) consist of two complexes linked by the adaptor protein Inscuteable. The Par polarity complex consisting of Bazooka/aPKC/Par-6 is the first complex to localize to the neuroblast cortex and is primarily involved in excluding basally localized proteins (red) from the apical cortex. The second apical protein complex consisting of Pins/ Mud/Gαi is generally involved in regulating mitotic spindle formation and alignment during asymmetric cell divisions. Lines indicate physical interactions and arrows indicate positive regulation. Adapted from (Chia et al., 2008).

4.2 MATERIALS AND METHODS

4.2.1 Fly strains and genetics

The following lines were obtained from Bloomington Stock Centre: *Insc-GAL4*, *Insc-GAL4*;*UAS-chRFP-Tubulin*, *UAS-Lifeact-GFP*, *UASp-Rok.RBD-GFP*, *pins*^{193}, *UAS-Moe*^{dsRNA} (#31872), *UAS-Moe.IR.327-775* (Moe IR; #8629) *UAS-Cdc42*^{dsRNA} (#35756), *UAS-Par6*^{dsRNA} (#38361), *UAS-aPKC*^{dsRNA} (#34334), and *UAS-Lgl*^{dsRNA} (#35773). *UAS-Moe*^{dsRNA} (y^1 sc* v^1; P[TRiP.HM05265]attP2) and *UAS-Moe.IR.327-775* was combined with *UAS-Dicer*. *Moe*^{G0323} 19A FRT/FM7, Krupple-GFP was obtained from R. Fehon (Speck et al., 2003). *Slik*^{1} 42D FRT/CyO, actin-GFP was obtained from D. Hipfner (Hipfner and Cohen, 2003). When necessary, stocks were maintained over *actin-GFP* balancer chromosomes and larvae of interest were chosen by lack of GFP. *w*^{1118} flies were used as wild-type control. Flies were maintained on: 5 g/L agar, 75 g/L cornmeal, 32 g/L yeast, 90 g/L sucrose and 2.5 g/L Methyl 4-hydroxybenzoate (Schwarz et al., 2014).

Time course experiments: Embryos were collected for 2 hours (Moe^{dsRNA} and control experiments) and 4 hours (*slik*^{1} mutant and control experiments) on apple juice plates. Embryos or non-GFP larvae were transferred to petri dishes containing food (recipe mentioned above) and covered with a plastic cage (100 ml plastic beaker with cut out bottom and covered with mesh) which was parafilmed to the dish. Cages containing embryos/larvae were sprayed twice daily with water to maintain moisture and larvae were dissected at indicated hours after larval hatching (approximately 22-24 hours after egg laying (AEL)). The above setup was used for all Moe knockdown, *slik*^{1}, *pins*^{193} experiments and respective controls, as these larvae are very weak.

4.2.2 Immunofluorescence

Larvae were dissected in 1X PBS and fixed in 4% paraformaldehyde for 20 min. Dissected tissues were rinsed at least 5 times in 1X PBS and blocked in 0.1% Triton X-100, and 1% normal donkey serum in 1X PBS (PTN) for at least 1 hr at room temperature (RT). Tissues were incubated in primary antibodies in PTN overnight at 4°C. Tissues were rinsed/washed for at least 1 hr in PTN at RT and incubated in secondary antibodies in PTN for 2-4 hours at RT. Tissues were rinsed/washed for at least 2 hours in PTN at RT. Tissues were incubated in DAPI (1:10 000) for 10 min and rinsed at least 3 times in PTN and at least 3 times in 1X PBS prior to mounting in ProLong® Gold Antifade Reagent (Invitrogen). For rabbit anti-phospho-Ezrin (Thr567)/Radixin (Thr564)/Moe (thr558) and mouse anti-rho1: Dissected tissues were fixed in 10% trichloroacetic acid (Hayashi et al., 1999) for 45 min on ice and rinsed at least 5 times in 30 mM glycine in 1X PBS. For rabbit anti-phospho-Myosin light

chain 2: Dissected tissues were fixed in 4% paraformaldehyde containing 0.5 mM EGTA and 5 mM $MgCl_2$ for 20 min and rinsed at least 5 times in 0.3% Triton X-100 in 1X PBS. Primary antibodies used were: Guinea pig anti-Sip1 (1:1000), rat anti-DE-Cadherin (1:200; DSHB) rabbit anti-phospho-Ezrin (Thr567)/Radixin (Thr564)/Moe (thr558) (1:100; Cell Signaling #3149 and #3726; referred to as p-Moesin), mouse anti-rho1 (1:50; Developmental Studies Hybridoma Bank (DSHB) p1D9), rabbit anti-phospho-Myosin light chain 2 (1:30; Cell Signaling #3671; referred to as p-MyoII), rabbit anti-Moe D44 (1:20 000; D. Kiehart; referred to as Moesin), rat anti-α-tubulin (1:100; Bio-Rad MCA77G), mouse anti-β-tubulin (1:1000; DSHB E7), rabbit anti-Bazooka (1:1000; A. Wodarz), rabbit anti-Pins (1:1000; F. Yu), rabbit anti-PKC ζ (1:500; Santa Cruz sc-216), rabbit anti-Par-6 (1:500; J. Knoblich), guinea pig anti-Par-6 (1:1000; A. Wodarz), mouse anti-Miranda (1:200; F. Matsuzaki), guinea pig anti-Miranda (1:1000; A. Wodarz), guinea pig anti-Numb (1:1000; J. Skeath), rabbit anti-Dpn (1:1000; Y. N. Jan), mouse anti-Prospero (1:500; DSHB MR1A), rat anti-Elav (1:500; DSHB 7E8A10), rabbit anti-Phospho-histone H3 (1:2000; Millipore #06-570), mouse anti-Phospho-histone H3 (1:1000; Abcam 14955), guinea pig anti-Slik (1:10 000; D. Hipfner), mouse anti-GFP 3E6 (1:500; Invitrogen), and Phalloidin Alexa Fluor 546 (1:1000; Invitrogen). Secondary antibodies used were: Donkey anti-Rabbit, -Mouse, -Guinea pig, and -Rat Alexa Fluor® 488/555/647 (1:2000; Abcam). Imaging was performed using a Zeiss LSM 700 confocal microscope using 20× NA 0.8 objective (Plan-Apochromat; Zeiss), 40× NA 1.3 oil immersion objective (EC Plan-Neofluar; Zeiss), and 63× NA 1.4 oil immersion objective (Plan-Apochromat; Zeiss). The acquisition software used was Zen 2009 and Adobe Photoshop/Illustrator were used to generate figures.

4.2.3 Neuroblast quantification and measurements

Quantification of neuroblasts and mitotic neuroblasts: Central brain neuroblasts (Type I and II; excluded intermediate progenitors based on size, proximity, and location within the brain lobe) fluorescently labelled using anti-Deadpan and anti-phosho-histone H3 (PH3) were quantified per brain lobe from confocal sections taken at approximately 0.4 µm intervals using the Zen 2 software. The number of PH3-positive and Dpn-positive cells were divided by total number of Dpn-positive cells per brain lobe to determine proportion (%) of PH3-positive, Dpn-positive cells. For Moesin knockdown experiments, 28-44 brain lobes were quantified.

Neuroblast diameter measurements: Neuroblast diameter was measured from maximum projections of central brain neuroblasts undergoing metaphase and fluorescently labelled with antibodies specific to apical polarity marker (aPKC, Bazooka, etc), Miranda, α-tubulin,

and phospho-histone H3. Using ImageJ software, the diameter was measured by averaging the axis bisecting the PH3-positive metaphase chromosomes and the orthogonal axis of the apical and basal crescents.

Quantification of neuroblasts in the stages of mitosis: Proportion of PH3-positive neuroblasts in the specific stages of mitosis were quantified from central brain neuroblasts fluorescently labelled with antibodies specific to aPKC, Miranda, α-tubulin, and PH3. Mitotic neuroblasts were confirmed using Miranda and PH3 as a neuroblast and mitotic marker, respectively. The stages of mitosis were determined using anti-PH3 and anti-α-tubulin to visualize the chromosomes and mitotic spindle, respectively: Prophase neuroblasts displayed condensed chromosomes and mitotic spindle poles forming as microtubule organizing centers. Metaphase neuroblasts were identified as the mitotic spindle aligning PH3-positive chromosomes at metaphase plate. Neuroblasts undergoing anaphase displayed the mitotic spindle separating chromosomes to their respective poles. Neuroblasts undergoing telophase were identified as cells that displayed separated chromatids at their respective poles and diffuse/basal Miranda localized to the cleavage furrow formation and the daughter cell.

4.2.4 Live imaging and processing

Lifeact-GFP and chRFP-Tubulin localization in wild-type and *Moesin* hypomorphic mutant neuroblasts were imaged in brains from third instar larval male progeny collected from the following crosses: *Insc-GAL4*; *UAS-Lifeact-GFP*, *UAS-chRFP-Tubulin* crossed to w^{1118} and Moe^{G0323}*/FM7c, P[Dfd-GMR-nvYFP]1* flies, respectively. The live imaging protocol was adapted from (Lerit et al., 2014). Larval brains were dissected in filter-sterilized Schneider's Insect medium (Sigma) supplemented with penicillin-streptomycin. Larval brains with ventral nerve cords facing down were submerged in 30 µl drop of supplemented media on 25 mm diameter round Deckgläser cover glass (neuVitro) placed in Attofluor cell chamber for microscopy (Invitrogen). Four drops of 30 µl Halocarbon oil 700 (Sigma-Aldrich) were placed on cover glass at four corners centered around the drop of media containing larval brains. YSI Model 5793 gas-permeable membrane (cut to size of round cover glass) was placed on top of cover glass with drops of media and halocarbon oil. Media and oil were allowed to disperse (5 min) before assembling cell chamber. Imaging was performed at 24°C using a Zeiss coupled to a Ultraview spinning disc confocal microscope (Perkin Elmer) using a 63x NA 1.4 oil immersion objective (Plan-Apochromat; Zeiss) and Hamamatsu C9100-50 camera. 15-25 z sections were taken at 1 µm intervals and recorded approximately every 30-60 seconds. The acquisition software used was Volocity 6.3.0

(PerkinElmer Inc.). ImageJ, Adobe Photoshop, and Illustrator were used for data analysis and figure formatting.

4.2.5 Expression analysis of Moesin transgenes

Epitope-tagged *Moesin* transgenes under UAS control were crossed to *actin-GAL4*/CyO, actin-GFP. Collected adult progeny (ten of each: males/females and non-CyO/CyO) in 1.5 mL tubes, froze with liquid nitrogen, and stored at -80°C. Flies were lysed in 2X SDS sample buffer (approximately 10 µL per fly) using a pestle and sheared using a tuberculin needle. Samples were boiled at 95°C for 10 min and 5 µL of samples were loaded onto SDS-page gel (3.5% stacking gel and 10% running gel). The gel was run at 150 V for approximately 1-1.5 hours and the gel was transferred onto nitrocellulose membrane at 100 V for 1 hour. The blots were blocked in LI-COR block and 1X PBS (1:1) for 2 hours at room temperature. The blots were incubated in the appropriate primary antibodies overnight in LI-COR block and 1X PBT (1:1): Rabbit anti-MYC (Sigma; 1:5000), rabbit anti-FLAG (Rockland; 1:2000), and mouse anti-β-tubulin (DSHB E7; 1:3000). Blots were rinsed in 1X PBT for 5 min (repeated 4 times). The blots were incubated in secondary antibodies at room temperature for 30 min in 1X PBT: Donkey anti-Rabbit IgG H&L Alexa Fluor 680 (1:10 000) and Donkey anti-Mouse IgG H&L Alexa Fluor 790 (1:50 000). The blots were rinsed in 1X PBT for 5 min (repeated 4 times) and twice in 1X PBS. The blots were scanned using the ODYSSEY infrared imaging system (LI-COR).

4.2.6 Immunoprecipitation and mass spectrometry

The FLAG-tagged *Moesin* transgene (SCH# 643) was expressed using *Insc-GAL4*. Third instar larval brains were dissected in 1X PBS containing protease inhibitor (Roche Complete ULTRA Tablets, EDTA-free protease inhibitor cocktail tablets) and phosphatase inhibitor (Roche PhosSTOP phosphatase inhibitor cocktail tablets) for 15 minutes. Larval brains were transferred into 1.5 mL tube containing PBS/inhibitor. The PBS/inhibitor was removed with a pipette, were frozen using liquid nitrogen, and stored at -80°C until enough brains were dissected for immunoprecipitation/mass spectrometry. Approximately 1000 brains were lysed in 1 mL of mild lysis buffer (MLB; 20 mM Hepes (pH 7), 50 mM NaCl, 1mM EDTA, 0.5mM EGTA, 1% Triton X-100, protease and phosphatase inhibitors) using a dounce homogenizer and a tuberculin needle. The sample was incubated on ice for 10 min and spun down at 16 000 xg for 10 min at 4°C. The supernatant was transferred into a 1.5 mL tube using a tuberculin needle (transferred fraction of supernatant and spun down multiple times to ensure minimal transfer of fat layer). 25 µL of supernatant was resuspended in 25 µL of 2X SDS sample buffer, boiled for 10 min at 95°C, and stored at -

20°C ("Input Lysate" control). The remaining supernatant (approximately 450 µL) was split into two 1.5 mL tubes ("IP" and "IgG control"). The primary antibody mouse anti-FLAG M2 (Sigma F3165; 1:200) was added to "IP" tube and IgG mouse serum (Sigma 15381; 1:200) was added to the "IgG control" tube. The tubes were incubated at room temperature with rocking for 6 hours. 60 µL of rinsed Protein G beads (Biovision; rinsed beads for 10 min in 1 mL of MLB and repeated 3 times) were added to the incubated lysates and the samples were incubated overnight at 4°C with rocking. The lysates/beads were spun down at 300 xg for 5 min. 100 µL of supernatant was resuspended in 100 µL of 2X SDS sample buffer and boiled for 10 min at 95°C ("Post-IP" controls). The remaining supernatant was discarded and the beads were rinsed in 1X PBS for 10 min (repeated 4 times) and rinsed again for 5 min in MLB. The beads were resuspended in 50 µL 2X SDS sample buffer and boiled for 10 min at 95°C. 100 µL of samples (Input lysate, IgG control, and FLAG IP) were loaded into a 10% Hoeffer SDS page gel (wiped glass plates, comb, and apparatus with 10% acetic acid and HPLC-grade water). The gel was run at 200V for approximately 2 hours. The gel was washed in HPLC water for 20 min (repeated 3 times), stained in Bio-safe coomassie stain for 1 hour, and washed in HPLC water for 1 hour. The HPLC water was replaced and washed overnight. The gel was sealed in a plastic bag. The bands of interest (bands present in FLAG IP and absent in IgG control lanes) were excised and placed in 1.5 mL tubes containing 40 µL HPLC water, under sterile conditions. The samples were processed at the Alberta Proteomics and Mass Spectrometry Facility. The candidate interacting proteins were validated as above, except approximately 250 larval brains were dissected and lysed in 500 µL MLB.

4.3 RESULTS

4.3.1 Sip1 localization and function in the neuroblasts

I found that Sip1 localized to the cytoplasm of the central brain neuroblasts and to the cortex of the surrounding differentiating cells (Figure 4-3). The localization of Sip1 within the neuroblasts was confirmed with Asense, which is expressed in all primary neuroblasts (Figure 4-4) (Brand et al., 1993). Many Asense-positive neuroblasts were Sip1-negative (Figure 4-4, yellow arrows), suggesting that Sip1 is present in a subset of neuroblasts during early larval brain development. Cytoplasmic EBP50 or Sip1 distribution has not been reported in physiologically normal cells. Thus, determining the functional significance of cytoplasmic Sip1 in normal neuroblasts, which have the ability to self-renew and differentiate, may reveal a novel role for Sip1 during development.

To determine the functional significance of Sip1 in the central brain neuroblasts, Sip1 was over-expressed using *Insc-GAL4*. When Sip1 was over-expressed in the neuroblasts, obvious defects in brain morphology or the differentiated cell markers, Elav and Prospero, were not observed (Figure 4-5). However, defects in the neuroblasts were observed by the dsRNA-mediated knockdown of Sip1 using *actin-GAL4*. In control larval brains, a single neuroblast was surrounded by a cluster of differentiated cells, referred to as a "neural cluster" (Figure 4-6, A-E). However, in the Sip1 knockdown, there appeared to be multiple neuroblasts forming within a given neural cluster (Figure 4-6, E-H; yellow arrowhead). These findings suggest that Sip1 may be important for the balance between neuroblast self-renewal and differentiation. Sip1 knockdown in the neuroblasts also altered polarity protein localization during metaphase (Figure 4-7). In control neuroblasts, aPKC and Miranda crescents formed at opposite poles during metaphase (Figure 4-7, A-F). When Sip1 levels were reduced in neuroblasts, normal aPKC and Miranda crescents were observed in some neuroblasts undergoing metaphase (Figure 4-7, G-I); however, neuroblasts with a diffuse polar distribution of aPKC and Miranda were also observed (Figure 4-7, J-L). Thus, Sip1 may be involved in polarity maintenance during asymmetric cell division.

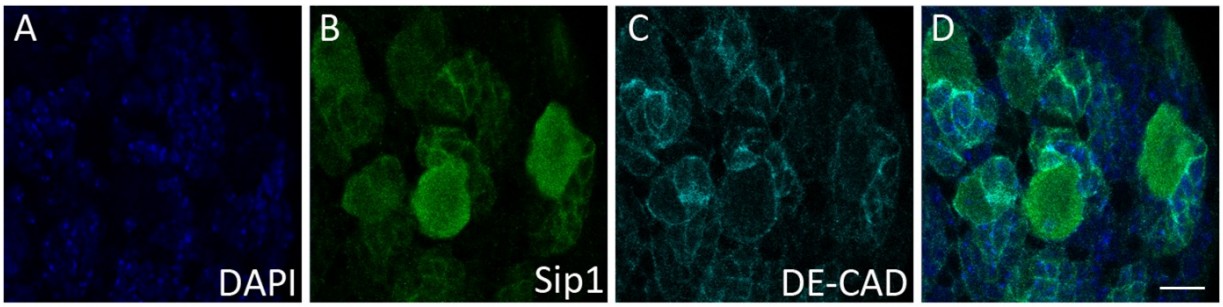

Figure 4-3: Sip1 localizes to the cytoplasm of central brain neuroblasts and to the cortex of differentiated ganglion mother cells. (A-D) Third instar larval brains were dissected and fluorescently labelled with (A) DAPI (blue), (B) anti-Sip1 (green), and (C) anti-DE-Cadherin (DE-CAD; cyan). Merge is shown in D. Scale bar represents 10 µm**.**

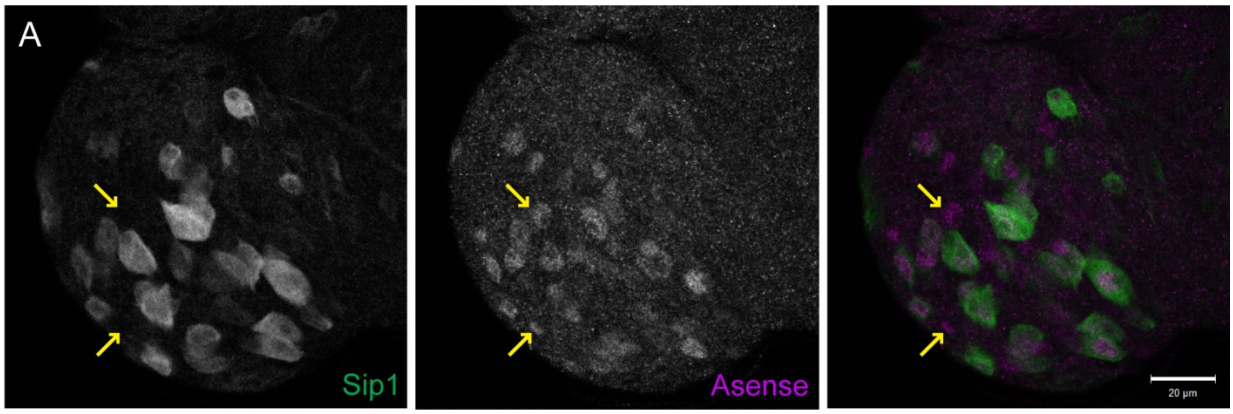

Figure 4-4: Sip1 localizes to Asense-positive neuroblasts in early larval brain lobes. (A-E) Larval brains were dissected 45-56 hours after egg laying and fluorescently labelled with anti-Sip1 (green) and anti-Asense (magenta), as shown in the merge. Sip1-positive neuroblasts also displayed nuclear Asense. There were Asense-positive neuroblasts that were Sip1-negative, as indicated by the yellow arrows. Scale bar represents 20 µm**.**

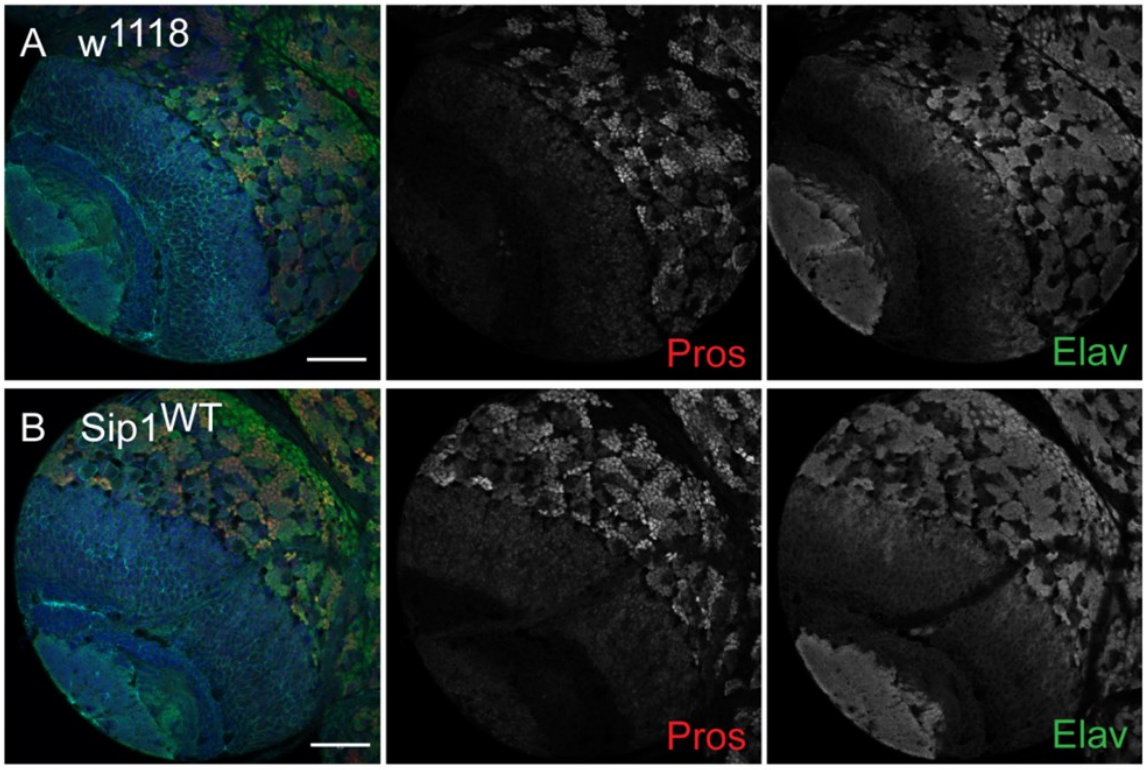

Figure 4-5: Over-expression of Sip1 in the neuroblasts does not alter larval brain morphology. The neuroblast GAL4 driver, *Insc-GAL4*, was crossed to (A) w^{1118} and (B) *UAS-MYC-Sip1* (Sip^{WT}). Third instar larval brains were dissected and fluorescently labelled with DAPI (blue), anti-Prospero (Pros; red), and anti-Elav (green), as shown in the merge panels. (B) The over-expression of Sip1 in the neuroblasts did not alter Moesin localization, differentiation markers, Pros and Elav, and overall brain morphology, when compared to (A) controls. Single focal plane images are shown. Scale bars represent 50 μm**.**

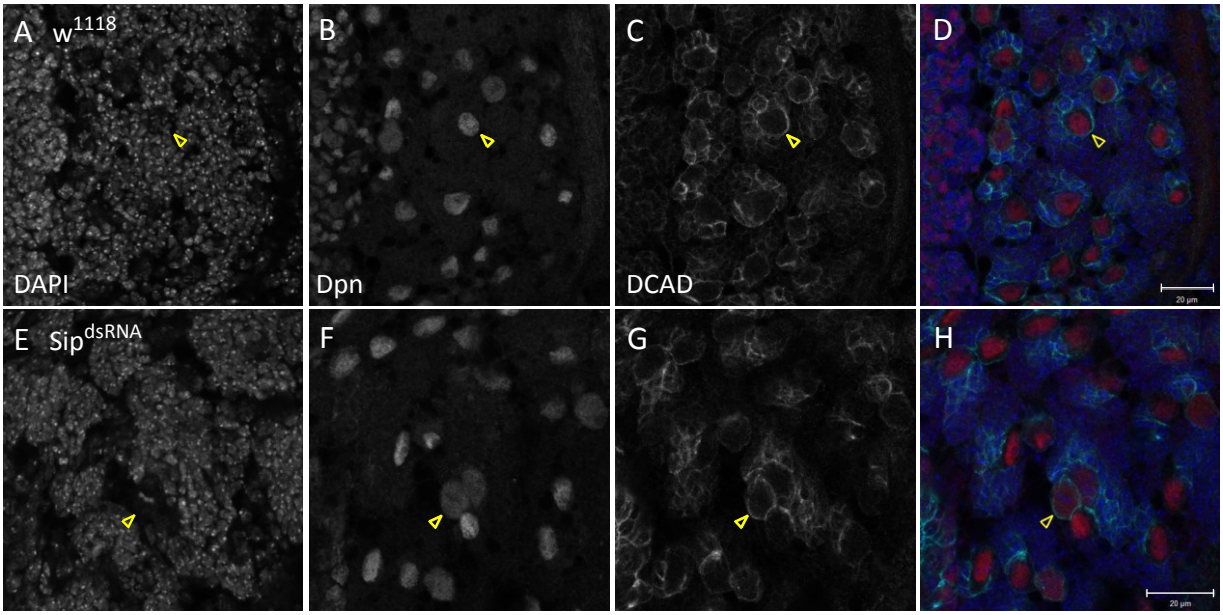

Figure 4-6: Reduced Sip1 levels lead to the presence of multiple neuroblasts within a neural cluster. The ubiquitous GAL4 driver, *actin-GAL4*, was crossed to (A-D) w^{1118} and (E-H) *UAS-Dicer;;Sip1*^{dsRNA} (Sip^{dsRNA}). Third instar larval brains were dissected and fluorescently labelled with DAPI (blue), anti-Deadpan (Dpn; red) and anti-DE-Cadherin (DCAD; cyan). (A-D) Within a given neural cluster, a single neuroblast and surrounding differentiated cells are present in controls (arrowheads in B and C). (E-H) Reduced Sip1 levels result in multiple neuroblasts forming within a given neural cluster, indicated by the close proximity of Dpn-positive cells (arrowheads in F and G). Scale bars represent 20 μm**.**

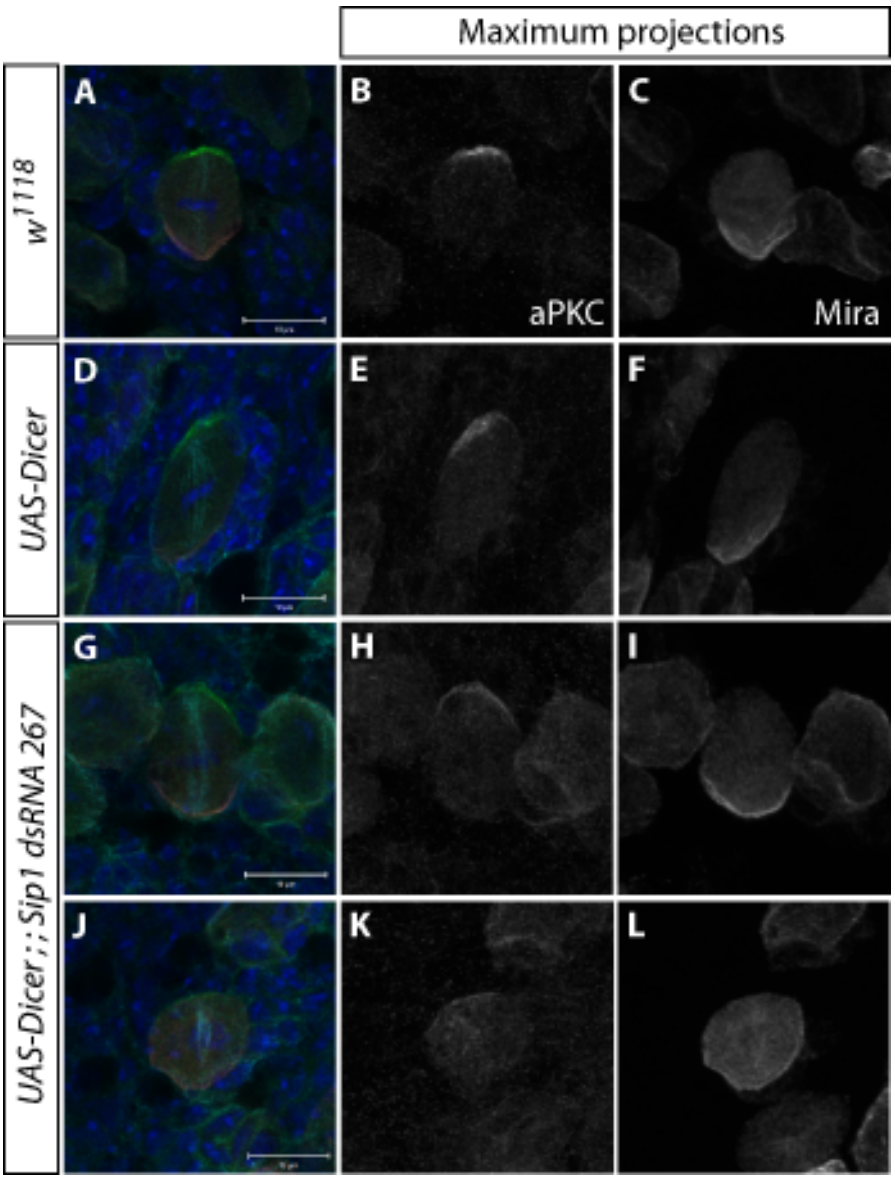

Figure 4-7: Reduced Sip1 in neuroblasts alters aPKC and Miranda localization. The neuroblast GAL4 driver, *Insc-GAL4*, was crossed to (D-F) *UAS-Dicer* and (G-L) *UAS-Dicer;;Sip1 dsRNA line 267*. Third instar larval brains were dissected and fluorescently labelled for DAPI (blue), anti-α-tubulin (cyan), anti-aPKC (green), and anti-Miranda (Mira; red), as shown in merge panels. (A-F) Standard (w^{1118}) and dicer control neuroblasts show aPKC and Mira crescents forming at opposite poles during metaphase. Reducing Sip1 in neuroblasts resulted in variable phenotypes, with (G-I) normal crescents and (J-L) diffuse polar distributions of aPKC and Mira forming at opposite poles during metaphase. Gray-scale images are maximum intensity projections. Scale bars represent 10 μm.

4.3.2 Potential upstream regulators of Sip1 localization in the neuroblasts

To identify potential upstream regulators of Sip1 localization in the neuroblasts, genes known to be involved in neuroblast self-renewal and differentiation were targeted by dsRNA-mediated knockdown using *Insc-GAL4*, and changes in Sip localization were examined (Table 3). Previously, Clueless was shown to localize to the cytoplasm of central brain neuroblasts and the loss of Clueless led to the mis-localization of polarity proteins in a proportion of dividing neuroblasts (Goh et al., 2013). However, the dsRNA-mediated knockdown of Clueless did not alter Sip1 localization, and Sip1 appeared cytoplasmic in the neuroblasts, similar to controls (Figure 4-8, A-B). When Bazooka was reduced, the Sip1 immunofluorescent signal appeared weaker compared to controls (Figure 4-8, C). Furthermore, ectopic Sip1 localization at the neuroblast cortex was observed in the Microtubule star (Mts) knockdown (Figure 4-8, D). These findings suggest that Bazooka and Mts may be important for Sip1 localization in the neuroblasts.

Table 3: Candidate dsRNA lines tested for changes in Sip1 localization in the neuroblasts.

Protein	Bloomington (BL) or Vienna (V) stock #	Change in Sip1 localization?	Reference
aPKC	BL38245	No	(Rolls et al., 2003)
Bazooka	BL39072	Yes	(Schober et al., 1999; Wodarz et al., 1999)
Cdc42	BL42861; BL35756	No; Variable	(Atwood et al., 2007)
Clueless	V42136; V42138	No; No	(Goh et al., 2013)
Lethal giant larvae	BL38989; BL35773	No; Variable	(Ohshiro et al., 2000; Peng et al., 2000)
Microtubule star	BL38337; BL27723	Yes; Yes	(Chabu and Doe, 2009)
Tre1	BL33718	Variable	(Yoshiura et al., 2012)

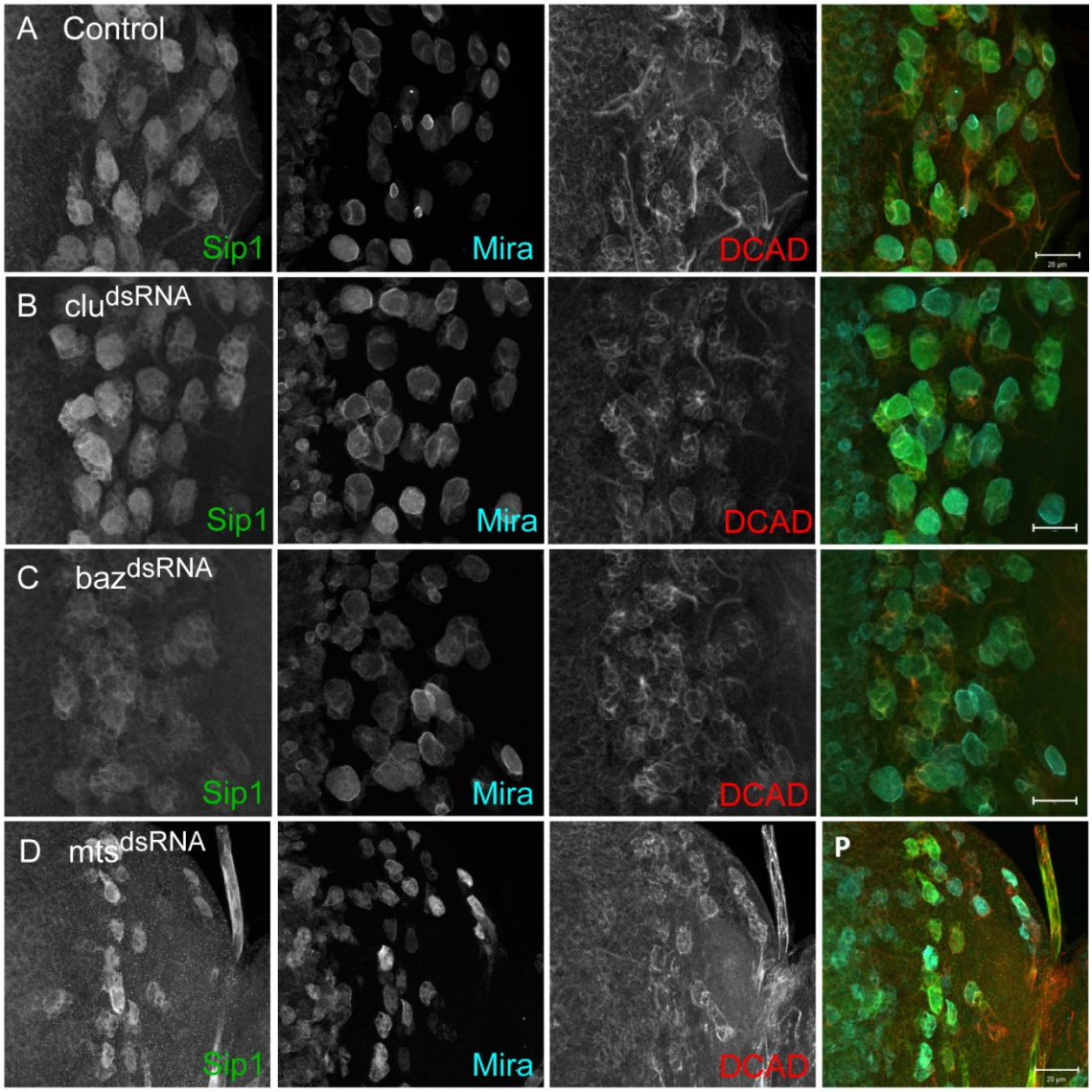

Figure 4-8: Loss-of-function analysis of genes involved in neuroblast self-renewal/differention and Sip1 localization. The neuroblast GAL4 driver, *Insc-GAL4*, was crossed to (A) w^{1118}, (B) *UAS-Clueless*^{dsRNA} (clu^{dsRNA}), (C) *UAS-Bazooka*^{dsRNA} (baz^{dsRNA}), and (D) *UAS-microtubule star*^{dsRNA} (mts^{dsRNA}). Third instar larval brains were dissected and fluorescently labelled for anti-Sip1 (green), anti-Miranda (Mira; cyan) and anti-DE-Cadherin (DCAD; red), as shown in merge panels. (B) Clueless knockdown did not alter Sip1 localization when compared to (A) controls. (C) Bazooka knockdown resulted in weaker Sip1 immunofluorescent signal and (D) Mts knockdown displayed Sip1 localizing more closely to the neuroblast cortex. Maximum intensity projections are shown. Scale bars represent 20 µm.

4.3.3 Loss of Sip1 does not alter phosphorylated Moesin in the neuroblasts

EBP50 and ezrin have been shown to co-localize in several epithelial tissues (Ingraffea et al., 2002) and appear to stabilize each other at the apical membrane of epithelial cells (Morales et al., 2004; Saotome et al., 2004). Furthermore, it was shown that Drosophila Sip1 mediates Moesin phosphorylation in the epithelial cells surrounding the developing oocyte (Hughes et al., 2010). Therefore, I asked whether Sip1 also regulated Moesin phosphorylation in the neuroblasts. Using an antibody specific to the conserved phosphorylated residue of mammalian ezrin/radixin/moesin (hereafter referred to as p-Moesin) (Hayashi et al., 1999), I found that p-Moesin was asymmetrically distributed in control neuroblasts undergoing metaphase (Figure 4-9, A yellow arrows). However, p-Moesin localization was not altered in metaphase neuroblasts when Sip1 was knocked down (Figure 4-9, B yellow arrows). Thus, Sip1 is not important for Moesin phosphorylation in metaphase neuroblasts. The functional significance of Moesin in the mitotic neuroblasts will be addressed in the following sections.

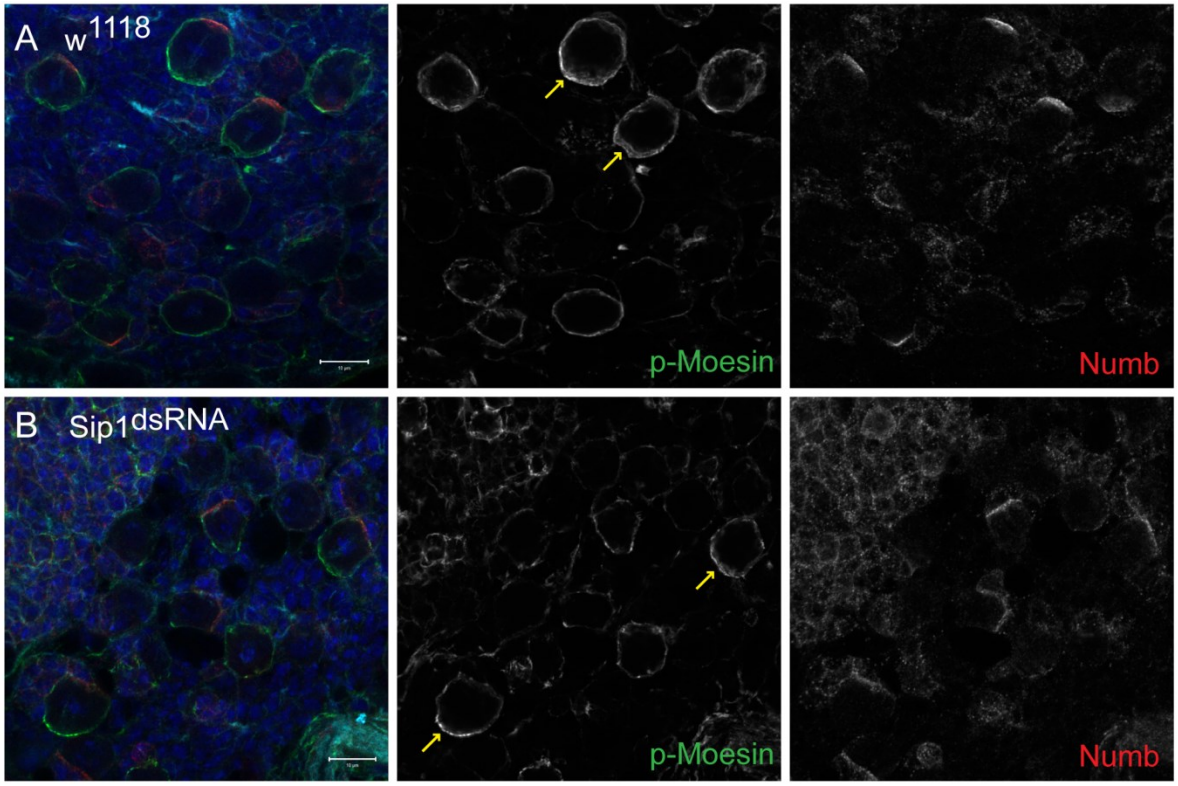

Figure 4-9: Reduced Sip1 in the neuroblasts does not alter p-Moesin localization. The neuroblast GAL4 driver, *Insc-GAL4*, was crossed to (A) w^{1118} and (B) *UAS-Dicer;;Sip1*^{dsRNA} (Sip1^{dsRNA}). Third instar larval brains were dissected and fluorescently labelled for DAPI (blue), anti-β-tubulin (cyan), anti-p-Moesin (green), and anti-Numb (red), as shown in merge panels. (B) Defects in p-Moesin localization were not observed with reduced Sip1 when compared to (A) controls, as p-Moesin was asymmetrically enriched at the cortical pole opposite of Numb (yellow arrows). Single focal plane images are shown. Scale bars represent 10 μm.

4.3.4 Phosphorylated Moesin is asymmetrically localized in mitotic neuroblasts

I found that the phosphorylated form of Moesin, the single Drosophila orthologue of the ERM proteins, localized to the cell cortex of both larval central brain and optic lobe neuroblasts (Figure 4-10, A). Phosphorylated Moesin (p-Moesin) was largely reduced in the surrounding differentiated cells indicated by the ganglion mother cell-specific marker, Prospero (Figure 4-10, A) (Matsuzaki et al., 1992). As mentioned previously, p-Moesin was asymmetrically distributed at the cell cortex in a few central brain neuroblasts (Figure 4-10, arrows in A). As neuroblast polarity is established at the onset of mitosis (Spana and Doe, 1995), the localization of p-Moesin was closely examined throughout neuroblast asymmetric cell division. I found that p-Moesin displayed an asymmetric and dynamic distribution in mitotic neuroblasts (Figure 4-10, B-E). During metaphase, p-Moesin was enriched at the apical cortex opposite of the basal polarity protein Numb (Figure 4-10, B). P-Moesin localization shifted more basally but remained enriched at the apical cortex during anaphase (Figure 4-10, C). During telophase, p-Moesin accumulated at the presumptive cleavage furrow site and was largely retained in the self-renewing neuroblast (Figure 4-10 D-E). The polar enrichment of p-Moesin was most likely established during the prophase-to-metaphase transition, as p-Moesin was cortical but discontinuous in 75% of neuroblasts and only 25% of neuroblasts showed a polar distribution of p-Moesin during prophase (n=20; Figure 4-11); whereas 100% of metaphase neuroblasts showed an apical enrichment of p-Moesin (n=27; Figure 4-10, B). In Drosophila S2 cells, p-Moesin was shown to increase at the cell cortex upon mitotic entry and remained uniformly distributed from prophase to metaphase (Carreno et al., 2008). In contrast to S2 cells, a polar distribution of p-Moesin was established by metaphase in neuroblasts, leading us to hypothesize that Moesin may be essential for the asymmetric properties of dividing neuroblasts.

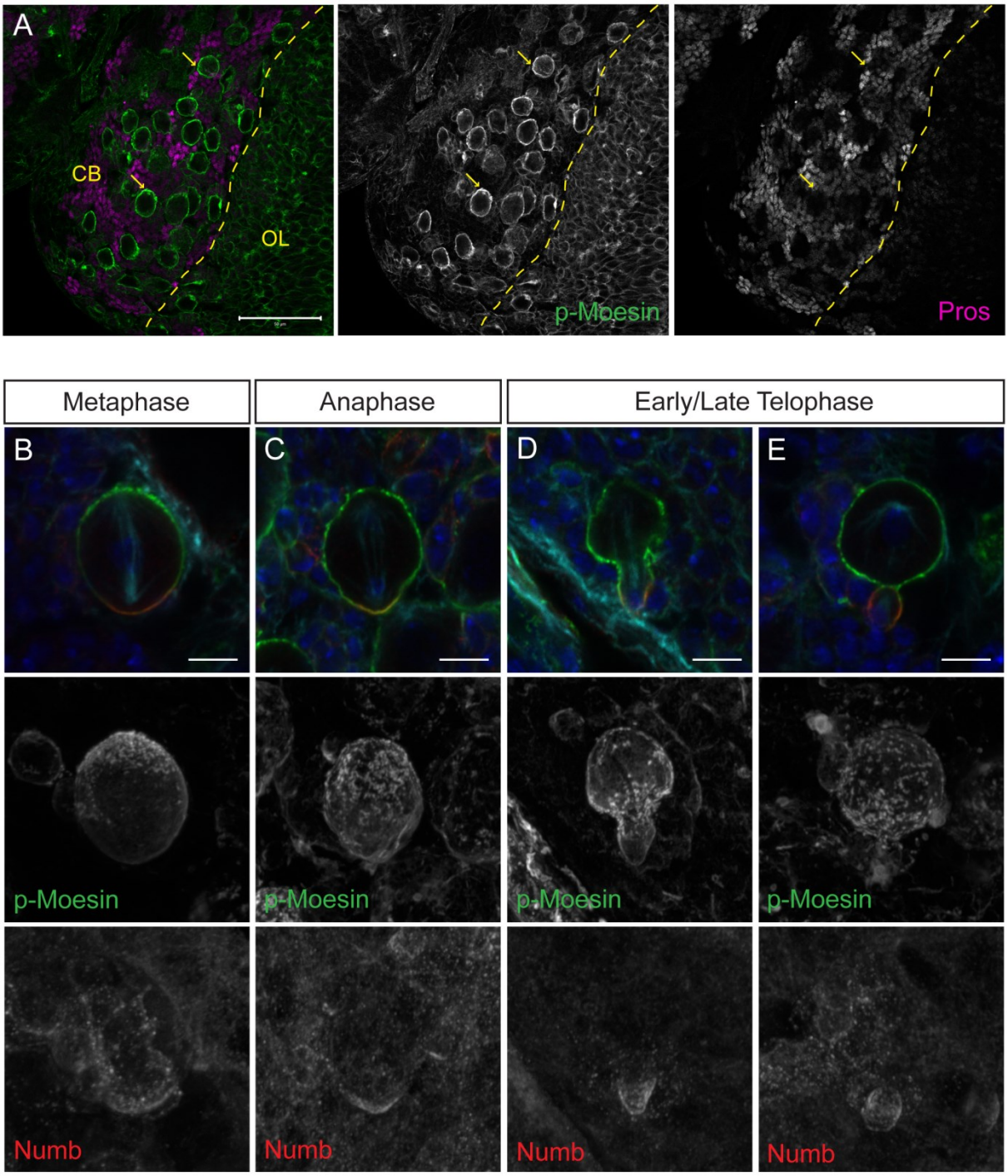
A
CB
OL
p-Moesin
Pros
Metaphase
Anaphase
Early/Late Telophase
B
C
D
E
p-Moesin
p-Moesin
p-Moesin
p-Moesin
Numb
Numb
Numb
Numb

Figure 4-10: Phosphorylated Moesin is enriched at the apical cortex of mitotic neuroblasts. (A) w^{1118} third instar larval brains were fluorescently labelled with anti-p-Moesin (green) and anti-Prospero (Pros; magenta), as shown in merge panel. P-Moesin localized to the cortex of neuroblasts within the central brain (CB) and optic lobe (OL). An asymmetric distribution of p-Moesin was observed, as indicated by yellow arrows. (B-E) w^{1118} larval neuroblasts were fluorescently labelled with DAPI (blue), anti-p-Moesin (green), anti-Numb (red), and anti-β-tubulin (cyan), as shown in merge panels. P-Moesin was apically enriched opposite of Numb during metaphase and (C) shifted more basally but remained in the apical half during anaphase. (D) P-Moesin accumulated at the cleavage furrow site and (E) was largely retained in the neuroblast during cytokinesis. (B-E) Merged panels are single focal plane images and gray-scale images are maximum intensity projections. Scale bars represent (A) 50 μm and (B-E) 5 μm.

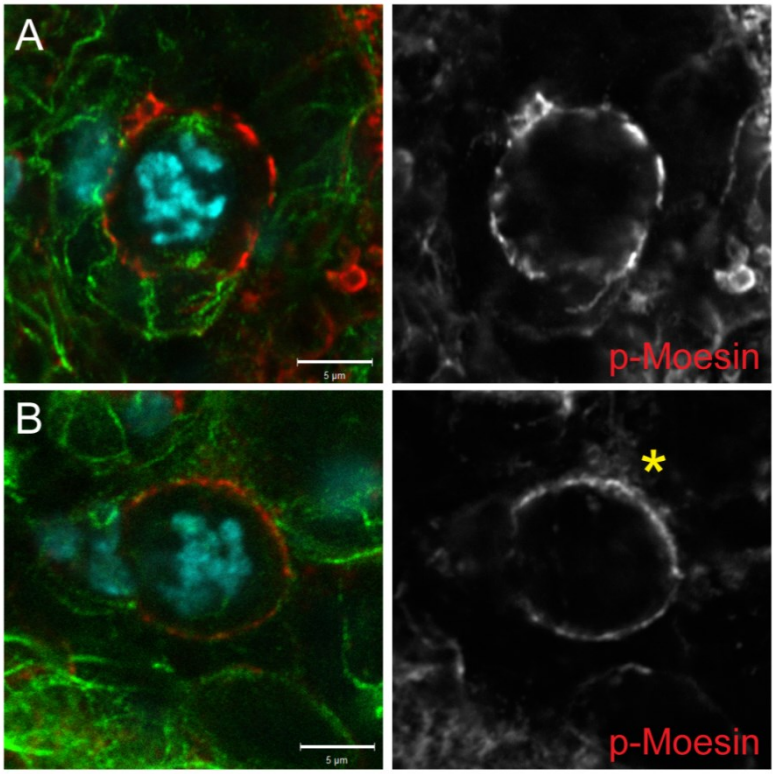

Figure 4-11: The asymmetric distribution of phosphorylated Moesin is likely established at the prophase to metaphase transition. In w^{1118} prophase neuroblasts, p-Moesin exhibited (A) a symmetric, uniform or discontinuous distribution at the cortex in 75% of neuroblasts and (B) an asymmetric distribution (yellow asterisk) in 25% of neuroblasts (*n*=20). Merged panels show p-Moesin (red), phospho-histone H3 (cyan), and α-tubulin (green). All panels shown are single focal plane images. Scale bars represent 5 μm.

4.3.5 Moesin is essential for neuroblast proliferation

To investigate the functional significance of Moesin in the larval neuroblasts, I analyzed the dsRNA-mediated knockdown of Moesin (Moe^{dsRNA}) in the neuroblasts, using *Insc-GAL4*. To enhance Moesin knockdown levels, Dicer was over-expressed as well. The p-Moesin immunofluorescent signal was reduced in the Moesin knockdown larval central nervous system, confirming loss of Moesin (Figure 4-12, A-B). At 96 hours after larval hatching (ALH), the overall size of the central nervous system was reduced in the Moesin knockdown larvae, compared to controls (Figure 4-12 and Figure 4-13, A-C). In control and Dicer alone crosses, the mitotic neuroblasts within the central nervous system were shown using the neuroblast-specific marker Deadpan (Dpn) and phospho-histone H3 (PH3) to mark mitotic cells (Figure 4-13, A-B) (Bier et al., 1992). When Moesin was knocked down, the central nervous system was reduced in size with fewer mitotic neuroblasts (Figure 4-13, C). Previous studies have shown that all neuroblasts, except the mushroom body neuroblasts, exit the cell cycle and either undergo apoptosis or become quiescent by late embryogenesis (Green et al., 1993; Peterson et al., 2002; Prokop et al., 1998; White et al., 1994; Younossi-Hartenstein et al., 1996). During early larval stages, neuroblasts enlarge, re-enter the cell cycle, and continue dividing throughout larval development, giving rise to the majority of adult neurons (Britton and Edgar, 1998; Ito and Hotta, 1992; Prokop and Technau, 1991; Truman and Bate, 1988). Thus, a reduced larval central nervous system size may be a result of the failure of neuroblasts to re-enter the cell cycle or decreased neuroblast divisions.

To examine whether neuroblast divisions were affected in the Moesin knockdown during larval development, the number and the proportion of mitotic neuroblasts per brain lobe was quantified at 24, 48, 72, and 96 hours ALH (Figure 4-13, D-E). The number of neuroblasts were reduced significantly in Moesin knockdown brains from 24 to 96 hours ALH, compared to controls (Figure 4-13, D). The proportion of mitotic neuroblasts increased from 24 to 48 hours ALH in control brains (Figure 4-13, E), the time at which neuroblasts exit quiescence (Ito and Hotta, 1992; Truman and Bate, 1988). However, in Moesin knockdown brains, the proportion of mitotic neuroblasts decreased from 24 to 48 hours and remained largely the same from 48 to 96 hours ALH (Figure 4-13, E). Furthermore, the optic lobes were reduced in size and no mitotic neuroblasts were observed in the ventral nerve cord in 87% of Moe^{dsRNA} larvae at 96 hours ALH (n=30; Figure 4-12, C). The neuroblasts within the Moesin knockdown ventral nerve cord also appeared smaller and the Deadpan immunofluorescent signal was weak and diffuse (Figure 4-12, C), shown previously to be characteristic of quiescent neuroblasts (Chell and Brand, 2010). I also

found that the few Moesin knockdown neuroblasts undergoing metaphase had a reduced cell diameter of 6.03 μm (median; maximum of 10.46 μm), compared to controls (median of 11.58 μm and maximum of 13.91 μm; Figure 4-13, F). Together, these findings indicate that neuroblast proliferation and size are impaired when Moesin levels are reduced.

To further examine the role of Moesin in mitotic neuroblasts, the proportion of PH3-positive neuroblasts in each mitotic stage was measured in the Moesin knockdown and control larval brains. I found a reduced proportion of mitotic neuroblasts undergoing stages prophase to telophase per Moe^{dsRNA} brain lobe compared to controls (Figure 4-13, G). There was a large proportion of PH3-positive Moesin knockdown neuroblasts that could not be classified to a particular stage of mitosis and thus were referred to as "mitotic defective" (Figure 4-13, G and Figure 4-14, A). In these mitotic defective neuroblasts, the spindle poles were not visible and only cortical microtubules were observed using α-tubulin (Figure 4-14, A). However, the nuclear envelope appeared to be broken down as Miranda was diffuse throughout the cytoplasm, aPKC polarity was not established and only PH3-positive condensed chromosomes were observed in these neuroblasts (Figure 4-14, A). To confirm specificity of the Moesin knockdown, I expressed a second independent *Moesin* dsRNA (Moe^{IR}) (Karagiosis and Ready, 2004)) using *Insc-GAL4* and mitotic defective neuroblasts were also observed (Figure 4-14, B). Thus, Moesin is essential for mitotic progression during neuroblast asymmetric cell division.

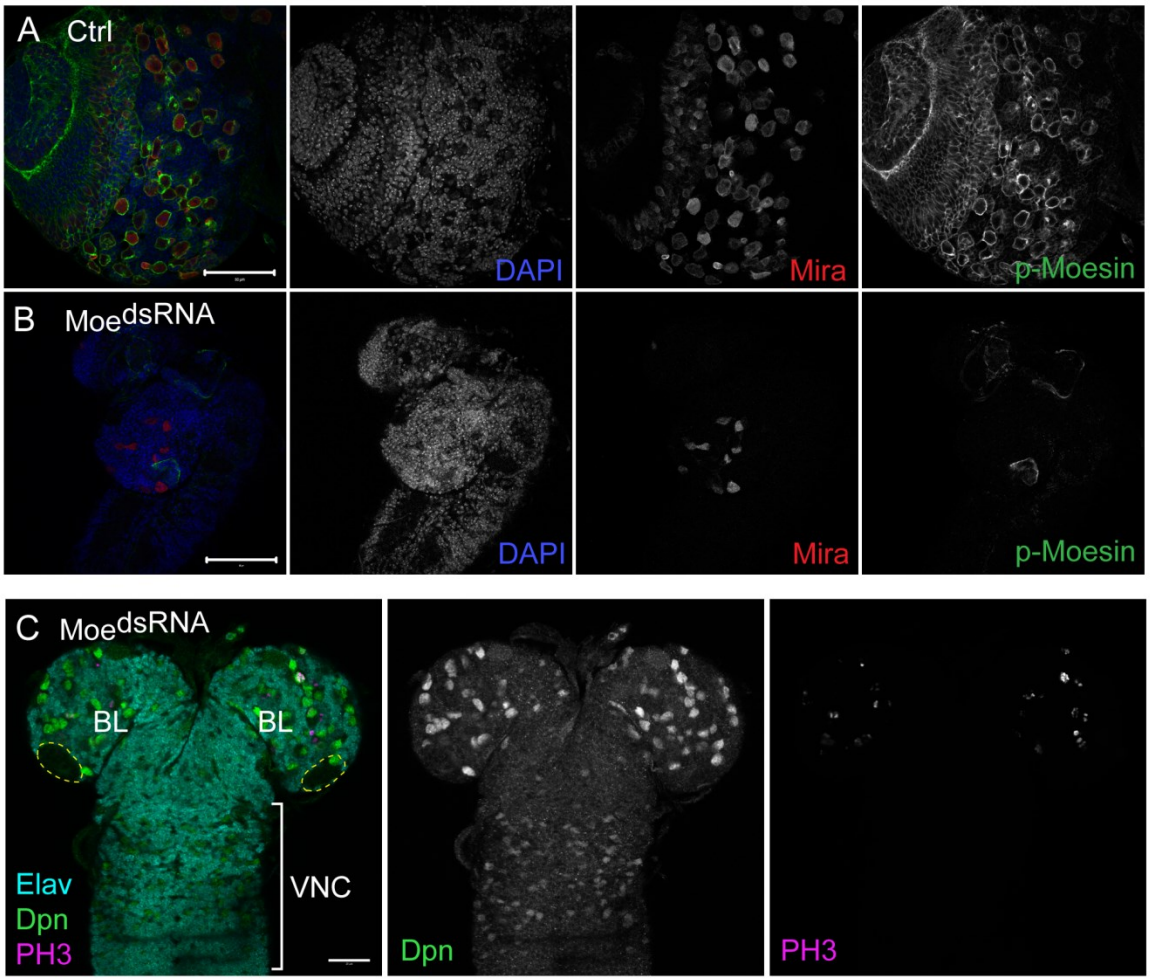

Figure 4-12: Reduced Moesin levels using *Insc-GAL4* display defects in neuroblast proliferation and optic lobe development. Larval central nervous systems isolated from progeny of *UAS-Dicer*;;*UAS-Moe*^{dsRNA} crossed to *w*^{1118} (Ctrl) and *Insc-GAL4* (Moe^{dsRNA}). (A) A single control larval brain lobe is shown. (B) Two larval brain lobes and the ventral nerve cord of the Moe^{dsRNA} are shown. The p-Moesin signal was largely reduced in the Moe^{dsRNA} larval neuroblasts. (A-B) Merge panel shows DAPI (blue), Miranda (Mira; red), and p-Moesin (green). (C) Larval brain lobes (BL) and the thoracic region of the ventral nerve cord (VNC) from Moe^{dsRNA} larvae at 96 hours after larval hatching (ALH). Deadpan (Dpn)-positive and phospho-histone H3 (PH3)-positive neuroblasts were present within the brain lobes, however no mitotic neuroblasts were observed in the thoracic region (87%, n=30) at 96 hours ALH. Yellow dashed line outlines the optic lobe primordium. (C) Merge panel shows Elav (cyan), Deadpan (green), and PH3 (magenta). Scale bars represent (A-B) 50 µm and (C) 20 µm.

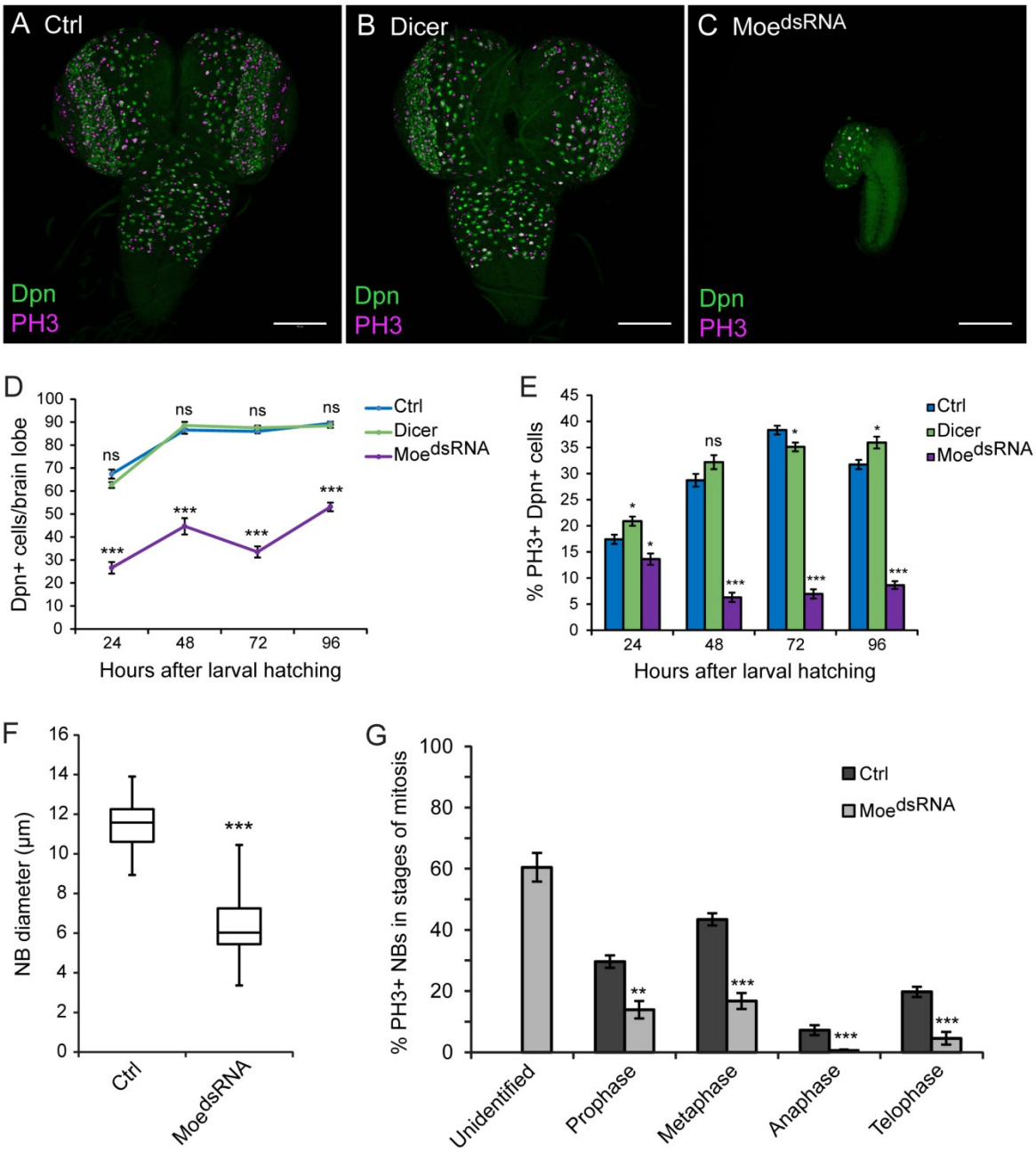
A Ctrl
B Dicer
C MoedsRNA
Dpn
PH3
D
Dpn+ cells/brain lobe
Hours after larval hatching
Ctrl
Dicer
MoedsRNA
ns
***
E
% PH3+ Dpn+ cells
Hours after larval hatching
Ctrl
Dicer
MoedsRNA
F
NB diameter (µm)
Ctrl
MoedsRNA
G
% PH3+ NBs in stages of mitosis
Ctrl
MoedsRNA
Unidentified
Prophase
Metaphase
Anaphase
Telophase

Figure 4-13: Moesin is essential for neuroblast proliferation. *UAS-Dicer*;;*UAS-Moe^{dsRNA}* was crossed to (A) *w^{1118}* (Ctrl) and (C) *Insc-GAL4* (Moe^{dsRNA}). (B) *UAS-Dicer* alone was crossed to *Insc-GAL4* (Dicer). (A-C) The larval central nervous systems fluorescently labelled with anti-Deadpan (Dpn; green) and anti-phospho-histone H3 (PH3; magenta) of Ctrl, Dicer, and Moe^{dsRNA} at 96 hours after larval hatching (ALH) are shown. (D) The mean number of Dpn-positive cells and (E) mean proportion of PH3-positive, Dpn-positive cells per central brain lobes of Ctrl, Dicer, and Moe^{dsRNA} at approximately 24, 48, 72, and 96 hours ALH (n=minimum of 28 brain lobes). (F) The median diameter of neuroblasts undergoing metaphase in Ctrl (n=23) and Moe^{dsRNA} (n=23) approximately 5-6 days after egg laying. (G) The mean proportion of PH3-positive, Dpn-positive cells undergoing the specific stages of mitosis per central brain lobe of Ctrl (n=28) and Moe^{dsRNA} (n=55). Scale bars represent (A-C) 100 μm. Error bars represent standard error. *$p<0.05$, **$p<0.001$, ***$p<0.0001$, and ns=not significant using Student's t-test.

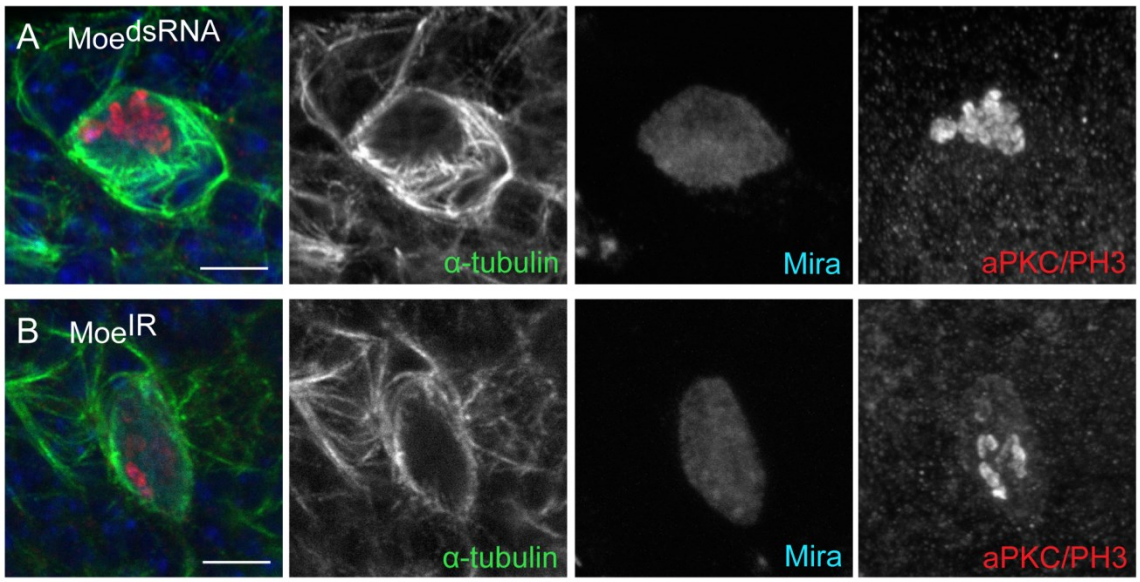

Figure 4-14: Mitotic defective neuroblasts are observed with reduced Moesin levels. Mitotic defective neuroblasts observed in larval brains isolated from *Insc-GAL4* crossed to (A) *UAS-Dicer*;;*UAS-Moe^{dsRNA}* (Moe^{dsRNA}) and (B) *UAS-Dicer*;;*UAS-Moe.IR.327-775* (Moe^{IR}). Mitotic defective neuroblasts were PH3-positive but lacked spindle poles (α-tubulin panel), even though the nuclear envelope appeared broken down (Mira panels). Merged panels show DAPI (blue), α-tubulin (green), aPKC/PH3 (red), and Miranda (Mira; cyan). Gray-scale panels of Mira and aPKC/PH3 are maximum intensity projections and the α-tubulin panel is a single focal plane image. Scale bars represent 5 μm.

4.3.6 Moesin is involved in apical polarity maintenance and mitotic spindle orientation

As p-Moesin was apically enriched in neuroblasts undergoing metaphase (Figure 4-10, B), I asked whether Moesin was required for apical polarity maintenance during neuroblast asymmetric cell division. Consistent with previous studies, I found that Bazooka and aPKC polarity was established during prophase in control neuroblasts (Figure 4-15, A and C) (Schober et al., 1999; Siegrist and Doe, 2006; Wodarz et al., 2000; Wodarz et al., 1999). In the Moesin knockdown neuroblasts, although spindle poles were visible using α-tubulin as a marker, Bazooka and aPKC crescents were not observed in a proportion of neuroblasts undergoing prophase (Figure 4-15, B and D, and Table 4). However, during metaphase, the majority of Moesin knockdown neuroblasts displayed an apical Bazooka crescent similar to controls (Table 4). The apical polarity protein Pins was also unaffected in the majority of Moesin knockdown neuroblasts undergoing metaphase (Table 4). Thus, although Bazooka polarity maintenance was initially affected in the Moesin knockdown neuroblasts undergoing prophase, this defect was less apparent during metaphase. Interestingly, I observed a more severe effect with aPKC and Par-6 polarity maintenance in metaphase neuroblasts when Moesin was knocked down. In the majority of Moesin knockdown neuroblasts, the Par-6 immunofluorescent signal was weak but polar (Figure 4-15, asterisk in F, and Table 4) or the polar crescent was absent during metaphase (Figure 4-15, G and Table 4). Similarly, a weak polar or absent polar aPKC signal was observed in the majority of metaphase Moesin knockdown neuroblasts (Figure 4-15, I-J, and Table 4). Although the basal polarity protein Miranda was mis-localized in a proportion of Moesin knockdown neuroblasts during metaphase, Miranda still localized to a cortical pole in the majority of neuroblasts. In Moesin knockdown neuroblasts with a weak polar aPKC signal, Miranda localized to the opposite cortical pole in 64% of metaphase neuroblasts (n=45; Figure 4-15, M). Even when an aPKC crescent was not observed in Moesin knockdown neuroblasts, Miranda still displayed a polar distribution in 63% of metaphase neuroblasts (n=16; Figure 4-15, N). Together, these findings suggest that Moesin may be important for overall apical polarity maintenance during prophase. During metaphase, Moesin is involved in Par-6 and aPKC polarity maintenance, but Bazooka and Pins localization at the apical cortex can occur in a partially Moesin-independent manner.

As larval development was severely disrupted in the Moesin knockdown, I examined a *Moesin* hypomorphic (partial loss-of-function) mutant (Moe^{G0323}), which displayed late larval lethality (Speck et al., 2003). The late larval brain morphology of the Moe^{G0323} mutant appeared largely normal and the number of neuroblasts per brain lobe was not statistically

different when compared to w^{1118} control brains (Figure 4-16). Thus, the Moe^{G0323} hypomorphic mutant phenotype was not as severe as the Moesin knockdown, although the p-Moesin immunofluorescent signal was reduced in the hypomorphic mutant (Figure 4-16).

As the Moe^{dsRNA} neuroblasts displayed defects in polarity maintenance, I examined apical/basal polarity and the mitotic spindle in Moe^{G0323} neuroblasts. In prometaphase control neuroblasts, the mitotic spindle had not fully extended to the cortical poles and weaker Miranda crescents were observed (Figure 4-17, A). In Moe^{G0323} mutant neuroblasts, the mitotic spindle did not reach the cortical poles and chromosome alignment appeared abnormal, although diffuse polar aPKC and polar Miranda immunofluorescent signals were observed (Figure 4-17, B-C). I also observed a misoriented mitotic spindle relative to the aPKC/Miranda polarity axis in Moe^{G0323} mutant neuroblasts (Figure 4-17, C). Furthermore, there appeared to be defects in spindle length with the loss of Moesin, as the mitotic spindle did not appear to extend to the cortical poles (Figure 4-17, B-C). It is unclear whether these Moe^{G0323} mutant neuroblasts are undergoing prometaphase or metaphase, which may be resolved with further live imaging analysis. In addition, future studies measuring the orientation and length of the mitotic spindle are essential for determining how Moesin affects the mitotic spindle during asymmetric cell division.

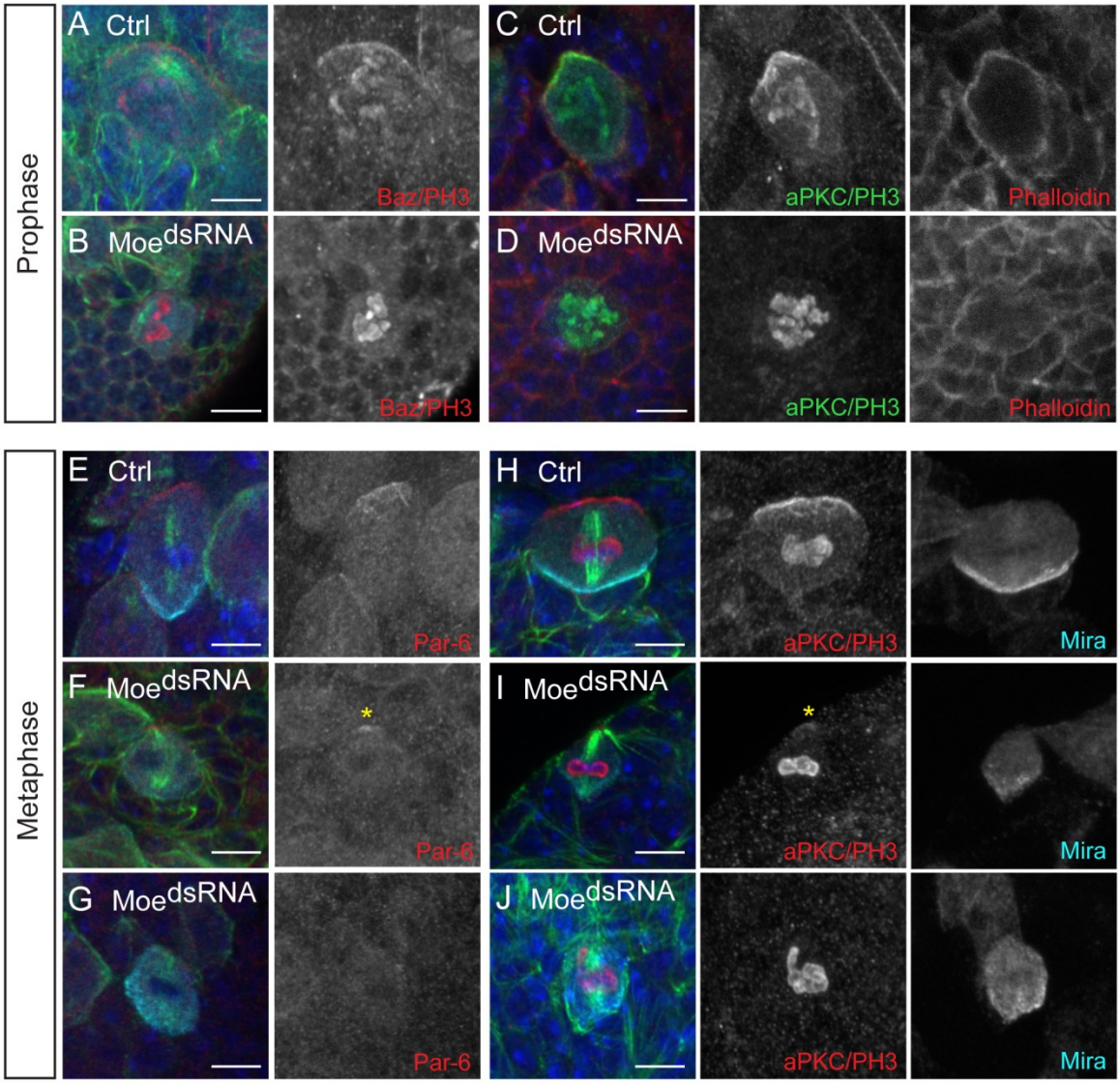
Prophase
A Ctrl
Baz/PH3
C Ctrl
aPKC/PH3
Phalloidin
B Moe dsRNA
Baz/PH3
D Moe dsRNA
aPKC/PH3
Phalloidin
Metaphase
E Ctrl
Par-6
H Ctrl
aPKC/PH3
Mira
F Moe dsRNA
*
Par-6
I Moe dsRNA
*
aPKC/PH3
Mira
G Moe dsRNA
Par-6
J Moe dsRNA
aPKC/PH3
Mira

Figure 4-15: Moesin regulates apical polarity maintenance in neuroblasts undergoing prophase and metaphase. *UAS-Dicer*;;*UAS-Moe*^{dsRNA} was crossed to *w*^{1118} (Ctrl) and *Insc-GAL4* (Moe^{dsRNA}) and larval neuroblasts undergoing (A-D) prophase and (E-J) metaphase were analyzed approximately 5-6 days after egg laying. (A) Bazooka (Baz) and (C) aPKC crescents formed in the majority of control neuroblasts during prophase. (B) Baz and (D) aPKC crescents were not observed in a proportion of Moe^{dsRNA} neuroblasts during prophase. (C-D) F-actin (Phalloidin; red) appeared disorganized in Moesin knockdown neuroblasts undergoing prophase, compared to controls. (E) Par-6 crescents formed in the majority of control neuroblasts during metaphase. (F) A weak or reduced polar Par-6 signal (yellow asterisk) and (G) an absent polar Par-6 signal was observed in Moe^{dsRNA} neuroblasts during metaphase. (H) aPKC crescents formed in the majority of control neuroblasts during metaphase. (I) A weak or reduced polar aPKC signal (yellow asterisk) and polar Miranda was observed in 64% of Moe^{dsRNA} neuroblasts during metaphase (n=55). (J) An absent polar aPKC crescent and polar Miranda was observed in 63% of Moe^{dsRNA} neuroblasts (n=22). Refer to Table 4 for summary of phenotypic proportions observed. Merged panels are single focal plane images and show DAPI (blue), Miranda (cyan), α-tubulin or aPKC/PH3 (green), and specified apical polarity proteins or Phalloidin (red). Gray-scale images are maximum intensity projections, with the exception of Phalloidin panels, which are single focal plane images. Scale bars represent 5 μm.

Table 4: Summary of apical phenotypic proportions observed in Moesin knockdown and control neuroblasts[a]

		Polar crescent		Weak/reduced crescent		Absent crescent	
		Control[b]	Moe^{dsRNA}[c]	Control	Moe^{dsRNA}	Control	Moe^{dsRNA}
Prophase	Bazooka	97% (*n*=29)	34% (*n*=29)	3% (*n*=29)	21% (*n*=29)	--	45% (*n*=29)
	aPKC	96% (*n*=44)	41% (*n*=49)	4% (*n*=44)	16% (*n*=49)	--	43% (*n*=49)
Metaphase	Bazooka	97% (*n*=73)	68% (*n*=66)	3% (*n*=73)	29% (*n*=66)	--	3% (*n*=66)
	Pins	100% (*n*=27)	69% (*n*=19)	--	26% (*n*=19)	--	5% (*n*=19)
	Par-6	92% (*n*=38)	16% (*n*=32)	8% (*n*=38)	44% (*n*=32)	--	37% (*n*=32)
	aPKC	97% (*n*=58)	27% (*n*=106)	3% (*n*=58)	52% (*n*=106)	--	21% (*n*=106)

[a] Refer to Figure 3 for examples of apical phenotypes observed

[b] Control represents progeny of *w*^{1118} crossed to *UAS-Dicer;;UAS-Moe*^{dsRNA}

[c] Moe^{dsRNA} represents progeny of *Insc-GAL4* crossed to *UAS-Dicer;;UAS-Moe*^{dsRNA}

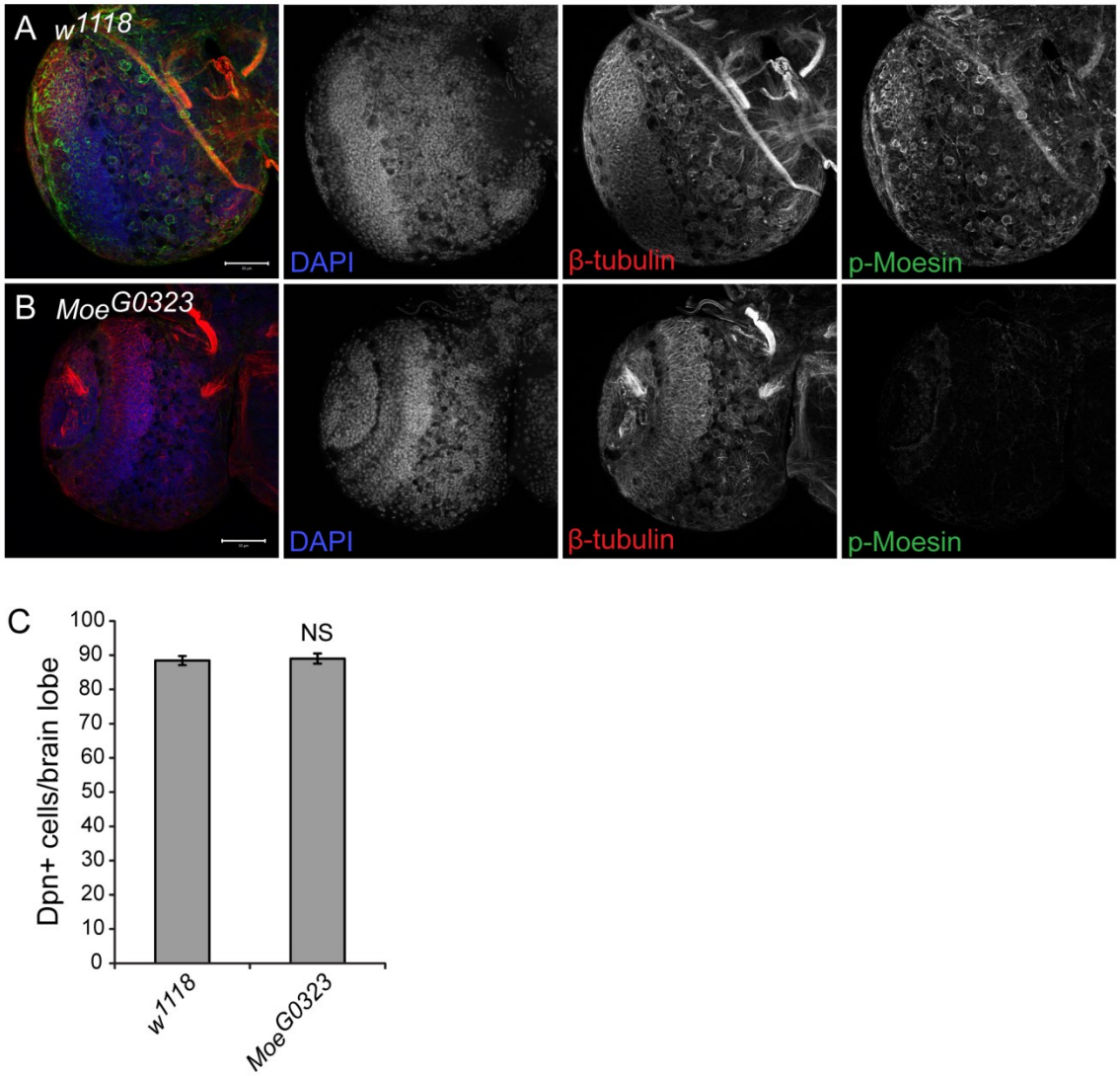

Figure 4-16: *Moesin* hypomorphic larval brains display reduced phosphorylated Moesin signal and normal brain morphology. (A) w^{1118} and (B) Moe^{G0323} third instar larval brains labelled with DAPI (blue), anti-β-tubulin (red), and anti-p-Moesin (green) are shown in merged panels. (C) Quantification of Deadpan (Dpn)-positive cells per central brain lobe in w^{1118} (n=27) and Moe^{G0323} (n=26). Scale bars represent 50 μm. ns=not significant using Student's t-test.

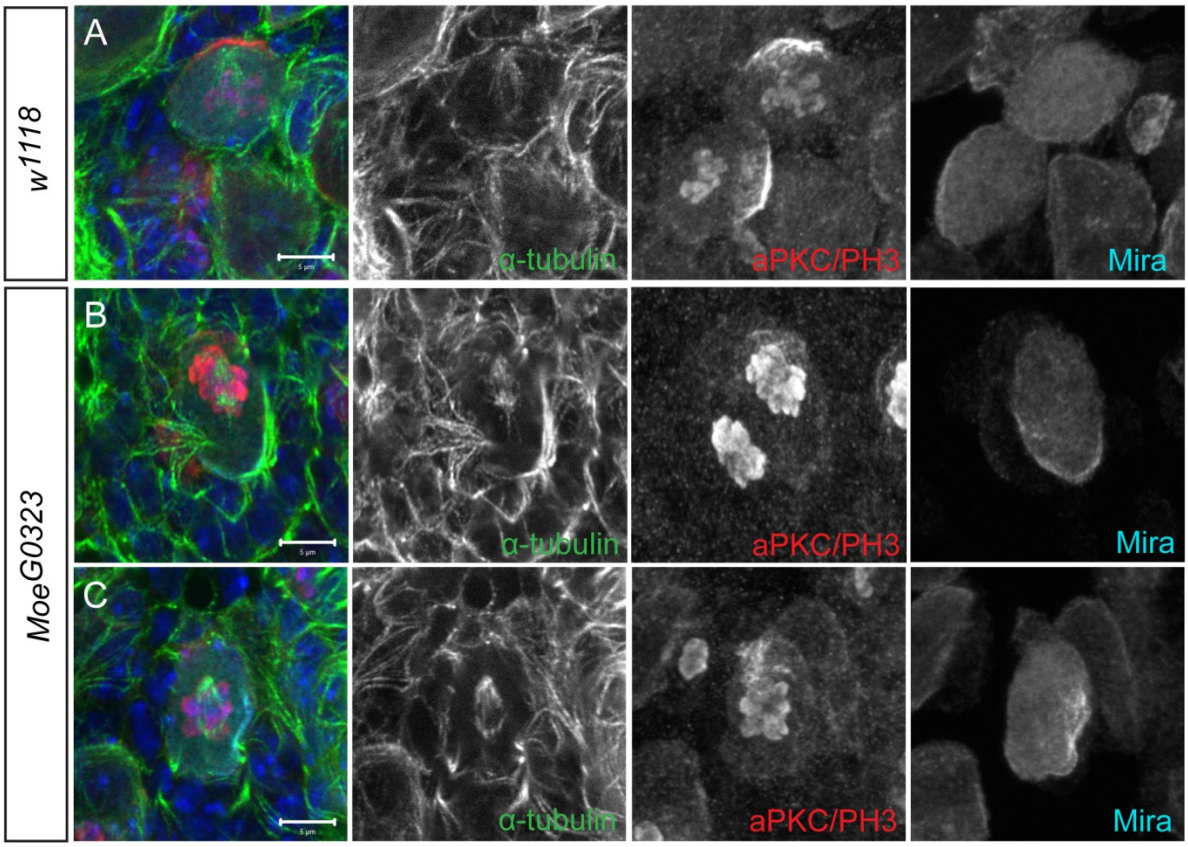

Figure 4-17: Moesin is involved in spindle orientation and chromosome alignment. (A) w^{1118} and (B-C) Moe^{G0323} third instar larval neuroblasts labelled with DAPI (blue), anti-α-tubulin (green), anti-aPKC/anti-phospho-histone H3 (aPKC/PH3; red), and anti-Miranda (Mira; cyan) as shown in merge panels. (A) In prometaphase control neuroblasts, the mitotic spindle had not fully extended to cortical poles and weaker Miranda crescents were observed. (B-C) In Moe^{G0323} mutant neuroblasts, the mitotic spindle did not reach the cortical poles and chromosome alignment appeared abnormal, although diffuse polar aPKC and polar Miranda crescents were observed. (C) A misoriented mitotic spindle relative to aPKC/Mira polarity was also observed in Moe^{G0323} mutant neuroblasts. Single focal plane images are shown in merge and α-tubulin panels. Maximum intensity projections are shown in aPKC/PH3 and Mira panels. Scale bars represent 5 μm.

4.3.7 Moesin is essential for cortical stability and remodelling during asymmetric cell division

Further analysis of aPKC polarity revealed that, in contrast to the Moesin knockdown, 98% of *Moe*^{G0323} mutant neuroblasts displayed a polar aPKC signal during metaphase (*n*=116). A polar aPKC crescent similar to controls was observed in 65% of *Moe*^{G0323} mutant neuroblasts. However, aPKC localized to ectopic sites at the neuroblast cortex in 35% of *Moe*^{G0323} mutant neuroblasts, when an aPKC crescent was also observed (*n*=75; Figure 4-18, arrow in B). Cortical instability was observed in mitotic *Moe*^{G0323} mutant neuroblasts, as indicated by the presence of cortical blebs (Figure 4-18, asterisk in B). In 21% of *Moe*^{G0323} mutant neuroblasts, the aPKC polar domain appeared disorganized and reduced in size compared to the polar aPKC crescents formed in controls (*n*=116; Figure 4-18, C). Miranda localized to the cortical pole opposite of aPKC in 74% of *Moe*^{G0323} mutant neuroblasts, although polar Miranda appeared reduced or diffuse in some cases (Figure 4-18, B and C). Thus, Moesin may regulate the integrity and organization of the polar domains, likely through regulating cortical stability during asymmetric cell division.

As the *Moesin* hypomorphic mutant phenotypes were not as severe, I was able to visualize neuroblasts undergoing anaphase and telophase, which were rarely observed in the Moesin knockdown (Figure 4-13, G). In control neuroblasts, basal furrow formation was induced by late anaphase, as indicated by Miranda localization at the smaller basal cortex and the segregating chromosomes reaching their respective poles (Figure 4-18, arrowheads in D). Although, aPKC and Miranda localized to opposite cortical poles in the majority of *Moe*^{G0323} neuroblasts undergoing anaphase (Figure 4-18, E), a misoriented polarity axis relative to the mitotic spindle was observed in 11% of *Moe*^{G0323} neuroblasts undergoing anaphase and early telophase (*n*=45). Furthermore, 64% of *Moe*^{G0323} neuroblast divisions appeared symmetric during initial constriction at the presumptive cleavage furrow site (*n*=11; Figure 4-18, arrowheads in E). However, during late cleavage furrow formation, 100% of the *Moe*^{G0323} neuroblast divisions appeared asymmetric similar to controls (*n*=20; Figure 4-18, F-G). Thus, the process of asymmetric membrane elongation and basal furrow induction may be impaired in the *Moesin* hypomorphic mutant neuroblasts undergoing anaphase.

Moesin has been implicated in driving cell shape changes in symmetrically dividing S2 cells (Roubinet et al., 2011). However, the function of Moesin in remodelling the cortex of asymmetrically dividing cells is unknown. To investigate cortical dynamics of control and *Moesin* hypomorphic mutant neuroblasts undergoing asymmetric cell division, live imaging was used to visualize filamentous actin and the mitotic spindle in neuroblasts expressing

LifeAct-GFP (Riedl et al., 2008) and chRFP-Tubulin (Rusan and Peifer, 2007). Asymmetric cell division of control neuroblasts lasted 12:21±0:22 (mean±standard error in minutes:seconds; *n*=24) measured from the point of nuclear envelope breakdown (NEB) to cytokinesis. In *Moe*^{G0323} mutant neuroblasts, asymmetric cell division lasted 16:13±0:55 (mean±standard error in minutes:seconds; p=0.0001 compared to controls, *n*=20). The increased time for asymmetric cell division to complete in the *Moe*^{G0323} mutant was due to a delay in anaphase onset, as the neuroblasts remained in metaphase for an extended period of time (Figure 4-19, A-B). In control neuroblasts, the cell cortex appeared round and stable during metaphase (Figure 4-19, A). However, in *Moe*^{G0323} neuroblasts, the metaphase cortex was unstable and irregular cortical actin dynamics were observed (Figure 4-19, B arrows). Thus, Moesin is essential for maintaining a round and stable metaphase cortex during asymmetric cell division.

Numerous studies have demonstrated that the ERM proteins both positively and negatively regulate Rho signaling (D'Angelo et al., 2007; Hatzoglou et al., 2007; Lee et al., 2004; Speck et al., 2003; Takahashi et al., 1998; Takahashi et al., 1997). To determine whether the non-uniform actin dynamics were due to defects in Rho1 signaling, Rho1 localization was examined in *Moe*^{G0323} mutant neuroblasts. *Moe*^{G0323} neuroblasts did not display any obvious differences in Rho1 localization during metaphase, when compared to controls (Figure 4-19, C-D). To further address potential changes in Rho1 activity, I analyzed the Rho1 downstream effector, Rho kinase, which phosphorylates and regulates cytoskeletal proteins, including Myosin II (Amano et al., 1996; Leung et al., 1995; Matsui et al., 1996). Neuroblasts expressing the Rho1 binding domain of Rho kinase (Rok) fused to GFP (Rok^{RBD}-GFP) (Abreu-Blanco et al., 2014) were analyzed in *w*^{1118} control and *Moe*^{G0323} mutant larval brains. A non-uniform distribution of phosphorylated Myosin Light Chain II (p-Myosin) was observed at the metaphase cortex, but no obvious difference in Rok^{RBD}-GFP was present in *Moe*^{G0323} mutant neuroblasts (Figure 4-19, E-F). Given these findings, the loss of Moesin does not appear to affect Rho1 during metaphase. Thus, the cortical instability observed during metaphase in the *Moe*^{G0323} neuroblasts is likely due to a defect in the ability of Moesin to crosslink the plasma membrane to the underlying actin cytoskeleton.

As the loss of Moesin led to defects in basal furrow induction and positioning (Figure 4-18, E), I further examined actomyosin organization during early anaphase. Control neuroblasts displayed restricted cortical actin at the site of furrow induction (Figure 4-20, A yellow arrowheads). In *Moe*^{G0323} neuroblasts, although basal furrow formation was induced following a delay in anaphase onset, cortical actin did not appear to be as restricted to the presumptive cleavage furrow site compared to controls (Figure 4-20, B yellow arrowheads).

Cortical instability was also observed throughout asymmetric cell division of *Moe*^{G0323} mutant neuroblasts, indicated by the presence of cortical blebbing (Figure 4-20, B yellow arrows). Previously, Myosin was shown to asymmetrically localize to the basal cortex in neuroblasts undergoing anaphase (Barros et al., 2003; Cabernard et al., 2010). The Myosin-induced basal furrow contributes to asymmetric cortical extension and formation of a basally displaced cleavage furrow, independent of the mitotic spindle (Cabernard et al., 2010; Connell et al., 2011). Consistent with previous studies, p-Myosin was enriched at the basal furrow in control neuroblasts undergoing early anaphase (80%, *n*=5; Figure 4-20, C). However, in *Moe*^{G0323} neuroblasts, p-Myosin was not enriched at the basal cortex during early anaphase (100%; *n*=5). The non-uniform distribution of p-Myosin at the lateral cortex observed in metaphase *Moe*^{G0323} neuroblasts (Figure 4-19, F) persisted into early anaphase, or p-Myosin localized to the equatorial region (Figure 4-20, D). These findings suggest that Moesin may function in the spindle-independent cleavage furrow positioning pathway. Thus, the initial appearance of symmetric divisions observed in *Moe*^{G0323} neuroblasts (Figure 4-18, E) is likely due to the absence of an induced p-Myosin basal furrow during early anaphase. However, during late cleavage furrow formation, p-Myosin localization in *Moe*^{G0323} neuroblasts was similar to controls and accumulated at the cleavage furrow site, supporting the observation that 100% of *Moe*^{G0323} neuroblast divisions eventually appeared asymmetric (*n*=20; Figure 4-18, G). Together, these findings suggest that Moesin regulates neuroblast cortical stability and actomyosin dynamics essential for timely mitotic progression and the initial establishment of cell size asymmetry.

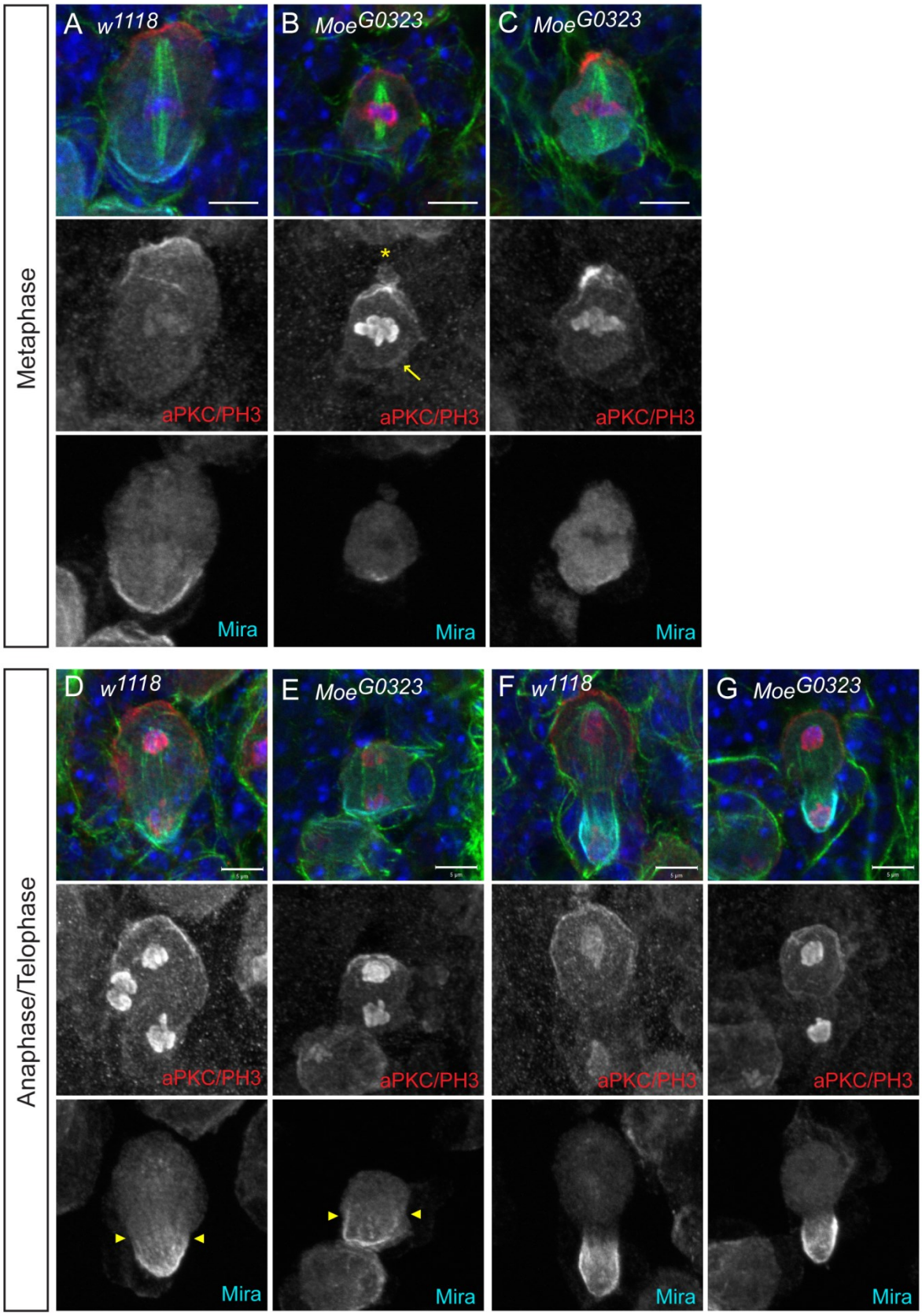
Metaphase
A w1118
B MoeG0323
C MoeG0323
aPKC/PH3
aPKC/PH3
aPKC/PH3
Mira
Mira
Mira
Anaphase/Telophase
D w1118
E MoeG0323
F w1118
G MoeG0323
aPKC/PH3
aPKC/PH3
aPKC/PH3
aPKC/PH3
Mira
Mira
Mira
Mira

Figure 4-18: Moesin is important for apical polarity integrity and cortical asymmetric divisions. Neuroblasts from w^{1118} and Moe^{G0323} third instar larvae were labelled with DAPI (blue), anti-α-tubulin (green), anti-aPKC/anti-phospho-histone H3 (aPKC/PH3; red) and anti-Miranda (Mira; cyan), as shown in merge panels. (A) A polar aPKC crescent formed in 91% of w^{1118} metaphase neuroblasts (*n*=23). (B) A polar aPKC crescent similar to controls formed in 65% of Moe^{G0323} metaphase neuroblasts (*n*=116), however aPKC localized to ectopic cortical sites in 35% of these Moe^{G0323} neuroblasts (yellow arrow; *n*=75). Cortical blebbing was also observed in Moe^{G0323} neuroblasts (yellow asterisk). (C) The polar aPKC domain appeared disorganized and reduced in size in 21% of Moe^{G0323} neuroblasts during metaphase (*n*=116). (B-C) Miranda localized to the opposite cortical pole of aPKC in 74% of Moe^{G0323} neuroblasts (*n*=116), although polar Miranda appeared reduced in size or diffuse, compared to control neuroblasts. (D) An asymmetric basal furrow was observed in w^{1118} neuroblasts undergoing anaphase (yellow arrowheads). (E) Divisions appeared symmetric in 64% of Moe^{G0323} neuroblasts undergoing initial constriction at the presumptive cleavage furrow site (yellow arrowheads; *n*=11). (G) During later stages of cleavage furrow formation, 100% of Moe^{G0323} neuroblast divisions appeared asymmetric (*n*=20). Merged panels are single focal plane images and gray-scale images are maximum intensity projections. Scale bars represent 5 μm.

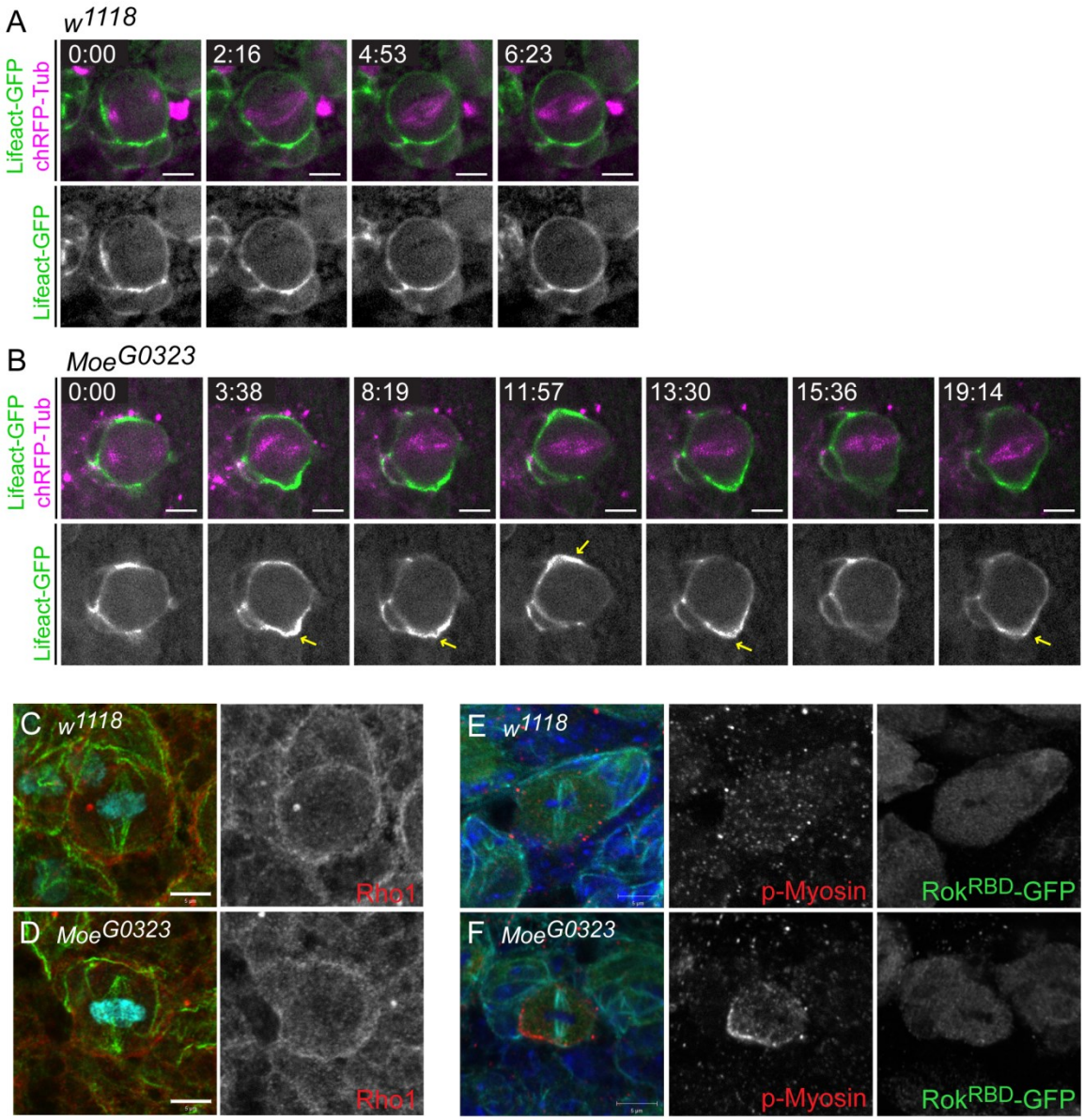
A
w1118
0:00
2:16
4:53
6:23
Lifeact-GFP
chRFP-Tub
Lifeact-GFP
B
MoeG0323
0:00
3:38
8:19
11:57
13:30
15:36
19:14
Lifeact-GFP
chRFP-Tub
Lifeact-GFP
C
w1118
Rho1
D
MoeG0323
Rho1
E
w1118
p-Myosin
RokRBD-GFP
F
MoeG0323
p-Myosin
RokRBD-GFP

Figure 4-19: Moesin is essential for maintaining a stable actomyosin cortex in metaphase neuroblasts. (A-B) Live imaging of *Insc-GAL4*; *UAS-ChRFP-Tub*, *UAS-Lifeact-GFP* crossed to (A) w^{1118} and (B) Moe^{G0323} to visualize filamentous actin (green) and the mitotic spindle (magenta) in the neuroblasts. Single focal plane images were shown to demonstrate cortical dynamics during metaphase. The time value in the top left corner of the merged panels is shown in minutes:seconds. Nuclear envelope breakdown (NEB) occurs at 0:00. (A) A round and stable metaphase cortex was observed in control neuroblasts. (B) The neuroblast cortex appeared unstable and non-uniform cortical actin (yellow arrows) was observed in Moe^{G0323} mutant neuroblasts during metaphase. (C-D) Obvious differences in cortical Rho1 were not observed in Moe^{G0323} mutant neuroblasts, compared to w^{1118} neuroblasts during metaphase. Merge panels show Rho1 (red), phospho-histone H3 (cyan), and α-tubulin (green). (E-F) Metaphase neuroblasts observed in larval brains isolated from *Insc-GAL4*; *UAS-Rok.Rho binding domain* (RBD)-*GFP* (Rok^{RBD}-GFP) crossed to (E) w^{1118} and (F) Moe^{G0323}. (E) Rok^{RBD}-GFP and phospho-Myosin Light Chain II (p-Myosin) appeared cytoplasmic in w^{1118} control neuroblasts. (F) Rok^{RBD}-GFP distribution in Moe^{G0323} mutant neuroblasts was similar to controls, although p-Myosin displayed an enriched, non-uniform distribution at the neuroblast cortex. Merge panels show DAPI (blue), p-Myosin (red), GFP (green), and α-tubulin (cyan). Scale bars represent 5 μm.

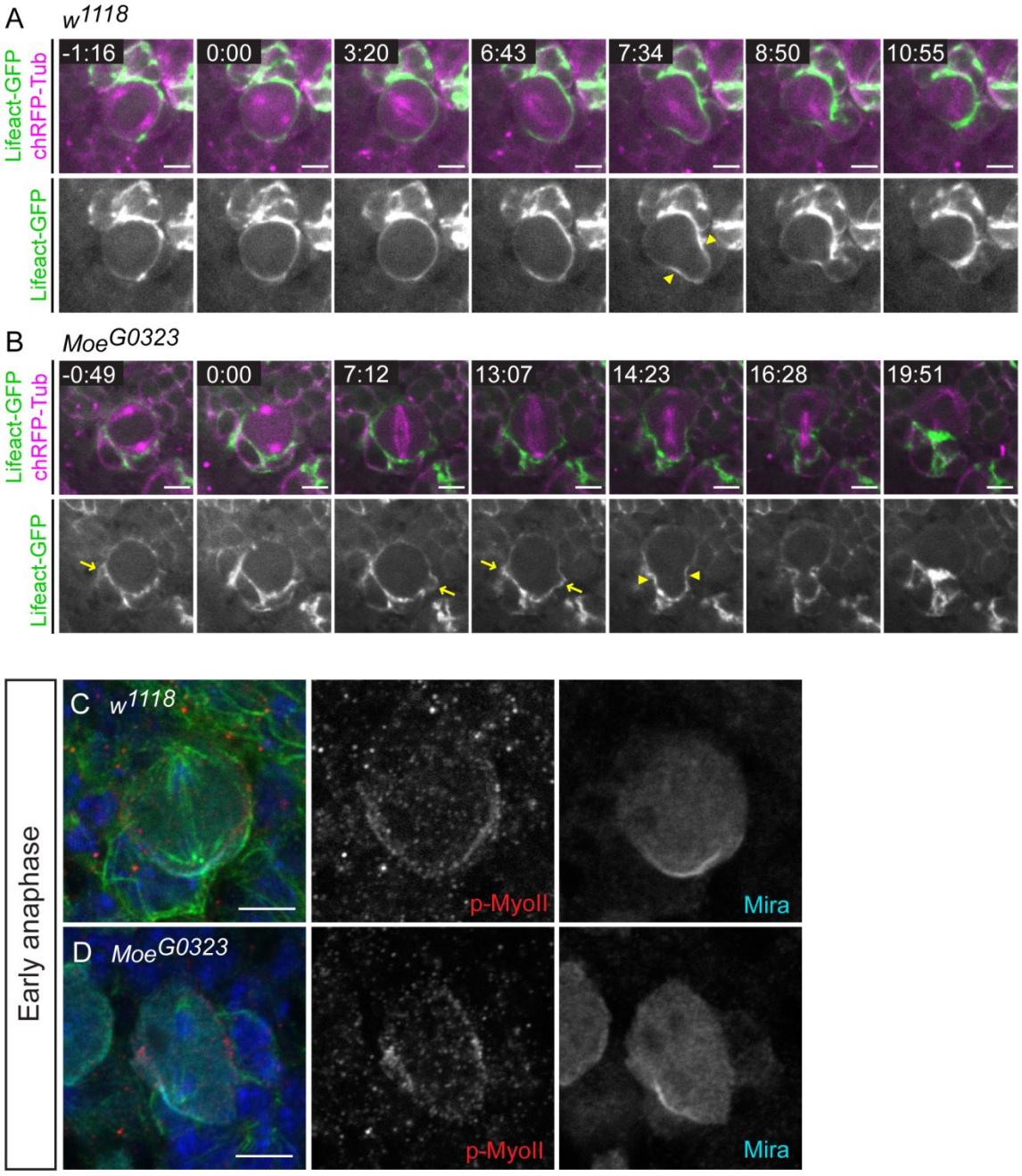
A
w1118
Lifeact-GFP
chRFP-Tub
-1:16
0:00
3:20
6:43
7:34
8:50
10:55
Lifeact-GFP
B
MoeG0323
Lifeact-GFP
chRFP-Tub
-0:49
0:00
7:12
13:07
14:23
16:28
19:51
Lifeact-GFP
Early anaphase
C
w1118
p-MyoII
Mira
D
MoeG0323
p-MyoII
Mira

Figure 4-20: Moesin regulates Myosin-induced furrow positioning during early anaphase. (A-B) Live imaging of *Insc-GAL4*; *UAS-ChRFP-Tub*, *UAS-Lifeact-GFP* crossed to w^{1118} and Moe^{G0323} to visualize filamentous actin (green) and the mitotic spindle (magenta) in the neuroblasts. The time value in the top left corner of the merged panels is shown in minutes:seconds. NEB occurs at 0:00. (A) Furrow induction (yellow arrowheads) showed restricted cortical actin at this site in the w^{1118} control neuroblast. (B) Cortical actin did not appear to be as restricted to the furrow site (yellow arrowheads) in the Moe^{G0323}, as in the w^{1118} neuroblast. Cortical blebbing (yellow arrows) was also observed throughout mitosis of Moe^{G0323} neuroblast. (C-D) w^{1118} and Moe^{G0323} larval neuroblasts undergoing early anaphase were labelled with DAPI (blue), anti-α-tubulin (green), anti-phospho-Myosin Light Chain II (p-Myosin; red), and anti-Miranda (Mira; cyan). (C) P-Myosin localized to the basal furrow in 80% of w^{1118} neuroblasts undergoing early anaphase (n=5). (D) P-Myosin localized to the cell equator in the Moe^{G0323} neuroblast shown and the p-Myosin basal furrow was not observed during early anaphase (100%; n=5). All panels shown are a single focal plane images. Scale bars represent 5 μm.

4.3.8 Examining the expression of Moesin transgenes in neuroblasts

To further characterize the functional significance of Moesin phosphorylation in the neuroblasts, I over-expressed wild-type Moesin (Moe^{WT}), a phosphomimetic or active form of Moesin (Moe^{T559D}), and a non-phosphorylated or inactive form of Moesin (Moe^{T559A}) using *Insc-GAL4*. Multiple tagged-*Moesin* transgenic lines were available in the lab stocks. Thus, the expression levels of the transgenic lines were examined using western blot analysis and lines that were expressed at similarly high levels were chosen for further analysis (Refer to Materials and Methods Section 4.2.5). The over-expression of Moe^{WT}, Moe^{T559D}, and Moe^{T559A} in the neuroblasts did not lead to obvious defects in overall brain morphology, proliferation (PH3), glial cell (Repo), and neuronal (Elav) markers when compared to control larval brain lobes (Figure 4-21). When the neuroblasts within the central brain were examined more closely, defects in the ganglion mother cells (Prospero) or overall central brain organization (DCAD) were not observed when the *Moesin* transgenes were over-expressed (Figure 4-22). The over-expression of Moe^{T559D} and Moe^{T559A} appeared to reduce neuroblast cell size as shown using cytoplasmic Sip1 as a neuroblast marker (Figure 4-22, C-D); however neuroblast diameter would need to be measured to confirm this finding. Furthermore, aPKC and Miranda crescents formed at opposite poles similar to controls, when the *Moesin* transgenes were over-expressed (Figure 4-23). However, spindle alignment appeared abnormal in metaphase neuroblasts over-expressing Moe^{T559A} (Figure 4-23**,** D). Together, these findings show that the phenotypes observed with the over-expression of the *Moesin* transgenes were subtle and variable, possibly due to the presence of endogenous Moesin.

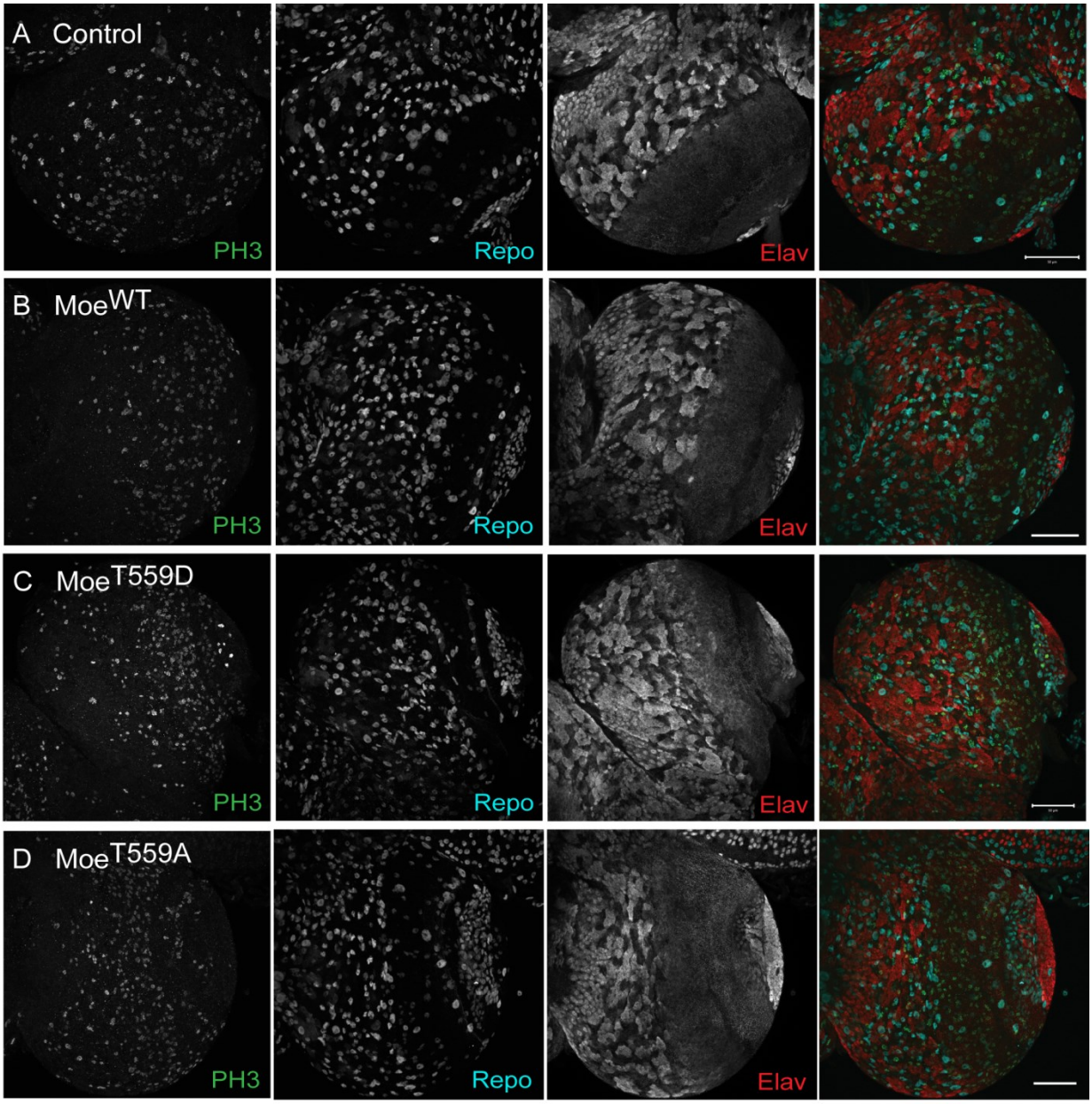
A Control
PH3
Repo
Elav
B MoeWT
PH3
Repo
Elav
C MoeT559D
PH3
Repo
Elav
D MoeT559A
PH3
Repo
Elav

Figure 4-21: Over-expression of *Moesin* transgenes using *Insc-GAL4* and larval brain morphology. The neuroblast GAL4 driver, *Insc-GAL4*, was crossed to (A) w^{1118}, (B) *UAS-Moesin* (Moe^{WT}), (C) *UAS-Moesin*^{T559D} (Moe^{T559D}), and (D) *UAS-Moesin*^{T559A} (Moe^{T559A}). Third instar larval brains were dissected and fluorescently labelled for anti-phospho-histone H3 (PH3; green), anti-Repo (cyan), and anti-Elav (red), as shown in merge panels. When the *Moesin* transgenes were over-expressed, proliferation, differentiated cell markers, Repo and Elav, and the overall brain morphology appeared similar to controls. Maximum intensity projections are shown. Scale bar represents 50 μm.

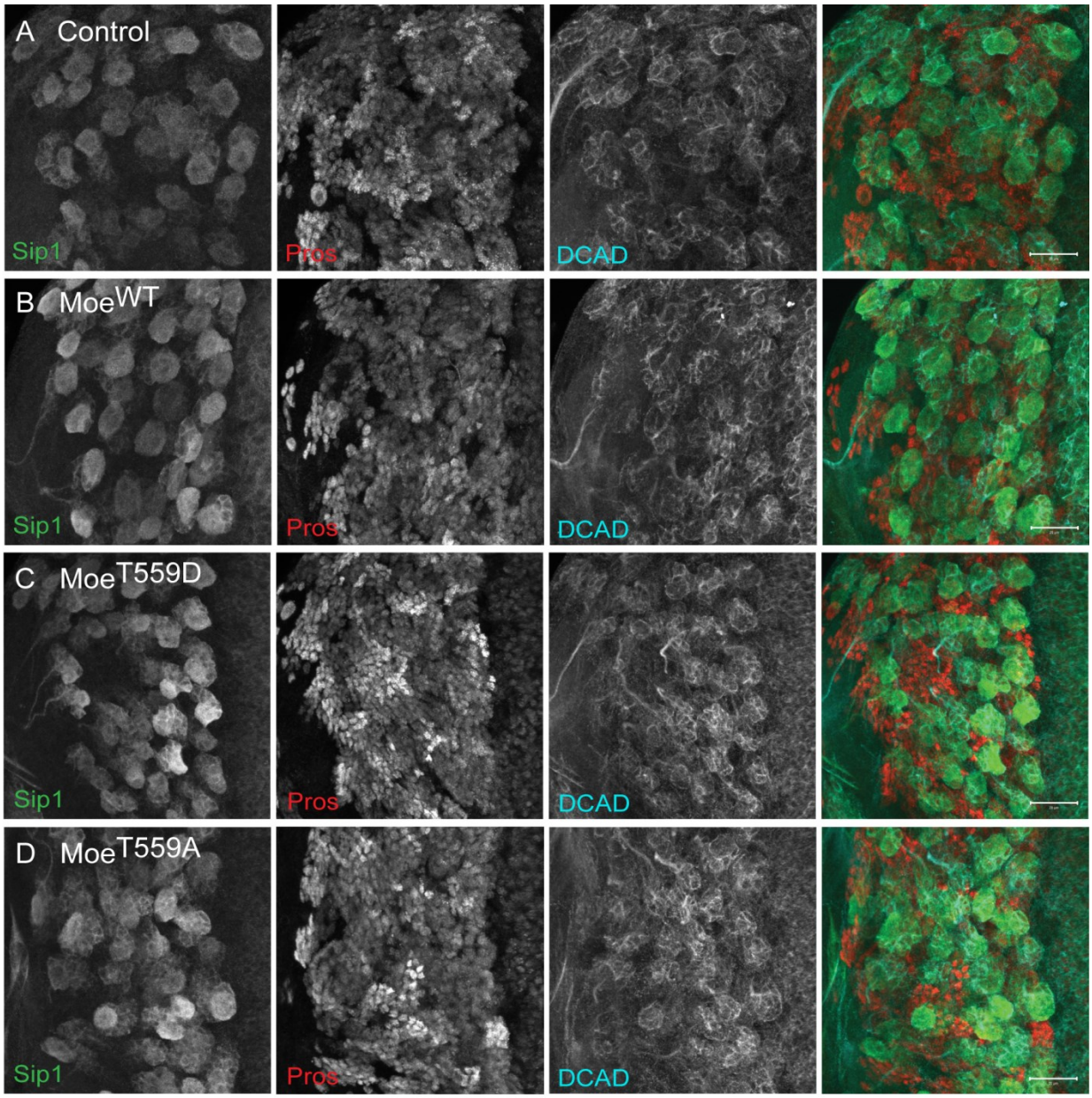
A Control
Sip1
Pros
DCAD
B MoeWT
Sip1
Pros
DCAD
C MoeT559D
Sip1
Pros
DCAD
D MoeT559A
Sip1
Pros
DCAD

Figure 4-22: Over-expression of *Moesin* transgenes using *Insc-GAL4* and central brain neuroblasts. The neuroblast GAL4 driver, *Insc-GAL4*, was crossed to (A) w^{1118}, (B) *UAS-Moesin* (Moe^{WT}), (C) *UAS-Moesin*^{T559D} (Moe^{T559D}), and (D) *UAS-Moesin*^{T559A} (Moe^{T559A}). Third instar larval brains were dissected and fluorescently labelled for anti-Sip1 (green), anti-Prospero (Pros; red), and anti-DE-Cadherin (DCAD; cyan), as shown in merge panels. When the *Moesin* transgenes were over-expressed, the ganglion mother cell marker, Pros, and DCAD appeared similar to controls. The over-expression of (C) Moe^{T559D} and (D) Moe^{T559A} may affect neuroblast cell size as shown in Sip1 panels. Maximum intensity projections are shown. Scale bar represents 20 μm.

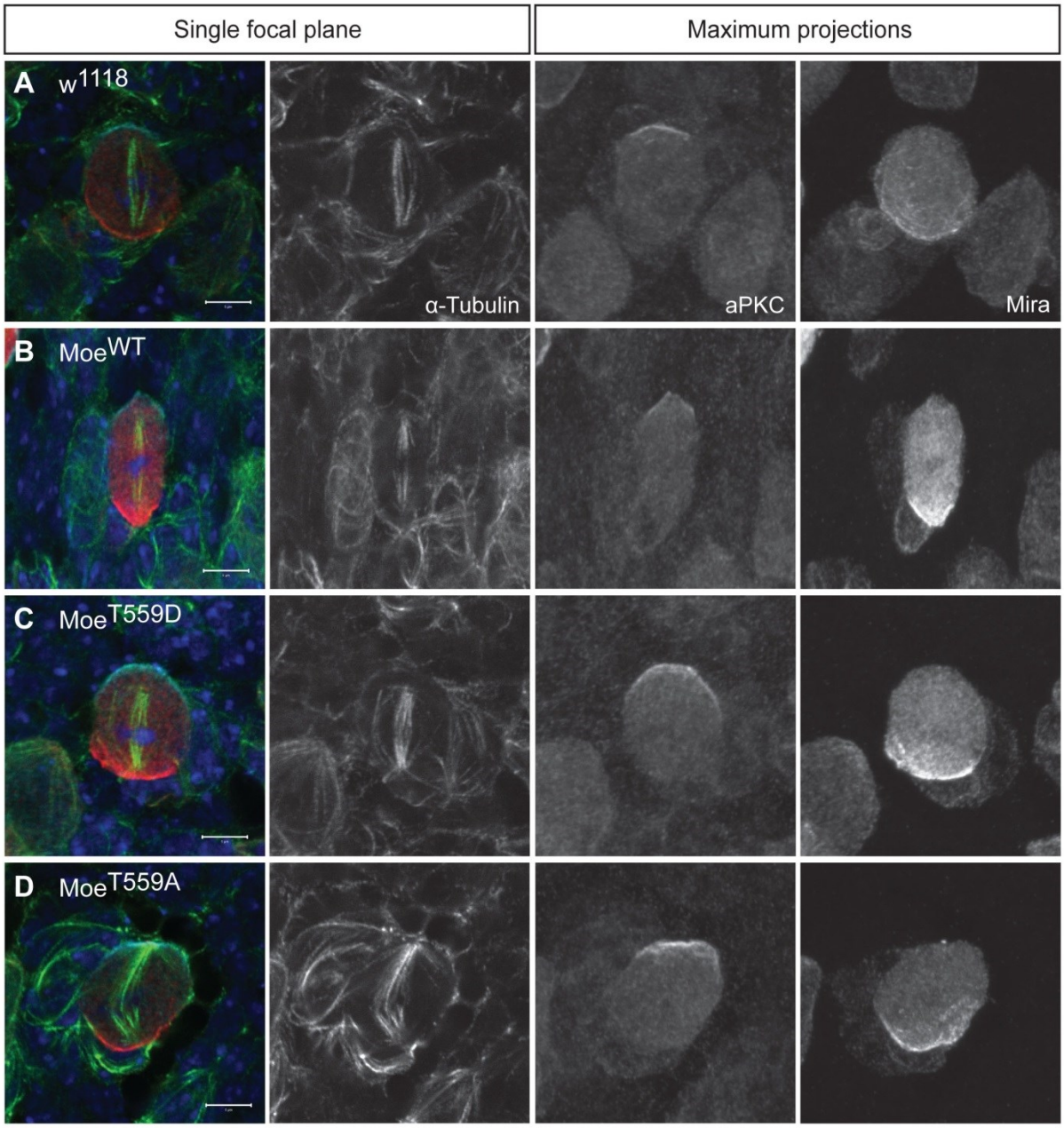
Single focal plane
Maximum projections
A w1118
α-Tubulin
aPKC
Mira
B MoeWT
C MoeT559D
D MoeT559A

Figure 4-23: Metaphase neuroblasts with the over-expression of *Moesin* transgenes. The neuroblast GAL4 driver, *Insc-GAL4*, was crossed to (A) w^{1118}, (B) *UAS-Moesin* (Moe^{WT}), (C) *UAS-Moesin*^{T559D} (Moe^{T559D}), and (D) *UAS-Moesin*^{T559A}. Third instar larval brains were dissected and fluorescently labelled for DAPI (blue), anti-aPKC (cyan), anti-Miranda (Mira; red), and anti-α-tubulin (green), as shown in merge panels. (B-D) Over-expression of Moe^{WT}, Moe^{T559D}, and Moe^{T559A} displayed normal aPKC and Miranda crescents forming at opposite poles in metaphase neuroblasts, similar to controls. (D) Over-expression of Moe^{T559A} resulted in abnormal spindle alignment. Single focal plane images are shown in merge and α-tubulin panels. Maximum intensity projection images are shown in aPKC and Mira panels. Scale bars represent 5 μm.

4.3.9 The apical polarity complex is important for asymmetric Moesin localization during metaphase

We then wanted to determine which proteins regulate the asymmetric distribution and activity of Moesin in mitotic neuroblasts. The loss of known apical polarity proteins were examined for defects in the apical enrichment of p-Moesin during metaphase. The dsRNA-mediated knockdown of apical polarity proteins Cdc42, Par-6, aPKC, and Lgl using *Insc-GAL4*, resulted in a uniform distribution of p-Moesin in a proportion of metaphase neuroblasts (Figure 4-24, A-E). Thus, Moesin not only regulates apical polarity maintenance and integrity, but components of the apical Par complex in turn regulate the asymmetric distribution of Moesin in neuroblasts.

I also examined whether the loss of Pins would affect p-Moesin distribution during metaphase. The *pins*^{193} hypomorphic mutant larval brains (Parmentier et al., 2000) displayed a wide range of phenotypes (Figure 4-24, F-K). P-Moesin and Numb displayed both a polar and uniform or discontinuous distribution at the cortex of *pins* mutant neuroblasts during metaphase (*n*=138; Figure 4-24, G-K). In 17% of *pins* mutant neuroblasts, polar p-Moesin and Numb crescents formed at opposite poles during metaphase, similar to control neuroblasts (Figure 4-24, F and G). However, in 19% of *pins* mutant neuroblasts, polar p-Moesin and Numb crescents formed at the same cortical pole (Figure 4-24, H). Although p-Moesin displayed a polar enrichment, Numb was also uniformly distributed at the cortex in a proportion of *pins* mutant neuroblasts (17%, n=138; Figure 4-24, I). A uniform or discontinuous distribution of p-Moesin was also observed in *pins* mutant neuroblasts, with either a polar (16%, n=138) or a uniform (20%, n=138) distribution of Numb at the cortex (Figure 4-24, J and K, respectively). Furthermore, of the *pins* mutant neuroblasts that formed either p-Moesin or Numb crescents, the mitotic spindle was misoriented relative to either crescent in 41% of metaphase neuroblasts (n=108; Figure 4-24, merge panels in G, H, and J). These findings suggest that Pins is important for proper asymmetric distribution of p-Moesin opposite of Numb and relative to the mitotic spindle during metaphase. Thus, known apical polarity proteins are important for the apical distribution of p-Moesin during metaphase, confirming that Moesin is a novel player essential for neuroblast asymmetric cell division.

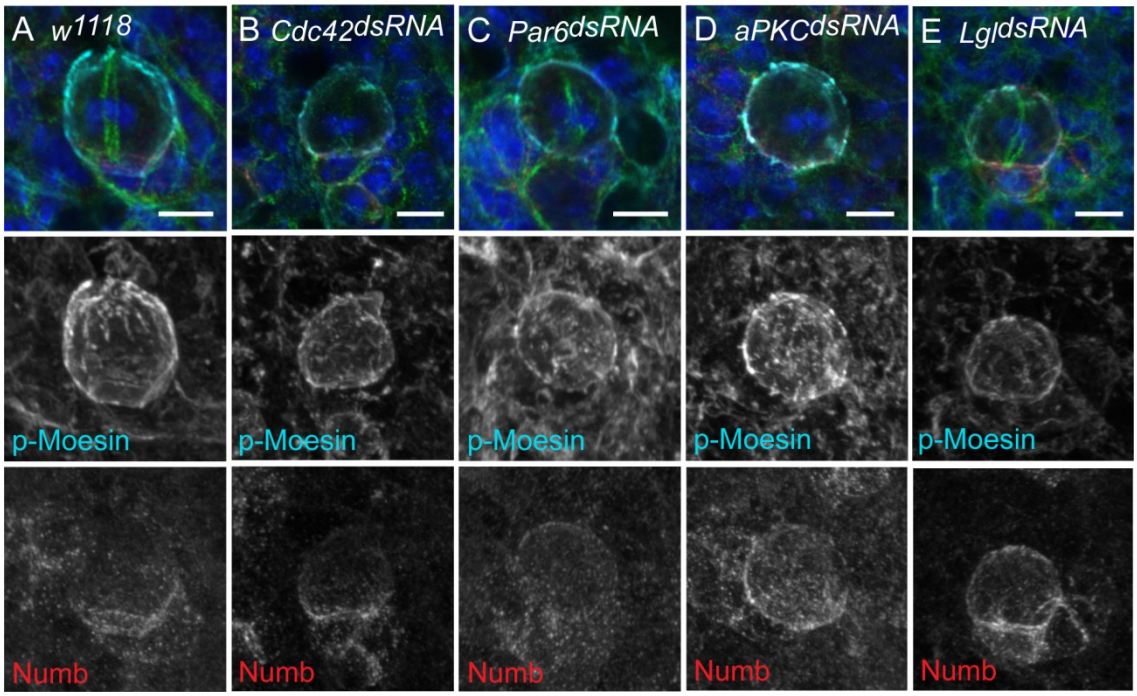
A w1118
B Cdc42dsRNA
C Par6dsRNA
D aPKCdsRNA
E LgldsRNA
p-Moesin
p-Moesin
p-Moesin
p-Moesin
p-Moesin
Numb
Numb
Numb
Numb
Numb

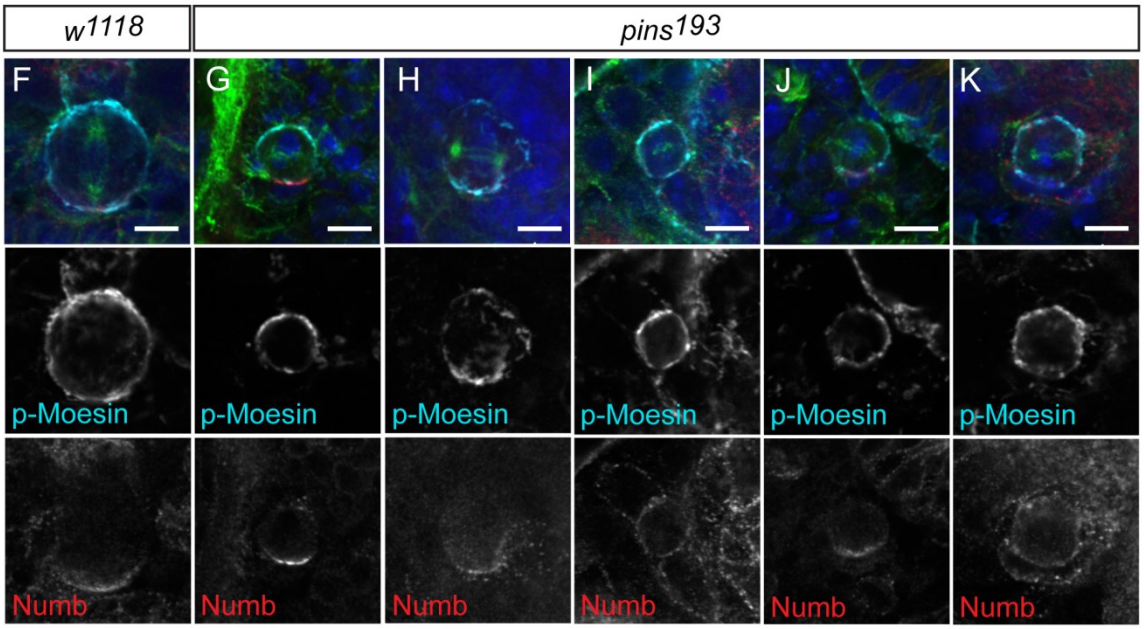
w1118
pins193
F
G
H
I
J
K
p-Moesin
p-Moesin
p-Moesin
p-Moesin
p-Moesin
p-Moesin
Numb
Numb
Numb
Numb
Numb
Numb

Figure 4-24: Apical polarity proteins regulate the asymmetric distribution of Moesin during metaphase. Third instar larval neuroblasts of (A) w^{1118}, (B) *UAS-Cdc42*^{dsRNA}, (C) *UAS-Par6*^{dsRNA}, (D) *UAS-aPKC*^{dsRNA}, and (E) *UAS-Lgl*^{dsRNA} crossed to *Insc-GAL4.* P-Moesin was uniformly cortical in (B) 45% (*n*=9), (C) 42% (*n*=28), (D) 45% (*n*=29), and (E) 26% (*n*=39) metaphase neuroblasts of respective knockdowns, compared to (A) w^{1118} controls (100%, *n*=21). (F-K) w^{1118} and *pins*^{193} larval neuroblasts undergoing metaphase approximately 5-6 days after egg laying. (G-K) Multiple phenotypes were observed in *pins*^{193} mutant neuroblasts during metaphase (*n*=138). (G) Polar p-Moesin and Numb localized to opposite poles (17%), (H) polar p-Moesin and Numb localized to the same pole (19%), (I) polar p-Moesin and uniform Numb (17%), (J) uniform/discontinuous p-Moesin and polar Numb (16%), and (K) uniform/discontinuous p-Moesin and uniform Numb (20%) were all observed. Merged panels are single focal plane images and show DAPI (blue), p-Moesin (cyan), Numb (red), and β-tubulin (green). Gray-scale images in (A-E) are maximum intensity projections and (F-K) are single focal plane images. Scale bars represent 5 μm.

4.3.10 Slik kinase is required for neuroblast asymmetric cell division and Moesin phosphorylation in the neuroblasts

The Sterile20-like kinase, Slik, has been shown to regulate Moesin phosphorylation in wing imaginal discs and follicle cell epithelium (Carreno et al., 2008; Hipfner et al., 2004; Hughes and Fehon, 2006). As a role for Slik in Drosophila neuroblasts is unknown, I first examined Slik localization in the larval neuroblasts. Slik was uniformly distributed at the neuroblast cortex and partially co-localized with Moesin (Figure 4-25, A). In addition, Slik localized to the cortex of the differentiated ganglion mother cells, as marked by Prospero (Figure 4-25, A). To determine the functional significance of Slik in the larval central nervous system, I analyzed the *slik*^{1} null mutant (Hipfner and Cohen, 2003). The *slik* mutant central nervous system was reduced in size (Figure 4-25, B-C) with a decrease in neuroblast numbers at 96 hours ALH, compared to controls (Figure 4-25, D). There was a reduced proportion of proliferating neuroblasts per brain lobe in the *slik* mutant (Figure 4-25, E), suggesting that neuroblast proliferation and differentiation were affected with the loss of Slik. In addition, the few *slik* mutant neuroblasts undergoing metaphase had a reduced diameter of 6.98 μm (median; maximum of 9.85 μm), compared to controls (median of 12.42 μm and maximum of 15.39 μm; Figure 4-25, F). These phenotypes observed in the *slik* mutant were very similar to what was observed in the Moesin knockdown (Figure 4-13). Indeed, the p-Moesin immunofluorescent signal was largely reduced in *slik* mutant larval neuroblasts undergoing metaphase (Figure 4-25, G-H), suggesting that Slik regulates Moesin phosphorylation during asymmetric cell division.

We then wanted to examine whether Slik also regulated aPKC polarity maintenance and found that in 94% of *slik* mutant neuroblasts, an aPKC crescent did not form during prophase, compared to control neuroblasts (n=16; Figure 4-26, A-B). During metaphase, 67% of *slik* mutant neuroblasts formed a weak polar aPKC signal (n=15; Figure 4-26, asterisk in D). However, in 27% of *slik* mutant neuroblasts, an aPKC crescent was not present, although Miranda still appeared to localize basally in both cases (n=15; Figure 4-26, E). Together, these findings suggest that Slik is important for neuroblast proliferation and aPKC polarity maintenance during asymmetric cell division, likely through regulating Moesin activity.

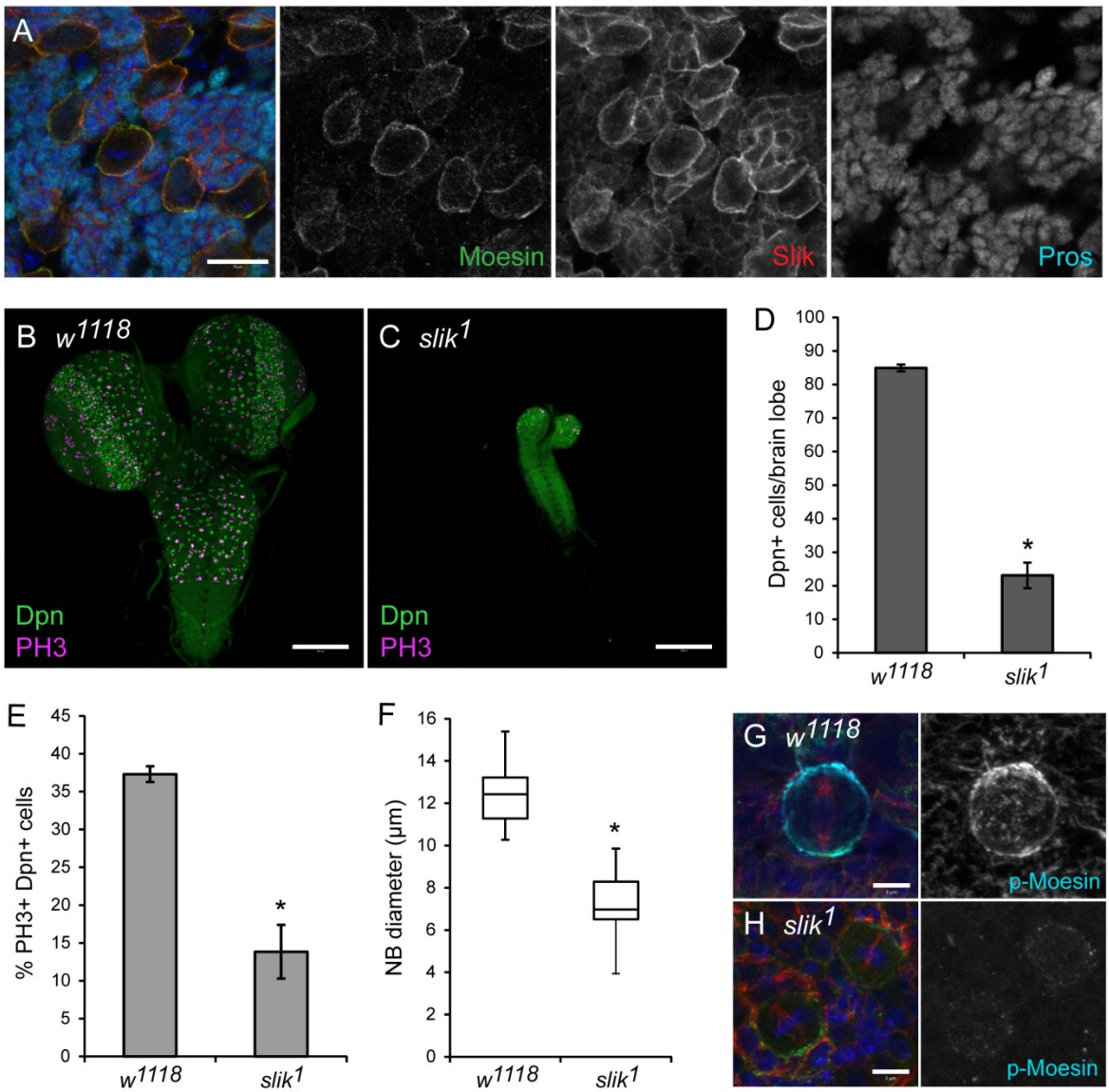
A
Moesin
Slik
Pros
B w1118
Dpn
PH3
C slik1
Dpn
PH3
D
Dpn+ cells/brain lobe
100
90
80
70
60
50
40
30
20
10
0
*
w1118
slik1
E
% PH3+ Dpn+ cells
45
40
35
30
25
20
15
10
5
0
*
w1118
slik1
F
NB diameter (µm)
16
14
12
10
8
6
4
2
0
*
w1118
slik1
G w1118
p-Moesin
H slik1
p-Moesin

Figure 4-25: Slik is essential for neuroblast proliferation and Moesin phosphorylation. (A) w^{1118} third instar larval brains labelled with anti-Slik (red), anti-Moesin (green), and anti-Prospero (cyan). Slik partially co-localized with Moesin at the neuroblast cortex and localized to the ganglion mother cell cortex. (B-C) w^{1118} and $slik^{1}$ larval central nervous systems labelled with anti-Deadpan (Dpn; green) and anti-phospho-histone H3 (PH3; magenta) at 96 hours after larval hatching (ALH). (D) The mean number of Dpn-positive cells and (E) the mean proportion of PH3-positive, Dpn-positive cells per central brain lobes of w^{1118} (n=35) and $slik^{1}$ (n=26) at 96 hours ALH. (F) The median diameter of neuroblasts undergoing metaphase in w^{1118} (n=25) and $slik^{1}$ (n=29) approximately 5-6 days after egg laying (AEL). (G-H) w^{1118} and $slik^{1}$ larval metaphase neuroblasts labelled with DAPI (blue), anti-p-Moesin (cyan), anti-Numb (green), and anti-β-tubulin (red) at approximately 5-6 days AEL. (H) The p-Moesin signal was reduced in $slik^{1}$ mutant neuroblasts compared to w^{1118} controls. Scale bars represent (A) 10 μm, (B-C) 100 μm, and (G-H) 5 μm. *$p<0.0001$ using Student's t-test.

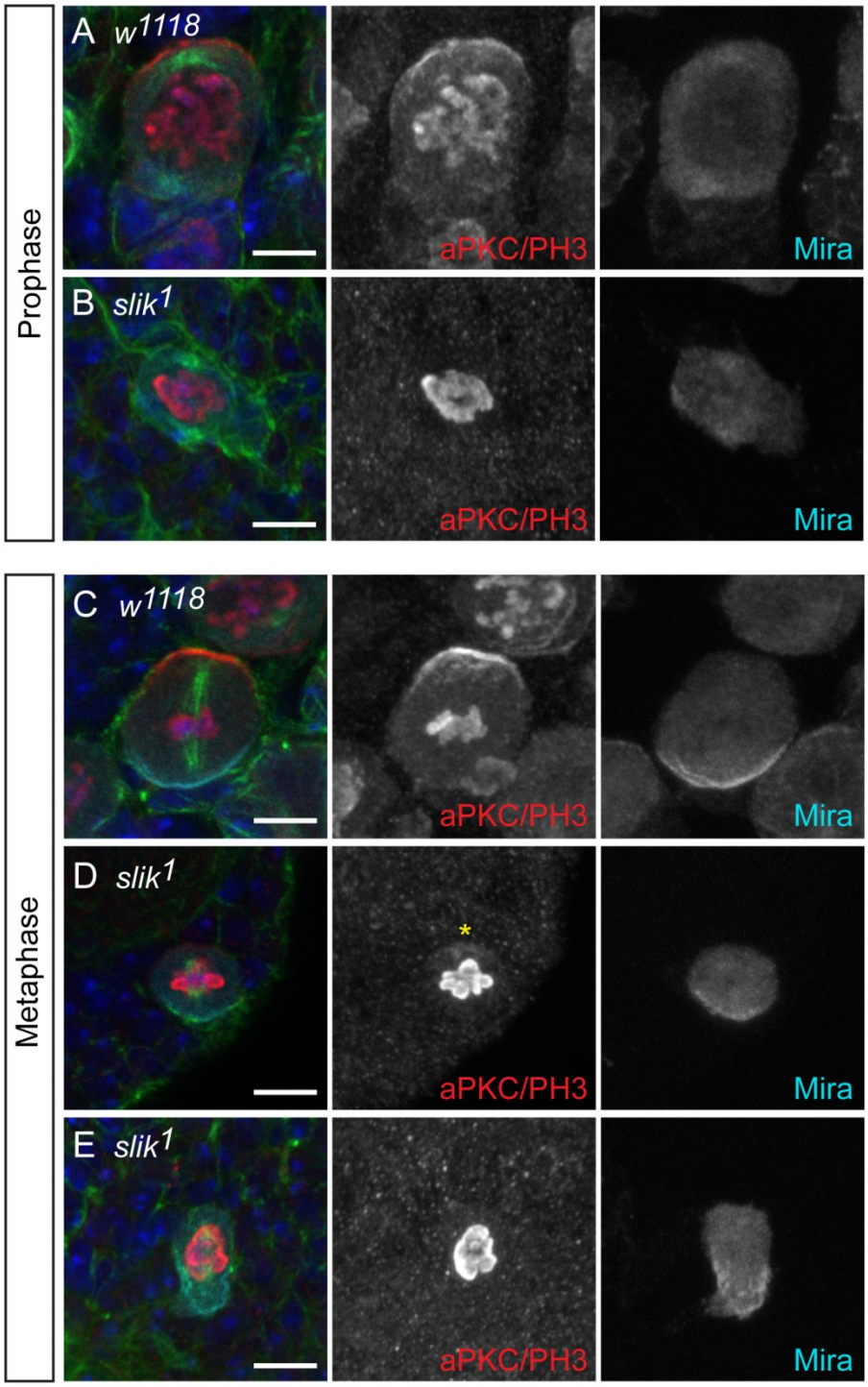
Prophase
A w1118
aPKC/PH3
Mira
B slik1
aPKC/PH3
Mira
Metaphase
C w1118
aPKC/PH3
Mira
D slik1
*
aPKC/PH3
Mira
E slik1
aPKC/PH3
Mira

Figure 4-26: Slik is important for aPKC polarity maintenance in neuroblasts. *w^{1118}* and *$slik^{1}$* larval neuroblasts labelled with DAPI (blue), anti-α-tubulin (green), anti-aPKC/anti-phospho-histone H3 (aPKC/PH3; red) and anti-Miranda (Mira; cyan), approximately 5-6 days AEL. (A) An aPKC crescent formed in *w^{1118}* neuroblasts undergoing prophase (95%, n=42). (B) An aPKC crescent was not observed in the majority of *$slik^{1}$* mutant neuroblasts undergoing prophase (94%, n=16). (C) An aPKC crescent was observed in *w^{1118}* metaphase neuroblasts (98%, n=59). (D) A weak polar aPKC signal was observed in 67% of *$slik^{1}$* neuroblasts, indicated by the yellow asterisk, and (E) a polar aPKC signal was absent in 27% *$slik^{1}$* neuroblasts during metaphase (n=15). Merged panels are single focal plane images and gray-scale images are maximum intensity projections. Scale bars represent 5 μm.

4.3.11 Investigating the role of phosphatases in neuroblasts

Previously, Flapwing and PP1-87B have been shown to regulate Moesin dephosphorylation in Drosophila epithelial tissues and cell culture (Kunda et al., 2012; Yang et al., 2012). To investigate whether Flapwing regulates Moesin phosphorylation in the neuroblasts, I over-expressed wild-type Flapwing in the neuroblasts using *Insc-GAL4* and examined p-Moesin localization. The over-expression of Flapwing did not alter p-Moesin and Numb localization in neuroblasts undergoing metaphase (Figure 4-27, A-B) and telophase (Figure 4-27, C-D). Furthermore, when I examined the dsRNA-mediated knockdown of Flapwing and PP1-87B in the neuroblasts, obvious defects in p-Moesin localization were not observed during metaphase (Figure 4-28, A-C) and telophase (Figure 4-28, D-F). However, cortical blebs were present at the apical pole in both the Flapwing and PP1-87B knockdown neuroblasts undergoing telophase (Figure 4-28, E-F), suggesting that the phosphatases may be involved in bleb retraction during telophase. Together, these findings suggest that Flapwing and PP1-87B phosphatases are not important for p-Moesin distribution during metaphase and telophase.

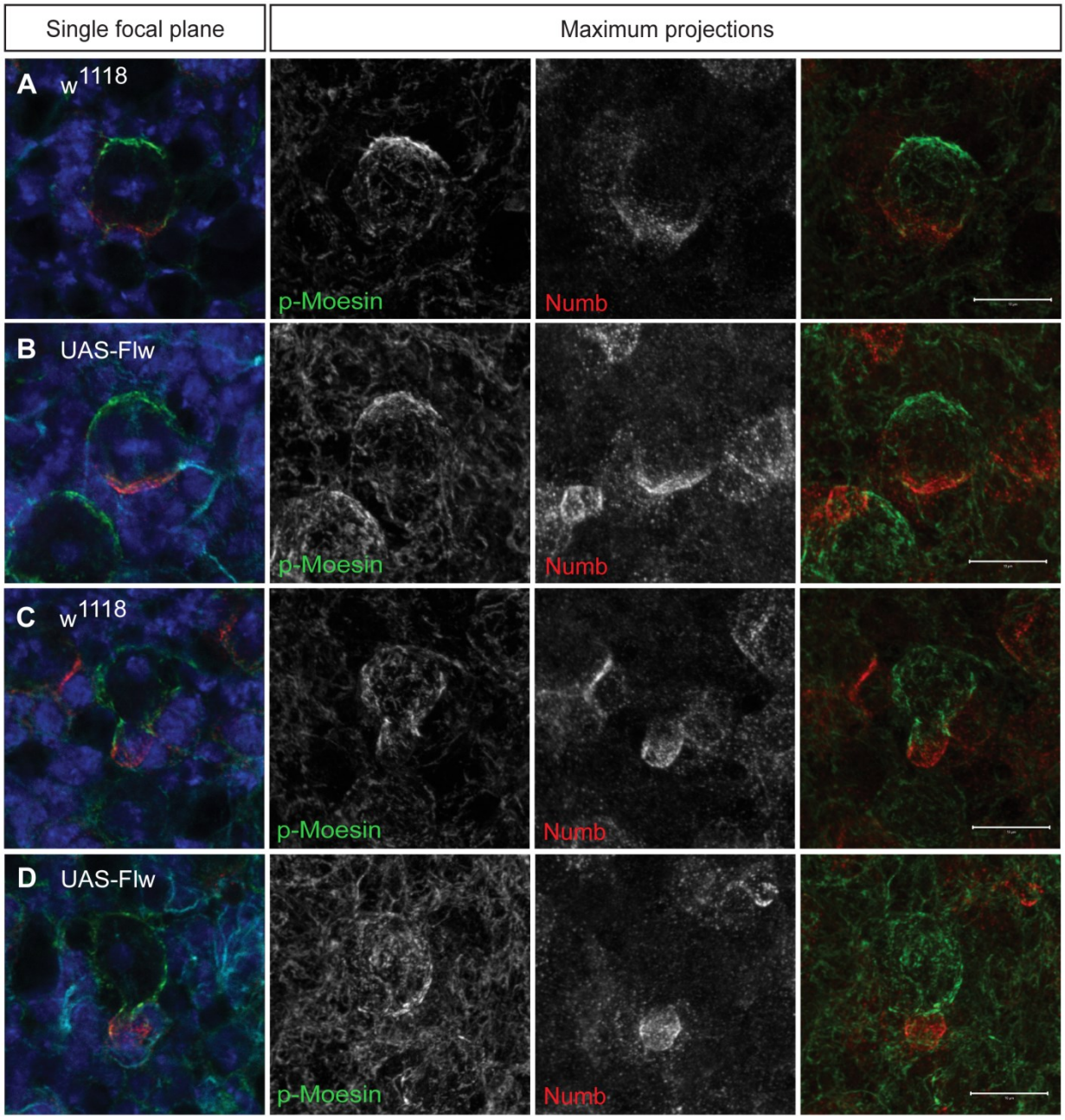
Single focal plane
Maximum projections
A
w1118
p-Moesin
Numb
B
UAS-Flw
p-Moesin
Numb
C
w1118
p-Moesin
Numb
D
UAS-Flw
p-Moesin
Numb

Figure 4-27: Over-expression of Flapwing does not alter p-Moesin and Numb localization during asymmetric cell division. The neuroblast GAL4 driver, *Insc-GAL4*, was crossed to (A and C) w^{1118}, and (B and D) *UAS-Flapwing* (UAS-Flw). Third instar larval brains were dissected and fluorescently labelled for DAPI (blue), anti-p-Moesin (green), anti-Numb (red), and anti-β-tubulin (cyan), as shown in merge panels. The over-expression of Flapwing did not alter p-Moesin and Numb localization in neuroblasts undergoing (A-B) metaphase and (C-D) telophase, when compared to controls. Single focal plane images are shown in far left merge panels. Maximum intensity projections are shown in gray-scale and far right merge panels. Scale bars represent 10 μm.

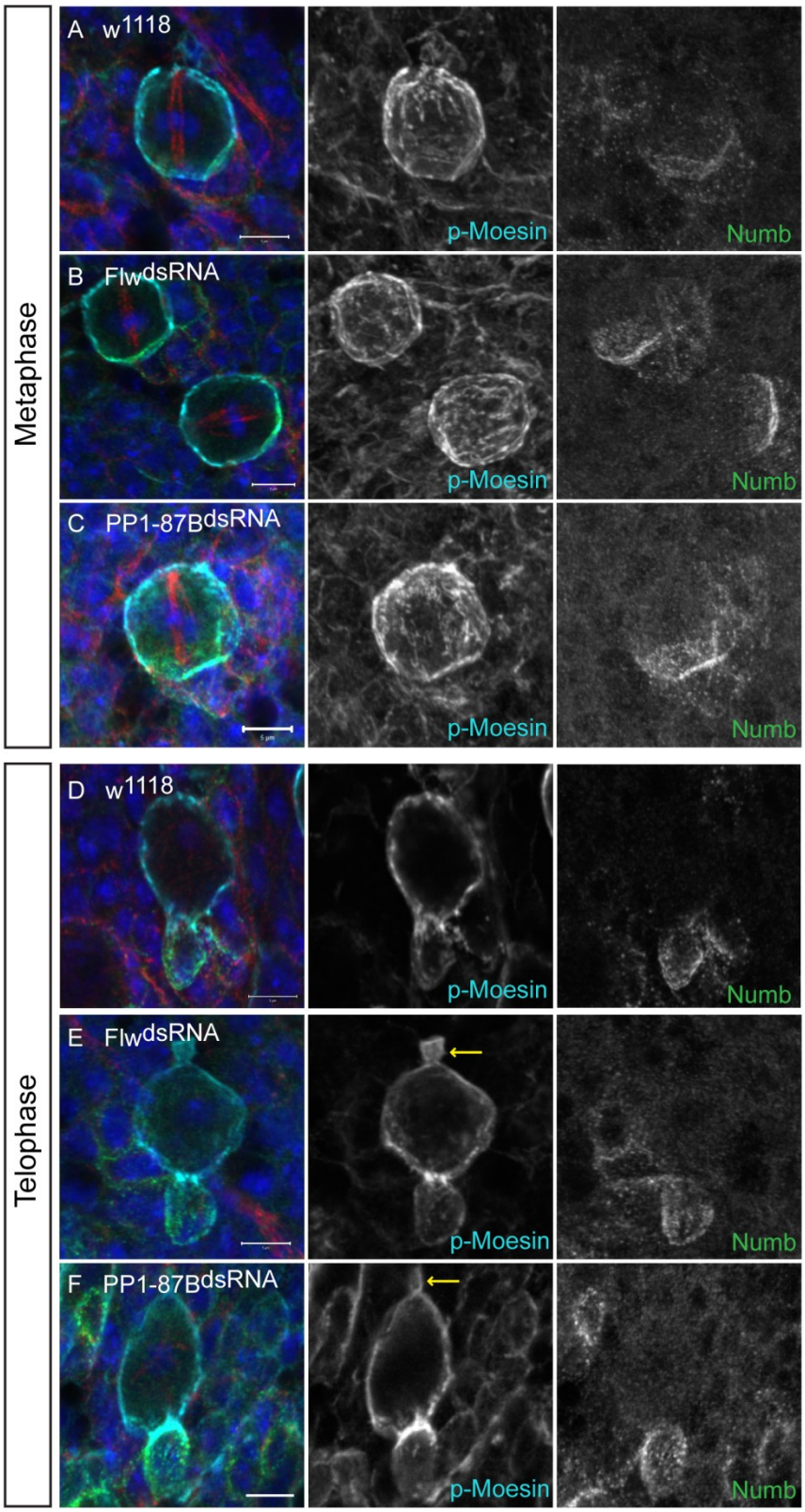
Metaphase
A w1118
p-Moesin
Numb
B Flw dsRNA
p-Moesin
Numb
C PP1-87B dsRNA
p-Moesin
Numb
Telophase
D w1118
p-Moesin
Numb
E Flw dsRNA
p-Moesin
Numb
F PP1-87B dsRNA
p-Moesin
Numb

Figure 4-28: Reduced Flw and PP1-87B does not alter p-Moesin localization in metaphase and telophase neuroblasts. The neuroblast GAL4 driver, *Insc-GAL4*, was crossed to (A and D) w^{1118}, (B and E) *UAS-Flw*^{dsRNA} (Flw^{dsRNA}), and (C and F) *UAS-PP1-87B*^{dsRNA} (PP1-87B^{dsRNA}). Third instar larval brains were dissected and fluorescently labelled for DAPI (blue), anti-p-Moesin (cyan), anti-Numb (green), and anti-β-tubulin (red) as shown in merge panels. Reduced Flapwing and PP1-87B did not alter p-Moesin localization in (A-C) metaphase and (D-F) telophase neuroblast. (E-F) Cortical blebbing was observed at the apical pole of Flapwing and PP1-87B knockdown neuroblasts undergoing telophase. Gray scale images in A-C are maximum intensity projections and D-F are single focal planes. Scale bars represent 5 μm.

4.3.12 Identification of additional Moesin protein interactions in neuroblasts

To identify novel protein interactions with Moesin in Drosophila neuroblasts, I performed immunoprecipitation experiments from larval brains followed by mass spectrometry, where an epitope-tagged construct of wild-type Moesin was expressed in the neuroblasts using *Insc-GAL4*. For further analysis, potential Moesin protein partners were chosen based on known function and whether they may play a role during neurogenesis (Table 5). Mass spectrometry revealed Lethal (2) giant larvae (Lgl), Na^+/K^+-ATPase α-subunit (ATPα), and Hu li tai shao (Hts), among many others, as potential Moesin interactors.

Previously, Lgl was shown to be important for the asymmetric distribution of p-Moesin in metaphase neuroblasts (Figure 4-24, E), thus the potential physical interaction between Moesin and Lgl was further examined. When FLAG-tagged *Moesin* was expressed in the neuroblasts using *Insc-GAL4* and immunoprecipitated from larval brains, Lgl did not appear to interact with Moesin via western blot analysis (Figure 4-29). Furthermore, I analyzed Moe^{G0323} hypomorphic mutant larval brains and did not observe any defects in Lgl localization in the neuroblasts (Figure 4-30). Thus, Moesin does not appear to interact with Lgl or regulate its localization in neuroblasts.

To determine whether Moesin influenced ATPα and Hts in the neuroblasts, I examined ATPα and Hts localization in control and Moe^{G0323} hypomorphic mutant larval brains. In control brains, ATPα appeared enriched at the glial niche surrounding the neuroblasts and the GMC daughter cells (Dumstrei et al., 2003) (Figure 4-30, A). I found no obvious defects in ATPα localization with the loss of Moesin, when compared to control brains (Figure 4-30, B). Furthermore, Hts localized to the cytoplasm and cortex of control mitotic neuroblasts (Figure 4-31, A yellow arrow) and was enriched at the neuroblast cortex during interphase (Figure 4-31, A yellow asterisk). *Moesin* hypomorphic mutant neuroblasts displayed no obvious defects in Hts localization in mitotic and interphase neuroblasts (Figure 4-31, B). Thus, Moesin does not appear to be essential for ATPα and Hts localization in the larval brain. I also examined whether the dsRNA-mediated knockdown of ATPα and Hts in the neuroblasts altered p-Moesin localization. During metphase, p-Moesin was enriched at the apical cortex in ATPα and Hts knockdown neuroblasts, similar to controls (Figure 4-32), suggesting that ATPα and Hts does not appear to regulate the asymmetric distribution of p-Moesin during metaphase.

Table 5: Candidate Moesin interactors in Drosophila neuroblasts

Protein	Coverage	Number of peptides	Functional relevance	Reference
Na^+/K^+-ATPase α-subunit	22.00	18	Septate junction component; Epithelial polarity protein	(Laprise et al., 2009; Paul et al., 2003)
Cullin-associated NEDD8-dissociated protein 1	11.46	12	Regulation of Cullin-RING ubiquitin ligases	(Higa et al., 2006; Kim et al., 2010)
Exportin-2	6.46	4	Nucleocytoplasmic transport	(Silverman-Gavrila and Wilde, 2006; Tekotte et al., 2002)
Cullin-1	4.65	3	Component of Cullin-RING ubiquitin ligases	(Filippov et al., 2000)
Lethal (2) giant larvae	5.68	5	Basal protein targeting in neuroblasts	(Ohshiro et al., 2000; Peng et al., 2000)
Hu li tai shao	3.03	2	Cytoskeletal protein	(Yue and Spradling, 1992)
Importin α	13.60	5	Nucleocytoplasmic transport	(Kussel and Frasch, 1995; Torok et al., 1995)
DE-Cadherin	2.06	2	Adherens junction component; Neuroblast proliferation	(Dumstrei et al., 2003; Oda et al., 1994)
Serine/threonine-protein phosphatase 4 regulatory subunit 3	2.45	2	Miranda localization in neuroblasts	(Sousa-Nunes et al., 2009)

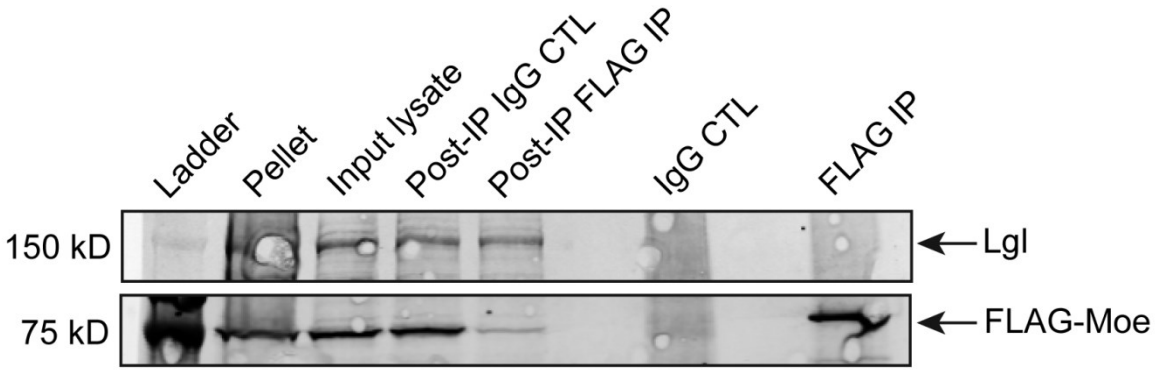

Figure 4-29: Moesin does not appear to interact with Lgl in larval neuroblasts. Western blot of FLAG immunoprecipitation from third instar larval brains expressing *UAS-FLAG-Moesin* in neuroblasts using *Insc-GAL4*. Blot was probed for anti-FLAG and anti-Lgl.

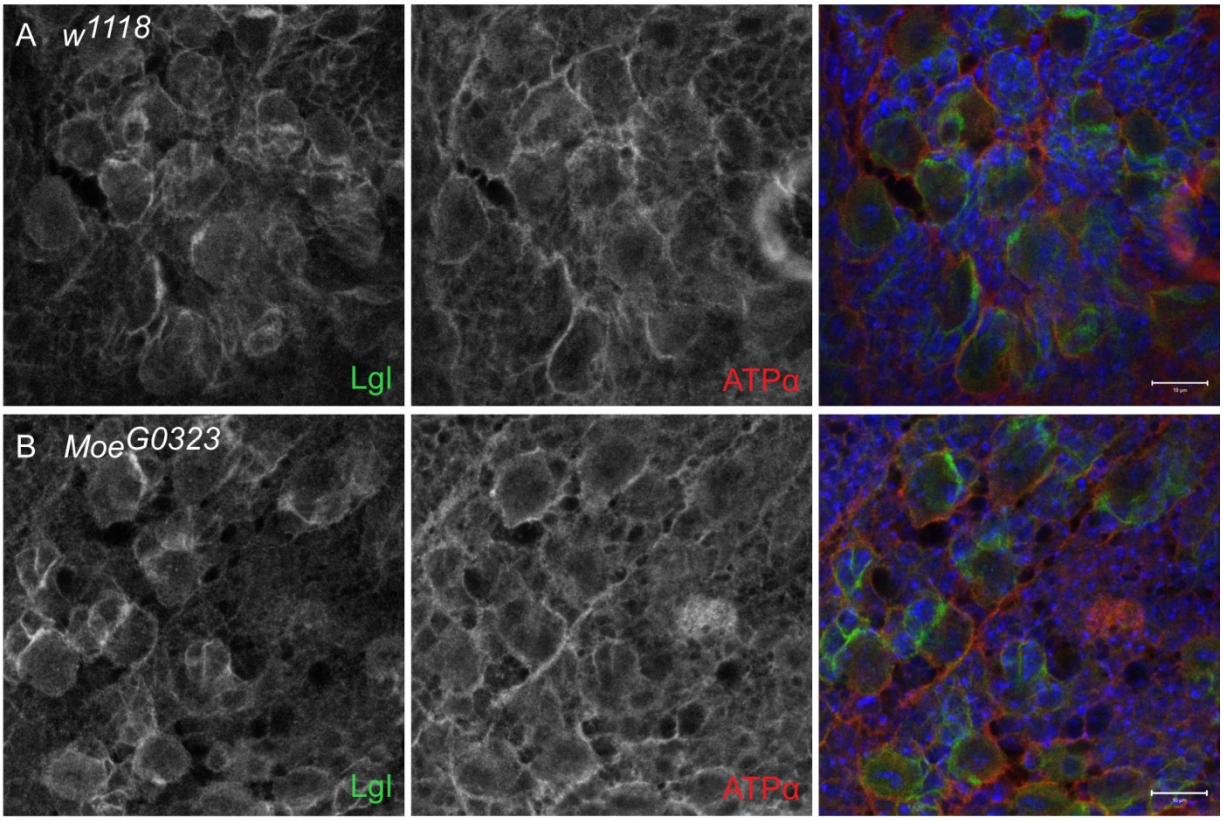

Figure 4-30: Loss of Moesin does not alter Lethal giant larvae and Na^+/K^+-ATPase α localization in the neuroblasts. Neuroblasts from (A) *w*^{1118} and (B) *Moe*^{G0323} third instar larvae were labelled with DAPI (blue), Lethal giant larvae (Lgl; green), and Na^+/K^+-ATPase α (ATPα; red), as shown in merge panels. (A) Lgl localized to the cortex and cytoplasm of control neuroblasts and GMCs. ATPα appeared enriched at the niche surrounding the neuroblasts and GMCs. (B) No obvious defects in Lgl and ATPα localization were observed with the loss of Moesin. Single focal plane images are shown. Scale bars represent 10 μm.

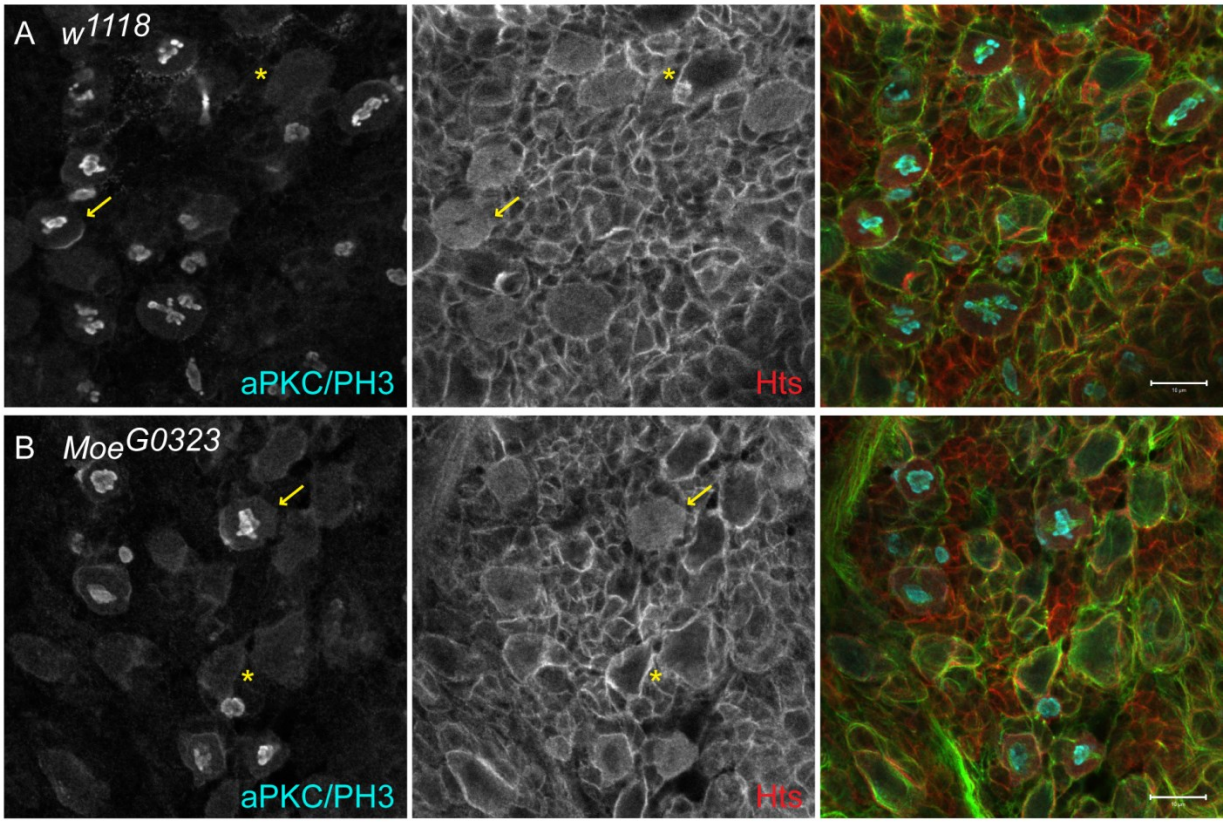

Figure 4-31: Loss of Moesin does not alter Hts localization in the neuroblasts. Neuroblasts from (A) *w*^{1118} and (B) *Moe*^{G0323} third instar larvae were labelled with aPKC/phospho-histone H3 (aPKC/PH3; cyan), Hts (red), and α-tubulin (green) as shown in merge panels. (A) Hts localized to the cytoplasm and cortex of mitotic control neuroblasts (PH3-positive; yellow arrows) and was largely cortical in control neuroblasts during interphase (non-PH3; yellow asterisk). (B) No obvious defects in Hts localization were observed in mitotic (yellow arrows) and interphase (yellow asterisk) neuroblasts with the loss of Moesin. Single focal plane images are shown. Scale bars represent 10 μm.

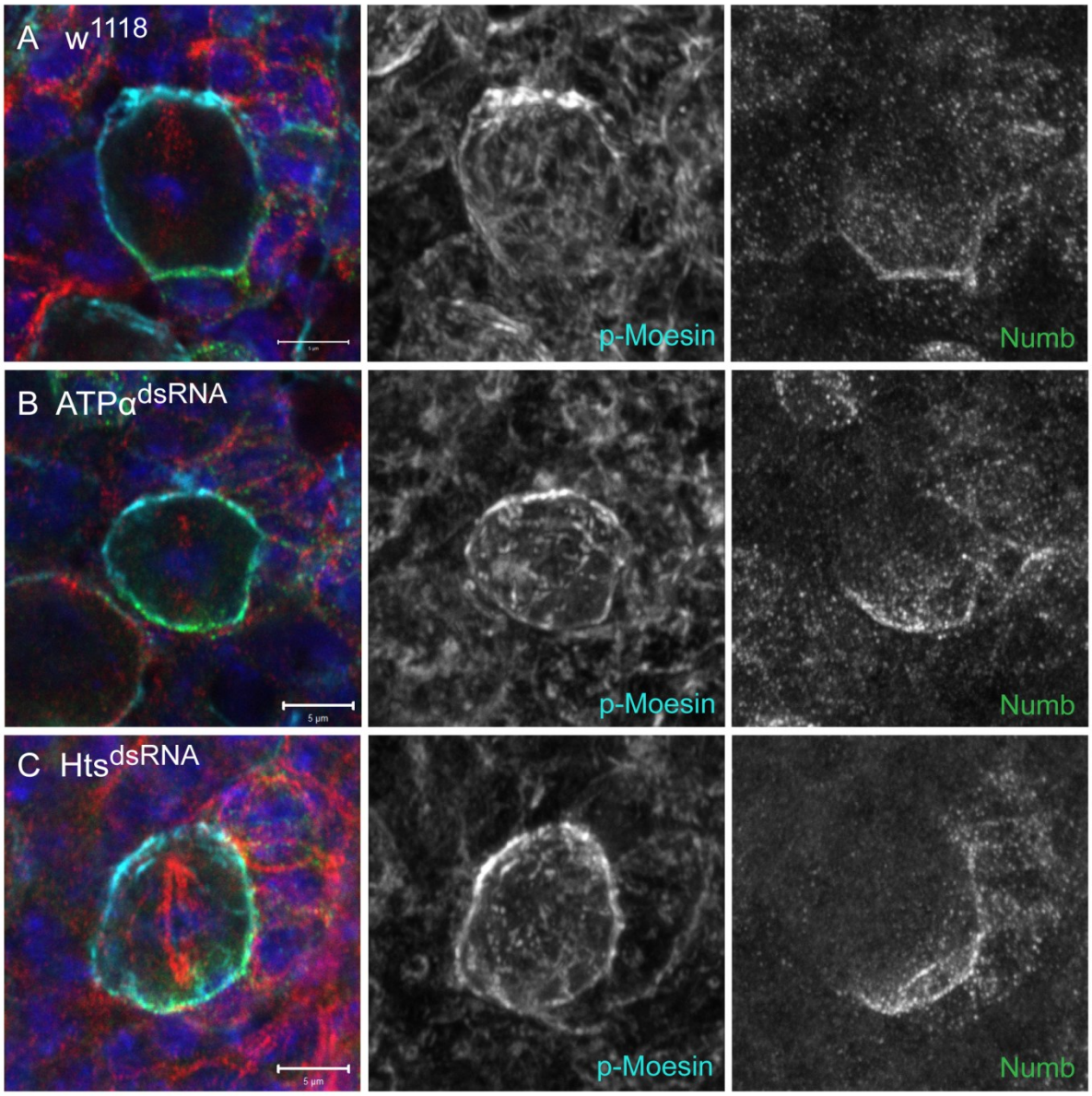

Figure 4-32: Reduced Na^+/K^+-ATPase α and Hts does not alter asymmetric p-Moesin distribution during metaphase. The neuroblast GAL4 driver, *Insc-GAL4*, was crossed to (A) w^{1118}, (B) *UAS-ATPα*^{dsRNA} (ATPα^{dsRNA}), and (C) *UAS-Hts*^{dsRNA} (Hts^{dsRNA}). Third instar larval brains were dissected and fluorescently labelled for DAPI (blue), anti-β-tubulin (red), anti-p-ERM (cyan), and anti-Numb (green) as shown in merge panels. (B-C) P-Moesin and Numb localized to opposite cortical poles in metaphase neuroblasts with reduced ATPα and Hts, similar to (A) controls. Gray-scale images are maximum intensity projections. Scale bars represent 5 μm.

4.4 DISCUSSION AND FUTURE DIRECTIONS

Both Drosophila Sip1 and the mammalian orthologue, NHERF1/EBP50, have not been reported to localize to the cytoplasm of physiologically normal cells. Thus, determining the functional significance of cytoplasmic Sip1 in Drosophila neuroblasts may reveal a novel role for Sip1 during development. Sip1 localization in the neuroblasts was confirmed by the presence of Asense, which is expressed in all primary neuroblasts (Brand et al., 1993). However, there were some primary neuroblasts that were Asense-positive and Sip1-negative, suggesting that Sip1 may function in only a subset of neuroblasts. Over-expressed EBP50 localizes to the cytoplasm of various cancer cells (Cardone et al., 2007; Shibata et al., 2003; Song et al., 2007; Stemmer-Rachamimov et al., 2001). It is proposed that cytoplasmic EBP50 plays an oncogenic role in tumour progression (Takahashi et al., 2006). This led to the hypothesis that cytoplasmic Sip1 may promote neuroblast self-renewal. However, I found that the over-expression of Sip1 did not lead to obvious defects in the neuroblasts or differentiated cells within the larval brain. When Sip1 was reduced in a ubiquitous manner, using *actin-GAL4*, neuroblast self-renewal was affected. Rather than a single neuroblast forming within a given neural cluster, multiple adjacent neuroblasts were observed in the Sip1 knockdown larval brains. These findings suggest that cytoplasmic Sip1 may be involved in inhibiting neuroblast self-renewal or promoting differentiation. Live imaging analysis of Sip1 knockdown neuroblasts undergoing asymmetric cell division may provide more insight into the underlying mechanism.

Studies investigating ERM function have highlighted the importance of the ERM proteins in regulating the mechanical properties of the cell cortex. We provide new insight into the role of Moesin in organizing the cortex of cells that establish intrinsic polarity and undergo asymmetric cell division *in vivo*. In larval brain neuroblasts, we find that Moesin is essential for neuroblast proliferation and mitotic progression, through regulating cortical stability and remodelling events during asymmetric cell division. During metaphase, Moesin is involved in maintaining apical integrity and the formation of a stable cell cortex. Slik kinase also appears to be essential for neuroblast proliferation and apical polarity maintenance, likely through regulating Moesin phosphorylation at the neuroblast cortex during asymmetric cell divisions. Furthermore, components of the apical polarity complex, including aPKC and Pins, regulate the asymmetric distribution of p-Moesin during metaphase. During early anaphase, Moesin contributes to myosin basal furrow positioning. Thus, the asymmetric and dynamic distribution of Moesin drives cortical remodelling of dividing neuroblasts, essential for the maintenance of apical polarity and cell size asymmetry.

When Moesin was knocked down using *Insc-GAL4*, the larval central nervous system was reduced in size due to a decrease in the proportion of dividing neuroblasts throughout larval development. We found that the Moesin knockdown using *Insc-GAL4* affected overall larval development and resulted in early larval lethality. However, viable progeny were obtained when Moesin levels were reduced using other neuroblast-GAL4 drivers, *asense-GAL4* (Zhu et al., 2006) and *worniu-GAL4* (Albertson et al., 2004). These differences in viability likely reflect differences in expression of the same transgene using these alternative GAL4 drivers. Recent studies which identified the Hippo pathway as an essential regulator of neuroblast quiescence also used *Insc-GAL4* in their analyses (Ding et al., 2016; Poon et al., 2016). Thus, we cannot exclude that the defects in neuroblast proliferation induced by dsRNA-mediated knockdown of Moesin using *Insc-GAL4* may be due to an overall delay or arrest in larval development. However, the observed defects in mitotic progression and polarity maintenance demonstrate a functional requirement of Moesin within the larval neuroblasts.

Proper regulation and function of the ERM proteins are required during cell division in both flies (Carreno et al., 2008; Cheng et al., 2011; Kunda et al., 2008) and mammals (Luxenburg et al., 2011). In Drosophila S2 cells, the increased and uniform distribution of p-Moesin at the metaphase cortex enhances cortical rigidity and cell rounding, proposed to be essential for stable spindle positioning (Carreno et al., 2008; Kunda et al., 2008). Thus, an asymmetric ERM distribution during metaphase would be predicted to influence spindle position and orientation accordingly. In human colorectal Caco2 cells, polarized ezrin was shown to locally stabilize actin, providing a physical platform for astral microtubule-mediated centrosome positioning during interphase (Hebert et al., 2012). Furthermore, HeLa cells cultured on L-shaped micropatterns displayed restricted ERM activation at the cell cortex adjacent to the adhesive substrate, which was essential for guiding spindle orientation (Machicoane et al., 2014; Thery et al., 2005). In Drosophila neuroblasts, we found that p-Moesin was apically enriched at the metaphase cortex; although the mitotic spindle has been reported to be symmetric and centrally located during metaphase (Cai et al., 2003; Kaltschmidt et al., 2000). Thus, p-Moesin at the apical cortex is likely not involved in generating spindle asymmetry during metaphase, but we cannot exclude the possibility of its involvement in preparing for the establishment of an asymmetric spindle during anaphase (Cai et al., 2003; Kaltschmidt et al., 2000; Yu et al., 2003). Drosophila Moesin was also shown to bind and stabilize microtubules at the cortex of cultured cells (Solinet et al., 2013). We found that the loss of Moesin affected spindle integrity and orientation in a proportion of metaphase neuroblasts; however Pins localization was normal

in the majority of Moesin knockdown neuroblasts. Thus, Moesin may not play a prominent role in spindle orientation during metaphase, likely due to the presence of a highly regulated Pins/Mud/Gαi complex in ensuring proper spindle formation and orientation (Bowman et al., 2006; Izumi et al., 2006; Schaefer et al., 2000; Siller et al., 2006; Yu et al., 2000). However, it is possible that the loss of both Moesin and Pins would lead to more severe defects in spindle orientation during metaphase.

We did observe that a large proportion of neuroblasts were PH3-positive but lacked visible spindle poles when Moesin was absent. The morphology of these mitotic defective neuroblasts were not round and may reflect the importance of Moesin in cell rounding during early mitosis, as previously shown using Drosophila cell culture (Carreno et al., 2008; Kunda et al., 2008). Alternatively, the mitotic defective neuroblasts may represent a population of neuroblasts that have failed to undergo cell division. As the loss of Moesin also resulted in a reduced proportion of mitotic neuroblasts undergoing the specific stages of mitosis, we conclude that Moesin is essential for mitotic progression during asymmetric cell division.

ERM proteins have been shown to localize to the apical cortex of a wide variety of polarized cells and are essential for maintaining the apical identity and surface properties of epithelial tissues across multiple organisms (Berryman et al., 1993; Gobel et al., 2004; Karagiosis and Ready, 2004; Louvet et al., 1996; Pilot et al., 2006; Saotome et al., 2004; Speck et al., 2003; Van Furden et al., 2004). Through the ability to bind directly to F-actin and link membrane-associated proteins to the underlying actin cytoskeleton (Algrain et al., 1993; Hirao et al., 1996; Turunen et al., 1994), the ERM proteins have shown to localize to numerous actin-rich structures (Berryman et al., 1993; Franck et al., 1993; Sato et al., 1992; Sato et al., 1991). Thus, it is possible that apical distribution of p-Moesin represents areas rich in actin filaments at the neuroblast cortex. Although, the actin cytoskeleton is important for cortical tethering of polarity complexes in neuroblasts (Broadus and Doe, 1997; Knoblich et al., 1997; Lu et al., 1999; Shen et al., 1998), F-actin does not display an obvious asymmetric distribution *in vitro* (Broadus and Doe, 1997) or *in vivo* (Hirata et al., 1995; Knoblich et al., 1995; Spana and Doe, 1995). Thus, the apical enrichment of p-Moesin may correlate with enhanced cortical stability at the apical cortex necessary for polarity maintenance and integrity. Confirming a role for p-Moesin in stabilizing cortical actin, we found that Bazooka and aPKC crescents were not observed in a proportion of Moesin knockdown neuroblasts undergoing prophase and the actin cytoskeleton appeared disorganized. As Bazooka and aPKC polarity is established by prophase (Schober et al., 1999; Siegrist and Doe, 2005; Wodarz et al., 2000; Wodarz et al., 1999), prior to the polar

enrichment of p-Moesin, we conclude that Moesin is involved in polarity maintenance rather than establishment. Similarly, in the *M. musculus* and *C. elegans* intestinal epithelium, ERM proteins are involved in apical membrane assembly and integrity, but do not appear to be required for polarity establishment (Saotome et al., 2004; Van Furden et al., 2004). During metaphase, we observed a proportion of Moesin knockdown neuroblasts lacking both Par-6 and aPKC polar crescents. However, the majority of Moesin knockdown neuroblasts displayed normal polar Bazooka and Pins crescents at the metaphase cortex. Neuroblasts lacking aPKC and Par-6 are still able to form an apical domain consisting of Bazooka, Inscuteable, Pins, and Discs large (Rolls et al., 2003). Thus, Moesin may be specifically involved in maintaining Par-6/aPKC polarity during metaphase, but have little effect on other apical polarity proteins, such as Bazooka and Pins. In contrast to what was observed in the Moesin knockdown, 98% of *Moesin* hypomorphic mutant neuroblasts displayed polar aPKC at the metaphase cortex. The differences in the phenotypes observed between the Moe^{dsRNA} and Moe^{G0323} hypomorphic mutant are likely due to differences in protein levels, as reflected in the severity of the lethality. The aPKC polar domain appeared disorganized and cortical blebbing was observed in the Moe^{G0323} mutant neuroblasts, strongly suggesting that Moesin regulates the integrity and maintenance of the apical domain, likely through affecting cortical stability during asymmetric cell division. We also found that the apical enrichment of p-Moesin was regulated by known apical polarity proteins (Cdc42, Par-6, aPKC, Lgl, and Pins) during metaphase. These findings support a mutually dependent interaction among the apical polarity proteins that has been extensively reported in neuroblasts (Atwood et al., 2007; Lee et al., 2006; Parmentier et al., 2000; Rolls et al., 2003; Schaefer et al., 2000; Schober et al., 1999; Wodarz et al., 2000; Wodarz et al., 1999; Yu et al., 2000). In addition to its role in localizing cell fate determinants to the basal cortex and orientation the mitotic spindle during metaphase, components of the apical polarity complexes also mediate spindle asymmetry and asymmetric cortical extension during anaphase, leading to the generation of unequal-sized daughter cells (Cabernard et al., 2010; Cai et al., 2003; Chenn and McConnell, 1995; Fuse et al., 2003). Interestingly, we found that Moesin also appeared to be involved in the initial establishment of cell size asymmetry during anaphase.

In Drosophila, the dynamic distribution of p-Moesin at the cortex of mitotic S2 cells has been correlated to sites of cortical contraction (Carreno et al., 2008; Kunda et al., 2008; Kunda et al., 2012; Roubinet et al., 2011). During anaphase onset, the reduction of p-Moesin at the cell poles lead to cortical relaxation and membrane elongation, facilitating cleavage furrow formation at the equatorial region in symmetrically dividing S2 cells

(Carreno et al., 2008; Kunda et al., 2008; Kunda et al., 2012; Rodrigues et al., 2015; Roubinet et al., 2011). However, we found that p-Moesin remained enriched at the apical cortex during early anaphase of asymmetrically dividing neuroblasts. Previous studies have shown that a polarized distribution of Myosin during early anaphase contributes to cortical extension at the opposing polar cortex, thus altering the cellular boundaries for furrow positioning (Connell et al., 2011; Kiyomitsu and Cheeseman, 2013; Ou et al., 2010). In Drosophila neuroblasts, a cortical polarity-induced pathway, consisting of Pins and the heterotrimeric G-proteins, is essential for Myosin accumulation at the basal cortex and the formation of a basally displaced furrow, independent of the mitotic spindle (Cabernard et al., 2010; Connell et al., 2011). We showed that the reduction of Moesin resulted in the absence of an induced p-Myosin basal furrow and the appearance of symmetric divisions during early anaphase. Given that p-Moesin can influence cortical remodelling through interaction with the actin cytoskeleton, we propose that the apical enrichment of p-Moesin is important for asymmetric cortical extension and furrow positioning during early anaphase, along with Pins and the heterotrimeric G-proteins. Apical p-Moesin may locally stabilize actin during early anaphase to counteract the forces generated from basal cortical contraction and cytoplasmic flow towards the apical cortex. However, unlike Pins, Moesin appears to influence Myosin-mediated cortical contractility during metaphase as well. The loss of Moesin resulted in a non-uniform distribution of p-Myosin at the metaphase cortex, revealing unstable actomyosin dynamics and a delay in anaphase onset. Although observable differences in cortical Rho1 signaling at the metaphase cortex were not observed in the *Moe*^{G0323} mutant metaphase neuroblasts, future studies using alternative biosensor approaches or pharmacological inhibition may allow for more precise visualization and analysis of Rho1 signaling (Verboon and Parkhurst, 2015). Alternatively, Rho1 signaling may function upstream of Moesin, as previously shown (Hirao et al., 1996; Mackay et al., 1997).

The complex spatiotemporal regulation of Moesin activity during mitosis has been demonstrated in Drosophila cell culture and requires the coordinated activities of PP1-87B phosphatase, Slik kinase, and regulators of phosphatidylinositol 4, 5-bisphosphate (PIP_2) levels at the cell cortex (Carreno et al., 2008; Kunda et al., 2008; Kunda et al., 2012; Roubinet et al., 2011). We showed that Slik was uniformly distributed at the neuroblast cell cortex. As Slik is regulated by phosphorylation (Panneton et al., 2015), it is possible that the phosphorylated form of Slik is asymmetrically distributed in mitotic neuroblasts. Furthermore, Slik was essential for neuroblast proliferation and polarity maintenance, likely through regulating Moesin phosphorylation at the neuroblast cortex. We found that the loss of Flapwing and PP1-87B phosphatases did not alter the apical enrichment of p-Moesin in

metaphase neuroblasts. However, the phosphatases or PIP_2 levels at the cell cortex may influence Moesin activity during anaphase or in interphase neuroblasts. To further examine the importance of Moesin phosphorylation on the cell cortex of dividing neuroblasts, the phosphomimetic and non-phosphorylated form of Moesin will need to be analyzed in the absence of endogenous Moesin. Furthermore, analysis of the mechanical properties of cultured neuroblasts will provide great insight into how Moesin function influences the mitotic cortex in the absence of physical constraint or external cues.

Chapter 5: General Discussion

We found that the relatively uncharacterized α-helical domain of Merlin interacts with the scaffold protein Sip1 *in vitro*. Mutation of conserved arginine residues within the α-helical domain of Merlin disrupted binding to Sip1 *in vitro* and *in vivo*. Our findings demonstrated that the Merlin and Sip1 interaction was important for the tumour suppressor function of Merlin and the maintenance of epithelial integrity. Thus, the α-helical domain plays an essential role in regulating Merlin binding and activity (Abeysundara et al., 2014). In support of this, crystal structural studies revealed that the central α-helical domain of moesin purified from ovarian insect cells formed multiple contacts with the FERM domain, suggesting that the α-helical domain contributes to masking ERM protein binding and activation sites (Li et al., 2007b). It was proposed that the α-helical domain of mammalian merlin acts in a similar manner and interactions between the α-helical and FERM domain are essential for maintaining merlin in its tumour suppressive form (Hennigan et al., 2010; Li et al., 2007b). Multiple non-truncating missense mutations associated with NF2 were found in the α-helical domain, supporting the clinical relevance of this domain for the tumour suppressor activity of merlin (Li et al., 2007b). Furthermore, we showed that the phosphomimetic form of Merlin binds to Sip1 to a greater extent than the non-phosphorylated form of Merlin (Abeysundara et al., 2014). We propose that Sip1 binding promotes Merlin dephosphorylation and activation, as altering Sip1 levels affected Merlin phosphorylation. The phosphomimetic form of merlin S518D was also shown to bind EBP50 (Ali Khajeh et al., 2014), however it remains to be determined whether EBP50 regulates mammalian merlin phosphorylation. Future studies investigating the relationship between merlin regulation, subcellular localization, and its interacting partners are essential for further understanding the growth suppressive function of merlin.

To examine the functional significance of Merlin and Sip1 in a neuronal context, I utilized the developing larval optic lobe as a model for neuroepithelial cell proliferation and differentiation. Merlin and Sip1 appear to be important for the neuroepithelial cell transition into medulla neuroblasts, although the precise mechanisms still remain unclear. *Nf2* mRNA was shown to be highly expressed in the neuroepithelial cells of the developing mammalian embryonic cortex (McLaughlin et al., 2007). The loss of merlin resulted in neuroepithelial cell detachment from the apical surface due to a lack in apico-lateral junctional complex formation and a portion of these detached cells appeared to undergo apoptosis (McLaughlin et al., 2007). When *Merlin* null mutant clones were generated in the neuroepithelial cells of the Drosophila optic lobe using MARCM, I observed a low frequency of mutant clones that were only generated at the dorsal and ventral tips of the OPC. Thus, it is possible that the loss of Merlin in the other areas of the OPC promotes neuroepithelial cell detachment and

apoptosis, as observed in the mammalian embryonic cortex. Previously, merlin was shown to limit expansion of the neural progenitor pool through inhibition of Yap activity in the mouse dorsal telencephalon and dorsal root ganglia (Lavado et al., 2013; Serinagaoglu et al., 2015). Furthermore, merlin loss in meningioma cell lines led to increased proliferation and enhanced nuclear localization of human YAP (Striedinger et al., 2008). These defects were rescued with the siRNA-mediated knockdown of YAP, suggesting that merlin regulates meningioma cell growth by inhibiting YAP activity (Striedinger et al., 2008). Merlin also regulates growth and glial differentiation of spinal cord progenitor cells (Garcia and Gutmann, 2014), which are likely the cells of origin for ependymomas arising in the spinal cord (Johnson et al., 2010; Taylor et al., 2005). However, in spinal cord progenitor cells and differentiated forebrain astrocytes, merlin loss was associated with increased ErbB2 activity (Garcia and Gutmann, 2014; Houshmandi et al., 2009). Therefore, merlin may influence different signaling pathways depending on the cellular context. In the Drosophila larval optic lobe, multiple signaling pathways, including the Hippo and EGFR pathways, are required for neuroepithelial cell proliferation and differentiation (Reddy et al., 2010; Yasugi et al., 2010). Thus, examining whether Merlin coordinately regulates these pathways during optic lobe development may provide further insight into Merlin function in neural progenitor cells. Interestingly, Lavado *et al*. demonstrated that merlin loss in the mammalian brain, which resulted in the expansion of the neural progenitor pool, did not alter mRNA expression levels of cell cycle regulators but led to the upregulation of genes involved in cell-cell junctions and mediators of the extracellular matrix (Lavado et al., 2013). In addition, merlin was shown to be essential for cell cycle exit and terminal differentiation of fiber cells during lens development in mice (Wiley et al., 2010). These authors further showed that the conditional deletion of *Nf2* in the lens led to defects in adhesion and polarity (Wiley et al., 2010). NF2 patients may also develop posterior subcapsular cataracts, which are proposed to arise from abnormal proliferation of epithelial cells or defects in fiber cell differentiation (Eshaghian and Streeten, 1980; Kaiser-Kupfer et al., 1989; Streeten and Eshaghian, 1978). Given that the neuroepithelial cells within the Drosophila optic lobe proliferate while maintaining adhesion and disassemble cell junctions to undergo differentiation, future studies examining the role of Merlin in the maintenance of neuroepithelial integrity may be worthwhile to further understanding its role in coordinating proliferation and differentiation.

The ERM proteins were also found to be expressed in neural progenitors and differentiated cell types within the mammalian subventricular zone of the cerebral cortex and the rostral migratory stream (Cleary et al., 2006; Gronholm et al., 2005; Moon et al., 2013; Persson et al., 2010). Similar to our studies of Moesin in Drosophila neuroblasts,

radixin inhibition was found to decrease neuroblast proliferation in the rat rostral migratory stream (Persson et al., 2013). In apical progenitors of the mouse embryonic cortex, the phospho-ERM immunofluorescent signal increased at the metaphase cell cortex compared to surrounding interphase cells, where the ERM proteins have been implicated in regulating spindle symmetry and orientation (Delaunay et al., 2014; Machicoane et al., 2014). It is not known whether the ERM proteins are asymmetrically enriched at the cell cortex or whether they influence polarity and cortical remodelling in dividing mammalian neural progenitors. In addition, examining whether Moesin influences centrosome behaviour and mitotic spindle orientation in dividing embryonic neuroblasts would be essential to further characterizing Moesin function during Drosophila neuroblast asymmetric cell division. Interestingly, high moesin expression has been linked to high-grade glioblastoma tumours and glioblastoma cell lines (DeSouza et al., 2013; Wu et al., 2013; Zhu et al., 2013). Increased ezrin expression was also associated with enhanced cell growth and poor prognosis of malignant gliobastoma (Geiger et al., 2000; Mao et al., 2013; Tynninen et al., 2004). When Drosophila Moesin was over-expressed in the neuroblasts, I did not observe any obvious defects in overall larval brain morphology or apical/basal polarity in metaphase neuroblasts. However, the over-expression of Moesin in more differentiated cell types may provide further insight into mechanisms underlying increased ERM expression found in glioblastoma tumours. Furthermore, although phosphorylated ERM proteins were shown to be enriched at the cleavage furrow in dividing mammalian and Drosophila cells (Carreno et al., 2008; Kawano et al., 1999; Kunda et al., 2008; Sato et al., 1991), the functional significance remains largely unexplored. We found that Moesin may be involved in initially specifying the site of cleavage furrow formation in asymmetrically dividing neuroblasts. Future studies examining how the over-expression of Moesin affects cleavage furrow positioning in Drosophila neuroblasts may be of particular interest. In addition, determining whether the ERM proteins are involved in cleavage furrow positioning in asymmetrically dividing mammalian cells would be essential to further understanding ERM protein function at the cleavage furrow.

To identify additional Moesin interactions in the neuroblasts, FLAG-tagged Moesin was expressed in the neuroblasts, immunoprecipitated from larval brains, and mass spectrometry was performed. Mass spectrometry results revealed a variety of potential protein interactions with Moesin in the neuroblasts. Other than Lethal (2) giant larvae, polarity proteins known to be involved in neuroblast asymmetric cell divisions were not identified. The Na^+/K^+-ATPase α-subunit, ATPα, was identified as a potential Moesin interacting protein in larval neuroblasts. ATPα is a component of septate junctions (Paul et

al., 2003) and shown to be highly expressed in the surface glia or blood brain barrier surrounding the Drosophila adult brain (DeSalvo et al., 2014). Although, p-Moesin and ATPα localization did not appear to be interdependent, the two proteins may still interact and function together in the neuroblasts. The ATPα-Moesin interaction may be important for communication between the glial cells and neuroblasts in early larval brains, particularly during neuroblast cell cycle re-entry. Furthermore, Drosophila Cullin-1 is an essential ubiquitin ligase that functions during cell cycle progression (Filippov et al., 2000) and Cand1 regulates Cullin complex formation (Higa et al., 2006; Kim et al., 2010). Mass spectrometry results revealed both Cullin-1 and Cand1 as potential Moesin interacting proteins, thus Moesin may be important for proteasomal degradation in the neuroblasts. Alternatively, Moesin may be targeted by the proteasome. These findings suggest that further investigation of Moesin interactions in the neuroblasts may reveal novel mechanisms underlying neuroblast self-renewal and differentiation.

In summary, we find that the Merlin binding to Sip1 is important for Merlin function as a tumour suppressor and in epithelial organization. This work also highlights the importance of the α-helical domain in Merlin regulation and activity. Furthermore, preliminary evidence supports a role for Merlin and Sip1 in the optic lobe, providing a model to further investigate the function of FERM domain proteins and interacting partners in regulating neuroepithelial integrity, proliferation, and differentiation. We also find that Moesin is essential for polarity maintenance and cortical remodelling in asymmetrically dividing neuroblasts. Moesin appears to be involved in the spindle-independent mechanism of cleavage furrow positioning. Future studies investigating Moesin function in the neuroblasts may reveal important insight into the cortical properties regulating cleavage furrow positioning and the generation of unequal sized daughter cells during asymmetric cell division. Together, this work provides further insight into the roles of Merlin and Moesin in regulating cell or tissue organization during Drosophila development.

References

Abdelilah-Seyfried, S., D.N. Cox, and Y.N. Jan. 2003. Bazooka is a permissive factor for the invasive behavior of discs large tumor cells in Drosophila ovarian follicular epithelia. *Development*. 130:1927-1935.

Abeysundara, N., A.C. Leung, D.A. Primrose, and S.C. Hughes. 2014. Regulation of cell proliferation and adhesion by means of a novel region of drosophila merlin interacting with Sip1. *Developmental dynamics : an official publication of the American Association of Anatomists*. 243:1554-1570.

Abiatari, I., I. Esposito, T.D. Oliveira, K. Felix, H. Xin, R. Penzel, T. Giese, H. Friess, and J. Kleeff. 2010. Moesin-dependent cytoskeleton remodelling is associated with an anaplastic phenotype of pancreatic cancer. *Journal of cellular and molecular medicine*. 14:1166-1179.

Abreu-Blanco, M.T., J.M. Verboon, and S.M. Parkhurst. 2014. Coordination of Rho family GTPase activities to orchestrate cytoskeleton responses during cell wound repair. *Current biology : CB*. 24:144-155.

Akisawa, N., I. Nishimori, T. Iwamura, S. Onishi, and M.A. Hollingsworth. 1999. High levels of ezrin expressed by human pancreatic adenocarcinoma cell lines with high metastatic potential. *Biochemical and biophysical research communications*. 258:395-400.

Albertson, R., C. Chabu, A. Sheehan, and C.Q. Doe. 2004. Scribble protein domain mapping reveals a multistep localization mechanism and domains necessary for establishing cortical polarity. *Journal of cell science*. 117:6061-6070.

Albertson, R., and C.Q. Doe. 2003. Dlg, Scrib and Lgl regulate neuroblast cell size and mitotic spindle asymmetry. *Nature cell biology*. 5:166-170.

Alfthan, K., L. Heiska, M. Gronholm, G.H. Renkema, and O. Carpen. 2004. Cyclic AMP-dependent protein kinase phosphorylates merlin at serine 518 independently of p21-activated kinase and promotes merlin-ezrin heterodimerization. *The Journal of biological chemistry*. 279:18559-18566.

Algrain, M., O. Turunen, A. Vaheri, D. Louvard, and M. Arpin. 1993. Ezrin contains cytoskeleton and membrane binding domains accounting for its proposed role as a membrane-cytoskeletal linker. *The Journal of cell biology*. 120:129-139.

Ali Khajeh, J., J.H. Ju, M. Atchiba, M. Allaire, C. Stanley, W.T. Heller, D.J. Callaway, and Z. Bu. 2014. Molecular conformation of the full-length tumor suppressor NF2/Merlin--a small-angle neutron scattering study. *Journal of molecular biology*. 426:2755-2768.

Amano, M., M. Ito, K. Kimura, Y. Fukata, K. Chihara, T. Nakano, Y. Matsuura, and K. Kaibuchi. 1996. Phosphorylation and activation of myosin by Rho-associated kinase (Rho-kinase). *The Journal of biological chemistry*. 271:20246-20249.

Amieva, M.R., and H. Furthmayr. 1995. Subcellular localization of moesin in dynamic filopodia, retraction fibers, and other structures involved in substrate exploration, attachment, and cell-cell contacts. *Experimental cell research*. 219:180-196.

Amieva, M.R., K.K. Wilgenbus, and H. Furthmayr. 1994. Radixin is a component of hepatocyte microvilli in situ. *Experimental cell research*. 210:140-144.

Atwood, S.X., C. Chabu, R.R. Penkert, C.Q. Doe, and K.E. Prehoda. 2007. Cdc42 acts downstream of Bazooka to regulate neuroblast polarity through Par-6 aPKC. *Journal of cell science*. 120:3200-3206.

Awasaki, T., S.L. Lai, K. Ito, and T. Lee. 2008. Organization and postembryonic development of glial cells in the adult central brain of Drosophila. *The Journal of neuroscience : the official journal of the Society for Neuroscience*. 28:13742-13753.

Baeyens, N., I. Latrache, X. Yerna, G. Noppe, S. Horman, and N. Morel. 2013. Redundant control of migration and adhesion by ERM proteins in vascular smooth muscle cells. *Biochemical and biophysical research communications*. 441:579-585.

Bainton, R.J., L.T. Tsai, T. Schwabe, M. DeSalvo, U. Gaul, and U. Heberlein. 2005. moody encodes two GPCRs that regulate cocaine behaviors and blood-brain barrier permeability in Drosophila. *Cell*. 123:145-156.

Barros, C.S., C.B. Phelps, and A.H. Brand. 2003. Drosophila nonmuscle myosin II promotes the asymmetric segregation of cell fate determinants by cortical exclusion rather than active transport. *Developmental cell*. 5:829-840.

Bartholow, T.L., U.R. Chandran, M.J. Becich, and A.V. Parwani. 2011. Immunohistochemical staining of radixin and moesin in prostatic adenocarcinoma. *BMC clinical pathology*. 11:1.

Baser, M.E., A. De Rienzo, D. Altomare, B.R. Balsara, N.M. Hedrick, D.H. Gutmann, L.H. Pitts, R.K. Jackler, and J.R. Testa. 2002. Neurofibromatosis 2 and malignant mesothelioma. *Neurology*. 59:290-291.

Baumgartner, M., A.L. Sillman, E.M. Blackwood, J. Srivastava, N. Madson, J.W. Schilling, J.H. Wright, and D.L. Barber. 2006. The Nck-interacting kinase phosphorylates ERM proteins for formation of lamellipodium by growth factors. *Proceedings of the National Academy of Sciences of the United States of America*. 103:13391-13396.

Belkina, N.V., Y. Liu, J.J. Hao, H. Karasuyama, and S. Shaw. 2009. LOK is a major ERM kinase in resting lymphocytes and regulates cytoskeletal rearrangement through

ERM phosphorylation. *Proceedings of the National Academy of Sciences of the United States of America*. 106:4707-4712.

Benhamouche, S., M. Curto, I. Saotome, A.B. Gladden, C.H. Liu, M. Giovannini, and A.I. McClatchey. 2010. Nf2/Merlin controls progenitor homeostasis and tumorigenesis in the liver. *Genes & development*. 24:1718-1730.

Bensenor, L.B., K. Barlan, S.E. Rice, R.G. Fehon, and V.I. Gelfand. 2010. Microtubule-mediated transport of the tumor-suppressor protein Merlin and its mutants. *Proceedings of the National Academy of Sciences of the United States of America*. 107:7311-7316.

Berryman, M., Z. Franck, and A. Bretscher. 1993. Ezrin is concentrated in the apical microvilli of a wide variety of epithelial cells whereas moesin is found primarily in endothelial cells. *Journal of cell science*. 105 (Pt 4):1025-1043.

Bertet, C., X. Li, T. Erclik, M. Cavey, B. Wells, and C. Desplan. 2014. Temporal patterning of neuroblasts controls Notch-mediated cell survival through regulation of Hid or Reaper. *Cell*. 158:1173-1186.

Betschinger, J., K. Mechtler, and J.A. Knoblich. 2003. The Par complex directs asymmetric cell division by phosphorylating the cytoskeletal protein Lgl. *Nature*. 422:326-330.

Bier, E., H. Vaessin, S. Younger-Shepherd, L.Y. Jan, and Y.N. Jan. 1992. deadpan, an essential pan-neural gene in Drosophila, encodes a helix-loop-helix protein similar to the hairy gene product. *Genes & development*. 6:2137-2151.

Bilder, D., M. Li, and N. Perrimon. 2000. Cooperative regulation of cell polarity and growth by Drosophila tumor suppressors. *Science*. 289:113-116.

Boedigheimer, M., and A. Laughon. 1993. Expanded: a gene involved in the control of cell proliferation in imaginal discs. *Development*. 118:1291-1301.

Bonilha, V.L., S.C. Finnemann, and E. Rodriguez-Boulan. 1999. Ezrin promotes morphogenesis of apical microvilli and basal infoldings in retinal pigment epithelium. *The Journal of cell biology*. 147:1533-1548.

Bostwick, D.G., M.B. Amin, P. Dundore, W. Marsh, and D.S. Schultz. 1993. Architectural patterns of high-grade prostatic intraepithelial neoplasia. *Human pathology*. 24:298-310.

Bowman, S.K., R.A. Neumuller, M. Novatchkova, Q. Du, and J.A. Knoblich. 2006. The Drosophila NuMA Homolog Mud regulates spindle orientation in asymmetric cell division. *Developmental cell*. 10:731-742.

Brand, A.H., and N. Perrimon. 1993. Targeted gene expression as a means of altering cell fates and generating dominant phenotypes. *Development*. 118:401-415.

Brand, M., A.P. Jarman, L.Y. Jan, and Y.N. Jan. 1993. asense is a Drosophila neural precursor gene and is capable of initiating sense organ formation. *Development*. 119:1-17.

Brault, E., A. Gautreau, M. Lamarine, I. Callebaut, G. Thomas, and L. Goutebroze. 2001. Normal membrane localization and actin association of the NF2 tumor suppressor protein are dependent on folding of its N-terminal domain. *Journal of cell science*. 114:1901-1912.

Bretscher, A. 1983. Purification of an 80,000-dalton protein that is a component of the isolated microvillus cytoskeleton, and its localization in nonmuscle cells. *The Journal of cell biology*. 97:425-432.

Bretscher, A. 1989. Rapid phosphorylation and reorganization of ezrin and spectrin accompany morphological changes induced in A-431 cells by epidermal growth factor. *The Journal of cell biology*. 108:921-930.

Bretscher, A., D. Chambers, R. Nguyen, and D. Reczek. 2000. ERM-Merlin and EBP50 protein families in plasma membrane organization and function. *Annual review of cell and developmental biology*. 16:113-143.

Bretscher, A., K. Edwards, and R.G. Fehon. 2002. ERM proteins and merlin: integrators at the cell cortex. *Nature reviews. Molecular cell biology*. 3:586-599.

Britton, J.S., and B.A. Edgar. 1998. Environmental control of the cell cycle in Drosophila: nutrition activates mitotic and endoreplicative cells by distinct mechanisms. *Development*. 125:2149-2158.

Broadus, J., and C.Q. Doe. 1997. Extrinsic cues, intrinsic cues and microfilaments regulate asymmetric protein localization in Drosophila neuroblasts. *Current biology : CB*. 7:827-835.

Bruce, B., G. Khanna, L. Ren, G. Landberg, K. Jirstrom, C. Powell, A. Borczuk, E.T. Keller, K.J. Wojno, P. Meltzer, K. Baird, A. McClatchey, A. Bretscher, S.M. Hewitt, and C. Khanna. 2007. Expression of the cytoskeleton linker protein ezrin in human cancers. *Clinical & experimental metastasis*. 24:69-78.

Bryant, P.J., K.L. Watson, R.W. Justice, and D.F. Woods. 1993. Tumor suppressor genes encoding proteins required for cell interactions and signal transduction in Drosophila. *Dev Suppl*:239-249.

Cabernard, C., K.E. Prehoda, and C.Q. Doe. 2010. A spindle-independent cleavage furrow positioning pathway. *Nature*. 467:91-94.

Cai, Y., F. Yu, S. Lin, W. Chia, and X. Yang. 2003. Apical complex genes control mitotic spindle geometry and relative size of daughter cells in Drosophila neuroblast and pI asymmetric divisions. *Cell*. 112:51-62.

Capdevila, J., and I. Guerrero. 1994. Targeted expression of the signaling molecule decapentaplegic induces pattern duplications and growth alterations in Drosophila wings. *The EMBO journal*. 13:4459-4468.

Cardone, R.A., A. Bellizzi, G. Busco, E.J. Weinman, M.E. Dell'Aquila, V. Casavola, A. Azzariti, A. Mangia, A. Paradiso, and S.J. Reshkin. 2007. The NHERF1 PDZ2 domain regulates PKA-RhoA-p38-mediated NHE1 activation and invasion in breast tumor cells. *Molecular biology of the cell*. 18:1768-1780.

Carreno, S., I. Kouranti, E.S. Glusman, M.T. Fuller, A. Echard, and F. Payre. 2008. Moesin and its activating kinase Slik are required for cortical stability and microtubule organization in mitotic cells. *The Journal of cell biology*. 180:739-746.

Castelo, L., and D.G. Jay. 1999. Radixin is involved in lamellipodial stability during nerve growth cone motility. *Molecular biology of the cell*. 10:1511-1520.

Chabu, C., and C.Q. Doe. 2009. Twins/PP2A regulates aPKC to control neuroblast cell polarity and self-renewal. *Developmental biology*. 330:399-405.

Chell, J.M., and A.H. Brand. 2010. Nutrition-responsive glia control exit of neural stem cells from quiescence. *Cell*. 143:1161-1173.

Chen, J.Y., Y.Y. Lin, and T.S. Jou. 2012. Phosphorylation of EBP50 negatively regulates beta-PIX-dependent Rac1 activity in anoikis. *Cell death and differentiation*. 19:1027-1037.

Chen, P.Y., H. Manninga, K. Slanchev, M. Chien, J.J. Russo, J. Ju, R. Sheridan, B. John, D.S. Marks, D. Gaidatzis, C. Sander, M. Zavolan, and T. Tuschl. 2005. The developmental miRNA profiles of zebrafish as determined by small RNA cloning. *Genes & development*. 19:1288-1293.

Chen, Z., A. Del Valle Rodriguez, X. Li, T. Erclik, V.M. Fernandes, and C. Desplan. 2016. A Unique Class of Neural Progenitors in the Drosophila Optic Lobe Generates Both Migrating Neurons and Glia. *Cell reports*.

Cheng, H., J. Li, R. Fazlieva, Z. Dai, Z. Bu, and H. Roder. 2009. Autoinhibitory interactions between the PDZ2 and C-terminal domains in the scaffolding protein NHERF1. *Structure*. 17:660-669.

Cheng, J., A. Tiyaboonchai, Y.M. Yamashita, and A.J. Hunt. 2011. Asymmetric division of cyst stem cells in Drosophila testis is ensured by anaphase spindle repositioning. *Development*. 138:831-837.

Cheng, J.Q., W.C. Lee, M.A. Klein, G.Z. Cheng, S.C. Jhanwar, and J.R. Testa. 1999. Frequent mutations of NF2 and allelic loss from chromosome band 22q12 in malignant mesothelioma: evidence for a two-hit mechanism of NF2 inactivation. *Genes, chromosomes & cancer*. 24:238-242.

Chenn, A., and S.K. McConnell. 1995. Cleavage orientation and the asymmetric inheritance of Notch1 immunoreactivity in mammalian neurogenesis. *Cell*. 82:631-641.

Chia, W., W.G. Somers, and H. Wang. 2008. Drosophila neuroblast asymmetric divisions: cell cycle regulators, asymmetric protein localization, and tumorigenesis. *The Journal of cell biology*. 180:267-272.

Cleary, M.A., N. Uboha, M.R. Picciotto, and R.D. Beech. 2006. Expression of ezrin in glial tubes in the adult subventricular zone and rostral migratory stream. *Neuroscience*. 143:851-861.

Cole, B.K., M. Curto, A.W. Chan, and A.I. McClatchey. 2008. Localization to the cortical cytoskeleton is necessary for Nf2/merlin-dependent epidermal growth factor receptor silencing. *Molecular and cellular biology*. 28:1274-1284.

Conboy, J., Y.W. Kan, S.B. Shohet, and N. Mohandas. 1986. Molecular cloning of protein 4.1, a major structural element of the human erythrocyte membrane skeleton. *Proceedings of the National Academy of Sciences of the United States of America*. 83:9512-9516.

Connell, M., C. Cabernard, D. Ricketson, C.Q. Doe, and K.E. Prehoda. 2011. Asymmetric cortical extension shifts cleavage furrow position in Drosophila neuroblasts. *Molecular biology of the cell*. 22:4220-4226.

Cooper, J.A., and T. Hunter. 1981. Similarities and differences between the effects of epidermal growth factor and Rous sarcoma virus. *The Journal of cell biology*. 91:878-883.

Crepaldi, T., A. Gautreau, P.M. Comoglio, D. Louvard, and M. Arpin. 1997. Ezrin is an effector of hepatocyte growth factor-mediated migration and morphogenesis in epithelial cells. *The Journal of cell biology*. 138:423-434.

Curto, M., B.K. Cole, D. Lallemand, C.H. Liu, and A.I. McClatchey. 2007. Contact-dependent inhibition of EGFR signaling by Nf2/Merlin. *The Journal of cell biology*. 177:893-903.

Custer, M., B. Spindler, F. Verrey, H. Murer, and J. Biber. 1997. Identification of a new gene product (diphor-1) regulated by dietary phosphate. *The American journal of physiology*. 273:F801-806.

D'Angelo, R., S. Aresta, A. Blangy, L. Del Maestro, D. Louvard, and M. Arpin. 2007. Interaction of ezrin with the novel guanine nucleotide exchange factor PLEKHG6

promotes RhoG-dependent apical cytoskeleton rearrangements in epithelial cells. *Molecular biology of the cell*. 18:4780-4793.

Dai, J.L., L. Wang, A.A. Sahin, L.D. Broemeling, M. Schutte, and Y. Pan. 2004. NHERF (Na+/H+ exchanger regulatory factor) gene mutations in human breast cancer. *Oncogene*. 23:8681-8687.

Dard, N., S. Louvet-Vallee, A. Santa-Maria, and B. Maro. 2004. Phosphorylation of ezrin on threonine T567 plays a crucial role during compaction in the mouse early embryo. *Developmental biology*. 271:87-97.

Dard, N., S. Louvet, A. Santa-Maria, J. Aghion, M. Martin, P. Mangeat, and B. Maro. 2001. In vivo functional analysis of ezrin during mouse blastocyst formation. *Developmental biology*. 233:161-173.

De Lorenzo, C., D. Strand, and B.M. Mechler. 1999. Requirement of Drosophila I(2)gl function for survival of the germline cells and organization of the follicle cells in a columnar epithelium during oogenesis. *The International journal of developmental biology*. 43:207-217.

Delaunay, D., V. Cortay, D. Patti, K. Knoblauch, and C. Dehay. 2014. Mitotic spindle asymmetry: a Wnt/PCP-regulated mechanism generating asymmetrical division in cortical precursors. *Cell reports*. 6:400-414.

Deng, W.M., C. Althauser, and H. Ruohola-Baker. 2001. Notch-Delta signaling induces a transition from mitotic cell cycle to endocycle in Drosophila follicle cells. *Development*. 128:4737-4746.

DeSalvo, M.K., S.J. Hindle, Z.M. Rusan, S. Orng, M. Eddison, K. Halliwill, and R.J. Bainton. 2014. The Drosophila surface glia transcriptome: evolutionary conserved blood-brain barrier processes. *Frontiers in neuroscience*. 8:346.

DeSouza, L.V., A. Matta, Z. Karim, J. Mukherjee, X.S. Wang, O. Krakovska, G. Zadeh, A. Guha, and K.M. Siu. 2013. Role of moesin in hyaluronan induced cell migration in glioblastoma multiforme. *Mol Cancer*. 12:74.

Ding, R., K. Weynans, T. Bossing, C.S. Barros, and C. Berger. 2016. The Hippo signalling pathway maintains quiescence in Drosophila neural stem cells. *Nature communications*. 7:10510.

Doe, C.Q., Q. Chu-LaGraff, D.M. Wright, and M.P. Scott. 1991. The prospero gene specifies cell fates in the Drosophila central nervous system. *Cell*. 65:451-464.

Doi, Y., M. Itoh, S. Yonemura, S. Ishihara, H. Takano, T. Noda, and S. Tsukita. 1999. Normal development of mice and unimpaired cell adhesion/cell motility/actin-based

cytoskeleton without compensatory up-regulation of ezrin or radixin in moesin gene knockout. *The Journal of biological chemistry*. 274:2315-2321.

Duffy, J.B., D.A. Harrison, and N. Perrimon. 1998. Identifying loci required for follicular patterning using directed mosaics. *Development*. 125:2263-2271.

Dumstrei, K., F. Wang, and V. Hartenstein. 2003. Role of DE-cadherin in neuroblast proliferation, neural morphogenesis, and axon tract formation in Drosophila larval brain development. *The Journal of neuroscience : the official journal of the Society for Neuroscience*. 23:3325-3335.

Ebens, A.J., H. Garren, B.N. Cheyette, and S.L. Zipursky. 1993. The Drosophila anachronism locus: a glycoprotein secreted by glia inhibits neuroblast proliferation. *Cell*. 74:15-27.

Egger, B., J.Q. Boone, N.R. Stevens, A.H. Brand, and C.Q. Doe. 2007. Regulation of spindle orientation and neural stem cell fate in the Drosophila optic lobe. *Neural development*. 2:1.

Egger, B., K.S. Gold, and A.H. Brand. 2010. Notch regulates the switch from symmetric to asymmetric neural stem cell division in the Drosophila optic lobe. *Development*. 137:2981-2987.

Elliott, B.E., J.A. Meens, S.K. SenGupta, D. Louvard, and M. Arpin. 2005. The membrane cytoskeletal crosslinker ezrin is required for metastasis of breast carcinoma cells. *Breast cancer research : BCR*. 7:R365-373.

Elliott, B.E., H. Qiao, D. Louvard, and M. Arpin. 2004. Co-operative effect of c-Src and ezrin in deregulation of cell-cell contacts and scattering of mammary carcinoma cells. *Journal of cellular biochemistry*. 92:16-28.

Erclik, T., V. Hartenstein, H.D. Lipshitz, and R.R. McInnes. 2008. Conserved role of the Vsx genes supports a monophyletic origin for bilaterian visual systems. *Current biology : CB*. 18:1278-1287.

Erclik, T., X. Li, M. Courgeon, C. Bertet, Z. Chen, R. Baumert, J. Ng, C. Koo, U. Arain, R. Behnia, A. del Valle Rodriguez, L. Senderowicz, N. Negre, K.P. White, and C. Desplan. 2017. Integration of temporal and spatial patterning generates neural diversity. *Nature*. 541:365-370.

Eshaghian, J., and B.W. Streeten. 1980. Human posterior subcapsular cataract. An ultrastructural study of the posteriorly migrating cells. *Archives of ophthalmology*. 98:134-143.

Estecha, A., L. Sanchez-Martin, A. Puig-Kroger, R.A. Bartolome, J. Teixido, R. Samaniego, and P. Sanchez-Mateos. 2009. Moesin orchestrates cortical polarity of melanoma tumour cells to initiate 3D invasion. *Journal of cell science*. 122:3492-3501.

Evans, D.G., S.M. Huson, D. Donnai, W. Neary, V. Blair, V. Newton, and R. Harris. 1992. A clinical study of type 2 neurofibromatosis. *The Quarterly journal of medicine*. 84:603-618.

Fehon, R.G., T. Oren, D.R. LaJeunesse, T.E. Melby, and B.M. McCartney. 1997. Isolation of mutations in the Drosophila homologues of the human Neurofibromatosis 2 and yeast CDC42 genes using a simple and efficient reverse-genetic method. *Genetics*. 146:245-252.

Fernandez-Valle, C., Y. Tang, J. Ricard, A. Rodenas-Ruano, A. Taylor, E. Hackler, J. Biggerstaff, and J. Iacovelli. 2002. Paxillin binds schwannomin and regulates its density-dependent localization and effect on cell morphology. *Nature genetics*. 31:354-362.

Fievet, B.T., A. Gautreau, C. Roy, L. Del Maestro, P. Mangeat, D. Louvard, and M. Arpin. 2004. Phosphoinositide binding and phosphorylation act sequentially in the activation mechanism of ezrin. *The Journal of cell biology*. 164:653-659.

Filippov, V., M. Filippova, F. Sehnal, and S.S. Gill. 2000. Temporal and spatial expression of the cell-cycle regulator cul-1 in Drosophila and its stimulation by radiation-induced apoptosis. *The Journal of experimental biology*. 203:2747-2756.

Flynt, A.S., E.J. Thatcher, K. Burkewitz, N. Li, Y. Liu, and J.G. Patton. 2009. miR-8 microRNAs regulate the response to osmotic stress in zebrafish embryos. *The Journal of cell biology*. 185:115-127.

Fouassier, L., C.Y. Duan, A.P. Feranchak, C.H. Yun, E. Sutherland, F. Simon, J.G. Fitz, and R.B. Doctor. 2001. Ezrin-radixin-moesin-binding phosphoprotein 50 is expressed at the apical membrane of rat liver epithelia. *Hepatology*. 33:166-176.

Fouassier, L., M.T. Nichols, E. Gidey, R.R. McWilliams, H. Robin, C. Finnigan, K.E. Howell, C. Housset, and R.B. Doctor. 2005. Protein kinase C regulates the phosphorylation and oligomerization of ERM binding phosphoprotein 50. *Experimental cell research*. 306:264-273.

Fouassier, L., C.C. Yun, J.G. Fitz, and R.B. Doctor. 2000. Evidence for ezrin-radixin-moesin-binding phosphoprotein 50 (EBP50) self-association through PDZ-PDZ interactions. *The Journal of biological chemistry*. 275:25039-25045.

Franck, Z., R. Gary, and A. Bretscher. 1993. Moesin, like ezrin, colocalizes with actin in the cortical cytoskeleton in cultured cells, but its expression is more variable. *Journal of cell science*. 105 (Pt 1):219-231.

Funayama, N., A. Nagafuchi, N. Sato, S. Tsukita, and S. Tsukita. 1991. Radixin is a novel member of the band 4.1 family. *The Journal of cell biology*. 115:1039-1048.

Fuse, N., K. Hisata, A.L. Katzen, and F. Matsuzaki. 2003. Heterotrimeric G proteins regulate daughter cell size asymmetry in Drosophila neuroblast divisions. *Current biology : CB*. 13:947-954.

Garbett, D., D.P. LaLonde, and A. Bretscher. 2010. The scaffolding protein EBP50 regulates microvillar assembly in a phosphorylation-dependent manner. *The Journal of cell biology*. 191:397-413.

Garcia, C., and D.H. Gutmann. 2014. Nf2/Merlin controls spinal cord neural progenitor function in a Rac1/ErbB2-dependent manner. *PloS one*. 9:e97320.

Gary, R., and A. Bretscher. 1993. Heterotypic and homotypic associations between ezrin and moesin, two putative membrane-cytoskeletal linking proteins. *Proceedings of the National Academy of Sciences of the United States of America*. 90:10846-10850.

Gary, R., and A. Bretscher. 1995. Ezrin self-association involves binding of an N-terminal domain to a normally masked C-terminal domain that includes the F-actin binding site. *Molecular biology of the cell*. 6:1061-1075.

Gautreau, A., D. Louvard, and M. Arpin. 2000. Morphogenic effects of ezrin require a phosphorylation-induced transition from oligomers to monomers at the plasma membrane. *The Journal of cell biology*. 150:193-203.

Gavilan, H.S., R.M. Kulikauskas, D.H. Gutmann, and R.G. Fehon. 2014. In vivo functional analysis of the human NF2 tumor suppressor gene in Drosophila. *PloS one*. 9:e90853.

Gehlhausen, J.R., S.J. Park, A.E. Hickox, M. Shew, K. Staser, S.D. Rhodes, K. Menon, J.D. Lajiness, M. Mwanthi, X. Yang, J. Yuan, P. Territo, G. Hutchins, G. Nalepa, F.C. Yang, S.J. Conway, M.G. Heinz, A. Stemmer-Rachamimov, C.W. Yates, and D. Wade Clapp. 2015. A murine model of neurofibromatosis type 2 that accurately phenocopies human schwannoma formation. *Human molecular genetics*. 24:1-8.

Geiger, K.D., P. Stoldt, W. Schlote, and A. Derouiche. 2000. Ezrin immunoreactivity is associated with increasing malignancy of astrocytic tumors but is absent in oligodendrogliomas. *The American journal of pathology*. 157:1785-1793.

Genova, J.L., S. Jong, J.T. Camp, and R.G. Fehon. 2000. Functional analysis of Cdc42 in actin filament assembly, epithelial morphogenesis, and cell signaling during Drosophila development. *Developmental biology*. 221:181-194.

Georgescu, M.M., G. Cote, N.K. Agarwal, and C.L. White, 3rd. 2014. NHERF1/EBP50 controls morphogenesis of 3D colonic glands by stabilizing PTEN and ezrin-radixin-moesin proteins at the apical membrane. *Neoplasia*. 16:365-374 e361-362.

Giovannini, M., E. Robanus-Maandag, M. van der Valk, M. Niwa-Kawakita, V. Abramowski, L. Goutebroze, J.M. Woodruff, A. Berns, and G. Thomas. 2000. Conditional biallelic Nf2 mutation in the mouse promotes manifestations of human neurofibromatosis type 2. *Genes & development*. 14:1617-1630.

Gladden, A.B., A.M. Hebert, E.E. Schneeberger, and A.I. McClatchey. 2010. The NF2 tumor suppressor, Merlin, regulates epidermal development through the establishment of a junctional polarity complex. *Developmental cell*. 19:727-739.

Gobel, V., P.L. Barrett, D.H. Hall, and J.T. Fleming. 2004. Lumen morphogenesis in C. elegans requires the membrane-cytoskeleton linker erm-1. *Developmental cell*. 6:865-873.

Goh, L.H., X. Zhou, M.C. Lee, S. Lin, H. Wang, Y. Luo, and X. Yang. 2013. Clueless regulates aPKC activity and promotes self-renewal cell fate in Drosophila lgl mutant larval brains. *Developmental biology*. 381:353-364.

Gold, K.S., and A.H. Brand. 2014. Optix defines a neuroepithelial compartment in the optic lobe of the Drosophila brain. *Neural development*. 9:18.

Gonzalez-Agosti, C., T. Wiederhold, M.E. Herndon, J. Gusella, and V. Ramesh. 1999. Interdomain interaction of merlin isoforms and its influence on intermolecular binding to NHE-RF. *The Journal of biological chemistry*. 274:34438-34442.

Gonzalez-Agosti, C., L. Xu, D. Pinney, R. Beauchamp, W. Hobbs, J. Gusella, and V. Ramesh. 1996. The merlin tumor suppressor localizes preferentially in membrane ruffles. *Oncogene*. 13:1239-1247.

Gonzalez-Gomez, P., M.J. Bello, M.E. Alonso, J. Lomas, D. Arjona, J.M. Campos, J. Vaquero, A. Isla, L. Lassaletta, M. Gutierrez, J.L. Sarasa, and J.A. Rey. 2003. CpG island methylation in sporadic and neurofibromatis type 2-associated schwannomas. *Clinical cancer research : an official journal of the American Association for Cancer Research*. 9:5601-5606.

Gonzalez-Reyes, A., H. Elliott, and D. St Johnston. 1995. Polarization of both major body axes in Drosophila by gurken-torpedo signalling. *Nature*. 375:654-658.

Goode, S., and N. Perrimon. 1997. Inhibition of patterned cell shape change and cell invasion by Discs large during Drosophila oogenesis. *Genes & development*. 11:2532-2544.

Gould, K.L., A. Bretscher, F.S. Esch, and T. Hunter. 1989. cDNA cloning and sequencing of the protein-tyrosine kinase substrate, ezrin, reveals homology to band 4.1. *The EMBO journal*. 8:4133-4142.

Green, P., A.Y. Hartenstein, and V. Hartenstein. 1993. The embryonic development of the Drosophila visual system. *Cell and tissue research*. 273:583-598.

Gronholm, M., M. Sainio, F. Zhao, L. Heiska, A. Vaheri, and O. Carpen. 1999. Homotypic and heterotypic interaction of the neurofibromatosis 2 tumor suppressor protein merlin and the ERM protein ezrin. *Journal of cell science*. 112 (Pt 6):895-904.

Gronholm, M., T. Teesalu, J. Tyynela, K. Piltti, T. Bohling, K. Wartiovaara, A. Vaheri, and O. Carpen. 2005. Characterization of the NF2 protein merlin and the ERM protein ezrin in human, rat, and mouse central nervous system. *Molecular and cellular neurosciences*. 28:683-693.

Gutmann, D.H., C.A. Haipek, and K. Hoang Lu. 1999a. Neurofibromatosis 2 tumor suppressor protein, merlin, forms two functionally important intramolecular associations. *Journal of neuroscience research*. 58:706-716.

Gutmann, D.H., L. Sherman, L. Seftor, C. Haipek, K. Hoang Lu, and M. Hendrix. 1999b. Increased expression of the NF2 tumor suppressor gene product, merlin, impairs cell motility, adhesionand spreading. *Human molecular genetics*. 8:267-275.

Hales, K.G., C.A. Korey, A.M. Larracuente, and D.M. Roberts. 2015. Genetics on the Fly: A Primer on the Drosophila Model System. *Genetics*. 201:815-842.

Hall, R.A., R.T. Premont, C.W. Chow, J.T. Blitzer, J.A. Pitcher, A. Claing, R.H. Stoffel, L.S. Barak, S. Shenolikar, E.J. Weinman, S. Grinstein, and R.J. Lefkowitz. 1998. The beta2-adrenergic receptor interacts with the Na+/H+-exchanger regulatory factor to control Na+/H+ exchange. *Nature*. 392:626-630.

Hall, R.A., R.F. Spurney, R.T. Premont, N. Rahman, J.T. Blitzer, J.A. Pitcher, and R.J. Lefkowitz. 1999. G protein-coupled receptor kinase 6A phosphorylates the Na(+)/H(+) exchanger regulatory factor via a PDZ domain-mediated interaction. *The Journal of biological chemistry*. 274:24328-24334.

Hamada, K., A. Seto, T. Shimizu, T. Matsui, Y. Takai, S. Tsukita, S. Tsukita, and T. Hakoshima. 2001. Crystallization and preliminary crystallographic studies of RhoGDI in complex with the radixin FERM domain. *Acta crystallographica. Section D, Biological crystallography*. 57:889-890.

Hamaratoglu, F., K. Gajewski, L. Sansores-Garcia, C. Morrison, C. Tao, and G. Halder. 2009. The Hippo tumor-suppressor pathway regulates apical-domain size in parallel to tissue growth. *Journal of cell science*. 122:2351-2359.

Hamaratoglu, F., M. Willecke, M. Kango-Singh, R. Nolo, E. Hyun, C. Tao, H. Jafar-Nejad, and G. Halder. 2006. The tumour-suppressor genes NF2/Merlin and Expanded act through Hippo signalling to regulate cell proliferation and apoptosis. *Nature cell biology*. 8:27-36.

Hanono, A., D. Garbett, D. Reczek, D.N. Chambers, and A. Bretscher. 2006. EPI64 regulates microvillar subdomains and structure. *The Journal of cell biology*. 175:803-813.

Hatzoglou, A., I. Ader, A. Splingard, J. Flanders, E. Saade, I. Leroy, S. Traver, S. Aresta, and J. de Gunzburg. 2007. Gem associates with Ezrin and acts via the Rho-GAP protein Gmip to down-regulate the Rho pathway. *Molecular biology of the cell*. 18:1242-1252.

Hayashi, K., S. Yonemura, T. Matsui, and S. Tsukita. 1999. Immunofluorescence detection of ezrin/radixin/moesin (ERM) proteins with their carboxyl-terminal threonine phosphorylated in cultured cells and tissues. *Journal of cell science*. 112 (Pt 8):1149-1158.

Hayashi, Y., J.R. Molina, S.R. Hamilton, and M.M. Georgescu. 2010. NHERF1/EBP50 is a new marker in colorectal cancer. *Neoplasia*. 12:1013-1022.

Haynes, J., J. Srivastava, N. Madson, T. Wittmann, and D.L. Barber. 2011. Dynamic actin remodeling during epithelial-mesenchymal transition depends on increased moesin expression. *Molecular biology of the cell*. 22:4750-4764.

He, J., A.G. Lau, M.B. Yaffe, and R.A. Hall. 2001. Phosphorylation and cell cycle-dependent regulation of Na+/H+ exchanger regulatory factor-1 by Cdc2 kinase. *The Journal of biological chemistry*. 276:41559-41565.

Hebert, A.M., B. DuBoff, J.B. Casaletto, A.B. Gladden, and A.I. McClatchey. 2012. Merlin/ERM proteins establish cortical asymmetry and centrosome position. *Genes & development*. 26:2709-2723.

Hennigan, R.F., L.A. Foster, M.F. Chaiken, T. Mani, M.M. Gomes, A.B. Herr, and W. Ip. 2010. Fluorescence resonance energy transfer analysis of merlin conformational changes. *Molecular and cellular biology*. 30:54-67.

Higa, L.A., X. Yang, J. Zheng, D. Banks, M. Wu, P. Ghosh, H. Sun, and H. Zhang. 2006. Involvement of CUL4 ubiquitin E3 ligases in regulating CDK inhibitors Dacapo/p27Kip1 and cyclin E degradation. *Cell cycle*. 5:71-77.

Hipfner, D.R., and S.M. Cohen. 2003. The Drosophila sterile-20 kinase slik controls cell proliferation and apoptosis during imaginal disc development. *PLoS biology*. 1:E35.

Hipfner, D.R., N. Keller, and S.M. Cohen. 2004. Slik Sterile-20 kinase regulates Moesin activity to promote epithelial integrity during tissue growth. *Genes & development*. 18:2243-2248.

Hirao, M., N. Sato, T. Kondo, S. Yonemura, M. Monden, T. Sasaki, Y. Takai, S. Tsukita, and S. Tsukita. 1996. Regulation mechanism of ERM (ezrin/radixin/moesin) protein/plasma membrane association: possible involvement of phosphatidylinositol turnover and Rho-dependent signaling pathway. *The Journal of cell biology*. 135:37-51.

Hirata, J., H. Nakagoshi, Y. Nabeshima, and F. Matsuzaki. 1995. Asymmetric segregation of the homeodomain protein Prospero during Drosophila development. *Nature*. 377:627-630.

Hofbauer, A., and J.A. Camposortega. 1990. Proliferation Pattern and Early Differentiation of the Optic Lobes in Drosophila-Melanogaster. *Roux Arch Dev Biol*. 198:264-274.

Houshmandi, S.S., R.J. Emnett, M. Giovannini, and D.H. Gutmann. 2009. The neurofibromatosis 2 protein, merlin, regulates glial cell growth in an ErbB2- and Src-dependent manner. *Molecular and cellular biology*. 29:1472-1486.

Hrdlicka, L., M. Gibson, A. Kiger, C. Micchelli, M. Schober, F. Schock, and N. Perrimon. 2002. Analysis of twenty-four Gal4 lines in Drosophila melanogaster. *Genesis*. 34:51-57.

Huang, L., E. Ichimaru, K. Pestonjamasp, X. Cui, H. Nakamura, G.Y. Lo, F.I. Lin, E.J. Luna, and H. Furthmayr. 1998. Merlin differs from moesin in binding to F-actin and in its intra- and intermolecular interactions. *Biochemical and biophysical research communications*. 248:548-553.

Huang, L., T.Y. Wong, R.C. Lin, and H. Furthmayr. 1999. Replacement of threonine 558, a critical site of phosphorylation of moesin in vivo, with aspartate activates F-actin binding of moesin. Regulation by conformational change. *The Journal of biological chemistry*. 274:12803-12810.

Huang, Z., and S. Kunes. 1996. Hedgehog, transmitted along retinal axons, triggers neurogenesis in the developing visual centers of the Drosophila brain. *Cell*. 86:411-422.

Huang, Z., and S. Kunes. 1998. Signals transmitted along retinal axons in Drosophila: Hedgehog signal reception and the cell circuitry of lamina cartridge assembly. *Development*. 125:3753-3764.

Hughes, S.C., and R.G. Fehon. 2006. Phosphorylation and activity of the tumor suppressor Merlin and the ERM protein Moesin are coordinately regulated by the Slik kinase. *The Journal of cell biology*. 175:305-313.

Hughes, S.C., E. Formstecher, and R.G. Fehon. 2010. Sip1, the Drosophila orthologue of EBP50/NHERF1, functions with the sterile 20 family kinase Slik to regulate Moesin activity. *Journal of cell science*. 123:1099-1107.

Ikeshima-Kataoka, H., J.B. Skeath, Y. Nabeshima, C.Q. Doe, and F. Matsuzaki. 1997. Miranda directs Prospero to a daughter cell during Drosophila asymmetric divisions. *Nature*. 390:625-629.

Ingraffea, J., D. Reczek, and A. Bretscher. 2002. Distinct cell type-specific expression of scaffolding proteins EBP50 and E3KARP: EBP50 is generally expressed with ezrin in specific epithelia, whereas E3KARP is not. *European journal of cell biology*. 81:61-68.

Ito, K., and Y. Hotta. 1992. Proliferation pattern of postembryonic neuroblasts in the brain of Drosophila melanogaster. *Developmental biology*. 149:134-148.

Izumi, Y., N. Ohta, K. Hisata, T. Raabe, and F. Matsuzaki. 2006. Drosophila Pins-binding protein Mud regulates spindle-polarity coupling and centrosome organization. *Nature cell biology*. 8:586-593.

Izumi, Y., N. Ohta, A. Itoh-Furuya, N. Fuse, and F. Matsuzaki. 2004. Differential functions of G protein and Baz-aPKC signaling pathways in Drosophila neuroblast asymmetric division. *The Journal of cell biology*. 164:729-738.

James, M.F., N. Manchanda, C. Gonzalez-Agosti, J.H. Hartwig, and V. Ramesh. 2001. The neurofibromatosis 2 protein product merlin selectively binds F-actin but not G-actin, and stabilizes the filaments through a lateral association. *The Biochemical journal*. 356:377-386.

Jankovics, F., R. Sinka, T. Lukacsovich, and M. Erdelyi. 2002. MOESIN crosslinks actin and cell membrane in Drosophila oocytes and is required for OSKAR anchoring. *Current biology : CB*. 12:2060-2065.

Jiang, Y., and H. Reichert. 2014. Drosophila neural stem cells in brain development and tumor formation. *Journal of neurogenetics*. 28:181-189.

Jin, H., T. Sperka, P. Herrlich, and H. Morrison. 2006. Tumorigenic transformation by CPI-17 through inhibition of a merlin phosphatase. *Nature*. 442:576-579.

Johnson, K.C., J.L. Kissil, J.L. Fry, and T. Jacks. 2002. Cellular transformation by a FERM domain mutant of the Nf2 tumor suppressor gene. *Oncogene*. 21:5990-5997.

Johnson, R.A., K.D. Wright, H. Poppleton, K.M. Mohankumar, D. Finkelstein, S.B. Pounds, V. Rand, S.E. Leary, E. White, C. Eden, T. Hogg, P. Northcott, S. Mack, G. Neale, Y.D.

Wang, B. Coyle, J. Atkinson, M. DeWire, T.A. Kranenburg, Y. Gillespie, J.C. Allen, T. Merchant, F.A. Boop, R.A. Sanford, A. Gajjar, D.W. Ellison, M.D. Taylor, R.G. Grundy, and R.J. Gilbertson. 2010. Cross-species genomics matches driver mutations and cell compartments to model ependymoma. *Nature*. 466:632-636.

Kaiser-Kupfer, M.I., V. Freidlin, M.B. Datiles, P.A. Edwards, J.L. Sherman, D. Parry, L.M. McCain, and R. Eldridge. 1989. The association of posterior capsular lens opacities with bilateral acoustic neuromas in patients with neurofibromatosis type 2. *Archives of ophthalmology*. 107:541-544.

Kalamarides, M., M. Niwa-Kawakita, H. Leblois, V. Abramowski, M. Perricaudet, A. Janin, G. Thomas, D.H. Gutmann, and M. Giovannini. 2002. Nf2 gene inactivation in arachnoidal cells is rate-limiting for meningioma development in the mouse. *Genes & development*. 16:1060-1065.

Kalikin, L.M., X. Qu, T.S. Frank, R.F. Caduff, S.M. Svoboda, D.J. Law, and E.M. Petty. 1996. Detailed deletion analysis of sporadic breast tumors defines an interstitial region of allelic loss on 17q25. *Genes, chromosomes & cancer*. 17:64-68.

Kaltschmidt, J.A., C.M. Davidson, N.H. Brown, and A.H. Brand. 2000. Rotation and asymmetry of the mitotic spindle direct asymmetric cell division in the developing central nervous system. *Nature cell biology*. 2:7-12.

Kang, B.S., D.R. Cooper, Y. Devedjiev, U. Derewenda, and Z.S. Derewenda. 2002. The structure of the FERM domain of merlin, the neurofibromatosis type 2 gene product. *Acta crystallographica. Section D, Biological crystallography*. 58:381-391.

Kaphingst, K., and S. Kunes. 1994. Pattern formation in the visual centers of the Drosophila brain: wingless acts via decapentaplegic to specify the dorsoventral axis. *Cell*. 78:437-448.

Karagiosis, S.A., and D.F. Ready. 2004. Moesin contributes an essential structural role in Drosophila photoreceptor morphogenesis. *Development*. 131:725-732.

Kawano, Y., Y. Fukata, N. Oshiro, M. Amano, T. Nakamura, M. Ito, F. Matsumura, M. Inagaki, and K. Kaibuchi. 1999. Phosphorylation of myosin-binding subunit (MBS) of myosin phosphatase by Rho-kinase in vivo. *The Journal of cell biology*. 147:1023-1038.

Khanna, C., J. Khan, P. Nguyen, J. Prehn, J. Caylor, C. Yeung, J. Trepel, P. Meltzer, and L. Helman. 2001. Metastasis-associated differences in gene expression in a murine model of osteosarcoma. *Cancer research*. 61:3750-3759.

Kikuchi, S., M. Hata, K. Fukumoto, Y. Yamane, T. Matsui, A. Tamura, S. Yonemura, H. Yamagishi, D. Keppler, S. Tsukita, and S. Tsukita. 2002. Radixin deficiency causes

conjugated hyperbilirubinemia with loss of Mrp2 from bile canalicular membranes. *Nature genetics*. 31:320-325.

Kim, S.H., H.J. Kim, S. Kim, and J. Yim. 2010. Drosophila Cand1 regulates Cullin3-dependent E3 ligases by affecting the neddylation of Cullin3 and by controlling the stability of Cullin3 and adaptor protein. *Developmental biology*. 346:247-257.

Kimura, Y., H. Koga, N. Araki, N. Mugita, N. Fujita, H. Takeshima, T. Nishi, T. Yamashima, T.C. Saido, T. Yamasaki, K. Moritake, H. Saya, and M. Nakao. 1998. The involvement of calpain-dependent proteolysis of the tumor suppressor NF2 (merlin) in schwannomas and meningiomas. *Nature medicine*. 4:915-922.

Kino, T., H. Takeshima, M. Nakao, T. Nishi, K. Yamamoto, T. Kimura, Y. Saito, M. Kochi, J. Kuratsu, H. Saya, and Y. Ushio. 2001. Identification of the cis-acting region in the NF2 gene promoter as a potential target for mutation and methylation-dependent silencing in schwannoma. *Genes to cells : devoted to molecular & cellular mechanisms*. 6:441-454.

Kissil, J.L., K.C. Johnson, M.S. Eckman, and T. Jacks. 2002. Merlin phosphorylation by p21-activated kinase 2 and effects of phosphorylation on merlin localization. *The Journal of biological chemistry*. 277:10394-10399.

Kissil, J.L., E.W. Wilker, K.C. Johnson, M.S. Eckman, M.B. Yaffe, and T. Jacks. 2003. Merlin, the product of the Nf2 tumor suppressor gene, is an inhibitor of the p21-activated kinase, Pak1. *Molecular cell*. 12:841-849.

Kiyomitsu, T., and I.M. Cheeseman. 2013. Cortical dynein and asymmetric membrane elongation coordinately position the spindle in anaphase. *Cell*. 154:391-402.

Knoblich, J.A., L.Y. Jan, and Y.N. Jan. 1995. Asymmetric segregation of Numb and Prospero during cell division. *Nature*. 377:624-627.

Knoblich, J.A., L.Y. Jan, and Y.N. Jan. 1997. The N terminus of the Drosophila Numb protein directs membrane association and actin-dependent asymmetric localization. *Proceedings of the National Academy of Sciences of the United States of America*. 94:13005-13010.

Kobayashi, H., J. Sagara, H. Kurita, M. Morifuji, M. Ohishi, K. Kurashina, and S. Taniguchi. 2004. Clinical significance of cellular distribution of moesin in patients with oral squamous cell carcinoma. *Clinical cancer research : an official journal of the American Association for Cancer Research*. 10:572-580.

Kocher, O., N. Comella, A. Gilchrist, R. Pal, K. Tognazzi, L.F. Brown, and J.H. Knoll. 1999. PDZK1, a novel PDZ domain-containing protein up-regulated in carcinomas and mapped to chromosome 1q21, interacts with cMOAT (MRP2), the multidrug

resistance-associated protein. *Laboratory investigation; a journal of technical methods and pathology*. 79:1161-1170.

Kraut, R., and J.A. Campos-Ortega. 1996. inscuteable, a neural precursor gene of Drosophila, encodes a candidate for a cytoskeleton adaptor protein. *Developmental biology*. 174:65-81.

Kraut, R., W. Chia, L.Y. Jan, Y.N. Jan, and J.A. Knoblich. 1996. Role of inscuteable in orienting asymmetric cell divisions in Drosophila. *Nature*. 383:50-55.

Kreimann, E.L., F.C. Morales, J. de Orbeta-Cruz, Y. Takahashi, H. Adams, T.J. Liu, P.D. McCrea, and M.M. Georgescu. 2007. Cortical stabilization of beta-catenin contributes to NHERF1/EBP50 tumor suppressor function. *Oncogene*. 26:5290-5299.

Krieg, J., and T. Hunter. 1992. Identification of the two major epidermal growth factor-induced tyrosine phosphorylation sites in the microvillar core protein ezrin. *The Journal of biological chemistry*. 267:19258-19265.

Kunda, P., A.E. Pelling, T. Liu, and B. Baum. 2008. Moesin controls cortical rigidity, cell rounding, and spindle morphogenesis during mitosis. *Current biology : CB*. 18:91-101.

Kunda, P., N.T. Rodrigues, E. Moeendarbary, T. Liu, A. Ivetic, G. Charras, and B. Baum. 2012. PP1-mediated moesin dephosphorylation couples polar relaxation to mitotic exit. *Current biology : CB*. 22:231-236.

Kussel, P., and M. Frasch. 1995. Pendulin, a Drosophila protein with cell cycle-dependent nuclear localization, is required for normal cell proliferation. *The Journal of cell biology*. 129:1491-1507.

LaJeunesse, D.R., B.M. McCartney, and R.G. Fehon. 1998. Structural analysis of Drosophila merlin reveals functional domains important for growth control and subcellular localization. *The Journal of cell biology*. 141:1589-1599.

LaJeunesse, D.R., B.M. McCartney, and R.G. Fehon. 2001. A systematic screen for dominant second-site modifiers of Merlin/NF2 phenotypes reveals an interaction with blistered/DSRF and scribbler. *Genetics*. 158:667-679.

Lallemand, D., M. Curto, I. Saotome, M. Giovannini, and A.I. McClatchey. 2003. NF2 deficiency promotes tumorigenesis and metastasis by destabilizing adherens junctions. *Genes & development*. 17:1090-1100.

Lallemand, D., J. Manent, A. Couvelard, A. Watilliaux, M. Siena, F. Chareyre, A. Lampin, M. Niwa-Kawakita, M. Kalamarides, and M. Giovannini. 2009a. Merlin regulates transmembrane receptor accumulation and signaling at the plasma membrane in primary mouse Schwann cells and in human schwannomas. *Oncogene*. 28:854-865.

Lallemand, D., A.L. Saint-Amaux, and M. Giovannini. 2009b. Tumor-suppression functions of merlin are independent of its role as an organizer of the actin cytoskeleton in Schwann cells. *Journal of cell science*. 122:4141-4149.

Lamb, R.F., B.W. Ozanne, C. Roy, L. McGarry, C. Stipp, P. Mangeat, and D.G. Jay. 1997. Essential functions of ezrin in maintenance of cell shape and lamellipodial extension in normal and transformed fibroblasts. *Current biology : CB*. 7:682-688.

Lanet, E., A.P. Gould, and C. Maurange. 2013. Protection of neuronal diversity at the expense of neuronal numbers during nutrient restriction in the Drosophila visual system. *Cell reports*. 3:587-594.

Lankes, W., A. Griesmacher, J. Grunwald, R. Schwartz-Albiez, and R. Keller. 1988. A heparin-binding protein involved in inhibition of smooth-muscle cell proliferation. *The Biochemical journal*. 251:831-842.

Lankes, W.T., and H. Furthmayr. 1991. Moesin: a member of the protein 4.1-talin-ezrin family of proteins. *Proceedings of the National Academy of Sciences of the United States of America*. 88:8297-8301.

Laprise, P., K.M. Lau, K.P. Harris, N.F. Silva-Gagliardi, S.M. Paul, S. Beronja, G.J. Beitel, C.J. McGlade, and U. Tepass. 2009. Yurt, Coracle, Neurexin IV and the Na(+),K(+)-ATPase form a novel group of epithelial polarity proteins. *Nature*. 459:1141-1145.

Lau, A.G., and R.A. Hall. 2001. Oligomerization of NHERF-1 and NHERF-2 PDZ domains: differential regulation by association with receptor carboxyl-termini and by phosphorylation. *Biochemistry*. 40:8572-8580.

Laulajainen, M., T. Muranen, O. Carpen, and M. Gronholm. 2008. Protein kinase A-mediated phosphorylation of the NF2 tumor suppressor protein merlin at serine 10 affects the actin cytoskeleton. *Oncogene*. 27:3233-3243.

Laulajainen, M., T. Muranen, T.A. Nyman, O. Carpen, and M. Gronholm. 2011. Multistep phosphorylation by oncogenic kinases enhances the degradation of the NF2 tumor suppressor merlin. *Neoplasia*. 13:643-652.

Lavado, A., Y. He, J. Pare, G. Neale, E.N. Olson, M. Giovannini, and X. Cao. 2013. Tumor suppressor Nf2 limits expansion of the neural progenitor pool by inhibiting Yap/Taz transcriptional coactivators. *Development*. 140:3323-3334.

Lazar, C.S., C.M. Cresson, D.A. Lauffenburger, and G.N. Gill. 2004. The Na+/H+ exchanger regulatory factor stabilizes epidermal growth factor receptors at the cell surface. *Molecular biology of the cell*. 15:5470-5480.

Lee, C.Y., K.J. Robinson, and C.Q. Doe. 2006. Lgl, Pins and aPKC regulate neuroblast self-renewal versus differentiation. *Nature*. 439:594-598.

Lee, J.H., T. Katakai, T. Hara, H. Gonda, M. Sugai, and A. Shimizu. 2004. Roles of p-ERM and Rho-ROCK signaling in lymphocyte polarity and uropod formation. *The Journal of cell biology*. 167:327-337.

Lee, T., and L. Luo. 1999. Mosaic analysis with a repressible cell marker for studies of gene function in neuronal morphogenesis. *Neuron*. 22:451-461.

Legg, J.W., C.A. Lewis, M. Parsons, T. Ng, and C.M. Isacke. 2002. A novel PKC-regulated mechanism controls CD44 ezrin association and directional cell motility. *Nature cell biology*. 4:399-407.

Lerit, D.A., K.M. Plevock, and N.M. Rusan. 2014. Live imaging of Drosophila larval neuroblasts. *Journal of visualized experiments : JoVE*.

Leung, T., E. Manser, L. Tan, and L. Lim. 1995. A novel serine/threonine kinase binding the Ras-related RhoA GTPase which translocates the kinase to peripheral membranes. *The Journal of biological chemistry*. 270:29051-29054.

Li, J., P.I. Poulikakos, Z. Dai, J.R. Testa, D.J. Callaway, and Z. Bu. 2007a. Protein kinase C phosphorylation disrupts Na+/H+ exchanger regulatory factor 1 autoinhibition and promotes cystic fibrosis transmembrane conductance regulator macromolecular assembly. *The Journal of biological chemistry*. 282:27086-27099.

Li, J.G., C. Chen, and L.Y. Liu-Chen. 2002. Ezrin-radixin-moesin-binding phosphoprotein-50/Na+/H+ exchanger regulatory factor (EBP50/NHERF) blocks U50,488H-induced down-regulation of the human kappa opioid receptor by enhancing its recycling rate. *The Journal of biological chemistry*. 277:27545-27552.

Li, P., X. Yang, M. Wasser, Y. Cai, and W. Chia. 1997. Inscuteable and Staufen mediate asymmetric localization and segregation of prospero RNA during Drosophila neuroblast cell divisions. *Cell*. 90:437-447.

Li, Q., M.R. Nance, R. Kulikauskas, K. Nyberg, R. Fehon, P.A. Karplus, A. Bretscher, and J.J. Tesmer. 2007b. Self-masking in an intact ERM-merlin protein: an active role for the central alpha-helical domain. *Journal of molecular biology*. 365:1446-1459.

Li, Q., M. Wu, H. Wang, G. Xu, T. Zhu, Y. Zhang, P. Liu, A. Song, C. Gang, Z. Han, J. Zhou, L. Meng, Y. Lu, S. Wang, and D. Ma. 2008. Ezrin silencing by small hairpin RNA reverses metastatic behaviors of human breast cancer cells. *Cancer letters*. 261:55-63.

Li, S., H. Wang, and C. Groth. 2014. Drosophila neuroblasts as a new model for the study of stem cell self-renewal and tumour formation. *Bioscience reports*. 34.

Li, X., R. Zhuo, S. Tiong, F. Di Cara, K. King-Jones, S.C. Hughes, S.D. Campbell, and R. Wevrick. 2013. The Smc5/Smc6/MAGE complex confers resistance to caffeine and genotoxic stress in Drosophila melanogaster. *PloS one*. 8:e59866.

Lim, H.C., and T.S. Jou. 2016. Ras-activated RSK1 phosphorylates EBP50 to regulate its nuclear localization and promote cell proliferation. *Oncotarget*. 7:10283-10296.

Lomas, J., M.J. Bello, D. Arjona, M.E. Alonso, V. Martinez-Glez, I. Lopez-Marin, C. Aminoso, J.M. de Campos, A. Isla, J. Vaquero, and J.A. Rey. 2005. Genetic and epigenetic alteration of the NF2 gene in sporadic meningiomas. *Genes, chromosomes & cancer*. 42:314-319.

Lopez-Schier, H., and D. St Johnston. 2001. Delta signaling from the germ line controls the proliferation and differentiation of the somatic follicle cells during Drosophila oogenesis. *Genes & development*. 15:1393-1405.

Louvet, S., J. Aghion, A. Santa-Maria, P. Mangeat, and B. Maro. 1996. Ezrin becomes restricted to outer cells following asymmetrical division in the preimplantation mouse embryo. *Developmental biology*. 177:568-579.

Lu, B., L. Ackerman, L.Y. Jan, and Y.N. Jan. 1999. Modes of protein movement that lead to the asymmetric localization of partner of Numb during Drosophila neuroblast division. *Molecular cell*. 4:883-891.

Lu, B., M. Rothenberg, L.Y. Jan, and Y.N. Jan. 1998. Partner of Numb colocalizes with Numb during mitosis and directs Numb asymmetric localization in Drosophila neural and muscle progenitors. *Cell*. 95:225-235.

Luxenburg, C., H.A. Pasolli, S.E. Williams, and E. Fuchs. 2011. Developmental roles for Srf, cortical cytoskeleton and cell shape in epidermal spindle orientation. *Nature cell biology*. 13:203-214.

MacDougall, N., Y. Lad, G.S. Wilkie, H. Francis-Lang, W. Sullivan, and I. Davis. 2001. Merlin, the Drosophila homologue of neurofibromatosis-2, is specifically required in posterior follicle cells for axis formation in the oocyte. *Development*. 128:665-673.

Machicoane, M., C.A. de Frutos, J. Fink, M. Rocancourt, Y. Lombardi, S. Garel, M. Piel, and A. Echard. 2014. SLK-dependent activation of ERMs controls LGN-NuMA localization and spindle orientation. *The Journal of cell biology*. 205:791-799.

Mackay, D.J., F. Esch, H. Furthmayr, and A. Hall. 1997. Rho- and rac-dependent assembly of focal adhesion complexes and actin filaments in permeabilized fibroblasts: an essential role for ezrin/radixin/moesin proteins. *The Journal of cell biology*. 138:927-938.

Maeda, M., T. Matsui, M. Imamura, S. Tsukita, and S. Tsukita. 1999. Expression level, subcellular distribution and rho-GDI binding affinity of merlin in comparison with Ezrin/Radixin/Moesin proteins. *Oncogene*. 18:4788-4797.

Mahoney, P.A., U. Weber, P. Onofrechuk, H. Biessmann, P.J. Bryant, and C.S. Goodman. 1991. The fat tumor suppressor gene in Drosophila encodes a novel member of the cadherin gene superfamily. *Cell*. 67:853-868.

Mahowald, A.P. 1972. Ultrastructural observations on oogenesis in Drosophila. *Journal of morphology*. 137:29-48.

Maitra, S., R.M. Kulikauskas, H. Gavilan, and R.G. Fehon. 2006. The tumor suppressors Merlin and Expanded function cooperatively to modulate receptor endocytosis and signaling. *Current biology : CB*. 16:702-709.

Manfruelli, P., N. Arquier, W.P. Hanratty, and M. Semeriva. 1996. The tumor suppressor gene, lethal(2)giant larvae (1(2)g1), is required for cell shape change of epithelial cells during Drosophila development. *Development*. 122:2283-2294.

Manseau, L., A. Baradaran, D. Brower, A. Budhu, F. Elefant, H. Phan, A.V. Philp, M. Yang, D. Glover, K. Kaiser, K. Palter, and S. Selleck. 1997. GAL4 enhancer traps expressed in the embryo, larval brain, imaginal discs, and ovary of Drosophila. *Developmental dynamics : an official publication of the American Association of Anatomists*. 209:310-322.

Mao, J., X.R. Yuan, S.S. Xu, X.C. Jiang, and X.T. Zhao. 2013. Expression and functional significance of ezrin in human brain astrocytoma. *Cell Biochem Biophys*. 67:1507-1511.

Margolis, J., and A. Spradling. 1995. Identification and behavior of epithelial stem cells in the Drosophila ovary. *Development*. 121:3797-3807.

Martin, M., C. Roy, P. Montcourrier, A. Sahuquet, and P. Mangeat. 1997. Three determinants in ezrin are responsible for cell extension activity. *Molecular biology of the cell*. 8:1543-1557.

Matsui, T., M. Amano, T. Yamamoto, K. Chihara, M. Nakafuku, M. Ito, T. Nakano, K. Okawa, A. Iwamatsu, and K. Kaibuchi. 1996. Rho-associated kinase, a novel serine/threonine kinase, as a putative target for small GTP binding protein Rho. *The EMBO journal*. 15:2208-2216.

Matsui, T., M. Maeda, Y. Doi, S. Yonemura, M. Amano, K. Kaibuchi, S. Tsukita, and S. Tsukita. 1998. Rho-kinase phosphorylates COOH-terminal threonines of ezrin/radixin/moesin (ERM) proteins and regulates their head-to-tail association. *The Journal of cell biology*. 140:647-657.

Matsui, T., S. Yonemura, S. Tsukita, and S. Tsukita. 1999. Activation of ERM proteins in vivo by Rho involves phosphatidyl-inositol 4-phosphate 5-kinase and not ROCK kinases. *Current biology : CB*. 9:1259-1262.

Matsuzaki, F., K. Koizumi, C. Hama, T. Yoshioka, and Y. Nabeshima. 1992. Cloning of the Drosophila prospero gene and its expression in ganglion mother cells. *Biochemical and biophysical research communications*. 182:1326-1332.

Maudsley, S., A.M. Zamah, N. Rahman, J.T. Blitzer, L.M. Luttrell, R.J. Lefkowitz, and R.A. Hall. 2000. Platelet-derived growth factor receptor association with Na(+)/H(+) exchanger regulatory factor potentiates receptor activity. *Molecular and cellular biology*. 20:8352-8363.

McCartney, B.M., and R.G. Fehon. 1996. Distinct cellular and subcellular patterns of expression imply distinct functions for the Drosophila homologues of moesin and the neurofibromatosis 2 tumor suppressor, merlin. *The Journal of cell biology*. 133:843-852.

McCartney, B.M., R.M. Kulikauskas, D.R. LaJeunesse, and R.G. Fehon. 2000. The neurofibromatosis-2 homologue, Merlin, and the tumor suppressor expanded function together in Drosophila to regulate cell proliferation and differentiation. *Development*. 127:1315-1324.

McClatchey, A.I. 2003. Merlin and ERM proteins: unappreciated roles in cancer development? *Nature reviews. Cancer*. 3:877-883.

McClatchey, A.I., I. Saotome, K. Mercer, D. Crowley, J.F. Gusella, R.T. Bronson, and T. Jacks. 1998. Mice heterozygous for a mutation at the Nf2 tumor suppressor locus develop a range of highly metastatic tumors. *Genes & development*. 12:1121-1133.

McClatchey, A.I., I. Saotome, V. Ramesh, J.F. Gusella, and T. Jacks. 1997. The Nf2 tumor suppressor gene product is essential for extraembryonic development immediately prior to gastrulation. *Genes & development*. 11:1253-1265.

McLaughlin, M.E., G.M. Kruger, K.L. Slocum, D. Crowley, N.A. Michaud, J. Huang, M. Magendantz, and T. Jacks. 2007. The Nf2 tumor suppressor regulates cell-cell adhesion during tissue fusion. *Proceedings of the National Academy of Sciences of the United States of America*. 104:3261-3266.

Medina, E., J. Williams, E. Klipfell, D. Zarnescu, G. Thomas, and A. Le Bivic. 2002. Crumbs interacts with moesin and beta(Heavy)-spectrin in the apical membrane skeleton of Drosophila. *The Journal of cell biology*. 158:941-951.

Meinertzhagen, I.A., and T.E. Hanson. 1993. The development of the optic lobe. 1363-1491.

Meng, Y., Z. Lu, S. Yu, Q. Zhang, Y. Ma, and J. Chen. 2010. Ezrin promotes invasion and metastasis of pancreatic cancer cells. *Journal of translational medicine*. 8:61.

Mohler, P.J., S.M. Kreda, R.C. Boucher, M. Sudol, M.J. Stutts, and S.L. Milgram. 1999. Yes-associated protein 65 localizes p62(c-Yes) to the apical compartment of airway epithelia by association with EBP50. *The Journal of cell biology*. 147:879-890.

Molnar, C., and J.F. de Celis. 2006. Independent roles of Drosophila Moesin in imaginal disc morphogenesis and hedgehog signalling. *Mechanisms of development*. 123:337-351.

Moon, Y., J.Y. Kim, S.Y. Choi, H.M. Cho, H. Kim, and W. Sun. 2013. Expression of ezrin in subventricular zone neural stem cells and their progeny in adult and developing mice. *Histochem Cell Biol*. 139:403-413.

Morales, F.C., Y. Takahashi, E.L. Kreimann, and M.M. Georgescu. 2004. Ezrin-radixin-moesin (ERM)-binding phosphoprotein 50 organizes ERM proteins at the apical membrane of polarized epithelia. *Proceedings of the National Academy of Sciences of the United States of America*. 101:17705-17710.

Morales, F.C., Y. Takahashi, S. Momin, H. Adams, X. Chen, and M.M. Georgescu. 2007. NHERF1/EBP50 head-to-tail intramolecular interaction masks association with PDZ domain ligands. *Molecular and cellular biology*. 27:2527-2537.

Morante, J., D.M. Vallejo, C. Desplan, and M. Dominguez. 2013. Conserved miR-8/miR-200 defines a glial niche that controls neuroepithelial expansion and neuroblast transition. *Developmental cell*. 27:174-187.

Morata, G., and P. Ripoll. 1975. Minutes: mutants of drosophila autonomously affecting cell division rate. *Developmental biology*. 42:211-221.

Morrison, H., L.S. Sherman, J. Legg, F. Banine, C. Isacke, C.A. Haipek, D.H. Gutmann, H. Ponta, and P. Herrlich. 2001. The NF2 tumor suppressor gene product, merlin, mediates contact inhibition of growth through interactions with CD44. *Genes & development*. 15:968-980.

Murthy, A., C. Gonzalez-Agosti, E. Cordero, D. Pinney, C. Candia, F. Solomon, J. Gusella, and V. Ramesh. 1998. NHE-RF, a regulatory cofactor for Na(+)-H+ exchange, is a common interactor for merlin and ERM (MERM) proteins. *The Journal of biological chemistry*. 273:1273-1276.

Nakamura, F., M.R. Amieva, and H. Furthmayr. 1995. Phosphorylation of threonine 558 in the carboxyl-terminal actin-binding domain of moesin by thrombin activation of human platelets. *The Journal of biological chemistry*. 270:31377-31385.

Nakamura, F., L. Huang, K. Pestonjamasp, E.J. Luna, and H. Furthmayr. 1999. Regulation of F-actin binding to platelet moesin in vitro by both phosphorylation of threonine 558 and polyphosphatidylinositides. *Molecular biology of the cell*. 10:2669-2685.

Nassif, C., A. Noveen, and V. Hartenstein. 2003. Early development of the Drosophila brain: III. The pattern of neuropile founder tracts during the larval period. *Journal of Comparative Neurology*. 455:417-434.

Nestl, A., O.D. Von Stein, K. Zatloukal, W.G. Thies, P. Herrlich, M. Hofmann, and J.P. Sleeman. 2001. Gene expression patterns associated with the metastatic phenotype in rodent and human tumors. *Cancer research*. 61:1569-1577.

Ng, T., M. Parsons, W.E. Hughes, J. Monypenny, D. Zicha, A. Gautreau, M. Arpin, S. Gschmeissner, P.J. Verveer, P.I. Bastiaens, and P.J. Parker. 2001. Ezrin is a downstream effector of trafficking PKC-integrin complexes involved in the control of cell motility. *The EMBO journal*. 20:2723-2741.

Ngo, K.T., J. Wang, M. Junker, S. Kriz, G. Vo, B. Asem, J.M. Olson, U. Banerjee, and V. Hartenstein. 2010. Concomitant requirement for Notch and Jak/Stat signaling during neuro-epithelial differentiation in the Drosophila optic lobe. *Developmental biology*. 346:284-295.

Nguyen, R., D. Reczek, and A. Bretscher. 2001. Hierarchy of merlin and ezrin N- and C-terminal domain interactions in homo- and heterotypic associations and their relationship to binding of scaffolding proteins EBP50 and E3KARP. *The Journal of biological chemistry*. 276:7621-7629.

Niggli, V., C. Andreoli, C. Roy, and P. Mangeat. 1995. Identification of a phosphatidylinositol-4,5-bisphosphate-binding domain in the N-terminal region of ezrin. *FEBS letters*. 376:172-176.

Nipper, R.W., K.H. Siller, N.R. Smith, C.Q. Doe, and K.E. Prehoda. 2007. Galphai generates multiple Pins activation states to link cortical polarity and spindle orientation in Drosophila neuroblasts. *Proceedings of the National Academy of Sciences of the United States of America*. 104:14306-14311.

Oda, H., T. Uemura, Y. Harada, Y. Iwai, and M. Takeichi. 1994. A Drosophila homolog of cadherin associated with armadillo and essential for embryonic cell-cell adhesion. *Developmental biology*. 165:716-726.

Ohshiro, T., T. Yagami, C. Zhang, and F. Matsuzaki. 2000. Role of cortical tumour-suppressor proteins in asymmetric division of Drosophila neuroblast. *Nature*. 408:593-596.

Okada, T., M. Lopez-Lago, and F.G. Giancotti. 2005. Merlin/NF-2 mediates contact inhibition of growth by suppressing recruitment of Rac to the plasma membrane. *The Journal of cell biology*. 171:361-371.

Orihara-Ono, M., M. Toriya, K. Nakao, and H. Okano. 2011. Downregulation of Notch mediates the seamless transition of individual Drosophila neuroepithelial progenitors into optic medullar neuroblasts during prolonged G1. *Developmental biology*. 351:163-175.

Orsetti, B., F. Courjal, M. Cuny, C. Rodriguez, and C. Theillet. 1999. 17q21-q25 aberrations in breast cancer: combined allelotyping and CGH analysis reveals 5 regions of allelic imbalance among which two correspond to DNA amplification. *Oncogene*. 18:6262-6270.

Oshiro, N., Y. Fukata, and K. Kaibuchi. 1998. Phosphorylation of moesin by rho-associated kinase (Rho-kinase) plays a crucial role in the formation of microvilli-like structures. *The Journal of biological chemistry*. 273:34663-34666.

Ou, G., N. Stuurman, M. D'Ambrosio, and R.D. Vale. 2010. Polarized myosin produces unequal-size daughters during asymmetric cell division. *Science*. 330:677-680.

Paglini, G., P. Kunda, S. Quiroga, K. Kosik, and A. Caceres. 1998. Suppression of radixin and moesin alters growth cone morphology, motility, and process formation in primary cultured neurons. *The Journal of cell biology*. 143:443-455.

Pakkanen, R., K. Hedman, O. Turunen, T. Wahlstrom, and A. Vaheri. 1987. Microvillus-specific Mr 75,000 plasma membrane protein of human choriocarcinoma cells. *The journal of histochemistry and cytochemistry : official journal of the Histochemistry Society*. 35:809-816.

Pakkanen, R., and A. Vaheri. 1989. Cytovillin and other microvillar proteins of human choriocarcinoma cells. *Journal of cellular biochemistry*. 41:1-12.

Pakkanen, R., C.H. von Bonsdorff, O. Turunen, T. Wahlstrom, and A. Vaheri. 1988. Redistribution of Mr 75,000 plasma membrane protein, cytovillin, into newly formed microvilli in herpes simplex and Semliki Forest virus infected human embryonal fibroblasts. *European journal of cell biology*. 46:435-443.

Pang, S.T., X. Fang, A. Valdman, G. Norstedt, A. Pousette, L. Egevad, and P. Ekman. 2004. Expression of ezrin in prostatic intraepithelial neoplasia. *Urology*. 63:609-612.

Panneton, V., A. Nath, F. Sader, N. Delaunay, A. Pelletier, D. Maier, K. Oh, and D.R. Hipfner. 2015. Regulation of Catalytic and Non-catalytic Functions of the Drosophila Ste20 Kinase Slik by Activation Segment Phosphorylation. *The Journal of biological chemistry*. 290:20960-20971.

Parmentier, M.L., D. Woods, S. Greig, P.G. Phan, A. Radovic, P. Bryant, and C.J. O'Kane. 2000. Rapsynoid/partner of inscuteable controls asymmetric division of larval neuroblasts in Drosophila. *The Journal of neuroscience : the official journal of the Society for Neuroscience*. 20:RC84.

Paul, S.M., M. Ternet, P.M. Salvaterra, and G.J. Beitel. 2003. The Na+/K+ ATPase is required for septate junction function and epithelial tube-size control in the Drosophila tracheal system. *Development*. 130:4963-4974.

Pearson, M.A., D. Reczek, A. Bretscher, and P.A. Karplus. 2000. Structure of the ERM protein moesin reveals the FERM domain fold masked by an extended actin binding tail domain. *Cell*. 101:259-270.

Pelton, P.D., L.S. Sherman, T.A. Rizvi, M.A. Marchionni, P. Wood, R.A. Friedman, and N. Ratner. 1998. Ruffling membrane, stress fiber, cell spreading and proliferation abnormalities in human Schwannoma cells. *Oncogene*. 17:2195-2209.

Peng, C.Y., L. Manning, R. Albertson, and C.Q. Doe. 2000. The tumour-suppressor genes lgl and dlg regulate basal protein targeting in Drosophila neuroblasts. *Nature*. 408:596-600.

Pereanu, W., D. Shy, and V. Hartenstein. 2005. Morphogenesis and proliferation of the larval brain glia in Drosophila. *Developmental biology*. 283:191-203.

Perez-Gomez, R., J. Slovakova, N. Rives-Quinto, A. Krejci, and A. Carmena. 2013. A Serrate-Notch-Canoe complex mediates essential interactions between glia and neuroepithelial cells during Drosophila optic lobe development. *Journal of cell science*. 126:4873-4884.

Persson, A., O.R. Lindberg, and H.G. Kuhn. 2013. Radixin inhibition decreases adult neural progenitor cell migration and proliferation in vitro and in vivo. *Frontiers in cellular neuroscience*. 7:161.

Persson, A., C. Lindwall, M.A. Curtis, and H.G. Kuhn. 2010. Expression of ezrin radixin moesin proteins in the adult subventricular zone and the rostral migratory stream. *Neuroscience*. 167:312-322.

Pestonjamasp, K., M.R. Amieva, C.P. Strassel, W.M. Nauseef, H. Furthmayr, and E.J. Luna. 1995. Moesin, ezrin, and p205 are actin-binding proteins associated with neutrophil plasma membranes. *Molecular biology of the cell*. 6:247-259.

Peterson, C., G.E. Carney, B.J. Taylor, and K. White. 2002. reaper is required for neuroblast apoptosis during Drosophila development. *Development*. 129:1467-1476.

Petritsch, C., G. Tavosanis, C.W. Turck, L.Y. Jan, and Y.N. Jan. 2003. The Drosophila myosin VI Jaguar is required for basal protein targeting and correct spindle orientation in mitotic neuroblasts. *Developmental cell*. 4:273-281.

Petronczki, M., and J.A. Knoblich. 2001. DmPAR-6 directs epithelial polarity and asymmetric cell division of neuroblasts in Drosophila. *Nature cell biology*. 3:43-49.

Pietromonaco, S.F., P.C. Simons, A. Altman, and L. Elias. 1998. Protein kinase C-theta phosphorylation of moesin in the actin-binding sequence. *The Journal of biological chemistry*. 273:7594-7603.

Pilot, F., J.M. Philippe, C. Lemmers, and T. Lecuit. 2006. Spatial control of actin organization at adherens junctions by a synaptotagmin-like protein Btsz. *Nature*. 442:580-584.

Plummer, S.J., L. Adams, J.A. Simmons, and G. Casey. 1997. Localization of a growth suppressor activity in MCF7 breast cancer cells to chromosome 17q24-q25. *Oncogene*. 14:2339-2345.

Polesello, C., I. Delon, P. Valenti, P. Ferrer, and F. Payre. 2002. Dmoesin controls actin-based cell shape and polarity during Drosophila melanogaster oogenesis. *Nature cell biology*. 4:782-789.

Poon, C.L., K.A. Mitchell, S. Kondo, L.Y. Cheng, and K.F. Harvey. 2016. The Hippo Pathway Regulates Neuroblasts and Brain Size in Drosophila melanogaster. *Current biology : CB*. 26:1034-1042.

Presneau, N., K. Dewar, V. Forgetta, D. Provencher, A.M. Mes-Masson, and P.N. Tonin. 2005. Loss of heterozygosity and transcriptome analyses of a 1.2 Mb candidate ovarian cancer tumor suppressor locus region at 17q25.1-q25.2. *Molecular carcinogenesis*. 43:141-154.

Prokop, A., S. Bray, E. Harrison, and G.M. Technau. 1998. Homeotic regulation of segment-specific differences in neuroblast numbers and proliferation in the Drosophila central nervous system. *Mechanisms of development*. 74:99-110.

Prokop, A., and G.M. Technau. 1991. The origin of postembryonic neuroblasts in the ventral nerve cord of Drosophila melanogaster. *Development*. 111:79-88.

Pujuguet, P., L. Del Maestro, A. Gautreau, D. Louvard, and M. Arpin. 2003. Ezrin regulates E-cadherin-dependent adherens junction assembly through Rac1 activation. *Molecular biology of the cell*. 14:2181-2191.

Radford, D.M., K.L. Fair, N.J. Phillips, J.H. Ritter, T. Steinbrueck, M.S. Holt, and H. Donis-Keller. 1995. Allelotyping of ductal carcinoma in situ of the breast: deletion of loci on 8p, 13q, 16q, 17p and 17q. *Cancer research*. 55:3399-3405.

Raghuram, V., H. Hormuth, and J.K. Foskett. 2003. A kinase-regulated mechanism controls CFTR channel gating by disrupting bivalent PDZ domain interactions. *Proceedings of the National Academy of Sciences of the United States of America*. 100:9620-9625.

Reczek, D., M. Berryman, and A. Bretscher. 1997. Identification of EBP50: A PDZ-containing phosphoprotein that associates with members of the ezrin-radixin-moesin family. *The Journal of cell biology*. 139:169-179.

Reczek, D., and A. Bretscher. 1998. The carboxyl-terminal region of EBP50 binds to a site in the amino-terminal domain of ezrin that is masked in the dormant molecule. *The Journal of biological chemistry*. 273:18452-18458.

Reddy, B.V., C. Rauskolb, and K.D. Irvine. 2010. Influence of fat-hippo and notch signaling on the proliferation and differentiation of Drosophila optic neuroepithelia. *Development*. 137:2397-2408.

Reiter, L.T., L. Potocki, S. Chien, M. Gribskov, and E. Bier. 2001. A systematic analysis of human disease-associated gene sequences in Drosophila melanogaster. *Genome research*. 11:1114-1125.

Riedl, J., A.H. Crevenna, K. Kessenbrock, J.H. Yu, D. Neukirchen, M. Bista, F. Bradke, D. Jenne, T.A. Holak, Z. Werb, M. Sixt, and R. Wedlich-Soldner. 2008. Lifeact: a versatile marker to visualize F-actin. *Nature methods*. 5:605-607.

Rodrigues, N.T., S. Lekomtsev, S. Jananji, J. Kriston-Vizi, G.R. Hickson, and B. Baum. 2015. Kinetochore-localized PP1-Sds22 couples chromosome segregation to polar relaxation. *Nature*. 524:489-492.

Rolls, M.M., R. Albertson, H.P. Shih, C.Y. Lee, and C.Q. Doe. 2003. Drosophila aPKC regulates cell polarity and cell proliferation in neuroblasts and epithelia. *The Journal of cell biology*. 163:1089-1098.

Roth, S., F.S. Neuman-Silberberg, G. Barcelo, and T. Schupbach. 1995. cornichon and the EGF receptor signaling process are necessary for both anterior-posterior and dorsal-ventral pattern formation in Drosophila. *Cell*. 81:967-978.

Roubinet, C., B. Decelle, G. Chicanne, J.F. Dorn, B. Payrastre, F. Payre, and S. Carreno. 2011. Molecular networks linked by Moesin drive remodeling of the cell cortex during mitosis. *The Journal of cell biology*. 195:99-112.

Rouleau, G.A., P. Merel, M. Lutchman, M. Sanson, J. Zucman, C. Marineau, K. Hoang-Xuan, S. Demczuk, C. Desmaze, B. Plougastel, and et al. 1993. Alteration in a new gene encoding a putative membrane-organizing protein causes neuro-fibromatosis type 2. *Nature*. 363:515-521.

Rouleau, G.A., W. Wertelecki, J.L. Haines, W.J. Hobbs, J.A. Trofatter, B.R. Seizinger, R.L. Martuza, D.W. Superneau, P.M. Conneally, and J.F. Gusella. 1987. Genetic linkage of bilateral acoustic neurofibromatosis to a DNA marker on chromosome 22. *Nature*. 329:246-248.

Rusan, N.M., and M. Peifer. 2007. A role for a novel centrosome cycle in asymmetric cell division. *The Journal of cell biology*. 177:13-20.

Sainio, M., F. Zhao, L. Heiska, O. Turunen, M. den Bakker, E. Zwarthoff, M. Lutchman, G.A. Rouleau, J. Jaaskelainen, A. Vaheri, and O. Carpen. 1997. Neurofibromatosis 2 tumor suppressor protein colocalizes with ezrin and CD44 and associates with actin-containing cytoskeleton. *Journal of cell science*. 110 (Pt 18):2249-2260.

Saotome, I., M. Curto, and A.I. McClatchey. 2004. Ezrin is essential for epithelial organization and villus morphogenesis in the developing intestine. *Developmental cell*. 6:855-864.

Sarrio, D., S.M. Rodriguez-Pinilla, A. Dotor, F. Calero, D. Hardisson, and J. Palacios. 2006. Abnormal ezrin localization is associated with clinicopathological features in invasive breast carcinomas. *Breast cancer research and treatment*. 98:71-79.

Sato, N., N. Funayama, A. Nagafuchi, S. Yonemura, S. Tsukita, and S. Tsukita. 1992. A gene family consisting of ezrin, radixin and moesin. Its specific localization at actin filament/plasma membrane association sites. *Journal of cell science*. 103 (Pt 1):131-143.

Sato, N., S. Yonemura, T. Obinata, S. Tsukita, and S. Tsukita. 1991. Radixin, a barbed end-capping actin-modulating protein, is concentrated at the cleavage furrow during cytokinesis. *The Journal of cell biology*. 113:321-330.

Schaefer, M., M. Petronczki, D. Dorner, M. Forte, and J.A. Knoblich. 2001. Heterotrimeric G proteins direct two modes of asymmetric cell division in the Drosophila nervous system. *Cell*. 107:183-194.

Schaefer, M., A. Shevchenko, A. Shevchenko, and J.A. Knoblich. 2000. A protein complex containing Inscuteable and the Galpha-binding protein Pins orients asymmetric cell divisions in Drosophila. *Current biology : CB*. 10:353-362.

Scherer, S.S., and D.H. Gutmann. 1996. Expression of the neurofibromatosis 2 tumor suppressor gene product, merlin, in Schwann cells. *Journal of neuroscience research*. 46:595-605.

Schmucker, B., W.G. Ballhausen, and M. Kressel. 1997. Subcellular localization and expression pattern of the neurofibromatosis type 2 protein merlin/schwannomin. *European journal of cell biology*. 72:46-53.

Schober, M., M. Schaefer, and J.A. Knoblich. 1999. Bazooka recruits Inscuteable to orient asymmetric cell divisions in Drosophila neuroblasts. *Nature*. 402:548-551.

Schulz, A., S.L. Baader, M. Niwa-Kawakita, M.J. Jung, R. Bauer, C. Garcia, A. Zoch, S. Schacke, C. Hagel, V.F. Mautner, C.O. Hanemann, X.P. Dun, D.B. Parkinson, J. Weis, J.M. Schroder, D.H. Gutmann, M. Giovannini, and H. Morrison. 2013. Merlin isoform 2 in neurofibromatosis type 2-associated polyneuropathy. *Nature neuroscience*. 16:426-433.

Schulz, A., A. Kyselyova, S.L. Baader, M.J. Jung, A. Zoch, V.F. Mautner, C. Hagel, and H. Morrison. 2014. Neuronal merlin influences ERBB2 receptor expression on Schwann cells through neuregulin 1 type III signalling. *Brain : a journal of neurology*. 137:420-432.

Schwabe, T., R.J. Bainton, R.D. Fetter, U. Heberlein, and U. Gaul. 2005. GPCR signaling is required for blood-brain barrier formation in drosophila. *Cell*. 123:133-144.

Schwarz, S., Z. Durisko, and R. Dukas. 2014. Food selection in larval fruit flies: dynamics and effects on larval development. *Die Naturwissenschaften*. 101:61-68.

Scoles, D.R., D.P. Huynh, P.A. Morcos, E.R. Coulsell, N.G. Robinson, F. Tamanoi, and S.M. Pulst. 1998. Neurofibromatosis 2 tumour suppressor schwannomin interacts with betaII-spectrin. *Nature genetics*. 18:354-359.

Scott, R.O., W.R. Thelin, and S.L. Milgram. 2002. A novel PDZ protein regulates the activity of guanylyl cyclase C, the heat-stable enterotoxin receptor. *The Journal of biological chemistry*. 277:22934-22941.

Sekido, Y., H.I. Pass, S. Bader, D.J. Mew, M.F. Christman, A.F. Gazdar, and J.D. Minna. 1995. Neurofibromatosis type 2 (NF2) gene is somatically mutated in mesothelioma but not in lung cancer. *Cancer research*. 55:1227-1231.

Selleck, S.B., C. Gonzalez, D.M. Glover, and K. White. 1992. Regulation of the G1-S transition in postembryonic neuronal precursors by axon ingrowth. *Nature*. 355:253-255.

Selleck, S.B., and H. Steller. 1991. The influence of retinal innervation on neurogenesis in the first optic ganglion of Drosophila. *Neuron*. 6:83-99.

Serinagaoglu, Y., J. Pare, M. Giovannini, and X. Cao. 2015. Nf2-Yap signaling controls the expansion of DRG progenitors and glia during DRG development. *Developmental biology*. 398:97-109.

Shaw, R.J., A.I. McClatchey, and T. Jacks. 1998a. Localization and functional domains of the neurofibromatosis type II tumor suppressor, merlin. *Cell growth & differentiation :*

the molecular biology journal of the American Association for Cancer Research. 9:287-296.

Shaw, R.J., A.I. McClatchey, and T. Jacks. 1998b. Regulation of the neurofibromatosis type 2 tumor suppressor protein, merlin, by adhesion and growth arrest stimuli. *The Journal of biological chemistry*. 273:7757-7764.

Shaw, R.J., J.G. Paez, M. Curto, A. Yaktine, W.M. Pruitt, I. Saotome, J.P. O'Bryan, V. Gupta, N. Ratner, C.J. Der, T. Jacks, and A.I. McClatchey. 2001. The Nf2 tumor suppressor, merlin, functions in Rac-dependent signaling. *Developmental cell*. 1:63-72.

Shen, C.P., L.Y. Jan, and Y.N. Jan. 1997. Miranda is required for the asymmetric localization of Prospero during mitosis in Drosophila. *Cell*. 90:449-458.

Shen, C.P., J.A. Knoblich, Y.M. Chan, M.M. Jiang, L.Y. Jan, and Y.N. Jan. 1998. Miranda as a multidomain adapter linking apically localized Inscuteable and basally localized Staufen and Prospero during asymmetric cell division in Drosophila. *Genes & development*. 12:1837-1846.

Shenolikar, S., C.M. Minkoff, D.A. Steplock, C. Evangelista, M. Liu, and E.J. Weinman. 2001. N-terminal PDZ domain is required for NHERF dimerization. *FEBS letters*. 489:233-236.

Shenolikar, S., J.W. Voltz, C.M. Minkoff, J.B. Wade, and E.J. Weinman. 2002. Targeted disruption of the mouse NHERF-1 gene promotes internalization of proximal tubule sodium-phosphate cotransporter type IIa and renal phosphate wasting. *Proceedings of the National Academy of Sciences of the United States of America*. 99:11470-11475.

Sher, I., C.O. Hanemann, P.A. Karplus, and A. Bretscher. 2012. The tumor suppressor merlin controls growth in its open state, and phosphorylation converts it to a less-active more-closed state. *Developmental cell*. 22:703-705.

Sherman, L., H.M. Xu, R.T. Geist, S. Saporito-Irwin, N. Howells, H. Ponta, P. Herrlich, and D.H. Gutmann. 1997. Interdomain binding mediates tumor growth suppression by the NF2 gene product. *Oncogene*. 15:2505-2509.

Shibata, T., M. Chuma, A. Kokubu, M. Sakamoto, and S. Hirohashi. 2003. EBP50, a beta-catenin-associating protein, enhances Wnt signaling and is over-expressed in hepatocellular carcinoma. *Hepatology*. 38:178-186.

Shimizu, T., A. Seto, N. Maita, K. Hamada, S. Tsukita, S. Tsukita, and T. Hakoshima. 2002. Structural basis for neurofibromatosis type 2. Crystal structure of the merlin FERM domain. *The Journal of biological chemistry*. 277:10332-10336.

Short, D.B., K.W. Trotter, D. Reczek, S.M. Kreda, A. Bretscher, R.C. Boucher, M.J. Stutts, and S.L. Milgram. 1998. An apical PDZ protein anchors the cystic fibrosis transmembrane conductance regulator to the cytoskeleton. *The Journal of biological chemistry*. 273:19797-19801.

Shuster, C.B., and I.M. Herman. 1995. Indirect association of ezrin with F-actin: isoform specificity and calcium sensitivity. *The Journal of cell biology*. 128:837-848.

Siegenthaler, J.A., A.M. Ashique, K. Zarbalis, K.P. Patterson, J.H. Hecht, M.A. Kane, A.E. Folias, Y. Choe, S.R. May, T. Kume, J.L. Napoli, A.S. Peterson, and S.J. Pleasure. 2009. Retinoic acid from the meninges regulates cortical neuron generation. *Cell*. 139:597-609.

Siegrist, S.E., and C.Q. Doe. 2005. Microtubule-induced Pins/Galphai cortical polarity in Drosophila neuroblasts. *Cell*. 123:1323-1335.

Siegrist, S.E., and C.Q. Doe. 2006. Extrinsic cues orient the cell division axis in Drosophila embryonic neuroblasts. *Development*. 133:529-536.

Siller, K.H., C. Cabernard, and C.Q. Doe. 2006. The NuMA-related Mud protein binds Pins and regulates spindle orientation in Drosophila neuroblasts. *Nature cell biology*. 8:594-600.

Silverman-Gavrila, R.V., and A. Wilde. 2006. Ran is required before metaphase for spindle assembly and chromosome alignment and after metaphase for chromosome segregation and spindle midbody organization. *Molecular biology of the cell*. 17:2069-2080.

Simon-Assmann, P., N. Turck, M. Sidhoum-Jenny, G. Gradwohl, and M. Kedinger. 2007. In vitro models of intestinal epithelial cell differentiation. *Cell biology and toxicology*. 23:241-256.

Simons, P.C., S.F. Pietromonaco, D. Reczek, A. Bretscher, and L. Elias. 1998. C-terminal threonine phosphorylation activates ERM proteins to link the cell's cortical lipid bilayer to the cytoskeleton. *Biochemical and biophysical research communications*. 253:561-565.

Solinet, S., K. Mahmud, S.F. Stewman, K. Ben El Kadhi, B. Decelle, L. Talje, A. Ma, B.H. Kwok, and S. Carreno. 2013. The actin-binding ERM protein Moesin binds to and stabilizes microtubules at the cell cortex. *The Journal of cell biology*. 202:251-260.

Song, G.J., K.L. Leslie, S. Barrick, T. Mamonova, J.M. Fitzpatrick, K.W. Drombosky, N. Peyser, B. Wang, M. Pellegrini, P.M. Bauer, P.A. Friedman, D.F. Mierke, and A. Bisello. 2015. Phosphorylation of ezrin-radixin-moesin-binding phosphoprotein 50

(EBP50) by Akt promotes stability and mitogenic function of S-phase kinase-associated protein-2 (Skp2). *The Journal of biological chemistry*. 290:2879-2887.

Song, J., J. Bai, W. Yang, E.W. Gabrielson, D.W. Chan, and Z. Zhang. 2007. Expression and clinicopathological significance of oestrogen-responsive ezrin-radixin-moesin-binding phosphoprotein 50 in breast cancer. *Histopathology*. 51:40-53.

Sousa-Nunes, R., W. Chia, and W.G. Somers. 2009. Protein phosphatase 4 mediates localization of the Miranda complex during Drosophila neuroblast asymmetric divisions. *Genes & development*. 23:359-372.

Spana, E.P., and C.Q. Doe. 1995. The prospero transcription factor is asymmetrically localized to the cell cortex during neuroblast mitosis in Drosophila. *Development*. 121:3187-3195.

Speck, O., S.C. Hughes, N.K. Noren, R.M. Kulikauskas, and R.G. Fehon. 2003. Moesin functions antagonistically to the Rho pathway to maintain epithelial integrity. *Nature*. 421:83-87.

Sperfeld, A.D., C. Hein, J.M. Schroder, A.C. Ludolph, and C.O. Hanemann. 2002. Occurrence and characterization of peripheral nerve involvement in neurofibromatosis type 2. *Brain : a journal of neurology*. 125:996-1004.

Spradling, A.C., D. Stern, A. Beaton, E.J. Rhem, T. Laverty, N. Mozden, S. Misra, and G.M. Rubin. 1999. The Berkeley Drosophila Genome Project gene disruption project: Single P-element insertions mutating 25% of vital Drosophila genes. *Genetics*. 153:135-177.

Stemmer-Rachamimov, A.O., T. Wiederhold, G.P. Nielsen, M. James, D. Pinney-Michalowski, J.E. Roy, W.A. Cohen, V. Ramesh, and D.N. Louis. 2001. NHE-RF, a merlin-interacting protein, is primarily expressed in luminal epithelia, proliferative endometrium, and estrogen receptor-positive breast carcinomas. *The American journal of pathology*. 158:57-62.

Stork, T., D. Engelen, A. Krudewig, M. Silies, R.J. Bainton, and C. Klambt. 2008. Organization and function of the blood-brain barrier in Drosophila. *The Journal of neuroscience : the official journal of the Society for Neuroscience*. 28:587-597.

Streeten, B.W., and J. Eshaghian. 1978. Human posterior subcapsular cataract. A gross and flat preparation study. *Archives of ophthalmology*. 96:1653-1658.

Striedinger, K., S.R. VandenBerg, G.S. Baia, M.W. McDermott, D.H. Gutmann, and A. Lal. 2008. The neurofibromatosis 2 tumor suppressor gene product, merlin, regulates human meningioma cell growth by signaling through YAP. *Neoplasia*. 10:1204-1212.

Surace, E.I., C.A. Haipek, and D.H. Gutmann. 2004. Effect of merlin phosphorylation on neurofibromatosis 2 (NF2) gene function. *Oncogene*. 23:580-587.

Takahashi, K., T. Sasaki, A. Mammoto, I. Hotta, K. Takaishi, H. Imamura, K. Nakano, A. Kodama, and Y. Takai. 1998. Interaction of radixin with Rho small G protein GDP/GTP exchange protein Dbl. *Oncogene*. 16:3279-3284.

Takahashi, K., T. Sasaki, A. Mammoto, K. Takaishi, T. Kameyama, S. Tsukita, and Y. Takai. 1997. Direct interaction of the Rho GDP dissociation inhibitor with ezrin/radixin/moesin initiates the activation of the Rho small G protein. *The Journal of biological chemistry*. 272:23371-23375.

Takahashi, Y., F.C. Morales, E.L. Kreimann, and M.M. Georgescu. 2006. PTEN tumor suppressor associates with NHERF proteins to attenuate PDGF receptor signaling. *The EMBO journal*. 25:910-920.

Takeuchi, K., N. Sato, H. Kasahara, N. Funayama, A. Nagafuchi, S. Yonemura, S. Tsukita, and S. Tsukita. 1994. Perturbation of cell adhesion and microvilli formation by antisense oligonucleotides to ERM family members. *The Journal of cell biology*. 125:1371-1384.

Tanentzapf, G., C. Smith, J. McGlade, and U. Tepass. 2000. Apical, lateral, and basal polarization cues contribute to the development of the follicular epithelium during Drosophila oogenesis. *The Journal of cell biology*. 151:891-904.

Tang, X., S.W. Jang, X. Wang, Z. Liu, S.M. Bahr, S.Y. Sun, D. Brat, D.H. Gutmann, and K. Ye. 2007. Akt phosphorylation regulates the tumour-suppressor merlin through ubiquitination and degradation. *Nature cell biology*. 9:1199-1207.

Taylor, M.D., H. Poppleton, C. Fuller, X. Su, Y. Liu, P. Jensen, S. Magdaleno, J. Dalton, C. Calabrese, J. Board, T. Macdonald, J. Rutka, A. Guha, A. Gajjar, T. Curran, and R.J. Gilbertson. 2005. Radial glia cells are candidate stem cells of ependymoma. *Cancer cell*. 8:323-335.

Tekotte, H., D. Berdnik, T. Torok, M. Buszczak, L.M. Jones, L. Cooley, J.A. Knoblich, and I. Davis. 2002. Dcas is required for importin-alpha3 nuclear export and mechano-sensory organ cell fate specification in Drosophila. *Developmental biology*. 244:396-406.

ten Klooster, J.P., M. Jansen, J. Yuan, V. Oorschot, H. Begthel, V. Di Giacomo, F. Colland, J. de Koning, M.M. Maurice, P. Hornbeck, and H. Clevers. 2009. Mst4 and Ezrin induce brush borders downstream of the Lkb1/Strad/Mo25 polarization complex. *Developmental cell*. 16:551-562.

Thery, M., V. Racine, A. Pepin, M. Piel, Y. Chen, J.B. Sibarita, and M. Bornens. 2005. The extracellular matrix guides the orientation of the cell division axis. *Nature cell biology*. 7:947-953.

Thurneysen, C., I. Opitz, S. Kurtz, W. Weder, R.A. Stahel, and E. Felley-Bosco. 2009. Functional inactivation of NF2/merlin in human mesothelioma. *Lung cancer*. 64:140-147.

Tio, M., M. Zavortink, X. Yang, and W. Chia. 1999. A functional analysis of inscuteable and its roles during Drosophila asymmetric cell divisions. *Journal of cell science*. 112 (Pt 10):1541-1551.

Tokunou, M., T. Niki, Y. Saitoh, H. Imamura, M. Sakamoto, and S. Hirohashi. 2000. Altered expression of the ERM proteins in lung adenocarcinoma. *Laboratory investigation; a journal of technical methods and pathology*. 80:1643-1650.

Torok, I., D. Strand, R. Schmitt, G. Tick, T. Torok, I. Kiss, and B.M. Mechler. 1995. The overgrown hematopoietic organs-31 tumor suppressor gene of Drosophila encodes an Importin-like protein accumulating in the nucleus at the onset of mitosis. *The Journal of cell biology*. 129:1473-1489.

Tran Quang, C., A. Gautreau, M. Arpin, and R. Treisman. 2000. Ezrin function is required for ROCK-mediated fibroblast transformation by the Net and Dbl oncogenes. *The EMBO journal*. 19:4565-4576.

Trofatter, J.A., M.M. MacCollin, J.L. Rutter, J.R. Murrell, M.P. Duyao, D.M. Parry, R. Eldridge, N. Kley, A.G. Menon, K. Pulaski, and et al. 1993. A novel moesin-, ezrin-, radixin-like gene is a candidate for the neurofibromatosis 2 tumor suppressor. *Cell*. 72:791-800.

Truman, J.W., and M. Bate. 1988. Spatial and temporal patterns of neurogenesis in the central nervous system of Drosophila melanogaster. *Developmental biology*. 125:145-157.

Tsukita, S., Y. Hieda, and S. Tsukita. 1989. A new 82-kD barbed end-capping protein (radixin) localized in the cell-to-cell adherens junction: purification and characterization. *The Journal of cell biology*. 108:2369-2382.

Tsukita, S., K. Oishi, N. Sato, J. Sagara, A. Kawai, and S. Tsukita. 1994. ERM family members as molecular linkers between the cell surface glycoprotein CD44 and actin-based cytoskeletons. *The Journal of cell biology*. 126:391-401.

Turunen, O., T. Wahlstrom, and A. Vaheri. 1994. Ezrin has a COOH-terminal actin-binding site that is conserved in the ezrin protein family. *The Journal of cell biology*. 126:1445-1453.

Turunen, O., R. Winqvist, R. Pakkanen, K.H. Grzeschik, T. Wahlstrom, and A. Vaheri. 1989. Cytovillin, a microvillar Mr 75,000 protein. cDNA sequence, prokaryotic expression, and chromosomal localization. *The Journal of biological chemistry*. 264:16727-16732.

Tynninen, O., O. Carpen, J. Jaaskelainen, T. Paavonen, and A. Paetau. 2004. Ezrin expression in tissue microarray of primary and recurrent gliomas. *Neuropathol Appl Neurobiol*. 30:472-477.

Valderrama, F., S. Thevapala, and A.J. Ridley. 2012. Radixin regulates cell migration and cell-cell adhesion through Rac1. *Journal of cell science*. 125:3310-3319.

Van Furden, D., K. Johnson, C. Segbert, and O. Bossinger. 2004. The C. elegans ezrin-radixin-moesin protein ERM-1 is necessary for apical junction remodelling and tubulogenesis in the intestine. *Developmental biology*. 272:262-276.

Verboon, J.M., and S.M. Parkhurst. 2015. Rho family GTPases bring a familiar ring to cell wound repair. *Small GTPases*. 6:1-7.

Voltz, J.W., M. Brush, S. Sikes, D. Steplock, E.J. Weinman, and S. Shenolikar. 2007. Phosphorylation of PDZ1 domain attenuates NHERF-1 binding to cellular targets. *The Journal of biological chemistry*. 282:33879-33887.

Wang, C.C., J.Y. Liau, Y.S. Lu, J.W. Chen, Y.T. Yao, and H.C. Lien. 2012. Differential expression of moesin in breast cancers and its implication in epithelial-mesenchymal transition. *Histopathology*. 61:78-87.

Wang, W., Y. Li, L. Zhou, H. Yue, and H. Luo. 2011a. Role of JAK/STAT signaling in neuroepithelial stem cell maintenance and proliferation in the Drosophila optic lobe. *Biochemical and biophysical research communications*. 410:714-720.

Wang, W., W. Liu, Y. Wang, L. Zhou, X. Tang, and H. Luo. 2011b. Notch signaling regulates neuroepithelial stem cell maintenance and neuroblast formation in Drosophila optic lobe development. *Developmental biology*. 350:414-428.

Weinman, E.J., D. Steplock, and S. Shenolikar. 1993. CAMP-mediated inhibition of the renal brush border membrane Na+-H+ exchanger requires a dissociable phosphoprotein cofactor. *The Journal of clinical investigation*. 92:1781-1786.

Weinman, E.J., D. Steplock, Y. Wang, and S. Shenolikar. 1995. Characterization of a protein cofactor that mediates protein kinase A regulation of the renal brush border membrane Na(+)-H+ exchanger. *The Journal of clinical investigation*. 95:2143-2149.

Weng, M., J.M. Haenfler, and C.Y. Lee. 2012. Changes in Notch signaling coordinates maintenance and differentiation of the Drosophila larval optic lobe neuroepithelia. *Developmental neurobiology*. 72:1376-1390.

Wheeler, D., W.B. Sneddon, B. Wang, P.A. Friedman, and G. Romero. 2007. NHERF-1 and the cytoskeleton regulate the traffic and membrane dynamics of G protein-coupled receptors. *The Journal of biological chemistry*. 282:25076-25087.

White, K., M.E. Grether, J.M. Abrams, L. Young, K. Farrell, and H. Steller. 1994. Genetic control of programmed cell death in Drosophila. *Science*. 264:677-683.

White, K., and D.R. Kankel. 1978. Patterns of cell division and cell movement in the formation of the imaginal nervous system in Drosophila melanogaster. *Developmental biology*. 65:296-321.

Wick, W., C. Grimmel, C. Wild-Bode, M. Platten, M. Arpin, and M. Weller. 2001. Ezrin-dependent promotion of glioma cell clonogenicity, motility, and invasion mediated by BCL-2 and transforming growth factor-beta2. *The Journal of neuroscience : the official journal of the Society for Neuroscience*. 21:3360-3368.

Wiley, L.A., L.K. Dattilo, K.B. Kang, M. Giovannini, and D.C. Beebe. 2010. The tumor suppressor merlin is required for cell cycle exit, terminal differentiation, and cell polarity in the developing murine lens. *Investigative ophthalmology & visual science*. 51:3611-3618.

Wodarz, A., A. Ramrath, A. Grimm, and E. Knust. 2000. Drosophila atypical protein kinase C associates with Bazooka and controls polarity of epithelia and neuroblasts. *The Journal of cell biology*. 150:1361-1374.

Wodarz, A., A. Ramrath, U. Kuchinke, and E. Knust. 1999. Bazooka provides an apical cue for Inscuteable localization in Drosophila neuroblasts. *Nature*. 402:544-547.

Wu, M., D.Y. Liu, X.R. Yuan, Q. Liu, X.J. Jiang, D. Yuan, J. Huang, X.J. Li, and Z.Q. Yang. 2013. The expression of moesin in astrocytoma: correlation with pathologic grade and poor clinical outcome. *Med Oncol*. 30:372.

Xiao, G.H., A. Beeser, J. Chernoff, and J.R. Testa. 2002. p21-activated kinase links Rac/Cdc42 signaling to merlin. *The Journal of biological chemistry*. 277:883-886.

Xu, H.M., and D.H. Gutmann. 1998. Merlin differentially associates with the microtubule and actin cytoskeleton. *Journal of neuroscience research*. 51:403-415.

Yang, H.S., and P.W. Hinds. 2003. Increased ezrin expression and activation by CDK5 coincident with acquisition of the senescent phenotype. *Molecular cell*. 11:1163-1176.

Yang, Y., D.A. Primrose, A.C. Leung, R.B. Fitzsimmons, M.C. McDermand, A. Missellbrook, J. Haskins, A.S. Smylie, and S.C. Hughes. 2012. The PP1 phosphatase flapwing regulates the activity of Merlin and Moesin in Drosophila. *Developmental biology*. 361:412-426.

Yasugi, T., A. Sugie, D. Umetsu, and T. Tabata. 2010. Coordinated sequential action of EGFR and Notch signaling pathways regulates proneural wave progression in the Drosophila optic lobe. *Development*. 137:3193-3203.

Yasugi, T., D. Umetsu, S. Murakami, M. Sato, and T. Tabata. 2008. Drosophila optic lobe neuroblasts triggered by a wave of proneural gene expression that is negatively regulated by JAK/STAT. *Development*. 135:1471-1480.

Yi, C., S. Troutman, D. Fera, A. Stemmer-Rachamimov, J.L. Avila, N. Christian, N.L. Persson, A. Shimono, D.W. Speicher, R. Marmorstein, L. Holmgren, and J.L. Kissil. 2011. A tight junction-associated Merlin-angiomotin complex mediates Merlin's regulation of mitogenic signaling and tumor suppressive functions. *Cancer cell*. 19:527-540.

Yonemura, S., M. Hirao, Y. Doi, N. Takahashi, T. Kondo, S. Tsukita, and S. Tsukita. 1998. Ezrin/radixin/moesin (ERM) proteins bind to a positively charged amino acid cluster in the juxta-membrane cytoplasmic domain of CD44, CD43, and ICAM-2. *The Journal of cell biology*. 140:885-895.

Yonemura, S., T. Matsui, S. Tsukita, and S. Tsukita. 2002. Rho-dependent and -independent activation mechanisms of ezrin/radixin/moesin proteins: an essential role for polyphosphoinositides in vivo. *Journal of cell science*. 115:2569-2580.

Yoo, N.J., S.W. Park, and S.H. Lee. 2012. Mutational analysis of tumour suppressor gene NF2 in common solid cancers and acute leukaemias. *Pathology*. 44:29-32.

Yoshiura, S., N. Ohta, and F. Matsuzaki. 2012. Tre1 GPCR signaling orients stem cell divisions in the Drosophila central nervous system. *Developmental cell*. 22:79-91.

Younossi-Hartenstein, A., C. Nassif, P. Green, and V. Hartenstein. 1996. Early neurogenesis of the Drosophila brain. *The Journal of comparative neurology*. 370:313-329.

Yu, F., Y. Cai, R. Kaushik, X. Yang, and W. Chia. 2003. Distinct roles of Galphai and Gbeta13F subunits of the heterotrimeric G protein complex in the mediation of Drosophila neuroblast asymmetric divisions. *The Journal of cell biology*. 162:623-633.

Yu, F., X. Morin, Y. Cai, X. Yang, and W. Chia. 2000. Analysis of partner of inscuteable, a novel player of Drosophila asymmetric divisions, reveals two distinct steps in inscuteable apical localization. *Cell*. 100:399-409.

Yue, L., and A.C. Spradling. 1992. hu-li tai shao, a gene required for ring canal formation during Drosophila oogenesis, encodes a homolog of adducin. *Genes & development*. 6:2443-2454.

Yun, C.H., S. Oh, M. Zizak, D. Steplock, S. Tsao, C.M. Tse, E.J. Weinman, and M. Donowitz. 1997. cAMP-mediated inhibition of the epithelial brush border Na+/H+ exchanger, NHE3, requires an associated regulatory protein. *Proceedings of the National Academy of Sciences of the United States of America*. 94:3010-3015.

Zhang, N., H. Bai, K.K. David, J. Dong, Y. Zheng, J. Cai, M. Giovannini, P. Liu, R.A. Anders, and D. Pan. 2010. The Merlin/NF2 tumor suppressor functions through the YAP oncoprotein to regulate tissue homeostasis in mammals. *Developmental cell*. 19:27-38.

Zhao, B., X. Wei, W. Li, R.S. Udan, Q. Yang, J. Kim, J. Xie, T. Ikenoue, J. Yu, L. Li, P. Zheng, K. Ye, A. Chinnaiyan, G. Halder, Z.C. Lai, and K.L. Guan. 2007. Inactivation of YAP oncoprotein by the Hippo pathway is involved in cell contact inhibition and tissue growth control. *Genes & development*. 21:2747-2761.

Zhou, L., A. Schnitzler, J. Agapite, L.M. Schwartz, H. Steller, and J.R. Nambu. 1997. Cooperative functions of the reaper and head involution defective genes in the programmed cell death of Drosophila central nervous system midline cells. *Proceedings of the National Academy of Sciences of the United States of America*. 94:5131-5136.

Zhu, S., S. Lin, C.F. Kao, T. Awasaki, A.S. Chiang, and T. Lee. 2006. Gradients of the Drosophila Chinmo BTB-zinc finger protein govern neuronal temporal identity. *Cell*. 127:409-422.

Zhu, X., F.C. Morales, N.K. Agarwal, T. Dogruluk, M. Gagea, and M.M. Georgescu. 2013. Moesin is a glioma progression marker that induces proliferation and Wnt/beta-catenin pathway activation via interaction with CD44. *Cancer research*. 73:1142-1155.